



UNIVERSITY*of*
TASMANIA

**Development of remote sensing products to investigate
the impact of tropical cyclones on natural vegetation
communities in the wet-dry tropics of northern Australia**

by

Grant Staben

BSc(Hons)

BEnvSc

Diploma: Lands, Parks and Wildlife Management

Submitted in fulfillment of the requirements for the degree of Doctor of Philosophy

University of Tasmania

March 2020

Declaration of Originality

"This thesis contains no material which has been accepted for a degree or diploma by the University or any other institution, except by way of background information and duly acknowledged in the thesis, and to the best of my knowledge and belief no material previously published or written by another person except where due acknowledgement is made in the text of the thesis, nor does the thesis contain any material that infringes copyright."

A handwritten signature in black ink, appearing to read "Grant Staben".

Grant Staben

31st March 2020

Authority of Access

The publishers of the papers comprising Chapters 2 to 3 hold the copyright for that content, and access to the material should be sought from the respective journals. The remaining non published content of the thesis may be made available for loan and limited copying and communication in accordance with the Copyright Act 1968.

Publications included in this thesis.

Chapters 2 and 3 in this thesis have been published in the peer reviewed journals detailed below.

Chapter 2 - Staben, G., Lucieer, A., Evans, K., Scarth, P. and Cook, G. (2016), ‘Obtaining biophysical measurements of woody vegetation from high resolution digital aerial photography in tropical and arid environments: Northern Territory, Australia’, International Journal of Applied Earth Observation and Geoinformation 52, 204–220. <http://linkinghub.elsevier.com/retrieve/pii/S0303243416300939>

Chapter 3 - Staben, G., Lucieer, A. and Scarth, P. (2018), ‘Modelling LiDAR derived tree canopy height from Landsat TM, ETM+ and OLI satellite imagery — A machine learning approach’, International Journal of Applied Earth Observation and Geoinformation 73, 666–681 <https://www.sciencedirect.com/science/article/pii/S0303243418303970>

Chapters 4 and 5 in this thesis have been or will be submitted for review or are under review in peer reviewed journals detailed below.

Chapter 4 - Staben, G., Scarth, P. and Lucieer, A., ‘Broad-scale mapping of tree canopy structure using optical satellite sensors, Sentinel-2 MSI and Landsat-8 OLI.’, Submitted for publication: Remote Sensing of Environment

Chapter 5 - Staben, G., Lucieer, A., and Scarth, P., Investigating structural dynamics of woody vegetation in northern Australia impacted by severe tropical cyclone Monica, using remote sensing. Submitted for publication: Remote Sensing Applications: Society and Environment



Grant Staben

31/3/2020

Statement of Co-Authorship

The following people and institutions contributed to the publication of work undertaken as part of this thesis:

Grant Staben, School of Technology, Environment and Design, University of Tasmania
Arko Lucieer, School of Technology, Environment and Design, University of Tasmania
Peter Scarth, Joint Remote Sensing Research Program, School of Geography, Planning and Environmental Management, University of Queensland
Garry Cook, CSIRO Ecosystem Sciences, Northern Territory, Australia
Ken Evans, Surface Water and Erosion Solutions, Northern Territory, Australia

Author details and their roles:

Chapter 2, Staben (90%), Lucieer (5%) Evans (2%), Scarth (2%), Cook (1%)

All authors contributed to design and development. Staben performed all analysis and writing of the chapter. Lucieer, Evans, Scarth and Cook provided editorial advice.

Chapter 3, Staben (90%), Lucieer (5%), Scarth (5%)

All authors contributed to design and development. Staben performed all analysis and writing of the chapter. Lucieer, and Scarth provided editorial advice.

Chapter 4, Staben (90%), Scarth (5%), Lucieer (5%)

All authors contributed to design and development. Staben performed all analysis and writing of the chapter. Lucieer, and Scarth provided editorial advice.

Chapter 5, Staben (94%), Cook (2%), Lucieer (2%) Scarth (2%),

All authors contributed to design and development. Staben performed all analysis and writing of the chapter. Cook, Lucieer and Scarth provided editorial advice.

We the undersigned agree with the above stated “proportion of work undertaken” for each of the above published (or submitted) peer-reviewed manuscripts contributing to this thesis:

Signed:

Candidate
Grant Staben
School of Technology
Environments and Design
University of Tasmania

Primary Supervisor
Professor Arko Lucieer
School of Technology
Environments and Design
University of Tasmania

Acting Head of School
Professor Elaine Stratford
School of Technology
Environments and Design
University of Tasmania

Date: 30/03/2020

31/03/2020

5 April 2020

ABSTRACT

Understanding ecological changes in native vegetation communities often requires information over long time periods. The influence of fire on woody vegetation structure in the Northern Territory has been well studied, however limited work has been undertaken to understand the impact of tropical cyclones, which can dramatically alter vegetation structure. Woody vegetation structure has been identified as an important metric for monitoring trends in biomass, primary productivity and biodiversity. Both cover and height have been identified as important structural attributes required for ecological studies investigating long term changes and trends. Satellite remote sensing products have the potential to provide information on cover and height at suitable spatial and temporal scales. Obtaining estimates of cover and height from satellite sensors requires the development of predictive models, often developed by relating field measured data to satellite imagery. The aim of this thesis is to develop remote sensing products measuring cover and height enabling the assessment of the impact of tropical cyclones on natural vegetation communities in the wet-dry tropics of northern Australia. To achieve the aim of the study, the following objectives were identified to develop mapping products that quantified and characterised woody vegetation structure based on cover and height.

The first objective was to develop and assess the suitability of using digital aerial photography to obtain woody vegetation biophysical parameters. This was done to enable validation of a Landsat satellite-based model predicting woody foliage projective cover, developed using field data collected over the state of Queensland. In this study, quantitative measurements obtained from digital aerial photography were compared to woody biophysical parameters measured from 1 ha field plots. There was a strong relationship ($R^2 \geq 0.85$) between all field measured woody canopy parameters and aerial derived green woody cover measurements, however only foliage projective cover (FPC) was found to be statistically significant. The results of this study show that accurate woody biophysical parameters can be obtained from aerial photography from a range of woody vegetation communities across the Northern Territory.

The second objective was to develop a predictive model to estimate vertical tree canopy structure. A machine learning algorithm, random forest regression, was used to predict

canopy height from a single date Landsat-5 TM scene, using training data derived from a 1 m canopy height model produced from LiDAR. The overall accuracy of the model was expressed by an R^2 of 0.53 and RMSE of 2.8 m. The model was also applied to Landsat-7 Enhanced Thematic Mapper Plus (ETM+) resulting in an R^2 of 0.49, RMSE of 2.8 m. The model was applied to Landsat imagery over the years 1988 to 2016. This study demonstrated that canopy height can be predicted from Landsat imagery. The robustness of the model across a range of vegetation communities and three different Landsat sensors illustrated that the approach could be successfully used to explore changes in woody vegetation height through time.

The third objective was to develop a predictive model to estimate a range of structural metrics characterising tree canopy structure from Sentinel-2 MSI and Landsat-8 OLI satellite sensors. Models were developed at 10 m, 20 m and 30 m spatial resolution for Sentinel-2 models, which enabled comparisons with the Landsat-8 results. To address limitations identified in the second objective, models were developed from seasonal composites (annual and dry season) for the respective satellite sensors, using training datasets captured across the Northern Territory. Of the seven models H_{99} (representing maximum canopy height) had the strongest relationship for both Sentinel-2 and Landsat-8 with R^2 values ranging from 0.7 to 0.81, and RMSE% between 22.9 and 33.8. Model accuracy was found to improve as spatial resolution decreased, with models produced at 30 m recording the highest overall accuracy. This study developed robust models predicting important forest structural metrics from Sentinel-2 and Landsat-8 satellite sensors, providing new insights into vertical tree canopy structure across an area covering 355,500 km² in the Northern Territory.

The fourth objective was to combine annual estimates of canopy cover and height (H_{99}) from Landsat satellite imagery to produce a structural classification product for a 30 year period (1988-2017). The structural mapping product was then used to investigate the dynamics of woody vegetation in a region ($\approx 11,500$ km²) impacted by severe tropical cyclone Monica in 2006. Landsat estimates of woody foliage projective cover (FPC) were validated and corrected for bias using estimates of FPC obtained from aerial photography, prior to being converted to canopy cover using a generalised model developed from field data. Independent datasets obtained from field data and LiDAR were used to validate the Landsat CC and height estimates. It was estimated that a total area of 3,551

km^2 was substantially impacted by cyclone Monica (2006). In 2017 it was estimated that an area of 70 km^2 was still severely impacted. The proportion of each structural class was used to gain insight into the dynamics and recovery of woody vegetation post cyclone Monica. The results show that recovery is occurring across the region, however the dynamics observed between the structural classes suggest that the region is still recovering 11 years after the cyclone.

This thesis has developed methodology to quantify woody vegetation structure using digital aerial photography, Landsat and Sentinel-2 satellite sensors. It enables the spatial and temporal assessment of historic (three decades) woody vegetation structure. The mapping products developed in this thesis have the potential to map and investigate woody vegetation (historic and contemporary) change across northern Australia.

ACKNOWLEDGEMENTS

I would first like to express my gratitude to my family, particularly my wife Jacqueline Staben for her support and encouragement over the years working on this thesis. Jacqui, without your support, encouragement and belief in me, which started when I was a TAFE student, this thesis would not have been written, I am forever grateful.

I would like to sincerely thank my supervisors Professor Arko Lucieer, Dr Peter Scarth, Dr Garry Cook and Dr Ken Evans. I am very grateful for the time you have all given me, I value the many discussions we have had. Thank you for expert guidance and advice and the many hours reading through the chapters in this thesis.

I would like to acknowledge the support of the Northern Territory Government. The satellite imagery used in this thesis was made available through a collaborative partnership between the Northern Territory Government's Department of Environment and Natural Resources and Queensland Governments, Department of Science, Information Technology, Innovation and the Arts, Remote Sensing Centre, I would like to thank all involved in this collaborative partnership. Field data used in this study were collected for a number of different projects between the years 2000 and 2018, I would like to thank the many people involved in the collection of these data.

The majority of the analysis undertaken in this thesis used open source programming languages, I would like to acknowledge and thank the open source community. I would like to thank Neil Flood for his advice and assistance in the use of the Python programming language.

I would also like to thank Nick Cuff and Peter Brocklehurst for sharing your knowledge of NT flora and veg mapping, our many discussions over the years have contributed to the development of the remote sensing products in this thesis.

TABLE OF CONTENTS

ABSTRACT	i
ACKNOWLEDGEMENTS	iv
LIST OF FIGURES	ix
LIST OF TABLES	xvii
1 Introduction	1
1.1 Background and rationale	1
1.2 Problem statement	6
1.3 Aim and objectives	7
1.4 Structure of the thesis	8
2 Obtaining biophysical measurements of woody vegetation from high resolution digital aerial photography in tropical and arid environments: Northern Territory, Australia.	9
2.1 Introduction	10
2.2 Methods	13
2.2.1 Study area	13
2.2.2 Aerial photography	14
2.2.3 Field data	15
2.2.4 Canopy biophysical parameters and aerial photography	19
2.2.5 Classification of aerial photographs	20
2.2.6 Segmentation	22
2.2.7 Classification	22
2.2.8 Classification method accuracy assessment	23
2.2.9 Stand basal area and aerial photography	24
2.2.10 Statistical analysis of relationship between field biophysical parameters and AP _{GWC}	24

2.3	Results	25
2.3.1	Classification accuracy assessment	25
2.3.2	Relationship between field biophysical parameters and AP _{GWC} . .	27
2.3.3	Comparison of the results between aerial photography captured at 15 cm and 30 cm GSD	30
2.3.4	Stand basal area	30
2.4	Discussion	32
2.5	Conclusion	38
3	Modelling LiDAR derived tree canopy height from Landsat TM, ETM+ and OLI satellite imagery:a machine learning approach.	40
3.1	Introduction	41
3.2	Data and Methods	44
3.2.1	Study Area	44
3.2.2	LiDAR Canopy Height Model	44
3.2.3	Satellite imagery	45
3.2.4	Training and Validation data	47
3.2.5	Random Forest Model Development	50
3.3	Results and discussion	53
3.3.1	Model Development Stage One: optimising number of trees	53
3.3.2	Model Development Stage Two: variable selection.	54
3.3.3	Model Development Stage Three: optimising number of variables.	55
3.3.4	Canopy height model	57
3.4	Conclusions	68
4	Broad-scale mapping of tree canopy structure using optical satellite sensors, Sentinel-2 MSI and Landsat-8 OLI.	70
4.1	Introduction	71
4.2	Data and Methods	73
4.2.1	Study Area	73
4.2.2	LiDAR	74
4.2.3	Sentinel-2 and Landsat satellite imagery	76
4.2.4	Model Training and Validation datasets	78

4.2.5	Model development	80
4.3	Results	81
4.3.1	Model development	81
4.4	Discussion	97
4.4.1	Important predictor variables	98
4.4.2	Scale effects	99
4.4.3	Structural metrics performance	100
4.4.4	Characterising tree canopy structural variability	101
4.5	Conclusion.	103
5	Remote sensing of structural dynamics of woody vegetation in north-ern Australia impacted by severe tropical cyclone Monica	105
5.1	Introduction	106
5.2	Data and Methods	108
5.2.1	Study area	109
5.2.2	Satellite imagery	110
5.2.3	Validation of Landsat canopy height product	113
5.2.4	Validation of the Landsat Woody FPC product	114
5.2.5	Correcting the bias in Landsat satellite estimates of foliage pro-jective cover.	116
5.2.6	Converting foliage projective cover to canopy cover	117
5.2.7	Structural classification	117
5.2.8	Time series Analysis.	118
5.3	Results	121
5.3.1	Woody FPC validation and bias corrections	121
5.3.2	Conversion of FPC to CC	123
5.3.3	Validation of tree height	125
5.3.4	Structural formation classes	126
5.3.5	Time series analysis - Cyclone Monica	127
5.4	Discussion	132
5.4.1	Development of the structural formation mapping product.	132
5.4.2	Assessment of Cyclone Monica	137
5.5	Conclusion	141

6	Conclusion	143
6.0.1	Chapter 2 - Obtaining biophysical measurements of woody vegetation from high resolution digital aerial photography in tropical and arid environments: Northern Territory, Australia	144
6.0.2	Chapter 3 - Modelling LiDAR derived tree canopy height from Landsat TM, ETM+ and OLI satellite imagery:a machine learning approach.	144
6.0.3	Chapter 4 - Broad-scale mapping of tree canopy structure using optical satellite sensors, Sentinel-2 MSI and Landsat-8 OLI	145
6.0.4	Chapter 5 - Investigating structural dynamics of woody vegetation in northern Australia impacted by severe tropical cyclone Monica, using remote sensing	146
6.0.5	Contributions to knowledge	147
6.0.6	Current operational use of the products developed in this thesis . .	149
6.0.7	Recommendations for future work	150
REFERENCES		152

Appendices

Appendix A	Supplementary material - Chapter 3	176
Appendix B	Supplementary material - Chapter 5	178
Appendix C	Supplementary material - Chapter 6	180

LIST OF FIGURES

2.1	Location of the study area Northern Territory (NT) Australia, major bioregions obtained from the Interim Biogeographic Regionalisation for Australia (IBRA) version 7 (http://www.environment.gov.au/land/nrs/science/ibra).	13
2.2	Example of four of the sites used in this study; 15 cm GSD aerial photograph (left) and corresponding field site photograph (right); (a) Mixed species Monsoon forest,(b) <i>Eucalyptus miniata</i> and <i>E. tetrodonta</i> woodland (c) <i>Acacia aneura</i> (Mulga) woodland and (d) Sparse Acacia shrubland.	16
2.3	(a) Location of all the field sites used in this study; (b) sites used to independently assess the relationship between digital aerial photography and predicted live SBA;(c) sites used to assess the relationship between tree canopy parameters and aerial photography GSD 15 cm; and (d) GSD 30 cm.	18
2.4	Example of the transect configuration of a 100 m × 100 m (1 ha) field site used to collect woody cover estimates, circles denote where tree basal area measurements were collected.	19
2.5	Example of the segmentation and classification of 15 cm digital aerial photography, showing that objects produced from the fine segmentation of the imagery which enable gaps in the tree canopy to be identified and classified.	21
2.6	Scatter plots showing the relationship between AP _{GWC} (x-axis) estimated from digital aerial photography captured at GSD 15 cm (a–e) and 30 cm (f–j) and field-measured U _{FPC} , UM _{FPC} , UMG _{FPC} , PPC and CC (y-axis), fitted line represents the 1:1 correspondence.	29

2.7	Scatter plot showing the relationship between AP _{GWC} derived from aerial photography captured at both 15 cm and 30 cm GSD for the same field site, fitted line represents the 1:1 correspondence.	31
2.8	Fitted line for the allometric relationship between field-measured UMG _{FPC} and live SBA m ² ha ⁻¹ ; the equation for the fitted line is shown in equ 2.1 and the best fit parameters are shown in Table 2.11	31
2.9	Scatter plot showing the predicted and observed live SBA estimates, plot (a) represents the 50 sites where live SBA was predicted from AP _{GWC} and plot (b) where live SBA was predicted from 44 field-measured UMG _{FPC}	32
2.10	Example of the seasonal differences in green woody vegetation captured in different date imagery (GSD 15 cm) for the same field site.	35
3.1	Location of the study area in Northern Territory of Australia.	45
3.2	Example of the canopy height model produced from the LiDAR data captured in 2009 (a) over Eucalyptus woodland (West) and transition to Mangrove forest (in the Eastern side of the figure), 15 cm digital aerial photography (b) shown for clarity.	46
3.3	Location of training and validation data within the extent of the LiDAR data.	50
3.4	Box plots showing the RMSE scores for the number of trees (n_estimator) in the random forest model, each box plot represents 100 iterations of the model where 10% of the training data is randomly selected to independently test each iteration of the model (dot = mean, box = 25 th and 75 th percentile, line = median, whiskers = show the range of the data). . .	54
3.5	Scatter plots showing the relationship between mean CHM and the 15 predictor variables identified in stage two of the development of the random forest model.	56
3.6	Mean R ² (a) and RMSE (b) values (based on 100 iterations) used to identify the number of predictor variables and the number of features used to grow the trees in the random forest model.	57

3.7 Random forest canopy height model applied to both (a) Landsat-5 TM (acquired 26/05/2009) and (b) Landsat-7 ETM+ (acquired 19/06/2009) imagery for path/row 106/68 to independently validate the accuracy of the model; black areas denote nodata values. Note, the region shown in this figure is the grey area shown in Figure 3.3.	58
3.8 Relative importance score for the 14 predictor variables used in the final random forest model.	59
3.9 Scatter plot showing the relationship between mean canopy height and the top four predictor variables, ratio of NIR and Green, GSAVI, SWIR1 reflectance and Red reflectance for three vegetation communities (Monsoon rainforest n= 759, Mangroves n= 1182, Eucalyptus n= 1159). Data points were subset from the training dataset within the extent of the 1:25,000 scale remnant vegetation mapping (Brock 1995).	60
3.10 Scatter plot showing the predicted and observed mean CHM for the validation region (a) Landsat-5 TM acquired 26/05/2009 (b) Landsat-7 ETM+ acquired 19/06/2009, solid line = 1:1 line.	61
3.11 Scatter plots showing the predicted CHM from Landsat-5 TM (26/05/2009) and Landsat-7 ETM+ (19/06/2009) for path/row p106r068 and the observed mean CHM (LiDAR, 03/07/2009) for broad vegetation communities located in the validation region; mapping by Brock (1995), solid line is the 1:1 line.	62
3.12 Scatter plots comparing mean canopy height estimates predicted from Landsat-5 TM, Landsat-7 ETM+ and Landsat-8 OLI in (a) 2009 (b) 2013 and (c) 2016, solid line is the 1:1 line and the dashed red line is the ridge regression. Statistics were only obtained from regions corresponding with valid Landsat-7 ETM+ pixels from the validation region for each year.	65
3.13 Canopy height estimates predicted from Landsat-5 TM, Landsat-7 ETM+ and Landsat-8 OLI for sites impacted by cyclone Tracy from 1987 to 2016 for a (a) mangrove forest, (b) monsoon rain forest, (c) Eucalyptus woodland with clearing and (d) Eucalyptus woodland.	67

3.14 Example of the damage to Eucalyptus communities (along McMillan's Road, Darwin) due to cyclone Tracy 25 th December 1974 and subsequent recovery and regrowth (a) photograph taken (by Roy Beames) 5 th July 1975 precise location on McMillan's Road unknown (b) photograph taken 27 th December 2016 at the location of time series Figure3.13 (d).	68
4.1 Location of the study area Northern Territory, Australia and the Sentinel-2 MSI and Landsat-8 OLI scenes used in this study.	74
4.2 Location of the LiDAR used in this study.	75
4.3 Example of the structural metrics derived from the LiDAR canopy height model resampled to 20 m spatial resolution.	77
4.4 Results of the variable reduction analysis showing the RMSE% and number of predictor variables for each structural metric predicted from Sentinel-2 (10 m, 20 m 30 m) and Landsat-8 imagery. Statistics were derived from five iterations of the model where 10% of the training data was selected (total n=74,000).	83
4.5 Example of the structural metrics applied to Sentinel-2 at 20 m spatial resolution, along with LiDAR canopy height (1 m) and very high resolution digital aerial photography.	85
4.6 Bar plots showing the predictor variables and relative importance score for each of the models predicting tree structure metrics from Sentinel-2 (10 m) imagery.	87
4.7 Violin plots showing summary statistics (mean, min, max) and the distribution of the observed (LiDAR derived) and predicted tree structure metrics from Sentinel-2 at spatial resolution 10 m for validation datasets Val01 and Val02.	88
4.8 Bar plots showing the predictor variables and relative importance score for each of the models predicting tree structure metrics from Sentinel-2 (20 m) imagery.	90

4.9	Violin plots showing summary statistics (mean, min, max) and the distribution of the observed (LiDAR derived) and predicted tree structure metrics from Sentinel-2 at spatial resolution 20 m for validation datasets Val01 and Val02.	91
4.10	Bar plots showing the predictor variables and relative importance score for each of the models predicting tree structure metrics from Sentinel-2 (30 m) imagery.	93
4.11	Violin plots showing summary statistics (mean, min, max) and the distribution of the observed (LiDAR derived) and predicted tree structure metrics from Sentinel-2 at spatial resolution 30 m for validation datasets Val01 and Val02.	94
4.12	Bar plots showing the predictor variables and relative importance score for each of the models predicting tree structure metrics from Landsat-8 (30 m) imagery.	96
4.13	Violin plots showing summary statistics (mean, min, max) and the distribution of the observed (LiDAR derived) and predicted tree structure metrics from Landsat-8 at spatial resolution 30 m for validation datasets Val01 and Val02.	97
4.14	Estimates of forest 99 th percentile canopy height (H_{99}) derived from 2018 Sentinel-2 satellite imagery at 10 m spatial resolution for the northern half of the Northern Territory.	98
4.15	Example of the misregistration errors between the LiDAR canopy height model and the 10 m Sentinel-2 pixels and the influence of different spatial resolutions in absorbing this error. All Sentinel-2 imagery displayed in the NIR, Red and Green spectral bands.	100
4.16	Differences in the level of mapping detail due to scale effects for the H_{99} Sentinel-2 at 10 m and Landsat-8 30 m spatial resolution.	101
4.17	Estimates of tree canopy structure (H_{99} , H_{mean} and H_{cov}) displayed as a three band composite (Red = H_{99} , Blue = H_{mean} and Green = H_{cov}) , derived from 2018 Sentinel-2 satellite imagery at 10 m spatial resolution for the northern half of the Northern Territory.	102

4.18 Example of tree canopy structure metrics displayed as a three band composite (a), H_{99} (b), H_{mean} (c) and H_{cov} (d) estimated from Sentinel-2 at 10 m spatial resolution. The 15 cm digital aerial photograph (e) was captured in 2018.	103
5.1 Schematic showing the work flow used to produce the Landsat tree structure mapping product.	108
5.2 Location of the study area in the Northern Territory, Australia (a) along with the track for cyclone Monica (BOM 2019), locations of the field sites used in this study and broad-scale vegetation structure (NVIS 1M) (b). The region used to assess the impact of cyclone Monica is also shown (c) and field sites at Narbarlek mine lease (d) and Gulungul Creek Catchment adjacent the town of Jabiru (e).	111
5.3 Location of the digital aerial photographs and LiDAR used to validate the woody FPC and canopy height estimates from Landsat imagery.	116
5.4 Graphical representations of the change detection analysis undertaken for each pixel over a 30 year period for (a) Eucalyptus Open forest and (b) Mangrove forest. Each of the 21 structural classes are shown on the y axis and year on the x axis. The circles represents the classification assigned to the pixel for each year and the squares represent the long term classification based on the mode. The light grey area represents the range of classes considered to be substantially different from the long term class which is identified as change, whereas the dark grey regions represent no change.	120
5.5 Example of the digital aerial photograph (2013) and the woody green class, with the 90x90 m grid overlay.	121
5.6 (a) Scatter plots showing the predicted (woody FPC from single date Landsat TM, ETM+ and OLI) and observed (aerial photo derived FPC) for sites located across the Northern Territory between the years 2008 and 2018 and (b) the non-linear fitted line used to correct the bias in Landsat woody FPC estimates.	122

5.7 Scatter plots showing the relationship between woody FPC estimates obtained from digital aerial photography and single date Landsat satellite imagery for (a) uncorrected and (b) bias corrected data. The black line represents the 1:1 line.	123
5.8 Scatter plots showing the predicted and observed CC estimates obtained from Landsat seasonal composites and field sites across the study area for the years 2000, 2016, 2017 and 2018. The black line represents the 1:1 line and the grey dashed lines represent the CC cover class ranges used in this study.	124
5.9 Scatter plots showing the predicted and observed CC estimates obtained from Landsat seasonal composites and field sites ($30\text{ m} \times 30\text{ m}$) impacted by cyclone Monica (a) 2005 and (b) 2006. The black line represents the 1:1 line. The location of the field sites is shown in Figure 5.2	124
5.10 Scatter plot showing the predicted (Landsat satellite seasonal composite) and observed (LiDAR) results for the validation of the canopy height metric H_{99} . The black line represents the 1:1 line and the grey dashed lines represent the height class ranges used in this study.	125
5.11 Scatter plots showing the predicted and observed tree canopy height (H_{99}) estimates obtained from Landsat seasonal composites and field sites ($30\text{ m} \times 30\text{ m}$) impacted by cyclone Monica (a) 2005 and (b) 2006. The black line represents the 1:1 line. The location of the field sites is shown in Figure 5.2	126
5.12 Structural formation classification for the year 2017 across the study area (Landsat path/rows: 106/68-72, 105/68-72, 104/68-72, 103/68-72, 102/68-72, 101/71-72).	127
5.13 The percentage area covered for each of the structural formation classes for the 2017 mapping shown in Fig 5.12.	127
5.14 Maps showing the extent of change in canopy cover and tree canopy height between 2005 and 2006 for the top-end of the Northern Territory.	128
5.15 Structural formation maps for the years 2005, 2006 and 2017 over the region impacted by severe tropical cyclone Monica.	130

5.16	Summary of the change detection analysis undertaken post severe tropical Cyclone Monica. The initial pixels ($30 \times 30 m$ area) identified as significant change are shown for 2006 along with the total number of times these pixels have been classified as a structure class below the long term structural class recorded in 2005 (pre Cyclone Monica).	131
5.17	Annual estimates of total area identified as severely impacted by Cyclone Monica in 2006 and the subsequent years until 2017 for the regions shown in Fig 5.16.	131
5.18	Time series plot showing the percentage area covered by six major structural formation classes for the years 2004 to 2017 over the region impacted by cyclone Monica (Extent shown in Fig 5.16).	132
5.19	Scatter plots showing the predicted and observed CC estimates obtained from Landsat single dates imagery and digital aerial photography across the study area for the years 2008-2018. The black line represents the 1:1 line and the grey dashed lines represent the CC cover class ranges used in this study.	134
5.20	Example of the (a) Structural formation classification for 2017 and (b) the structural formation classification produced from three years of data 2015, 2016 and 2017.	137
5.21	Example the disturbance/recovery mapping product and an area estimated as not recovered, in 2017. The digital aerial photography was captured in August 2013 and the damage is still evident. This site is located at Lat -12.226310 Long 133.287477 and in 2015 the damage is still evident in high resolution satellite imagery in Google Earth.	140
B.1	Decision matrix showing the conditions used to identify change (loss) between structural formation classes.	178
B.2	Bar graph detailing the coverage (km^2) of each structural formation class for the years 2004 to 2017 over the region impacted by Cyclone Monica (Extent shown in Fig 5.16).	179
C.1	Example of the structural classification mapping product showing the impact of two cyclone's, Lam and Nathan which impacted the Arnhem Land region in 2015.	180

LIST OF TABLES

2.1	Summary of the field sites used to investigate the relationship between tree biophysical parameters and 15 cm and 30 cm GSD aerial photographs, field sites are grouped into broad structural classes based on the National Vegetation Information System (Brocklehurst et al. 2007).	20
2.2	Summary statistics for the number of days between the field and image capture dates for the 15 cm GSD aerial photography.	20
2.3	Summary statistics for the number of days between the field and image capture dates for the 30 cm GSD aerial photography.	20
2.4	Example of the summary statistic for objects derived in the segmentation process and the number of objects used for the training of each class for sites shown in Figure 2.2. The letter in brackets in the site column corresponds to the 15 cm aerial photograph shown in Figure 2.2 and for two sites (a) and (b) where both GSD were captured the summary statistics for 30 cm imagery are also shown.	22
2.5	Accuracy of the 15 aerial photographs 15 cm (GSD) randomly selected to assess the object based classification, along with the NVIS structural class, broad climatic zone and dominant vegetation species taken from the field data.	26
2.6	Accuracy of the 15 aerial photographs 30 cm (GSD) randomly selected to assess the object based classification, along with the NVIS structural class, broad climatic zone and dominant vegetation species taken from the field data.	26
2.7	Error matrix showing the accuracy assessment results for the classification of 15 cm GSD digital aerial photography (n = 15 sites).	27
2.8	Error matrix showing the accuracy assessment results for the classification of 30 cm GSD digital aerial photography (n = 15 sites).	27

2.9	Results of assessment of the relationship between AP_{GWC} estimated from 15 cm digital aerial photography and field woody cover estimates (U_{FPC} , UM_{FPC} , UMG_{FPC} , PPC and CC).	28
2.10	Results of assessment of the relationship between AP_{GWC} estimated from 30 cm digital aerial photography and field woody cover estimates (U_{FPC} , UM_{FPC} , UMG_{FPC} , PPC and CC).	28
2.11	Best fit parameters for the allometric equation and summary statistics for live SBA predicted from field UMG_{FPC} and aerial derived AP_{GWC} using the allometric relationship developed between coincident field-measured live tree SBA (m^2ha^{-1}) and UMG_{FPC} (%).	32
3.1	Landsat-5 TM and 7 ETM+ imagery used in the development* and validation of the canopy height model.	47
3.2	Vegetation indices and band ratios used in this study.	48
3.3	Results for the predictor variable importance scores (Model development Stage One) for 512 decision trees (n_estimator).	55
4.1	Details of the LiDAR surveys used in this study	75
4.2	Details of the canopy height structural metrics derived from the 1 m canopy height models used in this study	76
4.3	Summary of the spectral bands for Sentinel-2 (MSI) and Landsat-8 (OLI) used in this study.	78
4.4	Vegetation indices used in this study (*denotes indices only applied to Sentinel-2.)	79
4.5	Number of variables used for each of the candidate models predicting tree structure metrics from Sentinel-2 (10 m, 20 m, 30 m) and Landsat-8 (30 m) imagery. The accuracy statistics are based on five iterations of the random forest model during the variable reduction analysis. For each iteration 10% of the training data were selected (n=74,000).	84
4.6	Model accuracy statistics for tree structure metrics derived from Sentinel-2 imagery at 10 m spatial resolution for validation dataset Val01 (n=37,000) and Val02 (n=29,811).	88

4.7	Model accuracy statistics for tree structure metrics derived from Sentinel-2 imagery at 20 m spatial resolution for validation dataset Val01 (n=37,000) and Val02 (n=29,922).	91
4.8	Model accuracy statistics for tree structure metrics derived from Sentinel-2 imagery at 30 m spatial resolution for validation dataset Val01 (n=37,000) and Val02 (n=29,864).	94
4.9	Model accuracy statistics for tree structure metrics derived from Landsat-8 imagery at 30 m spatial resolution for validation dataset Val01 (n=37,000) and Val02 (n=29,727).	97
5.1	Eleven status codes describing the level of impact of cyclone Monica on each tree ≥ 2 m in height.	113
5.2	Description of the classes used in the development of the digital aerial photography random forest classifier	115
5.3	Description of the structural formation classes used in this study, canopy cover classes are based on the NVIS/Walker and Hopkins scheme and the height classes have been adapted from Walker and Hopkins/NVIS scheme taking into account the measurement error in the Landsat derived CC and canopy height products and structural characteristic of woody vegetation in the study area.	118
5.4	Error matrix for the aerial photo classification	122
A.1	Details of the Landsat imagery used in the production of the time series plots.	176

CHAPTER 1

Introduction

1.1 Background and rationale

Globally, natural environments are under increased pressure from both natural and anthropogenic threats (Alleaume et al. 2018). Population growth is resulting in changes in land-use and land-cover which is putting pressure on natural ecosystems (Marques et al. 2019). Invasive species, habitat loss and changes in climate are all factors threatening global biodiversity (McGeoch et al. 2010, Smale et al. 2019). Tropical cyclones (also known as typhoons and hurricanes) are weather systems that develop in oceanic basins north and south of the equator, which have the potential to impact both man-made and natural environments (Lin et al. 2020, Pruitt et al. 2019, Noy 2016, Chi et al. 2015, de Gouvenain and Silander 2003). The destructive winds associated with tropical cyclones represent a natural disturbance agent that influences ecosystem structure and function at a local (Lewis and Bannar-Martin 2012) and global scale (Lin et al. 2020, Pruitt et al. 2019). For example, hurricane Katrina impacted the southeast United States in 2005 and it was estimated that 8300 km² of national forests were affected (Wang, Qu, Hao, Liu and Stanturf 2010) with approximately 320 million trees killed or damaged, representing a loss of 105 Tg of carbon equivalent to the annual terrestrial carbon sink of all United States forests (Chambers et al. 2007). The destructive winds of hurricane Hugo impacted northeast Puerto Rico in 1989, resulting in a 50 percent reduction in above ground biomass (at the Luquillo Experimental Forest). After 15 years, biomass had recovered along with increased species richness and stem densities when compared to pre-hurricane levels (Heartsill Scalley et al. 2010). Lewis and Bannar-Martin (2012) reported that the impact of cyclone Fanele (2009) on the dry deciduous forests of western Madagascar were likely to have long-term impacts on both flora and fauna in the region, however the full impact could only be determined with long-term monitoring. While tropical cyclones can have a significant impact on ecosystem function at a range of scales, Lin et al. (2020) contended that most of our ecological understanding (between 1989 and 2018) was gained from studies looking at cyclones in the North Atlantic Basin. They suggested that this gap is likely to have resulted in a bias in the global understanding of the impact of these storm events on ecosystem function (Lin

et al. 2020). Between 1989 and 2018 they reported that despite having 22 percent of cyclone activity globally, only 5 percent of studies were focused in the Indian Ocean Basin (Lin et al. 2020).

Tropical cyclones frequently occur across the northern Australian coastline. The impact of cyclonic winds are greatest on the coastal regions, however they also have the potential to cause significant disturbance further inland (Cook and Goyens 2008, Staben and Evans 2008). A number of studies have reported on the impact of cyclones on vegetation in the northern territory using a variety of techniques including field surveys (ground and aerial based) (Stocker 1976, Fox 1980, Cameron et al. 1983, Bowman and Panton 1994a, Cook and Goyens 2008, Woolley et al. 2018, Russell-Smith et al. 2019), aerial photography and satellite imagery (Staben and Evans 2008, Williamson et al. 2011, Hutley et al. 2013). These studies have largely focused on two severe tropical cyclones, cyclone Tracy which impacted the city of Darwin on the 25th of December 1974 and cyclone Monica which impacted the Arnhemland and Kakadu National Park region on the 24th of April 2006. Severe localised windstorms can also have an impact on woody vegetation resulting in significant tree damage (Williams and Douglas 1995, Franklin et al. 2010). Franklin et al. (2010) investigated the re-sprouting response of savanna trees after a tornado caused severe damage along a path estimated to be 3 km long by 300 m wide. Although cyclones are frequent and have the potential to be a major disturbance agent in ecosystems across the Northern Territory (Murphy 1984), very few studies have been undertaken to quantify the impact and potential role they play in driving the structure of these communities at a regional or continental (northern Australia) scale. While it is well recognised that fire and the stress of the seasonal drought, a characteristic of the wet-dry tropics of northern Australia, are frequent disturbance factors on vegetation communities very little focus has been given to the impact cyclones and storms have on these ecosystems (Cook and Goyens 2008, Hutley et al. 2013).

Biodiversity in northern Australia is under threat from, invasive species (flora and fauna), changes in fire regimes and climate (Davies et al. 2018, Woolley et al. 2018, Duke et al. 2017, Setterfield et al. 2010, Edwards and Russell-Smith 2009, Cook and Goyens 2008). Across the northern half of the Northern Territory there are a substantial number of endemic flora and fauna species which are both nationally and internationally significant (Woinarski et al. 2006, Allen et al. 2019). The development of long-term monitoring programs using information collected in a consistent and frequent manner has been identified as a way to help gain insight into the drivers of the change being observed (Lindenmayer et al. 2012, 2015). Tropical cyclones have the potential to alter the structure of natural ecosystem and while there has been a focus on the impact

of tropical cyclones in the wet tropics (Turton 2012), little attention has been given to the savannas of the wet-dry tropics as this region (globally) is largely not affected by tropical cyclones (Cook and Goyens 2008). Understanding the dynamics of tropical savannas is important globally, as these ecosystems play an important role in the global carbon cycle, contributing to approximately 30 % of the terrestrial net primary production (Murphy et al. 2010). Understanding change in woody vegetation structure is also important for biodiversity conservation management (Levick et al. 2019). Disturbance from cyclone and fire was found to be related to the availability of tree hollows, which are important habitat for many declining fauna species (Woolley et al. 2018). Understanding both the spatial and temporal distribution of the impact of cyclones on the structure of woody vegetation is important as it has the potential to increases the accuracy of carbon stock estimates (Cook et al. 2015, O'Grady et al. 2000, Hutley et al. 2013) and assist in identifying the location of large hollow-bearing trees, which are a keystone habitat in northern Australia for many fauna species (Woolley et al. 2018). There has been a substantial effort in monitoring landscape change (woody cover) in vegetation communities in the Alligator Rivers Region of the Northern Territory (Banfai and Bowman 2006, Bowman and Dingle 2006, Banfai and Bowman 2007, Lehmann et al. 2008, 2009, Bowman et al. 2010). These studies used manual interpretation techniques of aerial photography spanning a 40 year period (1964, 1984, 1991 and 2004) to measure changes in woody cover, and in general reported a trend in woody expansion and densification (Williamson et al. 2011). These studies also looked at a range of possible drivers responsible for the changes, which included increased rainfall, changes in feral animal populations, increased CO₂ levels and changes in fire regimes. Notably the effects of wind as a disturbance factor were largely not considered as a possible contributor to the changes they observed. Williamson et al. (2011) investigated the changes in vegetation of three swamps in the Darwin region covering an area of 30 km² which was severely impacted by cyclone Tracy and found that there was a 16.2 % increase in mangrove above the pre-cyclone distribution. They suggested that changes in sea level, changes in local hydrology and elevated CO₂ concentrations represent plausible reason for the increase in mangrove extent. While no definitive reason could be given for the changes observed in the suite of studies (Bowman and Dingle 2006, Lehmann et al. 2008, 2009, Bowman et al. 2010), it was suggested that research at a regional scale may help to gain a better understanding of the factors influencing the changes observed (Williamson et al. 2011). Hutley et al. (2013) used empirical models developed by Cook and Goyens (2008) to estimate the severity of tree damage and satellite imagery (moderate resolution imaging spectroradiometer (MODIS)) to assess gross primary productivity (GPP) and fire frequency post cyclone Monica. They found that GPP was suppressed for four years after cyclone Monica and that the increased fuel loads from destruction of the tree canopy did not dramatically shift fire regimes, however

there was evidence that fires were more frequent in areas with high levels of damage. The increased on-ground fuel loads as a result of cyclone Monica had the potential to represent $\approx 10\%$ of Australia's accountable green house emissions however, they concluded that the carbon balance is likely to be dominated by fire and termite consumption rather than infrequent extreme disturbance events such as cyclone Monica. Hutley et al. (2013) suggested that tracking recovery of highly damaged areas, monitoring fuel consumption and the rate of return of woody vegetation is required to gain a better understanding of cyclone disturbance and the impact it has on savanna structure and function (Hutley et al. 2013). It is clear from the level of disturbance a cyclone can have on a savanna ecosystems there is a need to gain a better understanding of their influence at a regional scale. Cook and Goyens (2008) proposed that to understand the role of tropical cyclones in the dynamics of the savanna ecosystems of northern Australia will require the knowledge of “(i) their immediate impacts; (ii) subsequent recovery processes and especially any interaction with fires; (iii) effects on landscape processes; and (iv) the probability of recurrence”

There is a clear need to produce information on vegetation structure that enables assessment of the impact of cyclones at appropriate spatial and temporal scales. Remote sensing provides the opportunity to objectively assess the landscape at a regional scale (Wallace et al. 2006, Karfs et al. 2009). The spectral and spatial resolution of the Landsat imagery combined with its temporal record make it valuable for monitoring woody cover change across large regions (Woodcock et al. 2001, Danaher et al. 2004, Gill et al. 2017). The development of regional or continental scale remote sensing monitoring programs has become feasible due to the open source policies of the United States Geological Survey (USGS) Landsat program and (more recently) the European Space Agency (ESA) Sentinel-2 satellite program (Wulder, Masek, Cohen, Loveland and Woodcock 2012). Remote sensing technology is particularly suited to the Northern Territory, due to the low population density, harsh climate and vast areas (Hill and Carter 1999, Staben and Evans 2008, Whiteside et al. 2011). The Northern Territory Government (NTG) is currently implementing a remote sensing monitoring program based on the Landsat and Sentinel-2 sensors. The development of the remote sensing programs is being undertaken under a partnership between the Northern Territory, Department of Environment and Natural Resources (DENR) and the Remote Sensing Centre (RSC) of the Queensland Government's Department of Environment and Science (DES). The aim of the remote sensing monitoring programs are to use quantitative information derived from both the historical archive and current Landsat and Sentinel-2 imagery to monitor and assess land cover change/condition across the Northern Territory.

To obtain quantitative information from optical satellite data relationships between bio-

physical variables need to be established (Moulin et al. 1998). Numerous studies have derived empirical relationships between satellite imagery and field-based measurements such as leaf area index (LAI) (Coops et al. 1997, Eriksson et al. 2006), above ground biomass of woody vegetation (Foody et al. 2003, Powell et al. 2010, Avitabile et al. 2012), fractional cover (Scarth et al. 2010), woody vegetation foliage projective cover (Danaher et al. 2004, Armston et al. 2009) and tree height (Hudak et al. 2002, Pascual et al. 2010, Hill et al. 2011, Ota et al. 2014, Ahmed et al. 2015, Lang et al. 2019). Currently the NTG is using fractional cover products developed by Scarth et al. (2010) that have been calibrated using field data captured across Australia, including the NT. These fractional cover products have been produced from both Landsat and Sentinel-2 satellite sensors, which are being used to monitor the pastoral estate and mangroves in Darwin Harbour (Staben et al. 2019). Estimates of woody FPC, which provide information on the horizontal structure of woody vegetation, are also routinely produced for all Landsat imagery captured across the Northern Territory. These estimates of woody FPC were produced using a multiple linear regression model developed from field data, collected in the state of Queensland (QLD), Australia (Armston et al. 2009). These Landsat based woody FPC products are used by the Queensland Government for the Statewide Land-cover and Trees Study (SLATS). As this woody FPC product was developed using field data collected in the state of Queensland, assessment of the accuracy of the woody FPC product needs to be undertaken to enable them to be used with confidence in the NT. Field data is typically used to assess the accuracy of remote sensing models. The collection of sufficient number of field sites to validate remote sensing products such as Landsat at a regional scale can be inhibited by both financial cost and logistical constraints (Laliberte et al. 2010, Armston et al. 2013). In addition to these constraints, assessment of the models applied to historical imagery needs to be compared to biophysical parameters measured at the time of the image capture. Aerial photography has been used to derive biophysical parameters to calibrate Landsat satellite imagery (Xu et al. 2003, Pu et al. 2003, Carreiras et al. 2006, Samani Majd et al. 2013), and provides the level of detail enabling it to be used as a surrogate for the collection of ground data (Mannel et al. 2006).

While a number of products currently exist that have the potential to be used to quantify horizontal structure of woody vegetation, the availability of products to assess the vertical structure, identified as a key parameter for inferring long term trends in biomass and carbon stock (Skidmore et al. 2015, Cook et al. 2015) is limited. Light detection and ranging (LiDAR) data is an efficient way to map and quantify woody vegetation structure (Lim et al. 2003, Wulder, White, Nelson, Næsset, Ørka, Coops, Hilker, Bater and Gobakken 2012, Goldbergs et al. 2018), however, the use of these data at a regional level can be prohibitive due financial constraints (Pascual et al. 2010). In addition to the

financial constraints, availability of LiDAR for long-term studies (multiple decades) is limited due to the paucity of data. A number of studies have used LiDAR data to develop predictive models, which have enabled estimates of vertical structure from Landsat (Hudak et al. 2002, Pascual et al. 2010, Hill et al. 2011, Ota et al. 2014, Ahmed et al. 2015, Matasci et al. 2018) and Sentinel (Lang et al. 2019) sensors with an aim to enhance the spatial and temporal coverage.

1.2 Problem statement

It is well known that tropical cyclones and windstorm can have a significant impact on native vegetation, however, very little is known about how these weather events influence the structural dynamics of woody vegetation across northern Australia (Cook and Goyens 2008, Turton 2012, Hutley et al. 2013). On average 11 tropical cyclones (based on data between 1981/1982 to 2012/2013 wet season) affect the Australian continent per year (Dowdy 2014). Numerous studies over the years have looked at the impact of cyclones on natural vegetation across northern Australia (Webb 1958, Grove et al. 2000, Nott 2006, Cook and Goyens 2008, Paling et al. 2008, Turton 2012, Hutley et al. 2013, Asbridge et al. 2018), however, given the number of cyclones that have impacted the Northern Territory (<http://www.bom.gov.au/cyclone/tropical-cyclone-knowledge-centre/history/tracks/>) there has been relatively little focus on the impact of these events in the Northern Territory (Turton 2008). Furthermore, there is very little to no information identifying the spatial extent of these disturbance events or any subsequent recovery.

A number of studies have looked at the dynamics of woody vegetation in the Northern Territory using a variety of methods including aerial photography and field surveys (Banfai and Bowman 2006, Bowman and Dingle 2006, Banfai and Bowman 2007, Lehmann et al. 2008, 2009, Bowman et al. 2010, Murphy et al. 2010, Williamson et al. 2011, Murphy et al. 2014). While these studies provide detailed information on the dynamics of woody vegetation over multiple decades and large areas (Murphy et al. 2010, 2014), in the Northern Territory context these studies cover relatively small geographical extents. With the availability of the Landsat and Sentinel-2 satellite image archives there is the potential to identify and quantify woody dynamics over much larger geographic areas, providing important information for natural resource management.

While a number of products have been developed that enable assessment of horizontal woody vegetation structure at a regional and Continental scale over a 30 year period (Armston et al. 2009, Scarth et al. 2010, Gill et al. 2017), the availability of products that enable assessment of vertical structure are limited. Information on vertical structure is important for the assessment of cyclone or windstorm damage to woody vegetation,

as generally larger trees are impacted (Williams and Douglas 1995, Cook and Goyens 2008), resulting in an initial loss of taller trees with larger canopies. Understanding change in woody vegetation structure is important for biodiversity conservation management (Levick et al. 2019). Disturbance from cyclones and fire have been found to be related to the availability of tree hollows, important keystone habitat for many declining fauna species in northern Australia for many fauna species (Woolley et al. 2018). Remote sensing products have the potential to provide new insights into the dynamics of vegetation structure and the role disturbance factors such as cyclones have on savanna ecosystems. The initial assessment of the damage using horizontal structure (Woody FPC or canopy cover) is likely to reflect the change, however it is possible that post the cyclone event, rapid regrowth of low woody vegetation may result in similar or higher levels of canopy cover being recorded by the satellite sensor. While the changes in the horizontal structure may reflect the woody cover on the ground, these changes may obscure the actual change in vertical structure, which has significant implications for identifying or characterising the longer term impacts of cyclones on natural ecosystems. It is also important to validate remote sensing models as this gives the users of the information confidence and enables the limitations to be taken into account when applying these data to change detection or vegetation mapping applications. While field data can be obtained to assess models derived from contemporary/current satellite imagery, assessment using field data can be prohibitive due the high costs and logistical constraints and often historic field data are not available.

1.3 Aim and objectives

The focus of this thesis is the development of remote sensing methods that enable the assessment of the structural dynamics of woody vegetation in response to storms and tropical cyclones. The key research objectives used to achieve the overall aim of the thesis were;

1. Development of methodology that enables the utility of very high resolution digital aerial photography to obtain woody vegetation biophysical parameters for use as a surrogate for the collection of field data.
2. Development of methodology to predict tree canopy height across a range of vegetation communities in the wet-dry tropics of northern Australia using Landsat-5 TM satellite sensor.
3. Investigate the utility of optical satellite imagery, Sentinel-2 MSI and Landsat-8 OLI for predicting tree canopy structure. This objective build onto objective 2 and develops models predicting seven tree canopy structure metrics at range of spatial scales to produce annual forest structure maps across northern Australia.

4. Develop an annual mapping product, detailing the spatial and temporal distribution of woody vegetation structure between the years 1988 and 2017 using the Landsat suite of sensors; and investigate the impact of severe tropical cyclone Monica (2006) and the assessment of subsequent recovery of woody vegetation over a 12 year period.

1.4 Structure of the thesis

This thesis consist of six chapters, with chapters 2-5 representing original research with the aim to fulfill the requirements of a thesis by publications. Chapters 2 and 3 have been published in the peer-review-journal "International Journal of Applied Earth Observation and Geoinformation".

The first three chapters of this thesis focus on the development of remote sensing products. In chapter 2 the relationship between estimates of woody FPC obtained from both field data and digital aerial photography is investigated and quantified. This provides a method to use digital aerial photography to validate historical satellite imagery predicting woody FPC. In chapter 3, a methodology is developed to predict tree canopy height (vertical structure) from single date Landsat satellite sensor. In chapter 4, further work is undertaken to refine and develop more robust models predicting annual estimates of tree canopy structure at a range of spatial scales using Sentinel-2 at (1 0m, 20 m 30 m) and Landsat-8 (3 0m). In chapter 5, the work undertaken in chapters 2, 3 and 4 is used to produce an annual mapping product detailing vegetation structure, based on woody FPC and tree canopy height derived from Landsat sensors over three decades. Change detection analysis is used to describe and quantify the impact of cyclones on woody vegetation structure using severe tropical cyclone Monica as a case study. Chapter 6 provides an synthesis and conclusion for the overall thesis. Chapter 6 also includes a discussion of the limitations and current operational use (by the Northern Territory Government) of the remote sensing products and methodologies developed in this thesis, and makes recommendations for future work.

CHAPTER 2

Obtaining biophysical measurements of woody vegetation from high resolution digital aerial photography in tropical and arid environments: Northern Territory, Australia.

Thesis context: The aim of this chapter is to assess the suitability of digital aerial photography to quantify woody vegetation biophysical parameters. The results of this study showed that estimates of woody foliage projective cover (FPC) were able to be obtained from digital aerial photography, enabling them to be used to validate and calibrate Landsat derived estimates of woody FPC, demonstrated in chapter 5 of this thesis. This chapter has been published in the "International Journal of Applied Earth Observation and Geoinformation".

Staben, G., Lucieer, A., Evans, K., Scarth, P. and Cook, G. (2016), 'Obtaining biophysical measurements of woody vegetation from high resolution digital aerial photography in tropical and arid environments: Northern Territory, Australia', International Journal of Applied Earth Observation and Geoinformation 52, 204–220. <http://linkinghub.elsevier.com/retrieve/pii/S0303243416300939>

Abstract

Biophysical parameters obtained from woody vegetation are commonly measured using field based techniques which require significant investment in resources. Quantitative measurements of woody vegetation provide important information for ecological studies investigating landscape change. The fine spatial resolution of aerial photography enables identification of features such as trees and shrubs. Improvements in spatial and spectral resolution of digital aerial photographic sensors have increased the possibility of using these data in quantitative remote sensing. Obtaining biophysical measurements from aerial photography has the potential to enable it to be used as a surrogate for the collection of field data. In this study, quantitative measurements obtained from digital aerial photography captured at ground sampling distance (GSD) of 15 cm ($n = 50$) and 30 cm ($n = 52$) were compared to woody biophysical parameters measured from 1 ha field plots. Supervised classification of the aerial photography using object based image analysis was used to quantify woody and non-woody vegetation components in the imagery. There was a high correlation ($r \geq 0.92$) between all field measured woody

canopy parameters (Foliage projective cover, Plant projective cover and Canopy cover) and aerial derived green woody cover measurements, however only foliage projective cover (FPC) was found to be statistically significant (paired t-test; $\alpha= 0.01$). There was no significant difference between measurements derived from imagery captured at either GSD of 15 cm and 30 cm over the same field site($n = 20$). Live stand basal area (SBA) (m^2ha^{-1}) was predicted from the aerial photographs by applying an allometric equation developed between field-measured live SBA and woody FPC. The results show that there was very little difference between live SBA predicted from FPC measured in the field or from aerial photography (R^2 , 0.88). The results of this study show that accurate woody biophysical parameters can be obtained from aerial photography from a range of woody vegetation communities across the Northern Territory.

2.1 Introduction

Biophysical parameters obtained from woody vegetation such as stand basal area, canopy cover and foliage projective cover are important information for studies investigating landscape change (Armston et al. 2013, Clewley et al. 2012). These attributes are commonly measured in the field and have been used extensively in ecological studies (Cook et al. 2005, Williams et al. 1997), for forest inventories (Wulder et al. 2008), and monitoring mine rehabilitation (Ludwig et al. 2003). A number of studies have shown that biophysical parameters from woody vegetation can be derived from aerial photography with reasonable levels of accuracy (Sharp and Bowman 2004, Fensham and Fairfax 2007, Fensham et al. 2007, Browning et al. 2009, Laliberte et al. 2010). Aerial photography represents one of the earliest forms of remote sensing and its use has been diverse (Campbell 1996), ranging from military reconnaissance, infrastructure mapping, natural disaster management and ecosystem monitoring. It has been used in a wide range of environmental studies, with applications ranging from invasive weed mapping (Robinson et al. 2008, Dorigo et al. 2012), rangeland mapping and assessment (Laliberte et al. 2010, Browning et al. 2009, Foran and Cellier 1980), forestry management (Coggins et al. 2008, Wulder, White, Coggins, Ortlepp, Coops, Heath and Mora 2012) and vegetation community mapping (Harvey and Hill 2001, Lucas et al. 2002, Lewis et al. 2013). The spatial resolution and historical record of aerial photography provide an important resource for landscape investigations (Morgan et al. 2010, Fensham et al. 2002). The fine spatial resolution(< 1 m ground sampling distance) of aerial photography enables features within the landscape, such as trees and shrubs to be identified (Morgan et al. 2010). It is also used as a source of information to produce calibration and validation data for use with coarser spatial resolution satellite imagery such as Landsat suite of sensors (Mellor et al. 2013, Wulder, White, Coggins, Ortlepp, Coops, Heath and Mora 2012, Pu et al. 2003, Xu et al. 2003, Congalton and Green 2009, Coops et al. 1997).

The development of digital sensors has led to a marked improvement in the spatial and spectral resolution of aerial photographic imagery (Rosso et al. 2008, Wulder, White, Coggins, Ortlepp, Coops, Heath and Mora 2012). These improvements have increased the potential use of these data for quantitative remote sensing (Laliberte et al. 2010). Coggins et al. (2008) used 10 cm ground sampling distance (GSD) digital aerial photography to extract individual tree canopy cover in forest in the Canadian Rocky Mountains. These canopy cover measurements were then related to field measured tree canopy cover and stem diameter to estimate stocking density. There was a significant correlation between estimates derived from the aerial photography and field data to enable them to be used as inputs into a model to predict the potential impacts of mountain pine beetle on these forest stands (Coggins et al. 2008, Wulder, White, Coggins, Ortlepp, Coops, Heath and Mora 2012). Laliberte et al. (2010) used ultra-high resolution digital aerial photography (4 cm GSD) to estimate percent cover of vegetation and bare ground for a range of vegetation communities in rangelands in south-western USA. They reported high correlations between shrub, grasses and non-vegetated surfaces derived from imagery and field-based measures (Laliberte et al. 2010). One of the motivating factors for their study was to develop reliable methods which enabled the assessment of plots at an equivalent scale and detail to field-based sampling measurements, over extensive and often remote areas (Laliberte et al. 2010).

Remote sensing technology is particularly suited to the Northern Territory, due to the low population density, harsh climate and vast areas (Hill and Carter 1999, Whiteside et al. 2011). The Northern Territory Government (NTG) is currently implementing a remote sensing monitoring program based on the Landsat suite of sensors. The temporal and spatial scales of these data has the potential to enable objective assessment of the landscape at a regional scale (Wallace et al. 2006, Karfs et al. 2009). The aim of this remote sensing program is to use quantitative information derived from both the historical archive and current Landsat imagery to monitor and assess land cover across the entire Northern Territory. This requires the development and assessment of models to predict biophysical parameters (e.g. woody cover estimates and fractional ground cover) from the suite of Landsat sensors. Studies that use coarser spatial resolution satellite imagery, such as Landsat (30 m GSD), to estimate biophysical parameters often develop predictive models by relating field measured data to the satellite imagery (Armston et al. 2009, Scarth et al. 2010). To enable these models to be developed, a sufficient quantity of field data covering the range of variability across the landscape is required. The collection of an adequate number of field sites to calibrate and validate products derived from sensors such as Landsat at a regional scale can be inhibited by both financial cost and logistical constraints (Laliberte et al. 2010, Armston et al. 2013). In addition to

these constraints, assessment of the models applied to historical imagery needs to be compared to biophysical parameters measured at the time of the image capture. The level of detail within aerial photography has enabled it to be used as a surrogate for the collection of ground data (Mannel et al. 2006). A number of studies have used aerial photography to derive biophysical parameters to calibrate Landsat satellite imagery (Xu et al. 2003, Pu et al. 2003, Carreiras et al. 2006, Samani Majd et al. 2013). Samani Majd et al. (2013) reported significant correlation between Landsat derived Normalised Difference Vegetation Index (NDVI) and fractional canopy cover measured from digital aerial photographs. In many instances, aerial photographs may be the only available data from which to assess the accuracy of results derived from coarse scale historical satellite imagery. Often when aerial photography is used to produce calibration and validation data, the assumption is made that the interpretation of the aerial photographs are correct, when in fact there may be significant errors in the interpretation which remain unknown unless validation of the results are undertaken (Congalton and Green 2009).

The NTG has a large archive of aerial photographs captured since 1940's (<http://www.ntlis.nt.gov.au/imfPublic/airPhotoimf.jsp>). In 2008 the NTG moved away from the traditional film aerial photography and now routinely captures imagery using digital format cameras. The extensive archive of very high resolution digital aerial photography held by the NTG has the potential to be a valuable source of calibration and validation data for use with coarser spatial resolution sensors. The combined spatial resolution and radiometric quality of the digital sensors (Leberl et al. 2012) used to capture the imagery across the Northern Territory has the potential to enable accurate measurements of biophysical parameters from woody vegetation. The spatial extent of these data would enable a large number of surrogate field sites to be randomly generated across the Northern Territory, representing a broad range of vegetation communities. To enable these data to be used as a surrogate for field data the biophysical parameters measured need to be first extracted from the imagery, and secondly, the accuracy of the information derived needs to be quantified. The objectives of this study are: (1) develop a methodology that enables the extraction of quantitative woody vegetation biophysical parameters from very high resolution digital aerial photography, (2) statistically quantify the relationship between digital aerial photography and field measured biophysical parameters, and (3) identify and assess the effect of different GSD on the biophysical parameters extracted from digital aerial photographs. The overall aim of this study is to investigate the utility of very high resolution digital aerial photography to be used as a surrogate for the collection of field data. This paper presents the methodology developed to extract biophysical parameters from digital aerial photography captured at both 15 cm and 30 cm GSD and evaluates the accuracy of the quantitative information derived from the imagery.

2.2 Methods

2.2.1 Study area

The field sites and aerial photography used in this study are distributed across the Northern Territory of Australia (2.1). The Northern Territory covers an area of 1,346,664 km², representing approximately 16.5% of the entire Australian landmass. It is sparsely populated with most people living in the main urban centres of Darwin, Katherine and Alice Springs. The climate is varied, ranging from wet dry tropics in the north, transitioning to semiarid and arid regions in the south (Ringrose et al. 1994). Temperatures are generally warm all year with the annual average temperature ranging from 32°C in Darwin, 34°C in Katherine, 32°C in Tennant creek and 29°C in Alice Springs. Much of the Northern Territory is influenced by a monsoonal climate with a majority of the rainfall occurring between the months of October and April (McDonald and McAlpine 1991). There is a distinct rainfall gradient moving south (Cook and Heerdegen 2001) with average annual rainfall of 1729 mm recorded at Darwin airport, 1133 mm in Katherine, 474 mm for Tennant Creek and 283 mm recorded in Alice Springs (www.bom.gov.au).

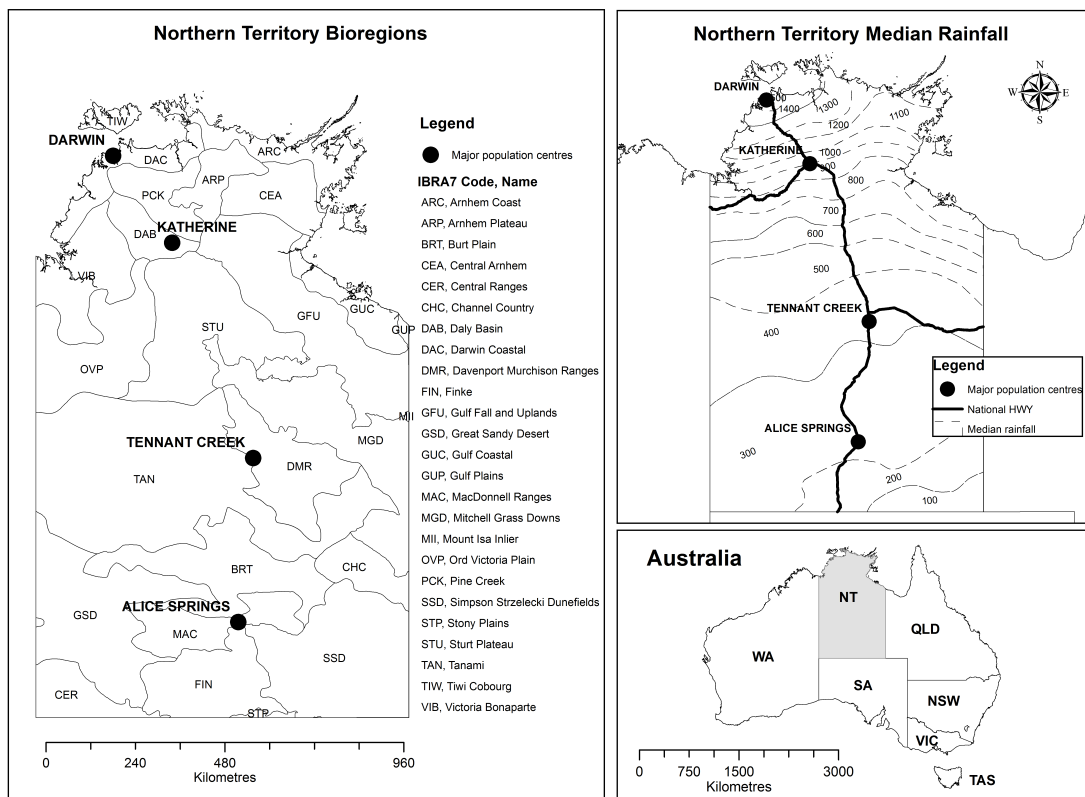


Fig. 2.1 Location of the study area Northern Territory (NT) Australia, major bioregions obtained from the Interim Biogeographic Regionalisation for Australia (IBRA) version 7 (<http://www.environment.gov.au/land/nrs/science/ibra>).

Woody vegetation in the Northern Territory is dominated by three main Genera, *Eucalyptus* and *Corymbia* in the north transitioning to *Acacia* communities in the arid south (Wilson et al. 1990). Large areas of the northern region are dominated by *Eucalyptus tetrodonta* and *E. miniata* woodlands to open forests containing a mid-stratum of mixed semi-deciduous to deciduous trees and shrubs and grasses (Williams et al. 1997). Melaleuca species are found on floodplains and river systems (Franklin et al. 2007), while pockets of dry and wet rain forests are scattered across the northern half of the Northern Territory (Wilson et al. 1990). Moving south into the semi-arid regions woodlands and low open woodlands consisting of *E. tectifica*, *Corymbia terminalis* and *E. chlorophylla* are common on undulating plains and plateaux (Wilson et al. 1990). In the coastal Gulf region (Fig 2.1, IBRA7 code GUC), both *E. tetrodonta* and *E. miniata* are more dominant, while *C. dichromophloia*, *E. tetrodonta* and *E. patellaris* are found on the undulating plains of the Sturt Plateau (IBRA7 code = STU). Large stands of *E. pruinosa* low woodlands are found in more poorly drained areas while Melaleuca woodlands are found on extensive low lying plains close to the coast (Wilson et al. 1990). Large areas of tussock grassland containing scattered trees and shrubs are found on cracking clay soils in the east (Barkly Tablelands, IBRA7 code MGD) and west (Victoria River Region, IBRA7 codes VIB, OVB). *E. microtheca* low open woodlands are found along clay-dominated water courses and intermittent swamps on clay plains and at the southern end of the semi-arid region (Wilson et al. 1990). Toward the southern edge of the semi-arid and into the arid region Acacia shrublands and open-shrublands are the most common woody vegetation communities. *Acacia aneura* (mulga) is the most common woody species in this region and it is found in a wide range of habitat types (Nicholas et al. 2009, Bowman et al. 1994), with open to sparse shrublands of *A. kempanana* dominate rocky calcareous landscapes (Wilson et al. 1990). Large tracts of spinifex (*Triodia* spp.) hummock grasslands are found across the sandy plains and dune fields of the central Australian deserts (Buckley 1981, Bowman et al. 2007). *Eucalyptus camaldulensis* is commonly found along the major sandy watercourses of the semi-arid and arid zones, while in areas fringing episodic water holes *E. microtheca* and *E. camaldulensis* low open woodlands and *Melaleuca glomerata* open-shrublands are common (Wilson et al. 1990). For a more detailed review of the diverse range of vegetation communities across the Northern Territory readers are directed to Wilson et al. (1990).

2.2.2 Aerial photography

A total of 31 aerial photograph mosaics captured between the years 2010 and 2013 were used in this study. They cover a broad range of structural formations and vegeta-

tion communities ranging from monsoon rainforests, savannah woodlands dominated by Eucalyptus and Corymbia trees, Mulga woodlands, Acacia shrublands and Triodia grasslands (Fig 2.2). The imagery used in this project has been captured on either a Vexcel Ultracam D or Ultracam X large-format digital camera. These cameras have four multispectral bands (red, green, blue and near infrared) and one panchromatic band, captured at 14-bit dynamic range (Gruber and Reitinger 2008, Leberl and Gruber 2005). The majority of digital aerial photography projects commissioned by the NTG are captured in the early dry season (around May–June) to reduce the impact of cloud, smoke, and haze on the imagery. To minimise the impact of shadow, imagery captured over areas with steep terrain and woody cover is restricted to times with a minimum solar altitude of 35° and for areas with open woody cover and flat terrain a minimum of 25°. Image processing is undertaken by the commercial contractors who produce a true colour (red, green, blue) orthorectified mosaic with a dynamic range of 8 bit. Imagery is supplied in a JPEG2000 compression format (10:1) with a reported spatial accuracy of $< \pm 1$ m. The ground sampling distances (GSD) of imagery captured is dependent on the requirements of the project. For this study, only 15 cm and 30 cm orthorectified mosaics supplied in true colour (red, green, blue) 8 bit dynamic range were available, captured between 2010 and 2013.

2.2.3 Field data

In total, 168 field sites located across the Northern Territory were available for use in this study (Fig 2.3 (a)). These field sites were sampled for a variety of projects undertaken by the NTG between the years 2009 and 2013. A number of the sites used in this study were part of a network of plots, which had been remeasured between the years 2010–2013 (Cuff and Brocklehurst 2015). In some instances, the same field sites were measured on different dates, these sites were used to assess aerial photography captured at either different GSD or on different dates. Locations of field sites were selected based on a methodology developed by the NTG rangelands monitoring unit to enable these data to be used with satellite imagery, this method is based on national Australian guidelines detailed in Muir et al. (2011). Sites were located within large homogeneous patches of vegetation 100 m from any boundary effect or disturbance (Muir et al. 2011). At each field site, a range of plant biophysical parameters and ground cover estimates were obtained over a 100 m \times 100 m quadrat. These data were measured using a point-based intercept method which obtains measurements at 1 m intervals along three 100 m tapes configured in a star shape (Fig 2.4). A densitometer sight tube (Stumpf 1993)

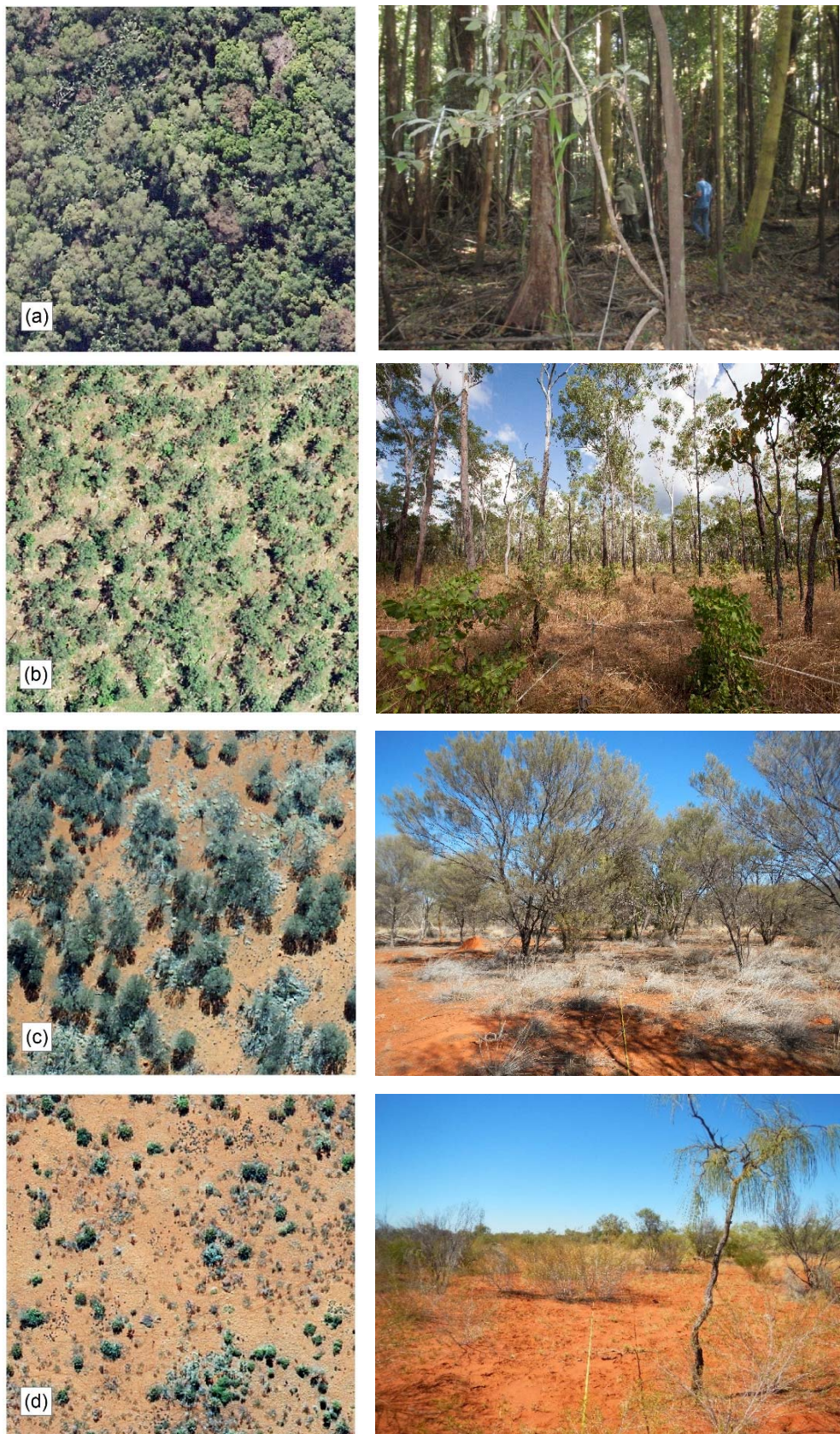


Fig. 2.2 Example of four of the sites used in this study; 15 cm GSD aerial photograph (left) and corresponding field site photograph (right); (a) Mixed species Monsoon forest,(b) *Eucalyptus miniata* and *E. tetrodonta* woodland (c) *Acacia aneura* (Mulga) woodland and (d) Sparse *Acacia* shrubland.

was used at the operator's eye height to record vertical intercepts of green leaf, dead leaf, branch, and sky within the extent of canopy for woody vegetation for the upper and mid stratum. Below the operators eye height an optical laser pointer was used to record the intercepts for woody vegetation in the ground stratum. In addition to the woody vegetation parameters, estimates of ground cover were also obtained along these transects. The ground layer measurements included green and dead leaf for herbs, forbs and grasses,litter, bare ground, rock and cryptogam. Stand basal area (SBA) estimates (m^2ha^{-1}) for individual woody species were also obtained for each site using a Haglöf factor gauge (Muir et al. 2011). At each site, seven individual basal sweeps were performed at predefined locations on the star transect (Muir et al. 2011). The mean of these measures were used to calculate the SBA (m^2ha^{-1}) for live and dead trees at each site. The centre of each plot was recorded using aver-aged GPS readings. Averaged GPS readings were recorded during the measurement of each field site which took between 1 to 3 h. Parameters for woody vegetation, such as total canopy cover, plant projective cover and foliage projective cover for the overstory, mid story and ground stratum are derived for each site. Foliage projective cover (FPC) represents the percentage of the sample site covered by the vertical projection of green foliage for woody vegetation. In this project, three broad vegetation strata were recorded, upper, mid and ground as defined in Brocklehurst et al. (2007). The number of strata recorded was dependent on the woody vegetation structure at each site. In some instance no upper or mid stratum existed, the height of vegetation in each strata is site specific and determined by the field team at the time of data collection. This enabled the proportion of FPC to be calculated for each stratum, U_{FPC} represents FPC for the upper canopy, UM_{FPC} is the combination of the upper and mid canopy FPC and UMG_{FPC} represents the total woody FPC for the site. Plant projective cover (PPC) represents the percentage of a site which is covered by the vertical projection of both green, dead foliage (dead leaf) and branches for woody vegetation for all three strata. Canopy Cover (CC) is defined as the percentage of the sample site within the periphery of the tree crown, treating the crown as opaque (Walker and Hopkins 1990). In this study, CC represented the area of the site covered by the vertical projection of PPC and sky (canopy gaps) recorded within the crowns of woody vegetation in the upper and mid stratum.

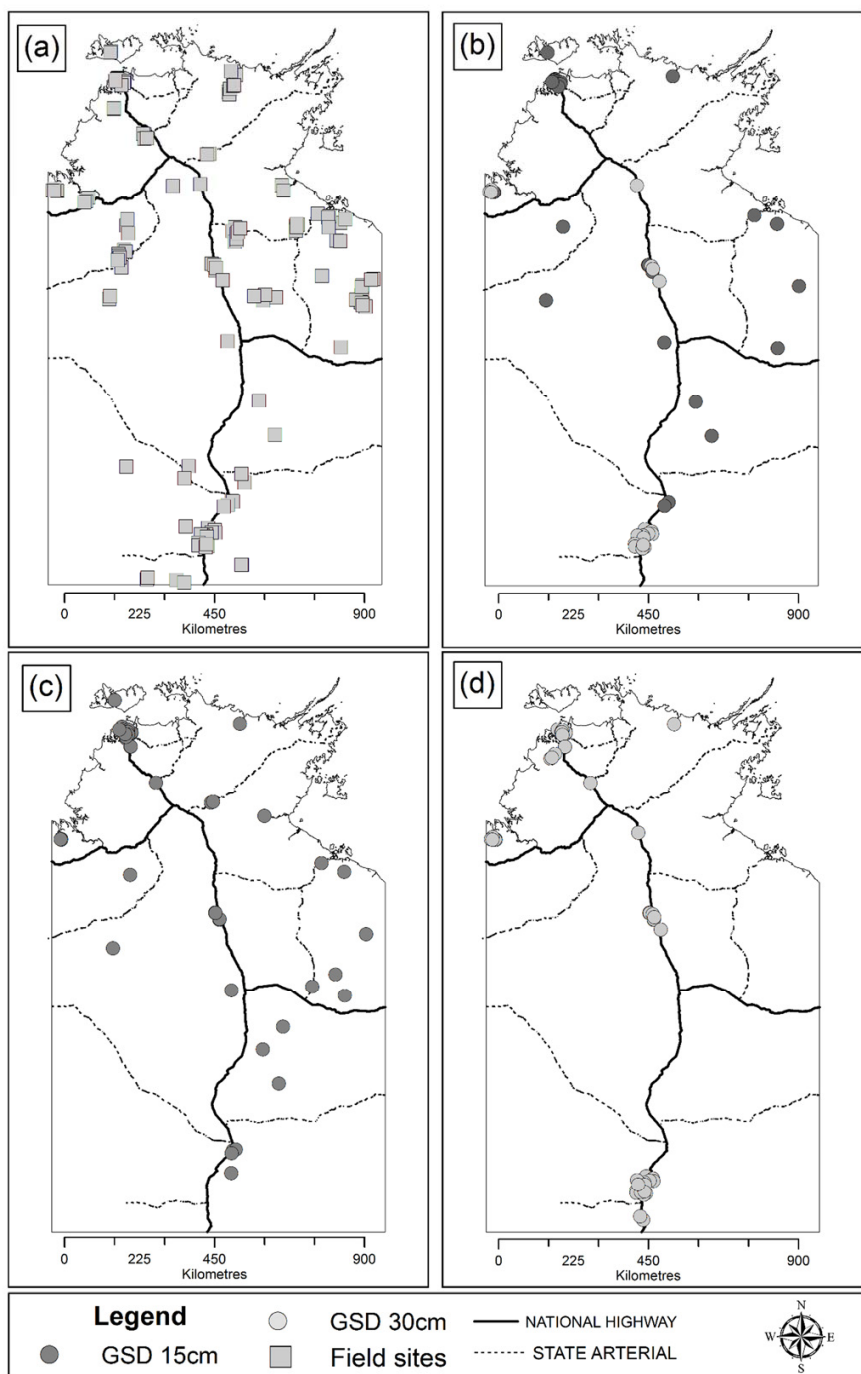


Fig. 2.3 (a) Location of all the field sites used in this study; (b) sites used to independently assess the relationship between digital aerial photography and predicted live SBA; (c) sites used to assess the relationship between tree canopy parameters and aerial photography GSD 15 cm; and (d) GSD 30 cm.

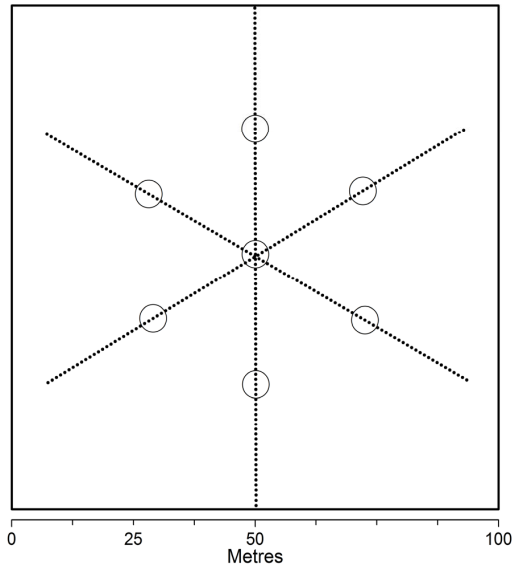


Fig. 2.4 Example of the transect configuration of a 100 m × 100 m (1 ha) field site used to collect woody cover estimates, circles denote where tree basal area measurements were collected.

2.2.4 Canopy biophysical parameters and aerial photography

Of the 168 sites available, 75 were located within the extent of digital aerial photography representing a broad range of structural classes (Table 2.1). These 75 field sites were used to assess the relationship between aerial photography and field measured woody biophysical canopy parameters. For aerial photography captured at 15 cm GSD, 50 individual field site measurements (on different sampling dates) from 46 sites were available, while 52 individual field site measurements recorded from 50 field sites were used to assess aerial photography captured at 30 cm GSD. Twenty of the 75 field sites used in this study had aerial photography captured at both 15 cm and 30 cm GSD and were used to investigate the difference between parameters derived from aerial photography at the same field sites. The difference between the field and image capture dates used in this study are summarised in Tables 2 and 3, with 75% of field sites measured <1 year of the image capture.

Table 2.1 Summary of the field sites used to investigate the relationship between tree biophysical parameters and 15 cm and 30 cm GSD aerial photographs, field sites are grouped into broad structural classes based on the National Vegetation Information System (Brocklehurst et al. 2007).

NVIS class	No. sites	Mean	range	Mean SBA	(range)	No. sites 15 cm GSD	No. sites 30 cm GSD
		CC (%)		(m ² ha ⁻¹)			
Low isolated shrubs	8	1.2	(0.33-3.99)	0.04	(0.00-0.19)	1	7
Low isolated trees	1	3.7		0.93			1
Low open forest	1	55.0		7.46			1
Low open woodland	10	13.3	(8.65 - 18.33)	2.11	(1.69 - 3.04)	6	4
Low sparse shrubs	2	6.3	(5.66 - 7.00)	0.02	(0.00 - 0.042)	1	1
Low tussock grassland	1	0.0		0.00			1
Low woodland	13	29.5	(20.00 - 37.33)	3.68	(0.35 - 6.60)	9	4
Mid closed forest	7	94.2	(89.63 - 100)	26.63	(17.78 - 34.2)	4	3
Mid hummock grassland	2	0.0		0.00			2
Mid isolated shrubs	1	0.7		0.00			1
Mid isolated trees	2	3.5	(2.33 - 4.65)	0.51	(0.00 - 0.09)		2
Mid open forest	22	64.2	(53.00 - 77.99)	13.74	(5.96 - 20.14)	13	9
Mid open woodland	6	11.6	(5.66 - 17.34)	1.44	(0.03 - 2.64)	3	3
Mid sparse shrubland	2	6.7	(6.31 - 7.00)	0.02	(0.00 - 0.04)		2
Mid woodland	20	34.9	(21.26 - 49.33)	5.66	(1.37 - 14.93)	10	10
Tall isolated shrubland	1	0.0		0.66			1
Tall open shrubland	1	28.0		3.94			1
Tall sparse shrubland	2	10.0	(6.00 - 14.00)	1.41	(0.11 - 2.71)	1	1

Table 2.2 Summary statistics for the number of days between the field and image capture dates for the 15 cm GSD aerial photography.

15 cm	< 1 year	1-2 years	2-3 years
n sites	34	10	6
min (days)	9	373	737
max (days)	350	493	1093
mean (days)	120	413	837

Table 2.3 Summary statistics for the number of days between the field and image capture dates for the 30 cm GSD aerial photography.

15 cm	< 1 year	1-2 years	2-3 years	4-5 years
n sites	43	3	5	1
min (days)	24	735	770	1477
max (days)	342	736	783	1477
mean (days)	143	735	776	

2.2.5 Classification of aerial photographs

For each of the field sites, a 100 m × 100 m subset was extracted from the digital aerial photo mosaic and classification of these data was performed using an object based image analysis (OBIA) approach in eCognition®Developer 8. A ruleset was developed that first segmented the image into meaningfully sized objects and then classified the image using a supervised nearest neighbour classification algorithm (Fig.2.5). This

studies area of interest encompasses a broad range of vegetation communities from the wet-dry tropics to the arid deserts of interior Australia. The digital number values representing green vegetation for the different vegetation communities across the NT were highly variable (see Fig. 2.2). Classification of imagery using an OBIA approach has been shown to reduce the salt and pepper effect in the imagery and increase accuracy of the classification over a per-pixel approach in northern Australia (Whiteside et al. 2011). Coggins et al. (2008) successfully used an OBIA supervised classification approach to obtain tree crown areas from aerial photography. Laliberte et al. (2010) developed an OBIA hierarchical classification approach which used a combination of rule based and supervised nearest neighbour algorithm to successfully classify ultra-high resolution aerial photography. They used the nearest neighbour algorithm to classify the image at the finer scale level as it enabled them to take into account the spectral variability of target objects in different images (Laliberte et al. 2010). The OBIA supervised classification method used in this study enables the user to rapidly train the classification algorithm taking into account the specific spectral variability within each aerial photograph sub-set. For a comprehensive review of OBIA readers are referred to Blaschke (2010) and Blaschke et al. (2014).

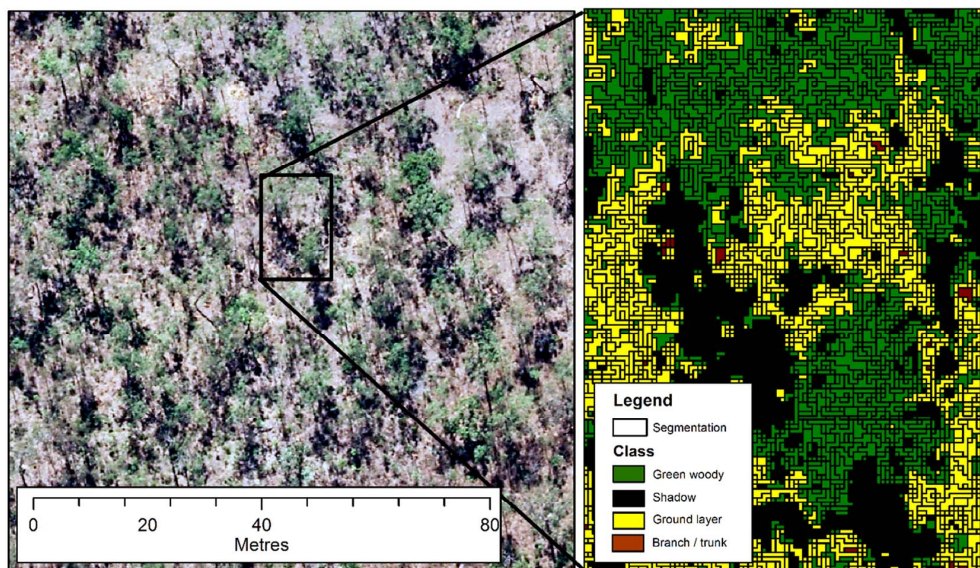


Fig. 2.5 Example of the segmentation and classification of 15 cm digital aerial photography, showing that objects produced from the fine segmentation of the imagery which enable gaps in the tree canopy to be identified and classified.

Table 2.4 Example of the summary statistic for objects derived in the segmentation process and the number of objects used for the training of each class for sites shown in Figure 2.2. The letter in brackets in the site column corresponds to the 15 cm aerial photograph shown in Figure 2.2 and for two sites (a) and (b) where both GSD were captured the summary statistics for 30 cm imagery are also shown.

Site	GSD	Total no.	Image Objects statistics			Training samples per class (no. objects)				
			Min no. pixels	Max no. pixels	Mean (SD) no. pixels	Green woody	Ground	Shadow	Trunk Branch	Green grass
HJ(a)	15 cm	168652	1	32	2.64 (2.37)	1587		35	7	
HJ	30 cm	37067	1	35	3.00 (2.62)	81		19	5	
HOW(b)	15 cm	152203	1	32	2.92 (2.64)	981	555	151	6	
HOW	30 cm	54740	1	20	2.03 (1.59)	71	211	47		
MURR(c)	15 cm	136948	1	40	3.48 (3.13)	67	1256	129	8	40
EPA(d)	15 cm	130327	1	50	3.63 (3.29)	136	2748	56		

2.2.6 Segmentation

The multi-resolution segmentation algorithm used by eCognition is a bottom-up region merging technique, starting with single pixel objects. During the hierarchical segmentation smaller image objects are merged into larger ones, based on unit-less parameters scale, colour and shape (Benz et al. 2004). These parameters define the growth in heterogeneity between adjacent image objects and this iterative process stops once the smallest growth exceeds the threshold defined by the scale parameter (Laliberte et al. 2007). To define the segmentation parameter, a number of different values were assessed to determine the optimal segmentation of the aerial photography for both GSD. This is a subjective process which relies on the operator's expert knowledge to select parameters that produce objects at a meaningful size. The main objective of this study was to identify green woody vegetation cover in a broad range of vegetation communities. Thus the final parameters for the segmentation of the 15 and 30 cm aerial photographs were chosen to reduce the spectral heterogeneity in the image while still retaining enough detail to identify gaps in individual tree canopies. The final parameters selected for the segmentation of both the 15 cm and 30 cm imagery were; scale 3, colour and shape 0.9/0.1 and smoothness/compactness 0.5/0.5 respectively. All three spectral bands were weighted evenly (weight value = 1) in the segmentation. An example of the number of objects and summary statistics for the aerial photographs for field sites shown in Figure 2.2 are detailed in Table 2.4.

2.2.7 Classification

The supervised nearest neighbour classification algorithm used in this study returns a value for each object indicating the probability of belonging to a certain class. If an object is identical to a sample it is given a value of one, while objects different from a sample are assigned a value between zero and one based on a fuzzy dependency of

the feature space distance to the nearest sample of a class (Trimble 2013). The user determines both the number of classes used in the classification and the features used to define the feature space. A large number of statistics describing colour, shape and texture characteristics derived from the image objects are available to define the feature space used in the classification (Blaschke 2010). In this study, only the mean digital numbers from each band were used to define the feature space used in the classification. For the majority of the aerial photograph subsets four main classes were defined (1) green woody vegetation, (2) branches or trunks, (3) shadow and (4) ground layer. Due to the dry season conditions at the time of a majority of the image capture dates, the ground layer class usually consisted of either bare ground or non-green vegetation. In some instances where the ground stratum had green grass present, a fifth class (green grass) was added to the classification to reduce confusion between green woody and no-woody vegetation. For each aerial photograph subset, samples were selected from across the image to train each of the classes. The number of training samples per class varied (see Table 2.4 for an example) and was dependent on the area covered by the particular class in the aerial photograph. On average, about 1% of the total objects were selected as training objects to classify each aerial photograph subset. It took between 20 and 30 min to process each aerial photo subset this included extracting the $100\text{ m} \times 100\text{ m}$ sub-set from the aerial photo mosaic, selecting the training samples for each class and running the classification and exporting the results. The results of the classification were exported to enable accuracy assessment of the classification and identify the proportion of area (m^2) for each class. The area attributed to the green woody vegetation class (AP_{GWC}) was used to estimate the percentage green woody cover for each 1 ha site. The green woody cover estimates derived from each of the aerial photograph subsets were then compared with the field measured tree biophysical parameters CC, PPC, UFPC, UM_{FPC} and UMG_{FPC} to identify any relationships between the estimates of AP_{GWC} obtained from the digital aerial photography. The AP_{GWC} estimates derived from the aerial photographs were also used to predict live woody SBA for each of the plots.

2.2.8 Classification method accuracy assessment

In order to assess the performance of the classifier's ability to predict the desired classes based on the training data, a test was undertaken to understand the classifier commission and omission error when used on novel data that were not used in the formation of the algorithm. This tests how well the method generalises to new examples from the same data domain (Baldi et al. 2000). This test requires the same expert operator who collected the training data to undertake labelling of additional random samples across the RGB digital aerial photograph. Assessment of the accuracy of the classified aerial

photographs was undertaken on a subset (30) of the 96 sites used in this study. Fifteen sites were randomly selected to represent each spatial resolution (GSD 15 cm and 30 cm). To produce a reference dataset to evaluate the classification, 200 points were randomly generated in a GIS for each of the 30 aerial photographs and overlayed on the 100 m × 100 m RGB aerial photograph subset. The 200 points were visually evaluated and assigned to one of the five classes used in the classification and the point vector files were then intersected with the corresponding classified image to produce the accuracy statistics. The results were then pooled into their respective GSD categories (15 cm = 3000 points, 30 cm = 3000 points) to calculate the producer (commission error) and user accuracy (omission error) for each class and the overall accuracy, which were presented in a standard error matrix (Congalton and Green 2009).

2.2.9 Stand basal area and aerial photography

An allometric relationship between coincident field measured UMG_{FPC} and live stand basal area (SBA) measurements was developed from 127 sites across the Northern Territory. This allometric relationship was developed using a non-linear power function based on a robust regression technique;

$$liveba = a * x^b + c * x^d \quad (2.1)$$

where a, b, c, and d are the best fit parameters and x is the field measured UMG_{FPC}. The field-based allometric relationship was then applied to estimates of AP_{GWC} derived from aerial photography, captured at 15 cm and 30 cm GSD to predict live SBA. A robust regression technique was chosen as the independent variables (field measured UMG_{FPC}) would not be free of measurement error and robust regression techniques are less impacted by outliers (Cohen et al. 2003). To independently assess the live SBA estimates derived from the aerial photography, 50 of the 168 field sites available in this study were not used in the development of the allometric equation. Forty four of the 50 sites were randomly selected from the 75 sites used in the assessment of canopy biophysical parameters and aerial photography. These 44 randomly selected sites contained both field measured UMG_{FPC} and live SBA, while only live SBA measurements were recorded during the field surveys at the remaining six sites. The allometric equation developed in this study was applied to field measured UMG_{FPC} ($n = 44$) and AP_{GWC} ($n = 50$) obtained from the independent sites.

2.2.10 Statistical analysis of relationship between field biophysical parameters and AP_{GWC}

The assumption in this study was that field measured biophysical parameters represent the accurate measure of these parameters at each location. A number of statistics were

used to identify and assess the relationships between measures derived from the aerial photographs and the field woody vegetation cover and live SBA measures. Pearson's product moment correlation coefficient (Zar 1984) was used to assess the correlation between the field-based biophysical parameters and photo-derived green woody cover and predicted live SBA. The root mean square error (RMSE) (Congalton and Green 2009) was used to assess the overall error (difference) between the field-measured biophysical parameters and the photo-derived estimates. Variance was used to assess the precision of the biophysical estimates from the aerial photography and the field-measured estimates. Bias was calculated to assess the average difference between the photo-derived and field-measured parameters and indicates the dispersion of data around the one-to-one line. To determine if there were statistically significant differences between AP_{GWC} derived from aerial photography and the field-measured biophysical parameters (CC, PPC, U_{FPC}, UM_{FPC}, UMG_{FPC}, live SBA) a paired t-test was used with a confidence level of 99% (Zar 1984).

2.3 Results

2.3.1 Classification accuracy assessment

The results of the accuracy assessment of the classified aerial photographs are presented in Tables 2.5, 2.6, 2.7 and 2.8. For sites captured at 15 cm GSD the minimum individual accuracy was 69.5%. This occurred in a *Eucalyptus tetrodonta* and *Euc miniata* open forest site located in the north half of the NT. The site with the highest accuracy (89%) occurred in a site dominated by *Eucalyptus tectifica* also located in the northern half of the NT. The overall accuracy for the 15 cm imagery was 80%, with the highest individual accuracy for the ground layer class. For the green woody vegetation class (the focus of this study) the producer and user accuracy was similar to the overall accuracy ($\approx 80\%$), with the majority of the commission and omission error between the ground layer and shadow classes. While there was minor omission and commission error between the green grass and branch/trunk class and green woody vegetation. The producer and user accuracy for the branch and trunk class was very low with commission error between the green woody vegetation, ground layer and shadow classes. Producer's accuracy for the green grass class was low with commission error between green woody vegetation and ground layer class, and omission error occurring as a result of confusion with the ground layer, shadow and green woody vegetation classes. For the 30 cm classification accuracy the lowest value (74.5%) occurred in a site located in the semi-arid zone dominated by the species *Bauhinia cunninghamii*. The highest accuracy (97%) occurred in two sites located in the arid zone. The accuracy for the classification for sites at 30 cm GSD was higher than the 15 cm imagery with an overall accuracy of 86%. While overall accuracy was higher than the 15 cm imagery the users and producers ac-

curacy for the green woody vegetation class for 30 cm imagery was slightly lower. As with the results of the 15 cm classification most of the omission and commission error for the green woody vegetation class occurred between the shadow and ground layer classes. The accuracy of the ground layer was high with most omission and commission error between the green woody vegetation, shadow and green grass classes. For the green grass class most omission and commission error occurred with the ground layer class. The branch and trunk class was not assessed as none were identified during the visual assessment of the 3000 randomly selected points.

Table 2.5 Accuracy of the 15 aerial photographs 15 cm (GSD) randomly selected to assess the object based classification, along with the NVIS structural class, broad climatic zone and dominant vegetation species taken from the field data.

NVIS class	Broad climate Zone	Dominant vegetation species	Accuracy
Low open woodland	Semi-arid	<i>Lophostemon lactifluus /Acacia auriculiformis</i>	81.5
Low woodland	Semi-arid	<i>Eucalyptus tetrodonta</i>	82.5
Low woodland	Humid	<i>Acacia estrophialata</i>	81.5
Low woodland	Arid	<i>Eucalyptus tetrodonta / Eucalyptus miniata</i>	70.0
Mid closed forest	Humid	<i>Eucalyptus tecifica</i>	89.0
Mid closed forest	Humid	<i>Bauhinia cunninghamii</i>	80.0
Mid open Forest	Humid	<i>Erythrophleum chlorostachys / Corymbia polycsiada</i>	80.5
Mid open forest	Humid	<i>Callitris intratropica</i>	77.0
Mid open forest	Humid	<i>Eucalyptus tetrodonta / Eucalyptus miniata</i>	69.5
Mid open woodland	Arid	<i>Corymbia opaca / Acacia coriacea</i>	80.0
Mid woodland	Semi-arid	<i>Eucalyptus tetrodonta / Eucalyptus miniata</i>	88.5
Mid woodland	Humid	<i>Eucalyptus tetrodonta / Eucalyptus miniata</i>	84.0
Mid woodland	Semi-arid	<i>Eucalyptus tetrodonta / Eucalyptus miniata</i>	79.5
Mid woodland	Humid	<i>Corymbia dichromophloia</i>	71.5
Tall sparse shrubland	Arid	<i>Eucalyptus tetrodonta / Eucalyptus miniata</i>	87.0

Broad climatic zones are defined by the median rainfall (Figure 5.2), Humid zone > 1000 mm, Semi-arid zone 500-1000 mm and Arid zone < 500 mm.

Table 2.6 Accuracy of the 15 aerial photographs 30 cm (GSD) randomly selected to assess the object based classification, along with the NVIS structural class, broad climatic zone and dominant vegetation species taken from the field data.

NVIS class	Broad climate Zone	Dominant vegetation species	Accuracy
Low open woodland	Semi-arid	<i>Lophostemon lactifluus /Acacia auriculiformis</i>	81.5
Low isolated shrubs	Arid	<i>Acacia kempeana</i>	90.0
Low isolated shrubs	Arid	<i>Acacia aneura/Eremphila spp</i>	89.5
Low isolated shrubs	Arid	<i>Sclerolaena laniscuspis/Enneapogon polyphyllus</i>	77.5
Low isolated trees	Arid	<i>Corymbia terminalis</i>	77.0
Low open forest	Semi-arid	<i>Eucalyptus tetrodonta/Eucalyptus miniata</i>	82.0
Low open woodland	Arid	<i>Acacia aneura/Senna spp</i>	79.0
Low open woodland	Semi-arid	<i>Bauhinia cunninghamii</i>	74.5
Mid closed forest	Humid	<i>Acacia auriculiformis/Carpentaria acuminata</i>	85.0
Mid isolated shrubs	Arid	<i>Eremphila duttonii</i>	97.0
Mid isolated trees	Humid	<i>Corymbia polycarpa</i>	92.5
Mid open woodland	Arid	<i>Eucalyptus microtheca</i>	93.5
Mid sparse shrubland	Arid	<i>Acacia aneura/Acacia kempeana</i>	97.0
Mid sparse shrubland	Arid	<i>Acacia kempeana</i>	90.0
Mid woodland	Arid	<i>Acacia aneura</i>	89.5
Mid woodland	Humid	<i>Eucalyptus tetrodonta/Eucalyptus miniata</i>	77.5

Broad climatic zones are defined by the median rainfall (Figure 5.2), Humid zone > 1000 mm, Semi-arid zone 500-1000 mm and Arid zone < 500 mm.

Table 2.7 Error matrix showing the accuracy assessment results for the classification of 15 cm GSD digital aerial photography (n = 15 sites).

Classified data	Reference data							Users accuracy
	Green woody	Shadow	Ground layer	Branches and trunks	Green grass	Total		
Green woody	726	72	100	4	12	914	79.4 %	
Shadow	97	389	48	1	0	535	72.7 %	
Ground layer	99	103	1232	3	8	1445	85.3 %	
Branches and trunks	1	0	5	1	0	7	14.3 %	
Green grass	6	16	22	0	55	99	55.6 %	
Total	929	580	1407	9	75	3000		
Producers accuracy	78.1 %	67.1	87.6	11.4	73.3			
Overall accuracy 80.1 %								

Table 2.8 Error matrix showing the accuracy assessment results for the classification of 30 cm GSD digital aerial photography (n = 15 sites).

Classified data	Reference data							Users accuracy
	Green woody	Shadow	Ground layer	Branches and trunks	Green grass	Total		
Green woody	306	51	57	0	3	417	73.4 %	
Shadow	60	220	23	0	5	308	71.4 %	
Ground layer	39	75	1942	0	26	2082	93.3 %	
Branches and trunks	3	0	0	0	0	3	0.0 %	
Green grass	6	17	52	0	115	190	60.5 %	
Total	436	345	2070	0	149	3000		
Producers accuracy	73.9 %	60.6	93.6	0.0	77.2			
Overall accuracy 86.1 %								

2.3.2 Relationship between field biophysical parameters and AP_{GWC}

2.3.2.1 15 cm aerial photography

The results show that there is a significant correlation between the field measured cover parameters (U_{FPC}, UM_{FPC}, UMG_{FPC}, PPC, CC) and 15 cm aerial derived AP_{GWC} estimates (n = 50) (Fig. 2.6, Table 2.9). Field-measured U_{FPC} and UM_{FPC} were overestimated by AP_{GWC} and conversely PPC and CC were underestimated (Fig. 6). The lowest RMSE value was found between UMG_{FPC} and AP_{GWC} while the variance was slightly lower between UM_{FPC} and AP_{GWC}. The lowest bias value was recorded between UMG_{FPC} and AP_{GWC} which is also reflected in the scatter around the 1 for 1 line (Fig. 6). A paired t-test ($\alpha=0.01$) was used to assess if there were differences in the mean values between field-based measurements and the aerial photo derived estimates (Fig. 2.6). The only field based cover parameter that was not significantly different to the mean of AP_{GWC} estimates was UMG_{FPC}.

Table 2.9 Results of assessment of the relationship between AP_{GWC} estimated from 15 cm digital aerial photography and field woody cover estimates (U_{FPC}, UM_{FPC}, UMG_{FPC}, PPC and CC).

Woody cover parameter	r	RMSE	Variance	Bias	T statistic	P value
U _{FPC}	0.92	10.85	62.85	7.49	-6.68	<0.001
UM _{FPC}	0.95	7.28	38.17	3.94	-4.51	<0.001
UMG _{FPC}	0.95	6.84	47.74	0.09	0.09	0.926
PPC	0.95	8.62	52.86	-4.74	4.61	<0.001
CC	0.95	14.83	88.12	-11.56	8.71	<0.001

2.3.2.2 30 cm aerial photography

The results for the 30 cm imagery ($n = 52$) are similar to the 15 cm imagery with high correlations between all field-measured woody cover parameters and AP_{GWC} (Fig. 2.6, Table 2.10). The scatter plots show that field measured U_{FPC} was overestimated by AP_{GWC}, while UM_{FPC} and UMG_{FPC} were scattered around the 1:1 line. Both PPC and CC were underestimated when compared to AP_{GWC} values. Based on the r, RMSE, variance and bias statistics shown in Table 2.10, both UM_{FPC} and UMG_{FPC} had the strongest relationship with AP_{GWC}, with UM_{FPC} having both the lowest RMSE and variance. Results from the paired t-test ($\alpha = 0.01$) show that both field measured UM_{FPC} and UMG_{FPC} were not significantly different to the mean values of AP_{GWC}.

Table 2.10 Results of assessment of the relationship between AP_{GWC} estimated from 30 cm digital aerial photography and field woody cover estimates (U_{FPC}, UM_{FPC}, UMG_{FPC}, PPC and CC).

Woody cover parameter	r	RMSE	Variance	Bias	T statistic	P value
U _{FPC}	0.92	8.81	56.98	4.66	-4.45	<0.001
UM _{FPC}	0.95	6.89	44.68	1.91	-2.06	0.045
UMG _{FPC}	0.94	7.39	53.48	-1.46	1.44	0.157
PPC	0.95	9.66	67.93	-5.16	4.51	<0.001
CC	0.95	15.88	141.14	-10.67	6.47	<0.001

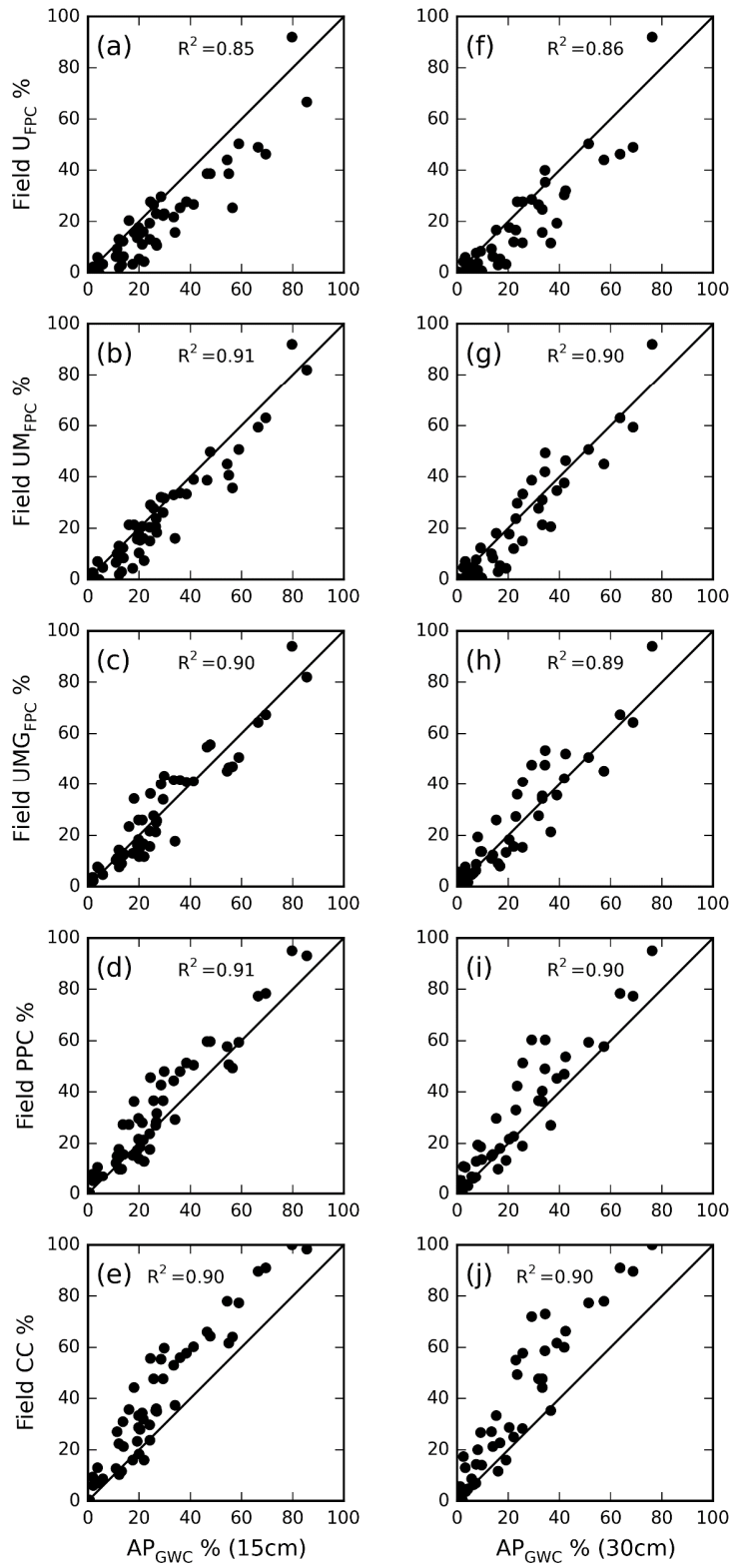


Fig. 2.6 Scatter plots showing the relationship between AP_{GWC} (x-axis) estimated from digital aerial photography captured at GSD 15 cm (a–e) and 30 cm (f–j) and field-measured U_{FPC}, UM_{FPC}, UMG_{FPC}, PPC and CC (y-axis), fitted line represents the 1:1 correspondence.

2.3.3 Comparison of the results between aerial photography captured at 15 cm and 30 cm GSD

The results show that the relationship between the field measured canopy parameters and imagery was stronger for 15 cm GSD in comparison to imagery captured at 30 cm GSD (Fig. 2.6). Overall the variance was lower for the 15 cm data for each of the parameters assessed, which is reflected in the spread of data in Fig. 2.6. Variance between field tree canopy parameters for both the 15 cm and 30 cm imagery was lowest between UM_{FPC} , however, for all other statistics the relationship was strongest with UMG_{FPC} for both 15 cm and 30 cm GSD. To further investigate the influence of the different GSD, comparisons were made between the AP_{GWC} values derived from 20 field sites where both 15 cm and 30 cm aerial photographs had been captured. A paired *t*-test was used to investigate if there was a statistically significant difference between the AP_{GWC} estimates derived from the two different GSD. There was a high correlation ($r = 0.94$) between AP_{GWC} derived from aerial photography at GSD of 15 cm and 30 cm for most sites (Fig.2.7). The results of the paired *t*-test indicated that there was no significant difference between the two spatial resolutions (T value = 1.35; P -value = 0.191; $\alpha= 0.01$). While most of these data points were close to the 1:1 line, a number of outliers were present, recording up to 22% difference in estimated AP_{GWC} between the different GSD.

2.3.4 Stand basal area

The best fit function for the allometric relationship between field-measured UMG_{FPC} and live SBA is shown in Fig. 2.7. The scatter around the best fit function highlights the variability in the relationship between UMG_{FPC} and live SBA, with the greatest variance occurring between the ranges of 30 and 60% UMG_{FPC} . Summary statistics for the non-linear power function and best fit parameters for the allometric equation are presented in Table 2.11. The allometric relationship was then applied to independent field measured UMG_{FPC} ($n = 44$) and aerial photograph ($n = 50$) measured AP_{GWC} to assess the accuracy of the predicted live SBA measures. The statistics used to assess the overall accuracy based on the predicted and observed values (Table 2.11) show that there was little difference between the 127 sites used to define the allometric relationship and the 50 independent sites. The predicted (Equ. 2.1) and observed live SBA estimates derived from aerial photography AP_{GWC} and field-measured UMG_{FPC} for the independent validation sites are presented in Figure 2.9. It shows that the predicted values above $10 \text{ m}^2\text{ha}^{-1}$ were generally underestimating live SBA, which may be a reflection on the limited number of sites used to independently assess the allometric relationship in this value range. A paired *t*-test between the 44 independent sites with field-measured UMG_{FPC} and aerial photography AP_{GWC} estimates showed that there

was no significant difference between live SBA estimated from either field or aerial photography AP_{GWC} (T value = 1.94; P -value = 0.059; $\alpha= 0.01$).

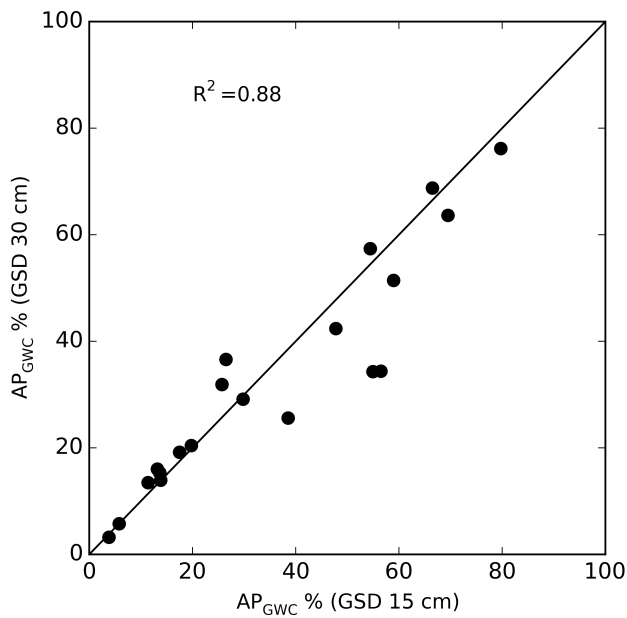


Fig. 2.7 Scatter plot showing the relationship between AP_{GWC} derived from aerial photography captured at both 15 cm and 30 cm GSD for the same field site, fitted line represents the 1:1 correspondence.

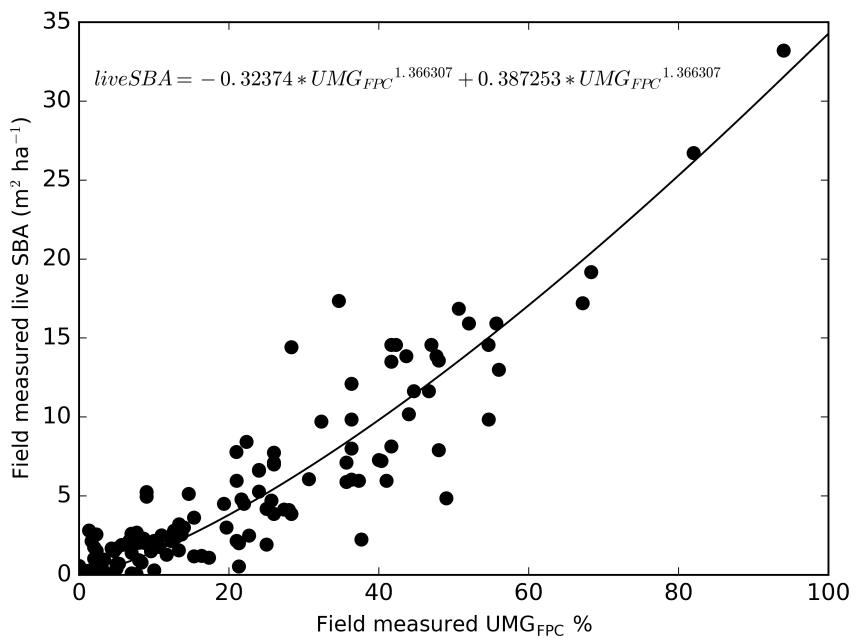


Fig. 2.8 Fitted line for the allometric relationship between field-measured UMG_{FPC} and live SBA $m^2 ha^{-1}$; the equation for the fitted line is shown in equ 2.1 and the best fit parameters are shown in Table 2.11

Table 2.11 Best fit parameters for the allometric equation and summary statistics for live SBA predicted from field UMG_{FPC} and aerial derived AP_{GWC} using the allometric relationship developed between coincident field-measured live tree SBA ($\text{m}^2 \text{ha}^{-1}$) and UMG_{FPC} (%).

Allometric relationship		Predicted vs observed	
		Field measured UMG _{FPC} vs observed live SBA	Aerial photography measured AP _{GWC} vs observed Live SBA
Best Fit	a = -0.32374		
Parameters	b = 1.366307		
	c = 0.387253		
	d = 1.366307		
No. field sites	127	44	50
r	0.92	0.95	0.95
RMSE	2.33	2.29	2.29
Variance	5.41	5.04	5.31
Bias	0.21	0.54	0.16

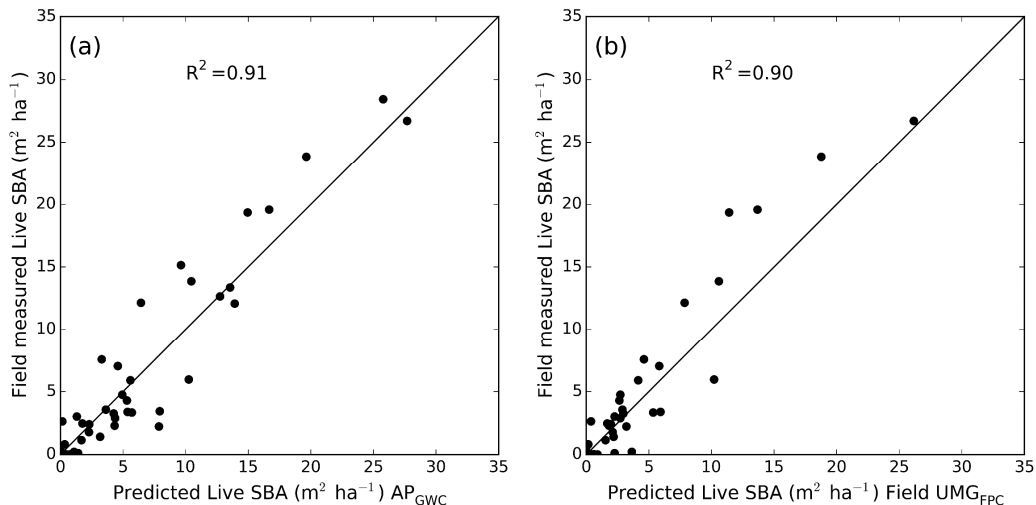


Fig. 2.9 Scatter plot showing the predicted and observed live SBA estimates, plot (a) represents the 50 sites where live SBA was predicted from AP_{GWC} and plot (b) where live SBA was predicted from 44 field-measured UMG_{FPC}.

2.4 Discussion

Estimates of tree biophysical parameters were extracted from very high resolution digital aerial photography captured at a GSD of 15 cm and 30 cm using OBIA. The very high spatial resolution of the digital aerial photography used in this project enabled estimates of green woody cover to be obtained over the 1 ha field sites. There was a high correlation between aerial photo derived AP_{GWC} and all the woody canopy parameters assessed (U_{FPC}, UM_{FPC}, UMG_{FPC}, PPC and CC). The relationship between all the field-measured canopy variables and aerial derived estimates were consistent across a

wide range of vegetation communities, structural classes, and across a large climate gradient, ranging from the monsoon tropics to the arid desert region. The strong relationship between all the field-based canopy parameters and aerial-derived values are likely to be due to the natural occurring relationships between these canopy attributes. Strong relationships between field-measured foliage projective cover (FPC) and CC were reported across a range of vegetation communities in the state of Queensland, Australia (Scarth et al. 2008). Scarth et al. (2008) found that FPC had a higher dynamic range than CC, saturating at around 75% and suggested that this relationship is likely to be similar elsewhere in Australia. While the number of sites used in this study with $CC > 75\%$ were limited, a non-linear relationship between CC and UMG_{FPC} obtained from field measurements is evident (unpublished data). Armston et al. (2009) showed how woody FPC at Landsat scale (30m spatial resolution) could be predicted from observed densitometer measurements recording the presence and absence of green leaf along transects. This is because estimates of vegetation cover fraction, which are proportions, can generally be scaled, unlike NDVI (Jiang et al. 2006). The ability to discriminate between different objects in any remotely sensed imagery is determined by the spatial and spectral limitations of the data (Blaschke 2010, Staben et al. 2012). Accuracy assessment of the supervised classification showed that while overall accuracy for imagery captured at 30 cm GSD was higher than 15 cm imagery, accuracy of the green woody class was higher in the 15 cm imagery. For the green woody class the majority of the commission and omission error occurred between the ground layer and shadow classes. It could be assumed that the ability to resolve green from non-green components in the 30 cm GSD would become more difficult, due to the increased mixing of these components in each pixel. This increased spectral homogeneity of 30 cm pixels may have reduced the ability of the classification algorithm to spectrally separate these classes. To enable parameters extracted from aerial photography to be used with any confidence the results need to be compared with field-measured data (Fensham and Fairfax 2007). In this study, the collection of the proportion of woody FPC for each stratum enabled the relationship between AP_{GWC} estimates and field-measured parameters to be better understood. The results show that parameters extracted from the 15 cm GSD aerial photography exhibited the strongest relationship with field-measured woody UMG_{FPC} . Relationships between estimates derived from imagery at GSD of 30 cm were not as clearly defined for UM_{FPC} and UMG_{FPC} with both showing statistically significant relationships. Not all field sites used in this study contained multiple strata, which can be seen in the underestimation of U_{FPC} and UM_{FPC} from the aerial photography for both GSD 15 cm and 30 cm (Fig. 2.6). In a number of the sites the only woody cover present were shrubs recorded in the ground strata. The parameters derived from the aerial photographs were generally lower when compared to field measured PPC and CC. Overall, there was less variance and scatter in the relationship between the field

parameters and measures derived from the higher spatial resolution 15 cm GSD imagery. It is possible that the increased scatter observed in the results for the 30 cm GSD imagery is due to the differences in the spatial resolution. Previous studies using film captured aerial photography to estimate CC from both 1:25,000 and 1:40,000 scales found that increase in photo scale resulted in overestimation of CC when compared to field-measured data (Fensham et al. 2002, Fensham and Fairfax 2007). The increased pixel size of the 30 cm imagery would lead to a reduction in the number of gaps visible in the canopy resulting in an overestimating of the green woody fraction at some sites. Examination of the scatter plots in Figure 2.6 indicates that PPC was in general being underestimated by the AP_{GWC} . This suggests something other than the non-green component of the canopy is influencing the scatter observed around the 1:1 line for UM_{FPC} and UMG_{FPC} . The increased error for the 30 cm imagery may be a result of small shrubs going undetected due the reduced spatial resolution. Previous studies have shown that detection of smaller shrubs can be problematic due to the spatial resolution of the imagery used (Robinson et al. 2008, Browning et al. 2009). Comparisons of twenty sites where imagery was captured at both GSD of 15 cm and 30 cm suggest that aerial AP_{GWC} measures were not significantly different. While the statistical tests indicate that there was no significant difference, a number of sites varied by up to 22%. These outliers (Figure 2.7) could be a result of real changes occurring at these sites due to the different image capture dates, up to 35 months in some instances. The difference observed could be due to factors such as fire which occur at these sites on a regular basis (Murphy et al. 2010) or storm events which result in wind-throw and damage to tree crowns (Staben and Evans 2008, Franklin et al. 2010). The differences in green woody vegetation may also be as a result of annual seasonal variation in FPC at these sites. Sites with the greatest difference in green woody vegetation were located in *Eucalyptus tetrodonta* and *E. miniata* dominated woodlands, which contain understories of mixed species. The differences measured in the aerial photography may represent natural variation in leaf fall and leaf flush, which occurs during the year (Williams et al. 1997, O'Grady et al. 2000). Williams et al. (1997) identified four main phenological types in the Darwin region, which included evergreen, brevidecidous or partly deciduous, semi-deciduous and fully deciduous species and reported that there were significant interannual, interspecific and intraspecific differences in leaf phenophases, over the 2.5 years period of their study. An example of seasonal variation in green woody vegetation visible in the imagery captured at 15 cm GSD on different dates is shown in Figure 2.10. Field measurements also captured the seasonal variability at this site with data collected on the 05/06/2012 and 23/05/2013 resulting in UMG_{FPC} values of 41% and 55% respectively. This example highlights the sensitivity of the imagery to detect the changes in green woody vegetation at this site.

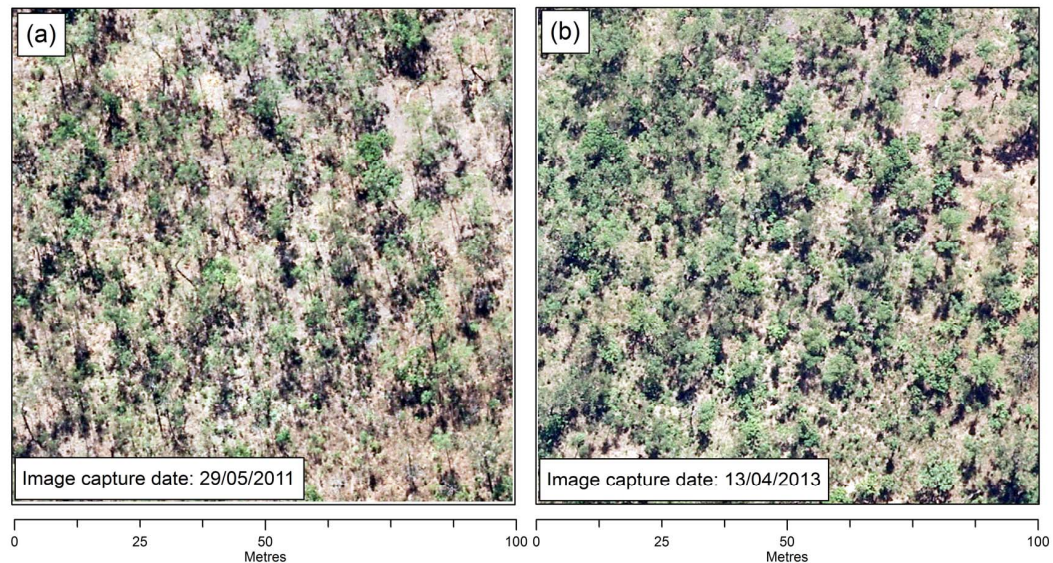


Fig. 2.10 Example of the seasonal differences in green woody vegetation captured in different date imagery (GSD 15 cm) for the same field site.

Some of the difference between field and image derived estimates could be due to error in the field surveys. The star transect used to measure these sites represents a sample of the woody cover over an area of 1 ha. In sites where there is a low density of tree cover it is possible that the configuration of the three 100 m transects may fail to detect individual trees, resulting in an underestimation of cover. This did occur on one site where no woody cover was measured along the three 100 m transects, however, there were clearly a number of trees visible in the imagery. While every effort is made to locate field sites in areas of homogeneous tree cover, the natural variability in the distribution of trees at a site may also result in an over or underestimation of woody cover. This is largely determined by the location of the star transect at the site, which may sample a disproportionate of either tree canopy or bare ground. This is one advantage in using aerial photography as it enables a complete census of the 1 ha plot, removing one of the limitations of the field survey in sites where there is scattered or uneven clumping of woody vegetation.

Shadow can also reduce the overall accuracy of estimates of canopy parameters from aerial photography with the shadow from taller trees obscuring adjacent lower tree canopy (Coggins et al. 2008). To reduce the impact of shadow in the imagery Coggins et al. (2008) recommended that imagery could be captured during overcast condition and during times that reduce the impact of the sun angle. While the timing of the capture of the aerial photography used in this study is restricted to reduce the effect of the sun angle in an image, shadow did impact on the estimates of AP_{GWC} in sites with high cover such as the monsoon rainforest. This was evident in the monsoon rainforest site

for both GSD 15 cm and 30 cm, where shadows from taller trees were obscuring the canopy of lower trees reducing the overall accuracy by 13% and 16% respectively. It is also possible that the underestimation in UMG_{FPC} in more open sites was due to shadows from taller trees obscuring woody vegetation in the mid and ground stratum. The addition of the infrared spectral band (not available in this study) would enable vegetation indices to be produced and may assist in the discrimination of green and non-green vegetation in the imagery. Standard image enhancement of the 8-bit imagery during the selection of segments to train the classification did not enable identification of vegetation within shadows. If the operator training the image classification is able to identify objects within shadow it may be possible to create an additional class to identify the fraction of green vegetation within shadow. The reduction in the radiometric resolution of the imagery limited the detection of vegetation within shadows, however, discrimination between green fractions for woody and non-woody vegetation was reasonably successful (Tables 2.7 and 2.8). While most aerial photography captured in the NT is during the dryer months when grass species are senescent, a number of the field sites used in this study contained non-woody green vegetation such as spinifex. Spinifex is a perennially green grass, which is found across large tracks of the Northern Territory (Wilson et al. 1990). Despite the limited radiometric resolution of the 8-bit data, the supervised nearest neighbour classification algorithm used in this project was able to spectrally separate the different green fractions for larger trees and non-woody spinifex species within imagery captured at 30 cm GSD. It should be noted that the method used in this study relies on the operator selecting the training samples in the imagery. If the operator selecting the training samples is not familiar with the objects visible in the imagery the results are likely to be erroneous. At one site located in the southern NT, separation of small shrubs (chenopods, height range 0.01–0.03 m) from non-woody green vegetation was not able to be achieved. In this example, the green component of the small shrub was not able to be identified in the 30 cm GSD imagery. The apparent shadow of these shrubs was visible in the imagery and classified accordingly. When the percentage of shadow in the imagery (2.97%) was compared with the woody cover measured in the field (2.33%) the results were very similar with only 0.64% difference. While the results at this site suggest that shadow was representative of the woody FPC it is likely that the green woody component of these shrubs were not able to be resolved in the 8-bit 30 cm imagery. The supervised classification method used in this study requires that the targets being classified are visible to the operator selecting the training classes. In this instance, imagery captured at a smaller GSD may enable these small shrubs to be identified and classified. Laliberte et al. (2010) reported high correlation between image-derived and field-measured shrub cover using very high resolution digital imagery captured at 4 cm GSD. They used an OBIA classification method and were able to classify all the dominant shrub species in their plots. In general, they found

that the image-derived shrub cover was higher than the field-measured cover, however, for some shrub species estimates derived from the imagery were lower, possibly due to smaller shrubs (< 12 cm x 12 cm) not being detected in the imagery (Laliberte et al. 2010).

The development of allometric relationships between tree structural attributes is well established (O'Grady et al. 2000, Cook et al. 2005, Williams et al. 2005, Suganuma et al. 2006, Armston et al. 2009). O'Grady et al. (2000) reported strong relationships between field-measured leaf area index (LAI) and basal area for the dominant woodland tree species *Eucalyptus tetrodonta* and *E. miniata* in the northern half of the NT. Allometric relationships based on field-measured parameters have also been developed to predict woody FPC from SBA across the state of Queensland, Australia, with reported RMSE of 7.26% (Armston et al. 2009). Similar allometric relationships between field-measured live SBA and UMG_{FPC} have been developed across the Northern Territory (based on 167 field sites), resulting in an RMSE of 7.48% (unpublished data). In this study, the inverse of this relationship was applied to 127 field sites to develop an allometric equation to predict live SBA from woody UMG_{FPC} measured in the field. A number of studies have developed models to predict SBA from CC estimates derived from aerial photography (Fensham et al. 2002, Coggins et al. 2008). Coggins et al. (2008) used digital aerial photography captured at 10 cm GSD to measure canopy crown area of individual lodgepole pine trees. Prediction equations were developed between field-measured tree crown area and stem diameter (cm) from individual trees, which were applied to the crown area estimated from the aerial photography to predict stocking densities (Coggins et al. 2008).

In this study, there was very little difference between the values of the error statistics for data used to develop the allometric relationship and data used independently to assess the overall accuracy of the predicted live SBA (Table 2.11). While there is inherent scatter in the relationship between live SBA and UMG_{FPC} (Fig. 2.8) the close agreement between live SBA values predicted from the independent validation sites from both field and aerial photographs supports the fact that UMG_{FPC} is being accurately estimated from aerial photographs at a similar accuracy level to the field measurements. Unless there is some sort of disturbance at a site, the live SBA is not likely to change dramatically during the year. The natural seasonal variability in woody FPC values due to the presence of deciduous species is likely to be contributing to the error in the estimates of live SBA derived from the aerial photography.

The close agreement demonstrated in this study between AP_{GWC} estimates obtained from the aerial photography and field measured UMG_{FPC} have the potential to be used

in a number of different applications, including the calibration and validation of image products derived from coarser spatial resolution satellite imagery such as Landsat. The prediction of biophysical parameters, such as woody FPC from coarser spatial resolution satellite imagery at a regional scale requires a significant quantity of samples representing the variability and range of woody FPC. This type of information is typically obtained from the collection of field data and represents a significant financial investment (Cohen et al. 2003). The methodology and assessment of the AP_{GWC} estimates derived from aerial photography in this study would enable a large number of surrogate field sites to be obtained from vegetation communities across the full spectrum of woody FPC values in the Northern Territory. The use of the digital aerial photography enables sites to be randomly selected, reducing bias in site selection, reducing the risk of spatial autocorrelation, and enabling sufficient sites to be produced for comprehensive accuracy assessments. While large numbers of surrogate field sites could be obtained, the need to collect field data can never be completely replaced by the methodology developed in this study. This is highlighted by the effect of shadow in the imagery where estimates in sites with high woody cover such as monsoon forests are likely to be underestimated. Analysis of digital aerial photography with the addition of the fourth multispectral infrared band and full dynamic range may reduce this error, and requires further investigation. One of the major benefits of this study is the ability to extract biophysical parameters from the historical archive of digital aerial photography. This is particularly relevant when the satellite imagery (such as Landsat-5 TM) is no longer operational and field estimates are required coincident with the image overpass. The results of this study show seasonal variability in green woody vegetation could be detected in the digital aerial photography. This sensitivity suggests that when relating biophysical parameters (derived from the aerial photography) to satellite imagery it is important to obtain satellite imagery coincident as possible with the capture date of the aerial photography.

2.5 Conclusion

The overall goal of this study was to investigate the use of digital aerial photography as a surrogate for the collection of field data. The findings of this study show that there is a strong relationship between field-measured woody UMG_{FPC} and AP_{GWC} derived from aerial photography captured across a broad range of vegetation communities in the Northern Territory (NT), Australia. To our knowledge this is the first study that looks at the relationship between field measured woody FPC (measured using the Australian national standard methodology), based on an extensive field dataset covering a diverse range of vegetation communities, and biophysical parameters from digital aerial photography in the NT. Statistical analysis shows that quantitative measurements of the

UMG_{FPC} can be extracted from digital aerial photography captured at GSD of 15 cm and 30 cm. Evidence of the relationship is further highlighted by the close agreement of live SBA predicted from both UMG_{FPC} and AP_{GWC} using allometric relationship developed from field measured data. The classification methodology presented in this paper relies on the operator's ability to identify green woody and non-green material in the imagery. Despite the reduced dynamic range (8-bit) of the aerial photography used in this project, the supervised classification of the aerial photography using an object based image analysis approach, enabled green woody components in the imagery to be quantified across a diverse range of vegetation communities. The use of aerial photography to obtain woody FPC estimates has advantages for sites with low tree density, as it samples the entire image ensuring all trees are detected. Shadow is likely to limit its use in areas with very high woody cover, however, it may be possible that imagery retaining the full dynamic range (14-bit) of the sensor and the addition of the near infrared band may enable green woody vegetation to be identified within shadow areas. The aerial photography classified in this study was subset to represent 100 m × 100 m field sites designed to be used for the calibration and validation of Landsat satellite sensors. However, it is also possible that larger areas could be classified, providing a source of calibration and validation data for other coarser spatial resolution sensors such as MODIS.

CHAPTER 3

Modelling LiDAR derived tree canopy height from Landsat TM, ETM+ and OLI satellite imagery:a machine learning approach.

Thesis context: The focus of this chapter is on the development of a remote sensing product that provides estimates of woody vegetation vertical structure (mean canopy height). The results demonstrated that canopy height can be predicted from Landsat satellite imagery at moderate to high levels of accuracy across a range of vegetation communities. The methodology developed and the limitations identified in this study were used to guide and refine the development of remote sensing products predicting seven woody vegetation structural metrics, characterising height from both Landsat-8 and Sentinel-2 satellite sensors (chapter 4). This chapter has been published in the "International Journal of Applied Earth Observation and Geoinformation".

Staben, G., Lucieer, A. and Scarth, P. (2018), 'Modelling LiDAR derived tree canopy height from Landsat TM, ETM+ and OLI satellite imagery — A machine learning approach', International Journal of Applied Earth Observation and Geoinformation 73, 666–681 <https://www.sciencedirect.com/science/article/pii/S0303243418303970>

Abstract

Understanding ecological changes in native vegetation communities often requires information over long time periods (multiple decades). Tropical cyclones can have a major impact on woody vegetation structure across northern Australia, however understanding the impacts on woody vegetation structure is limited. Woody vegetation structural attributes such as height are used in ecological studies to identify long term changes and trends. LiDAR has been used to measure woody vegetation structure, however LiDAR datasets cover relatively small areas and historical coverage is restricted, limiting the use of this technology for monitoring long-term change. The Landsat archive spans multiple decades and is suitable for regional/continental assessment. Advances in predictive modelling using machine learning algorithms have enabled complex relationships between dependent and independent variables to be identified. The aim of this study is to develop a predictive model to estimate woody vegetation height from Landsat imagery to assist in understanding change through space and time. A LiDAR canopy height model was produced covering a range of vegetation commun-

ties in northern Australia (Darwin region) for use as the dependent variable. A random forest regression model was developed to predict mean LiDAR canopy height (30 m spatial resolution) from Landsat-5 Thematic Mapper (TM). Validation of the random forest model was undertaken on independent data ($n = 30,500$) resulting in an overall $R^2 = 0.53$, RMSE of 2.8 m. Assessment of the RMSE within four broad vegetation communities ranged from 2.5 to 3.7 m with the two dominant communities in the study area Mangrove forests and Eucalyptus communities recording an RMSE value of 2.9 m and 2.5 m respectively. The model was also applied to Landsat-7 Enhanced Thematic Mapper Plus (ETM+) resulting in an R^2 of 0.49, RMSE of 2.8 m. The model was then applied to all cloud free Landsat-5 TM, Landsat-7 ETM+ and Landsat-8 Operational Land Imager (OLI) imagery (106/69 path/row) available between the months April, May and June for 1987 to 2016 to produce annual estimates (29 years) of canopy height. A number of time traces were produced to illustrate tree canopy height through time in the Darwin region which was severely impacted by cyclone (hurricane) Tracy on the 25th December 1974.

3.1 Introduction

The value of remote sensing in ecological studies has been well recognised (Roughgarden et al. 1991, Wang, Franklin, Guo and Cattet 2010, Pettorelli et al. 2014). Landsat satellites have been capturing multispectral imagery of the earth surface since 1972 representing the longest record of temporal space-borne land observations (Roy et al. 2010). Landsat data has been used for a variety of applications, such as natural hazard assessment (Barlow et al. 2003, Joyce et al. 2009), fire scar mapping (Gill et al. 2000, Goodwin and Collett 2014), coral reef mapping (Joyce et al. 2004), rangeland monitoring (Wallace et al. 2004, Scarth et al. 2010), temperate and tropical forest mapping (Brown et al. 2000, Renó et al. 2011), and many others. The characteristics of the Landsat sensors have been identified as valuable for regional monitoring applications (Cohen and Goward 2004). The spectral and spatial resolution of the Landsat imagery combined with its temporal record make it valuable for monitoring woody cover change across large regions (Woodcock et al. 2001, Danaher et al. 2004, Staben et al. 2016, Gill et al. 2017). Amongst its many applications Landsat imagery has been utilised to detect severe forest damage (Ekstrand 1996) including damage as a result of cyclonic (hurricane) winds (Preston 1987, Paling et al. 2008, Staben and Evans 2008).

Tropical cyclones occur on a frequent basis across the coastline of the Australian Northern Territory. The destructive winds associated with these cyclones can have a major impact on both the man-made and natural environments. The impact of cyclonic winds

are greatest on the coastal regions, however they also have the potential to cause significant disturbance further inland (e.g. Cyclone Monica) (Staben and Evans 2008). The impact on native vegetation can be significant, resulting in major structural changes to vegetation communities. A number of studies have reported on the impact of cyclones on vegetation in the Northern Territory (Stocker 1976, Fox 1980, Cameron et al. 1983, Bowman and Panton 1994b, Cook and Goyens 2008, Staben and Evans 2008, Williamson et al. 2011, Hutley et al. 2013). These studies have used a number of methods ranging from collection of field data, aerial photography and satellite imagery. Although cyclones are frequent and have the potential to be a major disturbance agent in ecosystems across the Northern Territory (Murphy 1984), very few studies have been undertaken to quantify the impact and potential role they play in driving the structure of these communities (Cook and Goyens 2008). While it is well recognised that fire and the stress of the seasonal drought (a characteristic of the wet-dry tropics of northern Australia) are frequent disturbance factors on vegetation communities, very little focus has been given to the impact cyclones have on these ecosystems (Cook and Goyens 2008, Hutley et al. 2013).

While severe damage to woody vegetation can be relatively easy to identify by comparing satellite imagery captured directly before and after the change event (e.g. cyclones), accurate assessment of the subtle changes through time is enhanced by relating biophysical variables to satellite remote sensing observations. To obtain quantitative information from optical satellite data relationships between biophysical variables need to be established (Moulin et al. 1998). Numerous studies have derived empirical relationships between Landsat imagery and field based measurements such as; leaf area index (Coops et al. 1997, Eriksson et al. 2006), above ground biomass of woody vegetation (Foody et al. 2003, Powell et al. 2010, Avitabile et al. 2012), fractional cover (Scarth et al. 2010) and woody vegetation foliage projective cover (Danaher et al. 2004, Armston et al. 2009). A variety of statistical methods have been used to develop these relationships including, linear and non-linear regression models based on single or multiple predictor variables (Cohen et al. 2003), while others have used machine learning algorithms such as neural networks, tree-based models, K-nearest neighbours and support vector machines (Labrecque et al. 2006, Li et al. 2010, Avitabile et al. 2012).

Vegetation height has been identified as a key parameter for inferring long term trends in biomass and carbon stock (Skidmore et al. 2015, Cook et al. 2015). Combined with species and site quality information vegetation height helps to inform estimates of stand age and successional stages (Stojanova et al. 2010). Light detection and ranging (LiDAR) data has been used extensively to measure woody vegetation structure, and while LiDAR is an efficient way to map and measure woody vegetation structure (Lim et al.

2003, Wulder, White, Nelson, Næsset, Ørka, Coops, Hilker, Bater and Gobakken 2012, Goldbergs et al. 2018), the use of these data at a regional level can be prohibitive due to financial constraints Pascual et al. (2010). Furthermore, the availability of LiDAR for long-term studies (multiple decades) is limited due to the paucity of data. Ecological processes can occur over long time frames, and understanding these processes often requires information recorded over multiple decades, captured at an appropriate spatial, spectral and temporal resolution. Numerous studies have used structural information obtained from LiDAR data to develop predictive models using Landsat sensors with an aim to enhance the spatial and temporal coverage (Hudak et al. 2002, Pascual et al. 2010, Hill et al. 2011, Ota et al. 2014, Ahmed et al. 2015). These studies have been undertaken across a variety of vegetation communities ranging from conifer forests (Ahmed et al. 2015) to tropical evergreen and deciduous forests (Ota et al. 2014, Hill et al. 2011, Wilkes et al. 2015). In southern Australia, Wilkes et al. (2015) predicted canopy height over a 2.9 million ha area of heterogeneous temperate forests by developing a relationship between LiDAR derived canopy height and a combination of satellite imagery (Landsat and Moderate Resolution Imaging Spectroradiometer) using the random forest algorithm. Machine learning techniques based on ensemble models such as random forest have been used successfully for a variety of remote sensing classification and regression modelling applications (Pal 2005, Avitabile et al. 2012, Mellor et al. 2013, Mascaro et al. 2014, Karlson et al. 2015, Wilkes et al. 2015, Mellor et al. 2015). These studies demonstrate the advantages of random forest algorithm such as its robustness to outliers in the training data, ability to handle non-parametric data, its ability to uncover complicated non-linear relationships between variables and the ease in tuning the models parameters.

In this study, we investigate the application of Landsat satellite sensors to predict woody vegetation canopy height and develop a model predicting canopy height across a range of vegetation communities in the wet-dry tropics of Northern Australia. While previous studies have demonstrated a fusion of different sensors and LiDAR to derive predictive models of canopy height in Australia (Wilkes et al. 2015), this study investigates the use Landsat sensors only for the estimation of canopy height over a long time series of multiple decades. To our knowledge, this is the first study to look at predicting LiDAR derived canopy height from Landsat sensors in the wet-dry tropics of northern Australia. A canopy height model (1 m spatial resolution) was produced from a LiDAR dataset captured in 2009 for use as the dependent variable. Random forest regression was used to produce a model to predict LiDAR derived canopy height from a single Landsat-5 Thematic Mapper (TM) image captured in 2009 (30 m spatial resolution). We developed a three-stage approach to identify the important independent variables and optimise the parameters used in the random forest model, which was applied to Landsat-5

TM, Landsat-7 Enhanced Thematic Mapper Plus (ETM+) and Landsat-8 Operational Land Imager (OLI) sensors.

3.2 Data and Methods

3.2.1 Study Area

This study was undertaken in the Darwin region, located in northern Australia's wet dry tropics (Figure 3.1). The average annual temperature for the Darwin region is 32° with average annual rainfall of 1729 mm, with the majority of the precipitation occurring during October and April. The study site covers an area of approximately 1,800 km² consisting of urban, peri-urban development and native vegetation. The dominant native vegetation communities occurring in the study area include Mangrove forests and Eucalyptus open forest to woodlands. Eucalyptus communities are dominated by *E tetrodonta* and *E. miniata* woodlands (average height 15 m) to open forests containing a mid-stratum of semi-deciduous to deciduous trees and shrubs such as *Corymbia polycsiada*, *E.porreota*, *Livistona humifis*, *Terminalia ferdinandiana* and *Xanthostemon paradoxus* and grasses (Brock 1995, Williams et al. 1997, O'Grady et al. 1999). Mangrove communities consist of a variety of species, the two dominate species mapped by Brocklehurst and Edmeades (1996) included *Ceriops tagal* closed to open forests (heights 1 m to 10 m) and *Rhizophora stylosa* closed forest, heights between 6 to 18 m tall. Stands of Melaleuca species are located on the floodplain and riparian zones across the study area (Brock 1995). Patches of wet and dry Monsoon forests are also found across the study area, containing a mix of species. Canopy height in wet monsoon forest rarely exceeds 25 m while dry monsoon forest canopies range from 10 m to 17 m (Bach 2002, Brock 1995).

3.2.2 LiDAR Canopy Height Model

The airborne LiDAR used in this study was captured between the 3rd and 5th of July 2009 using a LEICA ALS50-II laser scanner, on-board a Cessna 404 aircraft. LiDAR data were captured within two hours of low tide at a nominal flying height of 2012 m AGL. The LiDAR's foot print was 0.45 m in diameter with an average point density of 1.1 m². These data were pre-processed by contractors and supplied as las files containing 4 discrete returns. A pit filled canopy height model (CHM) was produced at a spatial resolution of 1 m using the suite of LAStools (Khosravipour et al. 2014) (Figure 3.2 (a)). The las files were first classified as either ground or non-ground using the lasground tool. These classified las files were then used to normalise the z coordinates

of the non-ground returns to represent relative height at ground level (LAsTools 2017). The final step was to produce the raster CHM using the lasgrid tool. As the LiDAR was captured with an average point density of 1.1 m^2 the pixel size for the output raster layer was set to 1 m. The parameter "-highest" was used as it ensures that only the highest z coordinate for each 1 m^2 pixel is used to produce the CHM. The parameter "-subcircle" which converts each point to a disc shape was used to remove pits within the tree canopies, for this study the subcircle parameter was set to 0.3 m^1 . At the time of the LiDAR capture (July, mid dry season), the native grasses in the study area were senescent. While the grass understory is senescent it would in some instances represent the highest z coordinate for a given pixel in the development of the CHM. As native grasses in the NT savannas are generally 0.5 m in height(Setterfield et al. 2010) pixels $\leq 0.5 \text{ m}$ were removed, resulting in a CHM with values ranging from 0.51-36.5 m used to produce the dependent variable, mean canopy height.

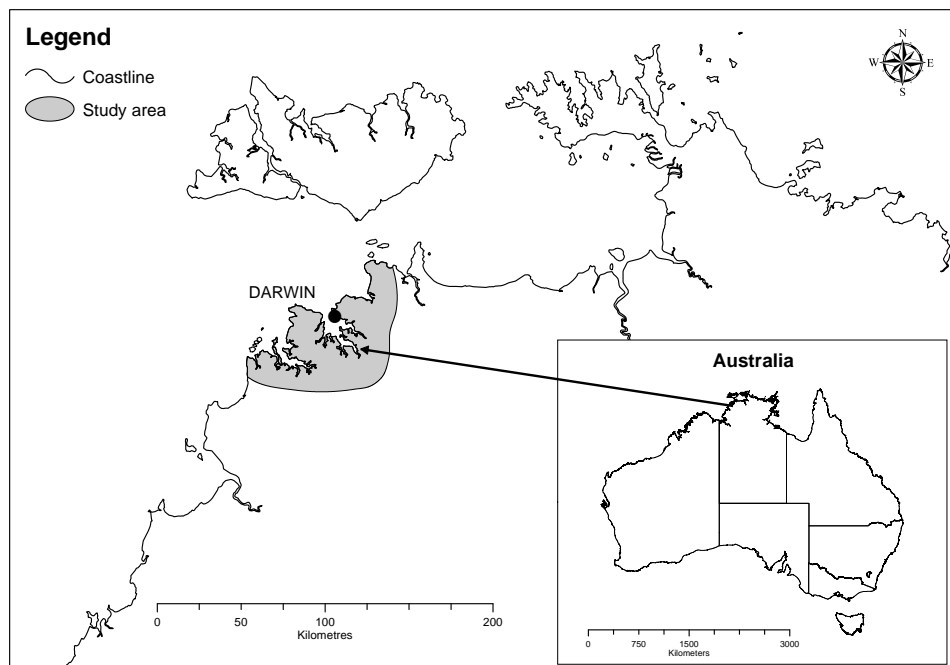


Fig. 3.1 Location of the study area in Northern Territory of Australia.

3.2.3 Satellite imagery

Details of the Landsat satellite imagery used to develop and validate the canopy height model in this project are shown in table 3.1. The canopy height model was developed using a Landsat-5 TM image captured on the 26th of May 2009. This image date was chosen as it was the first cloud free Landsat-5 TM image captured between the transition from the monsoon wet season to the dry season. A number of images capture in 2009, 2013 and 2016 were used to assess how well the final canopy height model generalised

¹<http://rapidlasso.com/2014/11/04/rasterizing-perfect-canopy-height-models-from-lidar/>

between sensors and years (table 3.1). Time series analysis was also undertaken to produce canopy height estimates from Landsat imagery captured between the years 1987 and 2016 to further evaluate the generalisation error. Details of the imagery used to produce the time series are provided as supplementary material.

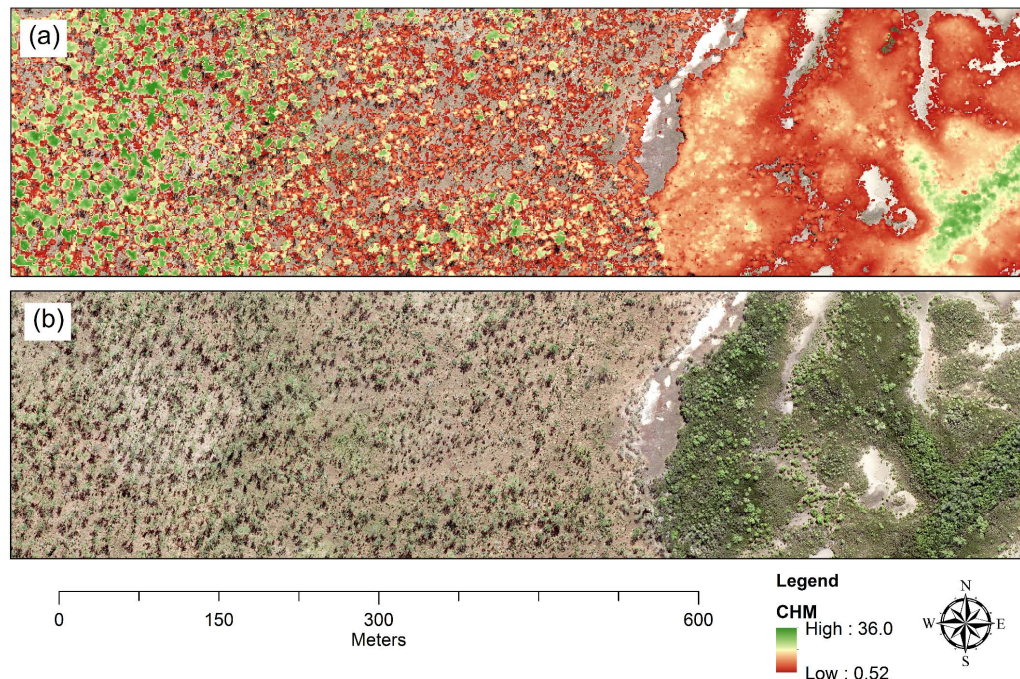


Fig. 3.2 Example of the canopy height model produced from the LiDAR data captured in 2009 (a) over Eucalyptus woodland (West) and transition to Mangrove forest (in the Eastern side of the figure), 15 cm digital aerial photography (b) shown for clarity.

Imagery captured in the early dry season was chosen to minimise the impact of fire scars in the imagery, as large areas of northern Australia are burnt each year with prescribed burning undertaken by land managers at the onset of the dry season as the grass under-story starts to become senescent (Edwards et al. 2013). While imagery captured later into the dry season (June - August) has the potential to provide greater spectral separability between woody and non-woody vegetation the impact of fire scars in the imagery limits the use of these data for producing woody vegetation structure maps. The Landsat image used in this study was atmospherically corrected using 6S radiative transfer code and a bi-directional reflectance distribution function (BRDF) model was applied to the imagery. This BRDF model takes into account topographic illumination effects and produces surface reflectance values to a standard view geometry (Flood 2014). For a detailed description of the image pre-processing applied to the Landsat imagery used in this study see Flood et al. (2013). To reduce noise introduced by differing atmospheric conditions between image dates, the Blue spectral band which is sensitive to

aerosol conditions (Flood 2014) was not used in the development of the canopy height model. In addition to the five multispectral bands (Green, Red, Near-Infrared (NIR), Short Wave Infrared 1 (SWIR1), Short Wave Infrared 2 (SWIR2)), a number of band ratios and vegetation indices were derived to investigate the relationship between mean canopy height and Landsat-5 TM derived predictor variables.

Table 3.1 Landsat-5 TM and 7 ETM+ imagery used in the development* and validation of the canopy height model.

Sensor	WRS-2 path/row	Capture date
Landsat-5 TM*	106/69	26/05/2009
Landsat-5 TM	106/68	26/05/2009
Landsat-7 ETM+	106/68	19/06/2009
Landsat-7 ETM+	106/69	27/04/2013
Landsat-8 OLI	106/69	19/04/2013
Landsat-7 ETM+	106/69	21/05/2016
Landsat-8 OLI	106/69	13/05/2016

3.2.3.1 Vegetation indices and band ratios

The vegetation indices investigated in this study included the more common NIR and Red band indices such as Normalised Difference Vegetation Index (NDVI) and Modified Simple Ratio (MSR), and several indices based on the SWIR and Green spectral bands. A combination of the ratios of all the five surface reflectance bands was also investigated. A total of 12 vegetation indices detailed in table 3.2 and 10 band ratios was calculated for this study.

3.2.4 Training and Validation data

The training and validation data were obtained from separate areas within the extent of the LiDAR CHM shown in figure 3.3.

3.2.4.1 Training data

The training data were located within the extent of Landsat scene 106/69 (path/row) while the validation data were located within the extent of the scene 106/68. Validation data were obtained from areas outside of the extent of the training data to reduce auto-correlation between the training and validation data. To produce the training dataset the mean value for the LiDAR CHM was calculated for each $30 \times 30\text{ m}$ pixel (excluding urban areas), resulting in CHM values ranging from 0 m to 29.1 m and a mean value of 10.5 m. While there is likely to be some misregistration between the location of the LiDAR canopy height model and pixels in the Landsat imagery, we chose a $30 \times 30\text{ m}$

Table 3.2 Vegetation indices and band ratios used in this study.

Spectral Index	Formula	Reference
Normalized Difference Vegetation Index	$NDVI = \frac{NIR - Red}{NIR + Red}$	Tucker (1979)
Green Soil Adjusted Vegetation Index	$GSAVI = \frac{(NIR + Green + 0.5) * (1 + 0.5)}{(NIR + Green)}$	Sripada et al. (2006)
Green Normalised Vegetation Index	$GNDVI = \frac{NIR - Green}{NIR + Green}$	Buschmann and Nagel (1993)
Chlorophyll Vegetation Index	$CVI = \frac{NIR}{Green} * \frac{Red}{Green}$	Vincini et al. (2008)
Normalized Difference Greenness Index NDGI	$NDGI = \frac{Green + Red}{NIR - SWIR2}$	Bannari et al. (1995)
Normalized Burn Ratio SWIR2 (Band 7)	$NBR = \frac{NIR + SWIR2}{NIR - SWIR1}$	Ji et al. (2011)
Normalized Burn Ratio SWIR1 (Band 5)	$NDII = \frac{NIR + SWIR1}{NIR + SWIR2}$	Ji et al. (2011)
Green Difference Vegetation Index	$GDVI = NIR - Green$	Sripada et al. (2006)
Modified Soil Adjusted Vegetation Index	$MSAVI = \frac{2 * NIR + 1 - \sqrt{(2 * NIR + 1)^2 - 8 * (NIR - Red)}}{2}$	Qi et al. (1994)
Difference Vegetation Index	$DVI = NIR - Red$	Tucker (1979)
Soil adjusted Vegetation index	$SAVI = \frac{NIR - Red}{(NIR + Red + 0.5) * (1 + 0.5)}$	Huete (1988)
Modified Simple Ratio	$MSR = \left(\frac{\sqrt{nir}}{\sqrt{Red}} \right) - 1$	Chen (1996)

window to ensure that the maximum mean LiDAR canopy height range was achieved in the training data. Increasing the window size (e.g. $90 \times 90\text{ m}$) to account for any misregistration between the two datasets reduces the maximum height values ($\approx 4\text{ m}$) in the training dataset. As the random forest algorithm will only predict within the bounds of the training data it was important to maintain as much of the height range as possible. It also ensures that as much of the variance in the spectral values of the Landsat image is seen by the model. A stratified random sampling approach for height ranges between 0 and 18 m was taken to ensure that the values of the dependent variable (mean canopy height) were evenly distributed across the height range in the study area (Figure 3.3). For canopy heights ranging between 19 m – 20 m, only 405 pixels were available, while for heights between 20 m and 29.1 m, only 927 pixels were present. In an attempt to create a more balanced training dataset and retain as much variance as possible, 500 pixels were randomly selected at 1 m intervals between 0.51 m and 18 m. An additional 500 pixels were randomly selected from pixels where no canopy height was recorded, resulting in a training dataset with 11,322 pixels.

3.2.4.2 Validation data

Canopy height estimates predicted from Landsat-5 TM and Landsat-7 ETM+ (Table 3.1) imagery for 106/68 (path/row) were obtained and compared with the mean LiDAR CHM values. Pixels in the Landsat-5 TM corresponding with the pixels affected by the scan-line corrector error in the Landsat-7 ETM+ imagery were removed from further analysis. Any pixels impacted by cloud, water or fire in both the Landsat-5 TM and Landsat-7 ETM+ imagery were also removed, resulting in a total of 30,500 pixels available to assess the accuracy of the final canopy height model. The CHM values from the validation pixels ranged from 0 m to 25.1 m and a mean value of 7.9 m. Additional assessment was also undertaken to produce accuracy statistics in four vegetation community groups in the region using 1:25,000 scale remnant vegetation mapping (Brock 1995). To further evaluate the generalisation error the canopy height model was applied to a time series of Landsat imagery captured between 1987 and 2016 for sites located in the Darwin region scene 106/69 (path/row).

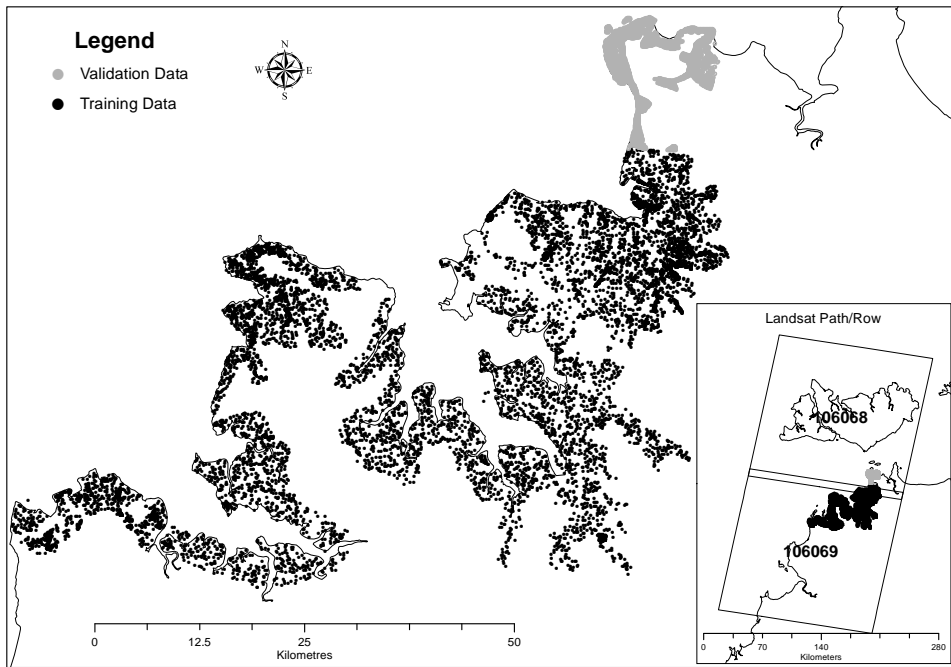


Fig. 3.3 Location of training and validation data within the extent of the LiDAR data.

3.2.5 Random Forest Model Development

Random forest is an ensemble learning algorithm (Breiman 2001) consisting of many decision trees built from a bootstrap sample of the training data. These individual decision trees are then combined to produce a more accurate model (Cutler et al. 2007). Random forest is able to handle thousands of input variables with complex non-linear relationships (Breiman 2001, Cutler et al. 2007). The random forest algorithm used in this study is implemented in the open source Python module Scikit-learn (Pedregosa et al. 2011). At a minimum there are two parameters that need to be set to produce a random forest model (Rodriguez-Galiano et al. 2012). These parameters define the number of trees (`n_estimators`) used and the number of prediction variables (`max_features`) used to grow the tree. One advantage of random forest is that it also calculates the relative feature importance for each predictor variable for the model (Strobl et al. 2008). In this study we undertook a number of experiments to identify the number of decision trees, important predictor variables and the number of features to grow the trees in the random forest model. This was undertaken to produce a model that would generalise through time and be computationally practical when applied to an archive of time series imagery (Landsat sensors TM, ETM+, OLI) used in this study.

3.2.5.1 Model Development Stage One: optimising number of trees

In the first stage, the optimal number of decision trees (`n_estimators` parameter) used to build the model was identified. Studies have shown that predictive accuracy of the

random forest algorithm converges with the increase in the number of decision trees (Oshiro et al. 2012, Rodriguez-Galiano et al. 2012, Gao et al. 2015). Similar to the study undertaken by Oshiro et al. (2012), we assessed a range of values (2, 4, 8, 16, 32, 64, 128, 256, 512, 1024, 2048, and 4096) to identify the optimal number of decision trees. For each of the n_estimator parameters assessed the random forest model was run 100 times and, for each iteration 90 % of the training data were randomly selected to train the model, while the remaining 10 % of these data (data unseen by the model) were used to assess the predictive accuracy of the random forest model using the root mean squared error (RMSE), defined as

$$RMSE = \sqrt{\frac{\sum (y_i - x_i)^2}{n}} \quad (3.1)$$

where n is the number of observations, y_i are the observed and x_i the predicted mean canopy height respectively. For each test of the random forest model, box plot statistics were produced for the 10 % test data's RMSE scores. The candidate n_estimator parameter was selected based on the consistency of the predictive accuracy for the 100 iterations of the model. The predictor variables feature importance scores were also calculated for each run of the model and the mean feature importance score for each n_estimator was recorded for the 27 parameters tested. The predictor variables feature importance scores (highest to lowest) for the candidate n_estimator were then used in the second stage of the models development. For the first stage the max_features parameter was set to the default “auto” in Scikit-learn which uses all features.

3.2.5.2 Model Development Stage Two: variable selection.

In the second stage, highly collinear predictor variables were identified and removed from further analysis. A correlation matrix was used to assess the linear and non-linear relationships between all predictor variables. Visual assessment of the correlation matrix identified a number of the band ratios and vegetation indices that were transformations of each other. Variables that were transformations of each other were identified and the least important variable based on the feature importance score highest to lowest output from stage one were removed from further analysis. For the remaining variables, the Pearson's correlation coefficient was calculated and any predictor variables with a score ≥ 0.95 were assessed and the least important of the two variables based on the feature importance score were removed from further analysis. Predictor variables were assessed from highest to lowest based on the feature importance score out put in stage one.

3.2.5.3 Model Development Stage Three: optimising number of variables.

In the third stage, a backward elimination process was undertaken to identify the number of predictor variables and the number of features used to grow the trees (max_features). In this analysis the number of decision trees (n_estimators) and predictor variables identified in stage one and two were used as inputs for the random forest model. Two max_features parameters (auto, log2) were evaluated to optimise the number of features used to grow the trees in the random forest model. The setting “auto” is the default setting which equates to using all predictor variables, while the “log2” is the logarithm base 2 of the number of predictor variables. For each suite of predictor variables the mean feature importance score was calculated, the least important variable was removed and the process repeated until only one variable remained. Again for each suite of predictor variables 100 iterations of the random forest were run (as described above) and the mean accuracy statistics based on the independent test data (randomly selected each permutation) were calculated. This approach was taken to expose the random forest model to as much variance in the training data as possible while still assessing the predictive accuracy of the model using an independent set of data. The final candidate model was selected using the accuracy statistics (test data R² and RMSE) derived from the 100 independent runs of the random forest model for each suite of predictor variables.

3.2.5.4 Final Model Validation

The optimal suite of predictor variables max_features and n_estimators identified in stages 1, 2 and 3 were used to produce a final model from all the training data (n = 11,322). The final model was then applied to Landsat-5 TM and Landsat-7 ETM+ imagery to predict mean canopy height for path/row 106/68. Accuracy of the model was evaluated using a number of statistics, including the coefficient of determination (Zar 1984), RMSE, variance and the bias. Variance was used to assess the precision of the predicted observations;

$$variance = \frac{1}{n-1} \sum_{i=1}^n ((x_i - y_i) - \bar{e})^2 \quad (3.2)$$

where \bar{e} is the mean of the error. Bias was used to assess the average difference between the predicted and observed mean canopy height values;

$$bias = \frac{1}{n} \sum_{i=1}^n x_i - y_i \quad (3.3)$$

Validation statistics were produced from Landsat-5 TM imagery captured on the same date as the models training data, while statistics produced from Landsat-7 ETM+ were

used to assess how transferable the model was to other Landsat sensors and image capture dates. The final model was also applied to Landsat-8 OLI imagery to enable comparisons between Landsat-7 ETM+ and produce examples of time series plots for a number of sites. Canopy heights predicted from the three Landsat sensors for the years 2009, 2013 and 2016 were also compared to investigate any bias between the different sensors. This was undertaken by producing scatter plots and using the slope of the regression line forced through the origin (using ridge regression) to identify any systematic bias between sensors (Flood 2014). The final canopy height model was also applied to all available Landsat imagery for scene 106/69 between the years 1987 to 2016 and a number of time traces were produced to show canopy height estimates for this period in sites that were severely impacted by cyclone Tracy in 1974.

3.3 Results and discussion

3.3.1 Model Development Stage One: optimising number of trees

To reduce the computational burden of the random forest model we undertook an experiment to identify the optimal number of decision trees, the results are presented as box plots in figure 3.4. Each box plot represents the RMSE values for the number of trees in the random forest model (based on 100 using independent test data) with mean RMSE values ranging between 3.18 m and 3.92 m. The lowest mean RMSE score was recorded for n_estimator values 512 and 4096. These results are consistent with other studies which have found that as the number of decision trees increase the overall accuracy converges (Oshiro et al. 2012, Gao et al. 2015, Rodriguez-Galiano et al. 2012, Belgiu and Drăgu 2016). A recent review of remote sensing applications using random forest reported the number of decision trees being used ranged between 70 and 5000, with a majority using 500 to build their models (Belgiu and Drăgu 2016). Based on these studies, Belgiu and Drăgu (2016) recommended that 500 represents a default value for remote sensing data. Based on the empirical results of this study we selected 512 decision trees for further use in the development of the random forest model.

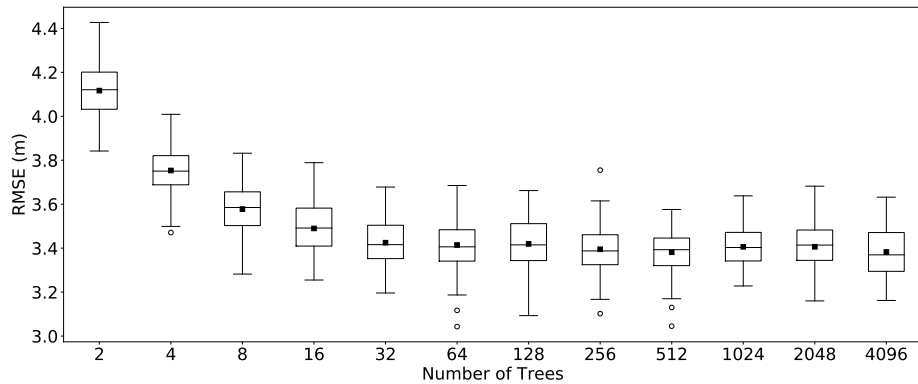


Fig. 3.4 Box plots showing the RMSE scores for the number of trees (`n_estimator`) in the random forest model, each box plot represents 100 iterations of the model where 10% of the training data is randomly selected to independently test each iteration of the model (dot = mean, box = 25th and 75th percentile, line = median, whiskers = show the range of the data).

3.3.2 Model Development Stage Two: variable selection.

While random forest is a non-parametric model that can handle complex interactions and high dimensional datasets (Breiman 2001, Strobl et al. 2008), to further increase the computational efficiency and obtain a more parsimonious model (Wilkes et al. 2015) we identified and removed predictor variables that were highly correlated. Visual assessment of a correlation matrix for the 27 predictor variables assessed in this study identified a number of the band ratios and vegetation indices that were transformations of each other. The predictor variable importance scores output for 512 decision trees (stage one, Table 3.3) were used to guide the decision on which of the correlated variables were removed. From the original 27 predictor variables, 12 were removed. Out of the 15 candidate variables, eight were combinations of band ratios, three were vegetation indices and the remaining were the single surface reflectance bands. The relationship between mean CHM and the remaining 15 candidate predictor variables are shown in scatter plots Figure 3.5. Interestingly none of the variables alone suggest a particularly strong relationship with mean LiDAR canopy height, and several variables clearly display a bimodal relationship.

Table 3.3 Results for the predictor variable importance scores (Model development Stage One) for 512 decision trees (n_estimator).

Predictor variable	Importance score	Predictor variable	Importance score
SWIR1	17.9480	SWIR2/SWIR1	1.4282
NIR/Green	14.5789	SWIR2/Green	1.3867
GNDVI	14.4570	SWIR2/NIR	1.3272
GSAVI	10.5619	NBR	1.3054
SWIR2	5.7975	CVI	1.2069
SAVI	4.7715	NIR	1.1859
SWIR1/Red	2.8598	SWIR2/Red	1.1787
SWIR1/Green	2.3242	Red	1.1585
MSR	2.2335	GDVI	0.8464
NIR/Red	2.2216	DVI	0.8196
NDVI	2.2197	MSAVI	0.8149
Green	1.9765	Red/Green	0.7292
NDII	1.9681	NDGI	0.7291
SWIR1/NIR	1.9652		

3.3.3 Model Development Stage Three: optimising number of variables.

To reduce over-fitting and further optimise the random forest model, we performed an experiment to assess different values of the max_features and the number of predictor variables used to build the model. The max_features parameter (in the scikit-learn implementation of random forest regressor) enables the user to determine the number of predictor variables randomly selected to split each node of the individual decision trees (Müller and Guido 2016). Reducing the max_features parameter increases the variance and conversely decreases the bias and produces weaker individual decision trees, however when combined in the ensemble of decision trees it increases the models overall accuracy (Breiman 2001, Rodriguez-Galiano et al. 2012). Accuracy statistics for the variable reduction and max_features parameters analysis are shown in figure 3.6. RMSE values ranged from 3.14 to 5.88 m while R² values ranged from 22% to 78%. Overall the accuracy statistics were similar for each of the max_features and number of predictor variables, with a decline in accuracy starting to occur around eight predictor variables. The highest R² value (78%) was recorded for max_features parameters “log2” and predictor variables between 11 and 15 (78%), while the lowest RMSE value was recorded for 14 predictor variables. Reducing the number of predictor variables randomly selected to split the nodes increased the overall accuracy of the model slightly; based on these results we selected the max_features parameter “log2” and the 14 predictor variables shown in Figure 3.8 to produce the canopy height model.

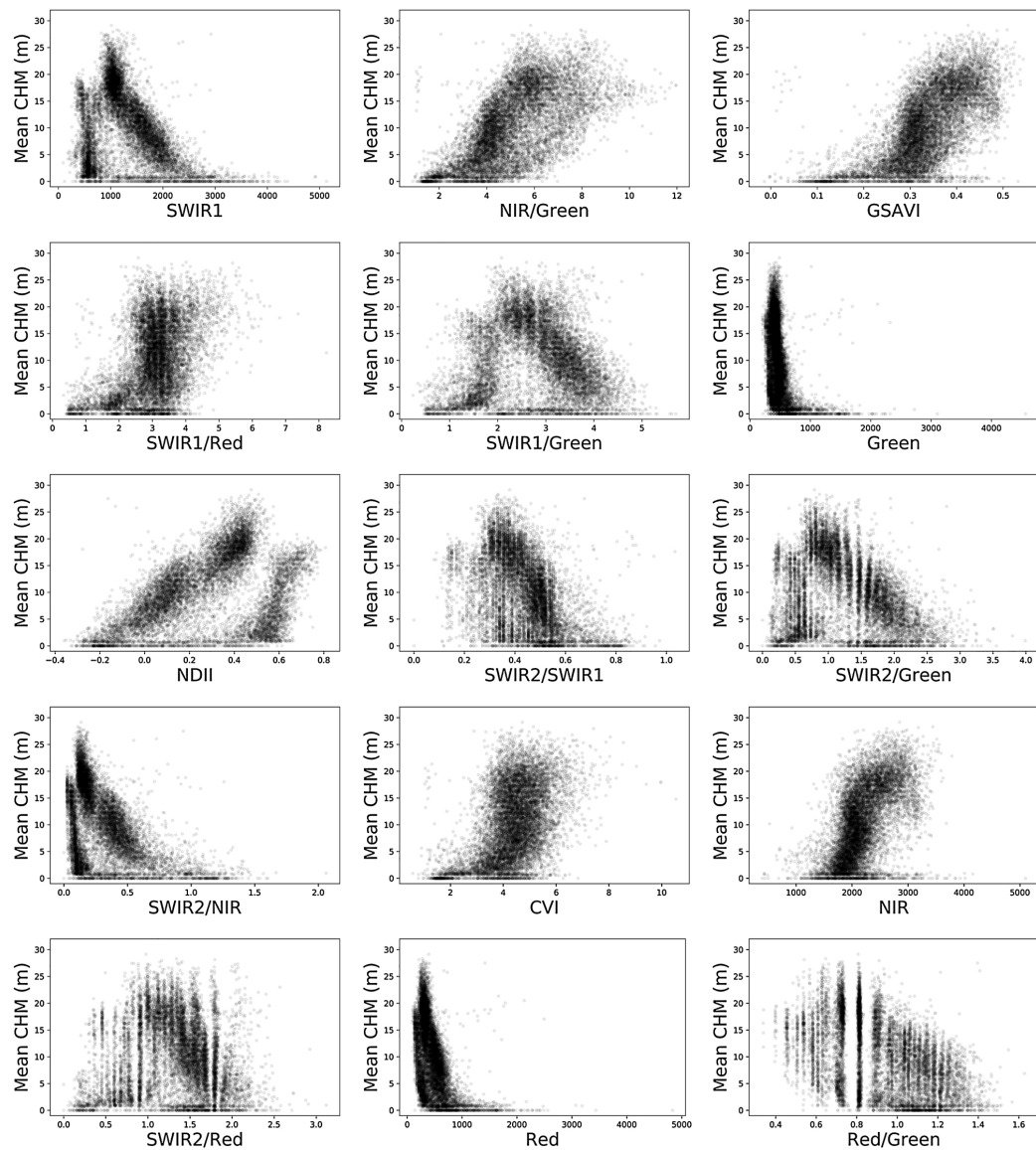


Fig. 3.5 Scatter plots showing the relationship between mean CHM and the 15 predictor variables identified in stage two of the development of the random forest model.

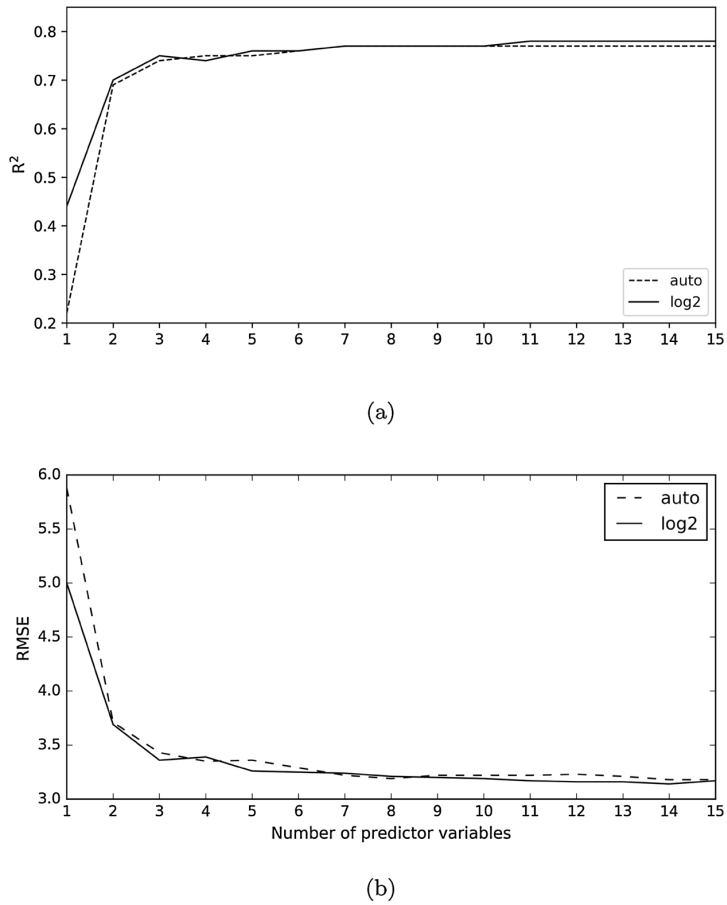


Fig. 3.6 Mean R^2 (a) and RMSE (b) values (based on 100 iterations) used to identify the number of predictor variables and the number of features used to grow the trees in the random forest model.

3.3.4 Canopy height model

The final canopy height model was developed using the following parameters; 512 decision trees, “log2” max_features parameter and 14 predictor variables based on all training data (11,322 data points). The random forest model was serialised to enable it to be applied to Landsat-5 TM, Landsat-7 ETM+ and Landsat-8 OLI imagery. To assess the accuracy of the model on independent data captured outside of the extent of the training data, the model was applied to Landsat-5 TM and Landsat-7 ETM+ imagery captured over path/row 106/68. Canopy height estimates derived from Landsat TM and ETM+ for the area used to validate the final random forest model is shown in Figure 3.7.

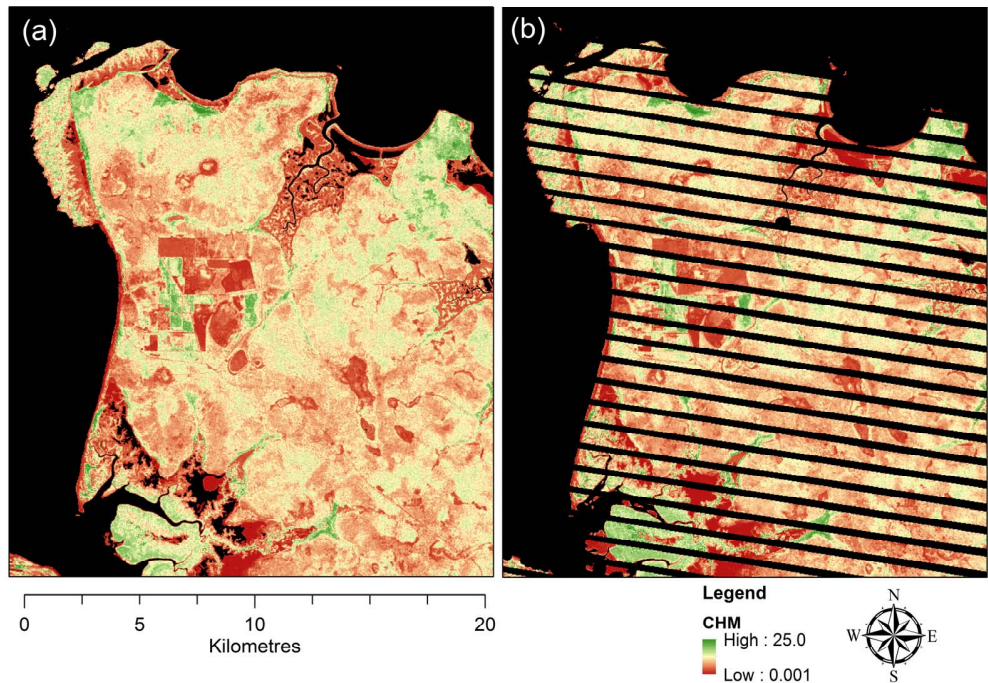


Fig. 3.7 Random forest canopy height model applied to both (a) Landsat-5 TM (acquired 26/05/2009) and (b) Landsat-7 ETM+ (acquired 19/06/2009) imagery for path/row 106/68 to independently validate the accuracy of the model; black areas denote nodata values. Note, the region shown in this figure is the grey area shown in Figure 3.3.

3.3.4.1 Predictor variable importance

The importance scores for the 14 predictor variables for the random forest model are shown in Figure 3.8. The most important predictor variable was the nir/green ratio followed by the vegetation index GSAVI and the SWIR1 band. A combination of band ratios were found to be important, representing eight of the 14 predictor variables. The green band featured six times, while the Red, NIR and SWIR1 bands occurred five times in either vegetation indices, band ratios or as individual bands. Hill et al. (2011) investigated the relationships between LiDAR derived canopy height and Landsat-7 ETM+ data for four tropical rainforest types. Their study showed that the NIR band was the most sensitive variable when related to mean and maximum canopy height followed by the green normalised vegetation index. They concluded that their study supported the hypothesis that canopy height distribution and shadow effects due to canopy complexity and emergent trees significantly influences spectral response for tropical rainforests (Hill et al. 2011). Hansen et al. (2016) mapped tree height distributions in Sub-Saharan Africa covering a wide range of vegetation community types using Landsat-7 ETM+ and Landsat-8 OLI. They used a regression tree model and found that seasonal derivatives (inter-percentile ranges) from the Red band were the top two important variables,

while the SWIR2 band was the third most important (Hansen et al. 2016). These studies highlight the complex relationships between woody vegetation height and spectral reflectance of the Landsat bands.

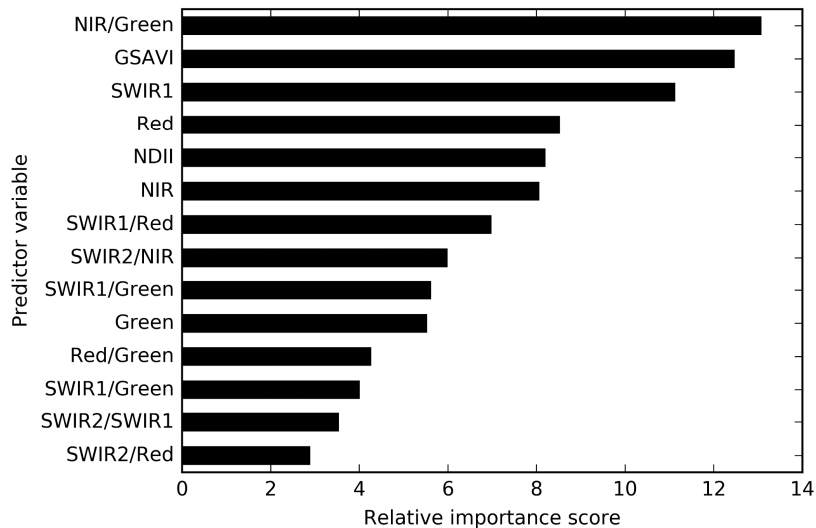


Fig. 3.8 Relative importance score for the 14 predictor variables used in the final random forest model.

In this study, the woody vegetation communities are structurally variable, ranging from closed forests, woodlands, open woodlands and grasslands with sparse trees. The variability in the relationship between the top four predictor variables and canopy height for three major vegetation communities in this study are shown in Figure 3.9. The distinct relationships between canopy height and ratio NIR/Green is evident for each of the three broad vegetation communities. As with Hill et al. (2011), it is likely that the shadow fraction contributed to the spectral reflectance in the Landsat pixels in many of the vegetation communities in this study. The SWIR bands, which are sensitive to leaf water content (Hunt and Rock 1989), featured eight times in the 14 predictor variables. Typically, the SWIR reflectance values will increase as leaf water content decreases (Ji et al. 2011). The bimodal relationship between SWIR1 reflectance and canopy height for three of the major vegetation communities in the study area can be seen in Figure 3.9. SWIR1 reflectance values for the Mangrove communities were low across the range of canopy heights, while mangrove canopy cover is dense and the leaf water content is likely to contribute to the low values, soil moisture and water would also be influencing the SWIR1 values. The Monsoon rainforests in the study area generally have dense canopy cover, resulting in low SWIR1 reflectance values clustered above the 12 m canopy height, while for Eucalyptus communities SWIR1 reflectance increases as canopy height declines. While the SWIR1 band was the third most important predictor

variable in the model the relationship between canopy height and Mangrove and Monsoon rainforest communities is low. It is clear from the individual relationships between the canopy height and the predictor variables in this study that no one variable has a particularly strong relationship (Figure 3.5, 3.9. One of the benefits and strengths of the random forest algorithm is its ability to handle non-parametric data and learn from the complex interactions between variables (Grömping 2009, Strobl et al. 2008, Avitabile et al. 2012).

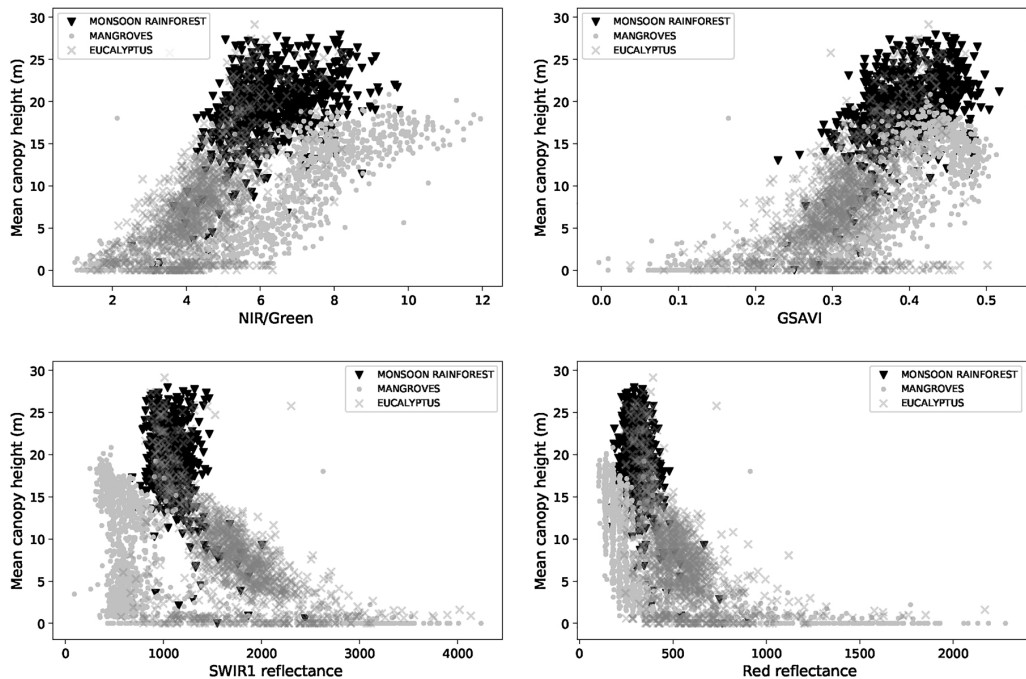


Fig. 3.9 Scatter plot showing the relationship between mean canopy height and the top four predictor variables, ratio of NIR and Green, GSAVI, SWIR1 reflectance and Red reflectance for three vegetation communities (Monsoon rainforest n= 759, Mangroves n= 1182, Eucalyptus n= 1159). Data points were subset from the training dataset within the extent of the 1:25,000 scale remnant vegetation mapping (Brock 1995).

3.3.4.2 Model validation

Accuracy statistics and the predicted and observed mean canopy height for Landsat-5 TM and Landsat-7 ETM+ (path/row 106/68) are shown in Figure 3.10. The model performance for the two sensors and image dates were very similar with only slight differences in the accuracy metrics. Canopy height predicted from Landsat-5 TM recorded a R^2 of 0.53 and RMSE value of 2.795 m, while Landsat-7 ETM+ recorded R^2 of 0.49 and RMSE 2.778 m, the variance and bias values were also very similar for both sensors. Even though the validation data were obtained from outside the extent of the training data, it would be expected that the Landsat-5 TM image would have achieved

a higher accuracy as it was captured on the same path (106) and date of the image used to develop the model, which is essentially the same image as it is captured on the same date and overpass of the sensor. The similar results between sensors suggests that the random forest model has transferred well to the Landsat-7 ETM+ sensor and has low generalisation error.

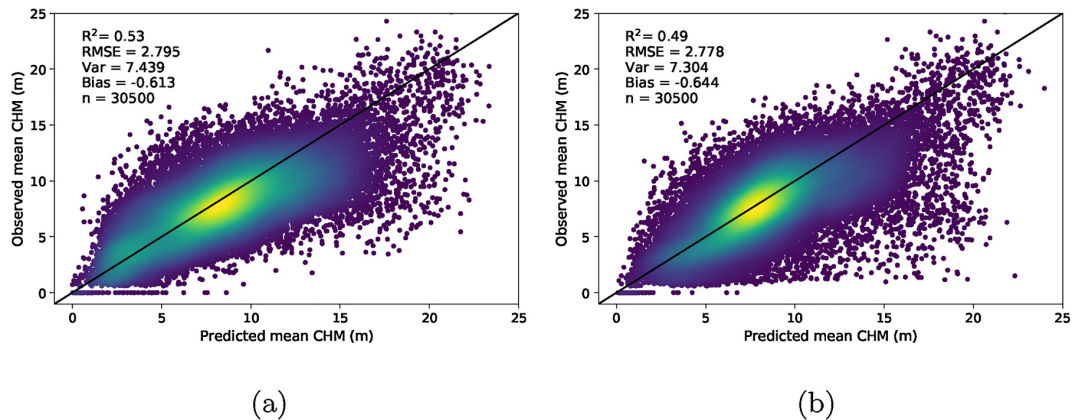


Fig. 3.10 Scatter plot showing the predicted and observed mean CHM for the validation region (a) Landsat-5 TM acquired 26/05/2009 (b) Landsat-7 ETM+ acquired 19/06/2009, solid line = 1:1 line.

To further evaluate the models performance and generalisation error, accuracy statistics were obtained for vegetation communities using existing mapping undertaken by Brock (1995). The predicted and observed mean canopy height and accuracy metrics for the four vegetation communities (Mangrove, Eucalyptus, Monsoon rainforest and Melaleuca) are shown in scatter plots Figure 3.11. There were variations in the models performance between sensors and vegetation communities. The lowest RMSE value 2.332 m was recorded for Eucalyptus communities predicted from Landsat-7 ETM+, while for Landsat-5 TM the lowest RMSE value (2.356 m) was recorded for the Eucalyptus communities, followed by the Mangrove communities (2.864 m). Bias was lowest for the Eucalyptus and Mangrove communities for both sensors with the predicted and observed data reasonably distributed around the 1:1 line. Bias in the model for both the Monsoon Rainforest and Melaleuca communities is clearly seen in Figure 3.11 with both sensors overestimating mean canopy height. Landsat-7 ETM+ recorded the lowest RMSE (3.037 m) for the Monsoon Rainforests, while Landsat-5 TM recorded the lowest RMSE for the Melaleuca communities (3.674 m). The Monsoon Rainforest in the study area is described as either wet or dry (Bach 2002). Wet monsoon rainforests are predominately evergreen with canopies rarely greater than 25 m, while dry monsoon forest are more diverse and contain deciduous species with a maximum canopy height of 12 m (Bach 2002).

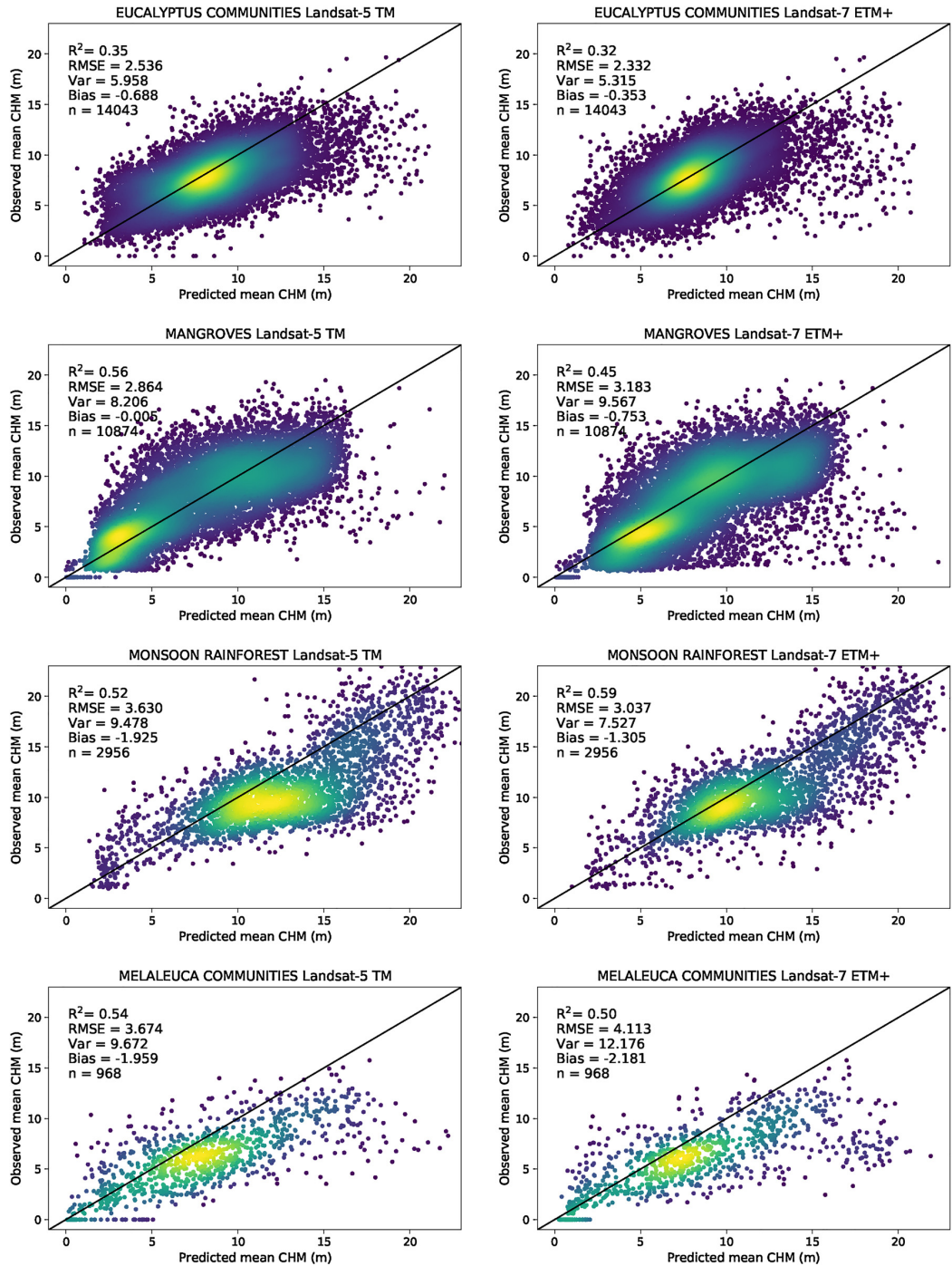


Fig. 3.11 Scatter plots showing the predicted CHM from Landsat-5 TM (26/05/2009) and Landsat-7 ETM+ (19/06/2009) for path/row p106r068 and the observed mean CHM (LiDAR, 03/07/2009) for broad vegetation communities located in the validation region; mapping by Brock (1995), solid line is the 1:1 line.

The overestimation of canopy height clustered around the 12 - 17 m range predicted from Landsat-5 TM are predominately located in dry monsoon rainforest patches. There is a slight improvement in the predictions from dry rainforests from Landsat-7 ETM+ captured later in the year (June), which is likely due to a reduction of the overall canopy greenness as a result of leaf fall in dry rainforests at this time of the year (Bach 2002).

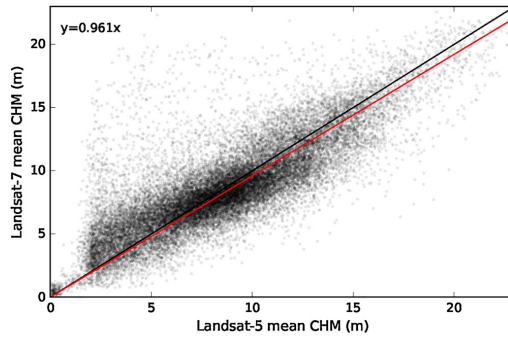
The bias observed in the dry monsoon rainforest and Melaleuca communities may be also due to the lower number of data points available to train the model. Avitabile et al. (2012) mapped woody biomass using random forest and stressed the importance of obtaining sufficient training data to capture the spectral variance within each classes. While the training data (section 2) in this study was stratified to obtain an even distribution across the height ranges, it is likely that there were insufficient samples from both the Dry Monsoon Rainforest and Melaleuca communities, as they represent a small percentage of the overall study area.

3.3.4.3 Model generalisation /time series

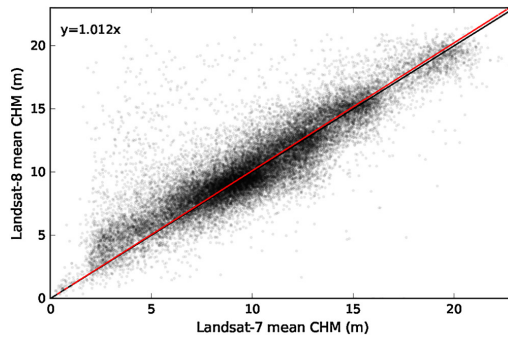
Pre-processing the imagery to standardise the reflectance values between image dates and sensors is important for time series analysis (Roy et al. 2016, Vicente-Serrano et al. 2008). In this study, the Landsat images were pre-processed (atmospheric, BRDF and topographic corrected) to a standardised solar-zenith angle of 45° (Flood et al. 2013, Flood 2014) which enabled the model developed from Landsat-5 TM to be directly applied to both Landsat-7 ETM+ and Landsat-8 OLI. Scatter plots comparing canopy heights predicted from Landsat-5 TM, Landsat-7 ETM+ and Landsat-8 OLI from the validation sites are shown in Figure 3.12. There was reasonable agreement between sensors, with the ridge regression slope close to 1 for all three years assessed. The results of this study are similar to Flood (2014) who reported similar regression values when comparing NDVI and a fractional cover model predicted from Landsat-7 ETM+ and Landsat-8 OLI imagery.

Canopy height estimates were obtained from 1 ha areas for sites located in the Mangrove community, wet Monsoon Rainforest, and Eucalyptus community predicted from Landsat imagery (captured between April and June) over a period of 29 years (1987 - 2016) are shown in figure 3.13. These sites were all severely impacted by cyclone Tracy on 25th December 1974 with large numbers of trees windthrown and damaged (Cameron et al. 1983, Stocker 1976, Fox 1980). In each time series, the individual canopy height estimates for each Landsat sensor are shown along with smoothed fitted line (dashed line) using a rolling median of three years. Variability in canopy height estimates for individual dates within a year is evident. It is likely that a number of factors are contributing to this variability, including differences in sensor characteristics, atmospheric conditions and seasonal variation in phenology between image capture dates. While pre-processing of imagery has been undertaken to standardise the reflectance values, it is likely that the 6S radiative transfer code used is unable to remove all the atmospheric effects resulting in variability in the spectral values recorded by the sensor.

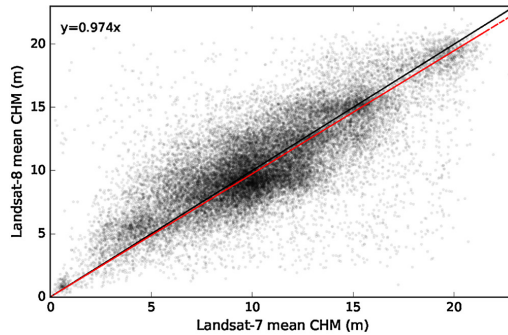
Differences in canopy height values could also be due to variability in spectral response due to differences in timing of leaf fall. The predictor variables used in the random forest model are all sensitive to changes in the level of photosynthetic vegetation and plant vigour. While the two dominant Eucalyptus species in the study region, are evergreen and canopy foliage projective cover remains reasonably high through the dry season (Williams et al. 1997). Many of the mid story tree species in the Eucalyptus communities in the study area are semi-deciduous or fully deciduous and timing of leaf fall varies between and within species and years (Myers et al. 1997, Williams et al. 1997).



(a)



(b)



(c)

Fig. 3.12 Scatter plots comparing mean canopy height estimates predicted from Landsat-5 TM, Landsat-7 ETM+ and Landsat-8 OLI in (a) 2009 (b) 2013 and (c) 2016, solid line is the 1:1 line and the dashed red line is the ridge regression. Statistics were only obtained from regions corresponding with valid Landsat-7 ETM+ pixels from the validation region for each year.

This variation in phenology is likely to be more pronounced in Eucalyptus communities where the upper canopy is more open and the mid-story vegetation is more visible to the sensor. The level of damage to Eucalyptus communities in the region (along McMillan's Road, Darwin) of the time trace (Figure 3.13 (d)) six months after cyclone Tracy is evident Figure 3.14 (a). For the Eucalyptus community sites shown in Figures 3.13 (c), 3.13 (d)) canopy height appears to be increasing and starts to reach an asymptote around

the mid to late 1990's for these sites. Wilson and Bowman (1987) undertook field work in the Howard Peninsula (located in the study area) in 1985 and reported dense regrowth and crown damage in the over story in the Eucalyptus communities and attributed it to the impact of cyclone Tracy in 1974. Likewise Brock (1995) also undertook field work during 1994 and 1995 in the study area and reported that within the Eucalyptus communities there were stands of vigorous uniform regrowth of *E. tetrodonta* and *E. miniata* to 10 m tall, and attributed this to recovery as a result of extensive damage from cyclone Tracy in 1974. The recovery observed in the 1994 - 1995 field surveys appears to be evident in the two Eucalyptus time trace examples with canopy heights around 8 m around that time period. The sudden drop in canopy height shown in Figure 3.13 (c) around 2013 is an example of land clearing for residential development in the area. In contrast to the Eucalyptus communities the wet Monsoon Rainforests example shows that canopy height remains consistent over the 29 years (Figure 3.13 (b)). This Monsoon Rainforest site was also severely impacted by cyclone Tracy with a large number of trees uprooted or having major branch or trunk damage (Stocker 1976). Regeneration months after cyclone Tracy in the Monsoon forest in the Darwin region was reported to be profuse (Fox 1980). Wilson and Bowman (1987) reported that Monsoon rainforest in the Howard Peninsula (located 15 km west of the time series Figure 3.13 (b)) 10 years after cyclone Tracy appeared to have no apparent evidence of damage, other than an absence of canopy emergents. The canopy height for the wet Monsoon rainforest shown in Figure 3.13 (b) is consistent with recovery (from cyclone Tracy) having occurred prior to the capture of the first Landsat image (1987) used in this study. The wet Monsoon rainforest time trace (Figure 3.13 (b)) shows less variability in canopy height between sensors, this may be due to the evergreen species in wet Monsoon rainforests resulting in more consistent foliage cover through time (Bach 2002). There is a clear spike in the rainforest canopy height recorded in 2009. This point represents data used to fit the random forest model and indicates that for this wet Monsoon forest it is likely that canopy height is being underestimated. This is in contrast with the dry Monsoon forest (discussed earlier) where canopy height is being overestimated.

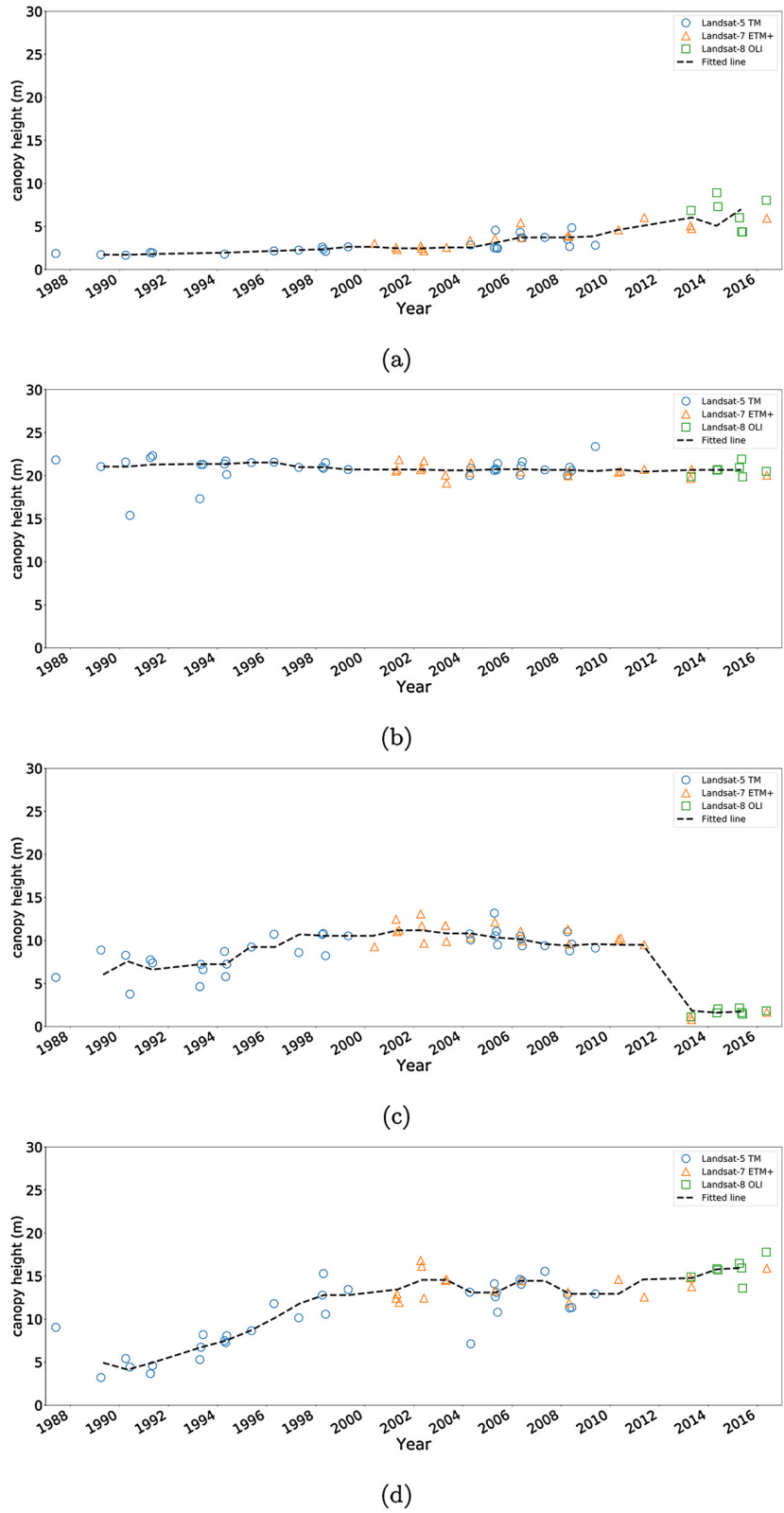


Fig. 3.13 Canopy height estimates predicted from Landsat-5 TM, Landsat-7 ETM+ and Landsat-8 OLI for sites impacted by cyclone Tracy from 1987 to 2016 for a (a) mangrove forest, (b) monsoon rain forest, (c) Eucalyptus woodland with clearing and (d) Eucalyptus woodland.



Fig. 3.14 Example of the damage to Eucalyptus communities (along McMillan's Road, Darwin) due to cyclone Tracy 25th December 1974 and subsequent recovery and re-growth (a) photograph taken (by Roy Beames) 5th July 1975 precise location on McMillan's Road unknown (b) photograph taken 27th December 2016 at the location of time series Figure 3.13 (d).

Damage to the Mangrove forests in the study area due to cyclone Tracy ranged from minor to severe (Stocker 1976) with mangrove death evident decades later in some areas (Rogers et al. 2017). Mangrove forests in the vicinity of the time trace (Figure 3.13 (a) were severely damaged during cyclone Tracy with dead trees still evident 26 years after the cyclone (Ferwerda et al. 2007). It appears that mangroves at this site have taken decades to recover from the cyclone damage with an increase in canopy height, starting to occur early 2000.

3.4 Conclusions

In this study we implemented a random forest regression model to predict canopy height from a single date Landsat-5 TM scene, across a variety of natural vegetation communities in the Northern Territory, Australia. The model was trained with a LiDAR-derived canopy height model (CHM) ($R^2 = 0.53$, RMSE = 2.8 m). A three-stage approach was undertaken to tune the random forest model and select the predictor variables used in the final model. Despite none of the individual independent predictor variables derived from Landsat-5 TM having a strong relationship with the dependent variable (LiDAR derived canopy height). The non-parametric random forest algorithm was able to account for the complex relationships between dependent and independent variables. The ability of the model to be applied to both Landsat-7 ETM+ and Landsat-8 OLI imagery was also assessed. The final canopy height model was applied to the first cloud-free Landsat-7 ETM+ image acquired after the LiDAR capture date resulting in a $R^2 = 0.49$ and RMSE = 2.8 m. The model was then applied to the three Landsat sensors to produce

time series plots for a period of 27 years (1987 – 2016). The results showed that the model could be transferred to Landsat-7 ETM+ and Landsat-8 OLI, however, there was variability between canopy height estimates likely to be due to seasonal variations in the image capture dates and sensors characteristics. The four time series plots used as example were all impacted by severe tropical cyclone Tracy in 1974. The canopy height estimates for the Monsoon forest example showed that it had recovered to the current height by 1987 (13 years post cyclone) while the two Eucalyptus community site were still in a state of recovery. The canopy height estimates for the Mangrove community indicate that this site has taken decades to recover and has only recently recovered to its pre-cyclone condition. It should be noted that the random forest regression model will not extrapolate beyond the range of canopy height values in the training dataset. In this study, the minimum and maximum heights in the validation dataset did not exceed the values in the training dataset, and the vegetation communities were similar in both regions. Further work is required to assess how well the random forest model transfers beyond the current study area. This study demonstrates that canopy height can be predicted from optical Landsat imagery at moderate to high levels of accuracy. The robustness of the model across a range of vegetation communities and three different Landsat sensors illustrate that our approach can be successfully used to explore changes in woody vegetation canopy height through time.

CHAPTER 4

Broad-scale mapping of tree canopy structure using optical satellite sensors, Sentinel-2 MSI and Landsat-8 OLI.

Thesis context: The focus of this chapter is the development of a remote sensing products predicting seven woody vegetation structural metrics from both Landsat-8 and Sentinel-2 satellite sensors. The models in this study produced annual estimates of tree canopy structure which were developed using training data derived from three LiDAR datasets captured in 2016, 2017 and 2018, representing a broad range of vegetation communities across the Northern Territory. The Landsat model was used to produce annual estimates of height for woody vegetation between the years 1988 and 2017 which was used in the development of the structural mapping product developed in chapter 5.

Abstract

This study has developed predictive models to obtain estimates of tree canopy structure from optical satellite sensors Sentinel-2 MSI and Landsat-8 OLI over an area covering 355,500 km² in the Northern Territory, Australia. Airborne LiDAR datasets were used to produce canopy height models for training and validation of the models. The machine learning algorithm Random Forest was used to develop regression models predicting seven structural metrics, which described characteristics of tree canopy height (99th, 95th, 75th, 25th percentiles, mean, standard deviation and coefficient of variation) at spatial resolutions of 10 m, 20 m and 30 m for Sentinel-2 MSI and 30 m for Landsat-8 OLI. Overall model accuracy improved as spatial resolution decreased, with models at 30 m recording the highest accuracy. The Sentinel-2 red-edge bands featured as important predictor variables, however they did not significantly improve model performance when compared with the models derived from Landsat-8. Of the seven structural attributes, the 99th percentile, representing maximum canopy height for a respective pixel had the strongest relationship for both Sentinel-2 and Landsat-8 with R² values ranging from 0.81 to 0.70 and RMSE% between 33.8 and 22.9. Model accuracy declined with a reduction in spatial resolution, however models at 10 m spatial resolution provided increased level of detail not available at 30 m. Combining the different structural metrics to produce three band composites provides insight into tree structure across the

landscape. This study demonstrates the utility of optical satellite sensors Sentinel-2 and Landsat-8 for broad-scale mapping of tree canopy structural metrics and has produced the first mapping products at 10 m spatial resolution identifying tree canopy structure across the northern half of the Northern Territory, Australia.

4.1 Introduction

The World's natural environments are under increased pressure from both natural and anthropogenic threats (Alleaume et al. 2018). Increase in the human population is resulting in changes in land-use and land-cover which is putting pressure on natural ecosystems (Marques et al. 2019). Invasive species, habitat loss and changes in climate are all factors threatening global biodiversity (McGeoch et al. 2010, Smale et al. 2019). In northern Australia, biodiversity is under threat from a number of factors including invasive species (flora and fauna), changes in fire regimes and climate (Davies et al. 2018, Woolley et al. 2018, Duke et al. 2017, Setterfield et al. 2010, Edwards and Russell-Smith 2009, Cook and Goyens 2008). There are a substantial number of endemic flora and fauna species in the northern half of the Northern Territory, which are both nationally and internationally significant (Woinarski et al. 2006, Allen et al. 2019). The development of long-term monitoring programs using information collected in a consistent and frequent manner has been identified as a way to help gain insight into the drivers of the change being observed (Lindenmayer et al. 2012, 2015).

Satellite remote sensing products have the potential to provide information at suitable spatial and temporal scales for long-term monitoring of important ecological variables (Alleaume et al. 2018, Luque et al. 2018, Pettorelli et al. 2016, Skidmore et al. 2015). Ecologists have identified classes of essential biodiversity variables which include, species traits and populations, ecosystem function and structure (Skidmore et al. 2015, Pereira et al. 2013). Forest structure has been identified as an important metric for monitoring trends in biomass, primary productivity and biodiversity (O'Grady et al. 2000, Cook et al. 2015, Skidmore et al. 2015, Pettorelli et al. 2016). Identifying the structural distribution of forests at a broader landscape scale is important, as it has the potential to increase the accuracy of carbon stock estimates (Cook et al. 2015, O'Grady et al. 2000) and assist in identifying the location of large hollow-bearing trees, which are a keystone habitat in northern Australia for many fauna species (Woolley et al. 2018). Fire, termites and cyclones are all drivers influencing vegetation structure in northern Australia (Woolley et al. 2018, Russell-Smith et al. 2019). The influence of fire on woody vegetation structure in the Northern Territory has been well studied (Anderson et al. 1998, Williams et al. 1999, Edwards and Russell-Smith 2009, Levick et al. 2019), however limited work has been undertaken to understand the impact of cy-

clones, which have the potential to dramatically alter tree structure (Cook and Goyens 2008, Hutley et al. 2013). Tree structure is commonly measured using Light Detection and Ranging (LiDAR) data and provides highly detailed information (Lim et al. 2003, Wulder, White, Nelson, Næsset, Ørka, Coops, Hilker, Bater and Gobakken 2012, Goldbergs et al. 2018, Levick et al. 2019). While the level of information available from LiDAR is very detailed, the use at a broad scale is cost prohibitive (Pascual et al. 2010, Lang et al. 2019). Numerous studies have used LiDAR to obtain tree structural information to develop predictive models from optical satellite sensors (Hudak et al. 2002, Pascual et al. 2010, Hill et al. 2011, Ota et al. 2014, Ahmed et al. 2015, Sohn and Mccoy 1997, Staben et al. 2018, Matasci et al. 2018, Lang et al. 2019). While the accuracy of the forest metrics obtained from optical sensors is reduced when compared with LiDAR, it does enable greater spatial and temporal coverage to be obtained. To develop long-term monitoring programs there is a need to produce information in a consistent manner through time (Lindenmayer et al. 2012). The open source policies for the United States Geological Survey (USGS) Landsat and European Space Agency (ESA) Sentinel-2 satellite programs have enabled the development of long-term monitoring programs at regional and global scales (Wulder, Masek, Cohen, Loveland and Woodcock 2012).

There is limited information available on the tree structure of the northern Territory. Scarth et al. (2019) recently published a mapping product detailing a structural classification based on height and woody foliage projective cover for the Australian continent using a fusion of sensors (ICESat/GLAS, ALOS PALSAR and Landsat imagery). While this structural classification provides insight into the forests across the Australian continent, it is produced from composites of data and provides a single snapshot in time. To enable long-term assessment of changes in forest structure across the Northern Territory, products need to be developed that identify change consistently through time. This study advances previous work (Staben et al. 2018) which demonstrated the utility of Landsat sensors in predicting mean canopy height across the Darwin region in the Northern Territory. Random forest regression was used to develop a model to predict mean canopy height from Landsat-5 Thematic mapper (TM) which was then applied to both Landsat-7 Enhanced Thematic Mapper Plus (ETM+) and Landsat-8 Operational Land Imager (OLI) sensors (Staben et al. 2018). Overall accuracy based on the root mean square error (RMSE) was 2.8 m for both Landsat-5 TM and Landsat-7 ETM+ (Staben et al. 2018). In this study seven structural metrics were modelled from Landsat-8 OLI and Sentinel-2 MSI sensors using training data captured in 2016, 2017 and 2018 obtained from a broad range of vegetation communities across three locations in the Northern Territory. Lang et al. (2019) developed models to predict vegetation height from composites of Sentinel-2 MSI satellite imagery captured over Gabon (Africa) and

Switzerland (Central Europe) and reported RMSE of 3.4 m and 5.6 m respectively for vegetation heights up to 50 m. The improved spectral resolution of both Landsat-8 OLI sensor and additional red-edge bands and increased spatial resolution available with Sentinel-2 sensors have the potential to develop more accurate models over our study area.

The aims of this study are to (1) investigate the utility of optical satellite imagery, Sentinel-2 MSI and Landsat-8 OLI in predicting tree canopy structural parameters derived from LiDAR canopy height models and; (2) produce tree canopy structure maps across the northern half of the Northern Territory to provide baseline information to natural resource managers. Seven metrics characterising tree canopy structure were extracted from 1 m canopy height models derived from LiDAR captured across the study area. As the Sentinel-2 satellite push-broom sensors capture imagery at different spatial resolutions, models were developed at 10 m and 20 m to assess the influence of different scales on model performance. Models were also developed at 30 m spatial resolution for Landsat-8 and Sentinel-2 imagery to enable comparisons between the two sensors.

4.2 Data and Methods

4.2.1 Study Area

This study was undertaken in the wet-dry tropics of the Northern Territory, Australia covering an area of approximately 355,500 km² (Figure 5.2). The average annual temperature is high with 32° on the coast (Darwin) to 34° for inland regions. The majority of the rainfall occurs between the months of October and April. There is a distinct rainfall gradient moving south (Cook et al. 2015), with a mean annual rainfall of 1725 mm for Darwin in the north and 790 mm at Borroloola in the south east of the study area (<http://www.bom.gov.au/>).

Vegetation communities across the study area are diverse, with mangrove forests found along the coastal regions (Rogers et al. 2017, Duke et al. 2017) and Melaleuca species found in poorly drained soils, along river systems and floodplains (Franklin et al. 2007). Pockets of dry and wet rainforests are scattered across the region (Bach 2002, Wilson et al. 1990). There are large sandstone plateaus which consist of a mix of woodlands and shrublands (Wilson et al. 1990). The study area is dominated by *Eucalyptus* and *Corymbia* species found on the undulating lateritic plains and plateaus (Wilson et al. 1990). Large areas of woodland and open forests are dominated by *Eucalyptus tetrodonta* and *E. miniata* which have mid-strata of mixed semi-deciduous to deciduous trees and shrubs and grasses (Williams et al. 1997).

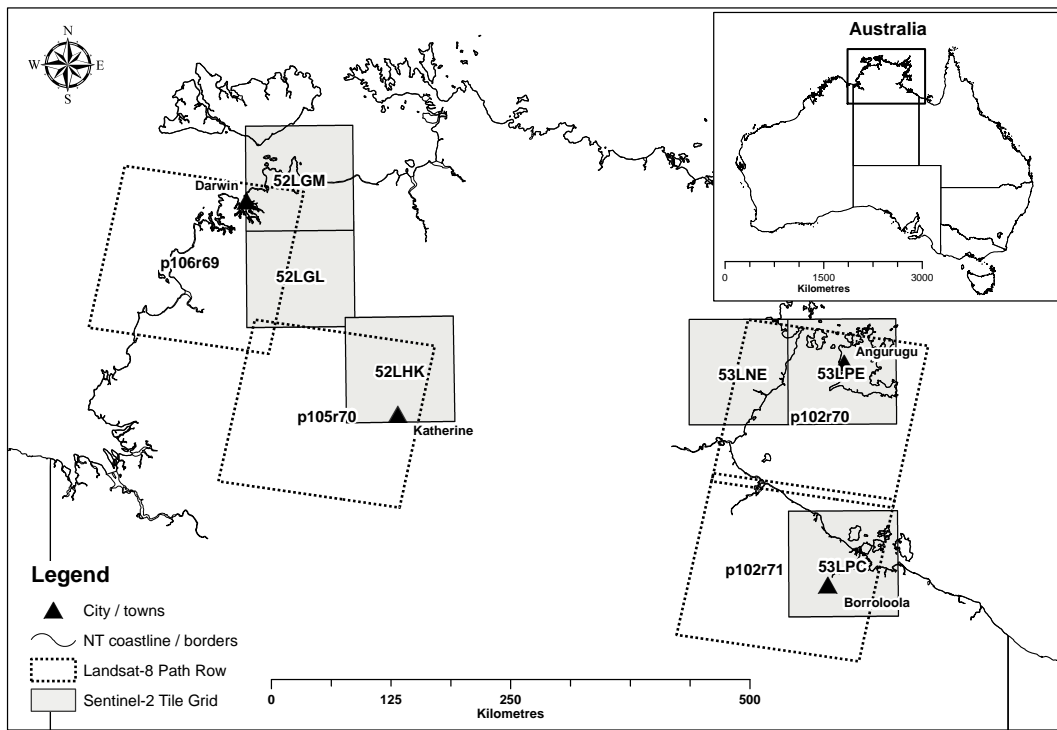


Fig. 4.1 Location of the study area Northern Territory, Australia and the Sentinel-2 MSI and Landsat-8 OLI scenes used in this study.

4.2.2 LiDAR

A number of airborne LiDAR datasets captured in 2016, 2017 and 2018 were used in this study (Figure 4.2). The 2018 LiDAR was captured over the Elizabeth River catchment in the Darwin region, covering an area approximately 300 km². The Elizabeth River catchment contains a mix of land use (urban, peri-urban, agricultural) and natural vegetation communities (Staben and Edmeades 2017). The 2016 LiDAR was captured inland over the town of Katherine, covering approximately 97 km². Land use consists of urban, peri-urban and agricultural with a mix of vegetation communities including tall riparian vegetation found along the banks of the Katherine River and woodlands. The LiDAR data captured in 2017 over the Gulf of Carpentaria were part of the investigation into the extensive Mangrove die-back event in 2015-2016 (Duke et al. 2017). The Gulf LiDAR consisted of flight lines captured along the coastline with a particular focus on capturing mangrove forests (http://wiki.auscover.net.au/wiki/LIDAR_data,_Gulf_of_Carpentaria). While large areas were acquired along the coast, we selected a number of the single flight lines consisting of both mangrove forests and upland vegetation communities, covering an area of approximately 54 km². All LiDAR data were processed by the respective data providers and supplied as classified point clouds. Details of the sensors used, point density and footprint for each LiDAR dataset are presented in Table 4.1. Canopy height models were produced at

1 m spatial resolution from each of the LiDAR datasets using the open source software Fusion (http://forsys.cfr.washington.edu/fusion/fusion_overview.html). Surface models were produced to enable the canopy heights to be normalised to the ground surface. All pixels in each of the canopy height models between the values >0 and 0.51 m were removed from further analysis. This was undertaken to account for the fact that the native grasses at the time of data capture were senescent and on average 0.5 m tall (Setterfield et al. 2010), and may represent the highest z value for a given pixel in the canopy height model.

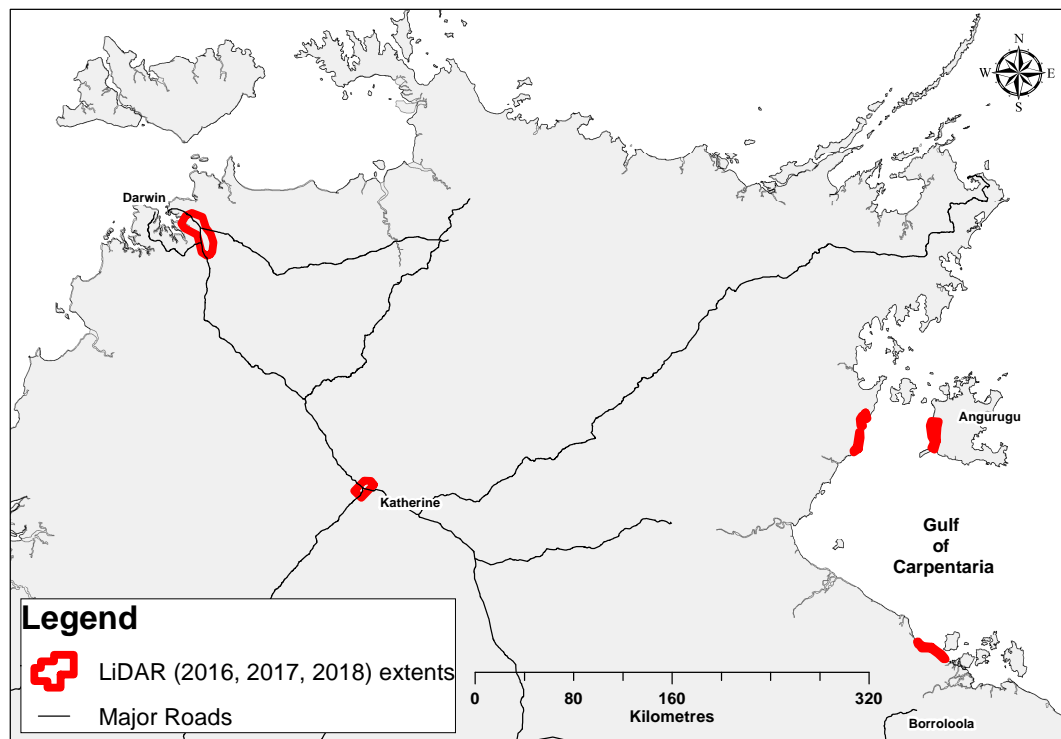


Fig. 4.2 Location of the LiDAR used in this study.

Table 4.1 Details of the LiDAR surveys used in this study

LiDAR	Acquisition Dates	Point density m^2	Foot print (m)	Sensor
Elizabeth River (Darwin)	18/19 May 2018	4	0.15	Trimble AX60
Katherine Region	18 May 2016	4	0.335	Riegl Q1560
Gulf of Carpentaria	16 Aug/2 Sep 2017	6-7	0.15	Riegl Q680i-S

A number of metrics were derived from the canopy height models to characterise woody vegetation structural attributes across the study area (Table 4.2). The structural metrics were calculated from 10×10 m, 20×20 m and 30×30 m plots, determined by the pixel size of the satellite imagery being used in the model development. The mean and a number of percentiles were calculated to characterise a range of woody vegetation heights. Metrics such as the 99th percentile represent the maximum canopy

height, while the mean canopy height (H_{mean}) provides information on how variable tree canopy is within the pixel. While a number of the percentiles were correlated, they were assessed to identify the optimal relationships with Sentinel-2 and Landsat-8 sensors. LiDAR also provides insight into the structural variability in woody vegetation (García et al. 2017, Carrasco et al. 2019). In this study, we calculated the standard deviation of the mean height and coefficient of variation from the canopy height models to assess variability in canopy height for each plot. Examples of these structural metrics estimated from 1 m canopy height model at 20 m spatial resolution are shown in Figure 4.3.

Table 4.2 Details of the canopy height structural metrics derived from the 1 m canopy height models used in this study

Metric	Description	Units
H_{99}	99 th percentile canopy height	m
H_{95}	95 th percentile canopy height	m
H_{75}	75 th percentile canopy height	m
H_{25}	25 th percentile canopy height	m
H_{mean}	Mean canopy height	m
H_{sd}	Standard deviation mean canopy height	m
H_{cov}	Coefficient of variation canopy height	%

4.2.3 Sentinel-2 and Landsat satellite imagery

Seasonal composites for both Sentinel-2 MSI and Landsat-8 OLI imagery captured over each of the three LiDAR datasets were produced for use as predictor variables. Two seasonal composites (annual and dry season) for each year were produced to exploit seasonal changes in vegetation growth through the year. The dry season composites were produced using imagery captured between May and September. Typically during this period the grass understory is senescent and provides greater spectral separability between woody and non-woody vegetation. The Landsat path/row and Sentinel tile grids used in this study are shown in Figure 5.2. The single date Sentinel-2 and Landsat-8 imagery were atmospherically corrected using 6S radiative transfer code and a bi-directional reflectance distribution function (BRDF) model was applied to take into account topographic illumination effects, producing surface reflectance values at nadir and a solar zenith angle of 45° (Flood 2014, 2017). The blue spectral bands, which are sensitive to aerosol conditions for both Landsat-8 and Sentinel-2, were not used in this study to reduce noise potentially introduced by differing atmospheric conditions between image dates (Flood 2014). A summary of the spectral bands used in this study for each sensor is shown in Table 4.3. To enable transfer of models from Landsat-8 to Landsat-5 TM and Landsat-7 ETM+ sensors, the reflectance values were converted to predict Landsat-7 reflectance using the coefficients published in Flood (2014). Cloud, shadow and water were masked from the single date images before producing the composite surface reflectance imagery using a multidimensional medoid (median) detailed

in Flood (2013). Vegetation indices and band ratios were also derived from each of the Landsat-8 and Sentinel-2 seasonal composites (Table 4.4). For Landsat-8, a total of 56 predictor variables consisting of surface reflectance bands, band ratio's and vegetation indices derived from the two seasonal composites (annual and dry season) were assessed, while for Sentinel-2 a total of 124 variables were available due to the addition of the red-edge bands.

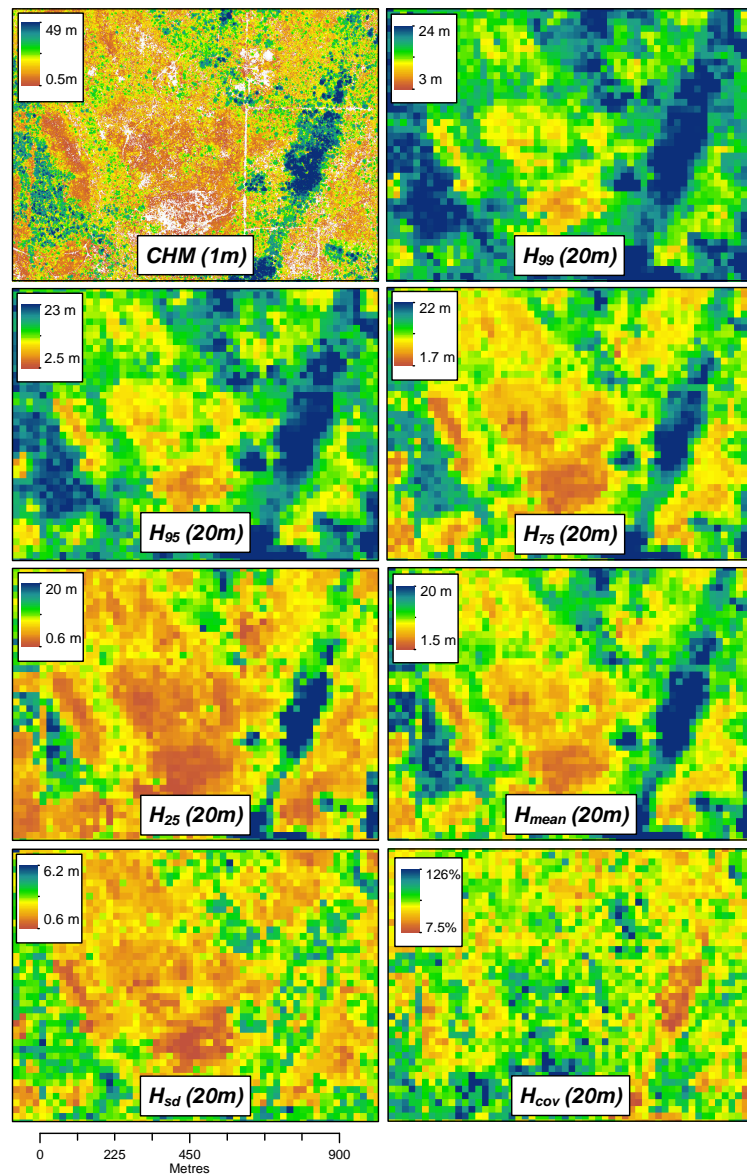


Fig. 4.3 Example of the structural metrics derived from the LiDAR canopy height model resampled to 20 m spatial resolution.

To assess the capacity of Sentinel-2 to predict forest structural metrics and make comparisons with Landsat-8 we developed four sets of models at differing spatial resolutions. For Sentinel-2 we produced models at 10 m, 20 m and 30 m and for Landsat-8,

models were produced at 30 m. Sentinel-2 seasonal (annual and dry season) composites were produced at 10 m, 20 m and 30 m by up or down sampling the respective bands. To produce the Sentinel-2 10 m stack the six 20 m bands were down-sampled to the pixel grid of the 10 m bands, while the 10 m bands were up-sampled to the 20 m pixel grid to produce the 20 m Sentinel stack, using cubic convolution. To produce the Sentinel-2 composites at 30 m resolution the Sentinel-2 20 m stack were resampled based on the pixel grid of the Landsat-8 composites.

Table 4.3 Summary of the spectral bands for Sentinel-2 (MSI) and Landsat-8 (OLI) used in this study.

Sentinel-2 Name (band)	2a Centre Wavelength (nm)	2b Centre Wavelength (nm)	Resolution (m)	Landsat-8 Name (band)	Centre wavelength (nm)	Resolution (m)
Green (B3)	559.8	559.0	10	Green (B3)	561.41	30
Red (B4)	664.6	664.9	10	Red (B4)	654.59	30
RE1 (B5)	704.1	703.8	20			
RE2 (B6)	740.5	739.1	20			
RE3 (B7)	782.8	779.7	20			
NIR (B8)	832.8	832.9	10	NIR (B5)	864.67	30
nNIR (B8a)	864.7	864.0	20			
SWIR1 (B11)	1613.7	1610.4	20	SWIR1 (B6)	1608.86	30
SWIR2 (B12)	2202.4	2185.7	20	SWIR2 (B7)	2200.73	30

4.2.4 Model Training and Validation datasets

Training and validation datasets were produced from the extent of the canopy height models. As fire is a frequent occurrence in northern Australian landscapes (Edwards et al. 2013, Williams et al. 1999) burnt areas within the Sentinel-2 and Landsat-8 composites were visually identified and removed from the training and validation datasets. Burnt areas were removed as the spectral response received by the satellite sensor is more representative of burnt vegetation and ash, which is seasonal and does not reflect tree canopy height. The predictor variables used to train the models were obtained from the respective seasonal composites the year the LiDAR data were captured. Producing a training dataset from LiDAR and satellite imagery captured in 2016, 2017 and 2018 was undertaken to capture inter-annual variability in the spectral response of the satellite data, due to seasonal conditions. To enable independent assessment of the accuracy of the final models, a number of regions within the extent of the Elizabeth River and Katherine LiDAR were excluded in the production of the training datasets. Polygon grids were produced for each of the Sentinel-2 and Landsat-8 images based on the pixel resolution (10 m, 20 m and 30 m) over the extent of each of the LiDAR datasets. These polygon grids were used to define the area for calculation of the tree structural parameters (detailed in Table 4.2) from the LiDAR-derived canopy height models. A total of 148,000 pixels were randomly selected from the Sentinel-2 and Landsat-8 imagery within the extent of the LiDAR for use as training data. Two validation datasets were produced to assess the final model performance; the first dataset (identified here after as Val01) was randomly selected from the same regions as the training dataset while the second (identified here after as Val02) was selected from regions independent of

Table 4.4 Vegetation indices used in this study (*denotes indices only applied to Sentinel-2.)

Spectral Index	Formula	Reference
Normalized Difference Vegetation Index	$NDVI = \frac{NIR - Red}{NIR + Red}$	Tucker (1979)
Green Soil Adjusted Vegetation Index	$GSAVI = \frac{(NIR + Green)(NIR - Green)}{(NIR + Green + 0.5)(NIR - Green + 0.5)}$	Sripada et al. (2006)
Green Normalised Vegetation Index	$GNDVI = \frac{NIR - Green}{NIR + Green}$	Buschmann and Nagel (1993)
Chlorophyll Vegetation Index	$CVI = \frac{NIR}{NIR + Red} * \frac{Green}{Green - Red}$	Vincini et al. (2008)
Normalized Difference Greenness Index NDGI	$NDGI = \frac{Green - Red}{Green + Red}$	Bannari et al. (1995)
Normalized Burn Ratio SWIR2 (Band 7)	$NBR = \frac{NIR + SWIR2}{NIR - SWIR1}$	Ji et al. (2011)
Normalized Burn Ratio SWIR1 (Band 5)	$NDII = \frac{NIR + SWIR1}{NIR - SWIR1}$	Ji et al. (2011)
Green Difference Vegetation Index	$GDI = NIR - Green$	Sripada et al. (2006)
Modified Soil Adjusted Vegetation Index	$MSAVI = \frac{2 * NIR + 1 - \sqrt{(2 * NIR + 1)^2 - 8 * (NIR - Red)}}{2}$	Qi et al. (1994)
Difference Vegetation Index	$DVI = NIR - Red$	Tucker (1979)
Soil adjusted Vegetation index	$SAVI = \frac{NIR - Red}{(NIR + Red + 0.5)(NIR + Red + 0.5)}$	Huete (1988)
Modified Simple Ratio	$MSR = \frac{(NIR - Red) - 1}{(\sqrt{\frac{nir}{Red}}) + 1}$	Chen (1996)
Normalized Difference Redness Index	$RI = \frac{Red - Green}{Red + Green}$	Escadafal and Huete (1991)
*Chlorophyll Index Green	$CIgreen = (\frac{Green}{RE3}) - 1$	Gitelson et al. (2003)
*Chlorophyll Index Redge	$CIgreen = (\frac{RE3}{RE1}) - 1$	Gitelson et al. (2003)
*Normalized Difference Red-Edge 1	$NDRE1 = \frac{RE2 - RE1}{RE2 + RE1}$	Barnes et al. (2000)
*Normalized Difference Red-Edge 2	$NDRE2 = \frac{RE3 + RE1}{RE3 + RE1}$	Barnes et al. (2000)

the training data. The second validation dataset (Val02) was produced to evaluate the model performance outside of the extent of the training data. While regions used in the production of Val02 were excluded from the production of the training dataset for the Elizabeth River and Katherine LiDAR, for the Gulf region a LiDAR transect was selected south (approximately 150 km) of the Gulf LiDAR transects used in the model development.

4.2.5 Model development

The machine learning algorithm random forest was used to investigate the relationships between forest structural metrics and Sentinel-2 and Landsat-8 satellite imagery. A total of 28 models were developed: three sets of seven models for Sentinel-2 at 10 m, 20 m, and 30 m spatial resolutions and seven models for Landsat-8 at 30 m resolution. Random forest is an ensemble of decision trees built from a bootstrap sample of the training data (Breiman 2001, Cutler et al. 2007). The use of the random forest algorithm in remote sensing applications has increased in recent times as it is non-parametric, can handle thousands of input data, and model complex non-linear relationships (Breiman 2001, Cutler et al. 2007, Belgiu and Drăgu 2016, Staben et al. 2018). In this study, we use the random forest algorithm implemented in the open source Python module Scikit-learn (Pedregosa et al. 2011). There is a minimum of two parameters which need to be defined to produce a model using random forest; (1) the number of trees (`n_estimators`) and (2) the number of prediction variables (`max_features`) used to grow the tree (Rodríguez-Galiano et al. 2012). Based on the results of previous work the `n_estimator` variable parameter was set to 512 trees and the `max_feature` parameter was set to 'log2' (logarithm to the base 2) (Staben et al. 2018). One of the valuable features of the random forest algorithm is the calculation of the relative importance score for each of predictor variables (Belgiu and Drăgu 2016, Strobl et al. 2008).

A number of steps were undertaken in the development of each model. In stage one, the most important predictor variables were identified using the mean importance score for all predictor variables, based on 20 iterations of the model. In the second stage, predictor variables which are non-linear transformations of each other and variables that are highly correlated ($r = \geq 95\%$) were identified. This was undertaken to remove redundant predictor variables and produce more parsimonious models. Variables removed from further analysis were based on the order of importance identified in stage one of the analysis.

To further optimise the models, variable reduction analysis was performed using the

predictor variables identified in stage two. The least important variable was identified based on the mean importance score for five iterations of the random forest model, and the model was then re-run until only one predictor variable remained. For each of the five iterations of the model, 10% of the training data was randomly selected to independently assess the accuracy of the model (total n=74,000). The final models were selected and evaluated using a number of statistics, including the coefficient of determination (Zar 1984), root mean squared error (RMSE), RMSE%, BIAS and BIAS%. The RMSE, RMSE%, BIAS and BIAS% are defined as;

$$RMSE = \sqrt{\frac{\sum (x_i - y_i)^2}{n}} \quad (4.1)$$

$$RMSE\% = \frac{RMSE}{\bar{y}} * 100 \quad (4.2)$$

$$BIAS = \frac{1}{n} \sum_{i=1}^n x_i - y_i \quad (4.3)$$

$$BIAS\% = \frac{BIAS}{\bar{y}} * 100 \quad (4.4)$$

where n is the number of observations, y_i are the observed and x_i the predicted structural metrics and \bar{y} is the mean of y_i .

Candidate models for each of the structural metrics for each sensor and spatial resolution were selected using the statistics R^2 , RMSE and RMSE%. Preference was given to models with high accuracy statistics and low numbers of predictor variables. The final models were then produced using all the training data (n=148,000). To independently assess the accuracy of each model the statistics R^2 , RMSE, RMSE%, BIAS and BIAS% were calculated for each of the candidate models using the two validation datasets (Val01, Val02).

4.3 Results

4.3.1 Model development

4.3.1.1 Stage 1 and 2

In the first two stages of model development, a large number of predictor variables were found to be highly correlated or non-linear transformations of each other. Of the 124 predictor variables assessed for Sentinel-2, between 50 and 60 predictor variables were retained for further model development while for Landsat-8, of the 56 predictor vari-

ables between 29 and 31 remained.

4.3.1.2 Stage 3

The results of the variable reduction analysis for each of the structural metrics for Sentinel-2 and Landsat-8 are shown in Figure 4.4. The results were consistent for each of the structural metrics assessed for Sentinel-2 and Landsat-8, with model RMSE% converging on a minimum for more than 10 predictor variables. From the results of the variable reduction analysis (Figure 4.4) the final candidate models for each structural metric were selected using the R^2 and lowest RMSE, RMSE% statistics and model with the minimum number of predictor variables. The summary statistics and the number of predictor variables used in each of the candidate models are shown in Table 4.5. For the Sentinel-2 models (10 m, 20 m and 30 m), the number of predictor variables ranged between 21 and 35 and for Landsat-8 models between 18 and 25 (specific details for each of the four test sets are provided in sections 4.3.1.3, 4.3.1.4, 4.3.1.5 and 4.3.1.6). The relationship between the structural metrics and Sentinel-2 and Landsat-8 varied with R^2 values ranging from 0.82 to 0.46 and RMSE% values from 22.8 to 60.1. A number of models (15) recorded RMSE% values below 30%. The strongest relationships between all of the models and test sets developed was for H_{99} with R^2 values ranging from 0.82 to 0.75 and RMSE% between 22.8 and 27.1. The weakest models were for H_{25} , which recorded the highest RMSE% values for the four model sets. Models developed using Sentinel-2 at 20 m recorded the highest R^2 values, while the lowest overall RMSE% values were recorded for Sentinel-2 and 30 m spatial resolution for all seven structural metrics. An example of each of the candidate structural metric predicted from Sentinel-2 imagery at 20 m spatial resolution are shown in Figure 4.5.

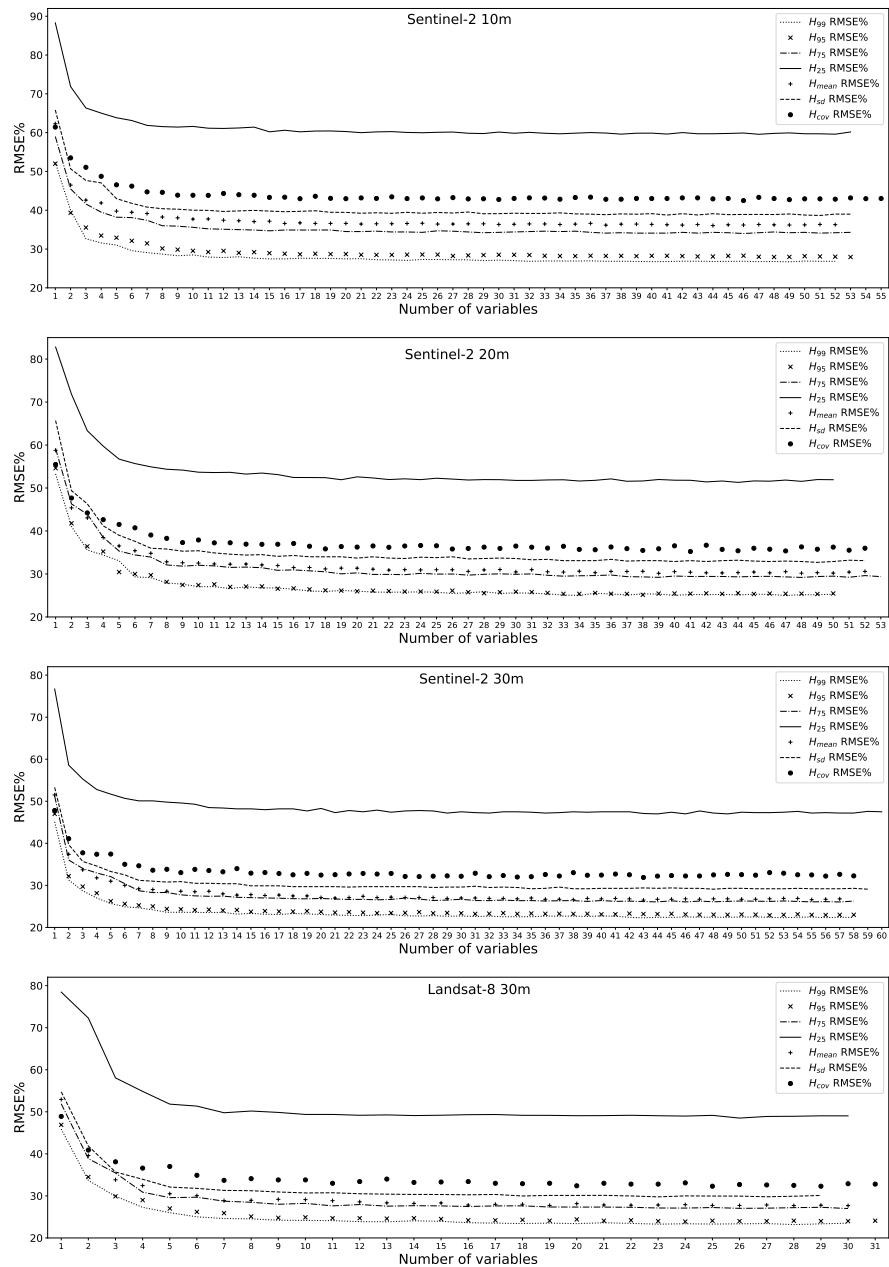


Fig. 4.4 Results of the variable reduction analysis showing the RMSE% and number of predictor variables for each structural metric predicted from Sentinel-2 (10 m, 20 m 30 m) and Landsat-8 imagery. Statistics were derived from five iterations of the model where 10% of the training data was selected (total n=74,000).

Table 4.5 Number of variables used for each of the candidate models predicting tree structure metrics from Sentinel-2 (10 m, 20 m, 30 m) and Landsat-8 (30 m) imagery. The accuracy statistics are based on five iterations of the random forest model during the variable reduction analysis. For each iteration 10% of the training data were selected (n=74,000).

Sensor/Metric	R ²	RMSE	RMSE %	No.var
S2 10m				
H ₉₉ (m)	0.77	3.1	27.1	24
H ₉₅ (m)	0.76	3.1	28.5	22
H ₇₅ (m)	0.70	3.1	34.2	29
H ₂₅ (m)	0.50	3.0	60.1	24
H _{mean} (m)	0.68	2.5	36.4	21
H _{sd} (m)	0.66	1.1	39.1	35
H _{cov} (%)	0.50	16.8	42.8	30
S2 20m				
H ₉₉ (m)	0.82	2.8	25.5	26
H ₉₅ (m)	0.82	2.6	25.8	27
H ₇₅ (m)	0.80	2.5	29.7	27
H ₂₅ (m)	0.61	2.1	51.9	29
H _{mean} (m)	0.79	1.9	30.5	30
H _{sd} (m)	0.77	0.9	33.1	33
H _{cov} (%)	0.59	14.6	35.8	26
S2 30m				
H ₉₉ (m)	0.77	3.0	22.8	23
H ₉₅ (m)	0.78	2.8	23.2	31
H ₇₅ (m)	0.76	2.5	26.4	28
H ₂₅ (m)	0.60	2.1	47.3	21
H _{mean} (m)	0.76	1.9	26.9	29
H _{sd} (m)	0.72	1.0	29.2	35
H _{cov} (%)	0.49	15.3	32.0	34
L8 30m				
H ₉₉ (m)	0.75	3.2	23.4	18
H ₉₅ (m)	0.75	3.0	24.2	16
H ₇₅ (m)	0.74	2.6	27.4	19
H ₂₅ (m)	0.57	2.2	49.2	19
H _{mean} (m)	0.74	2.0	27.7	19
H _{sd} (m)	0.70	1.0	29.8	23
H _{cov} (%)	0.46	15.6	32.3	25

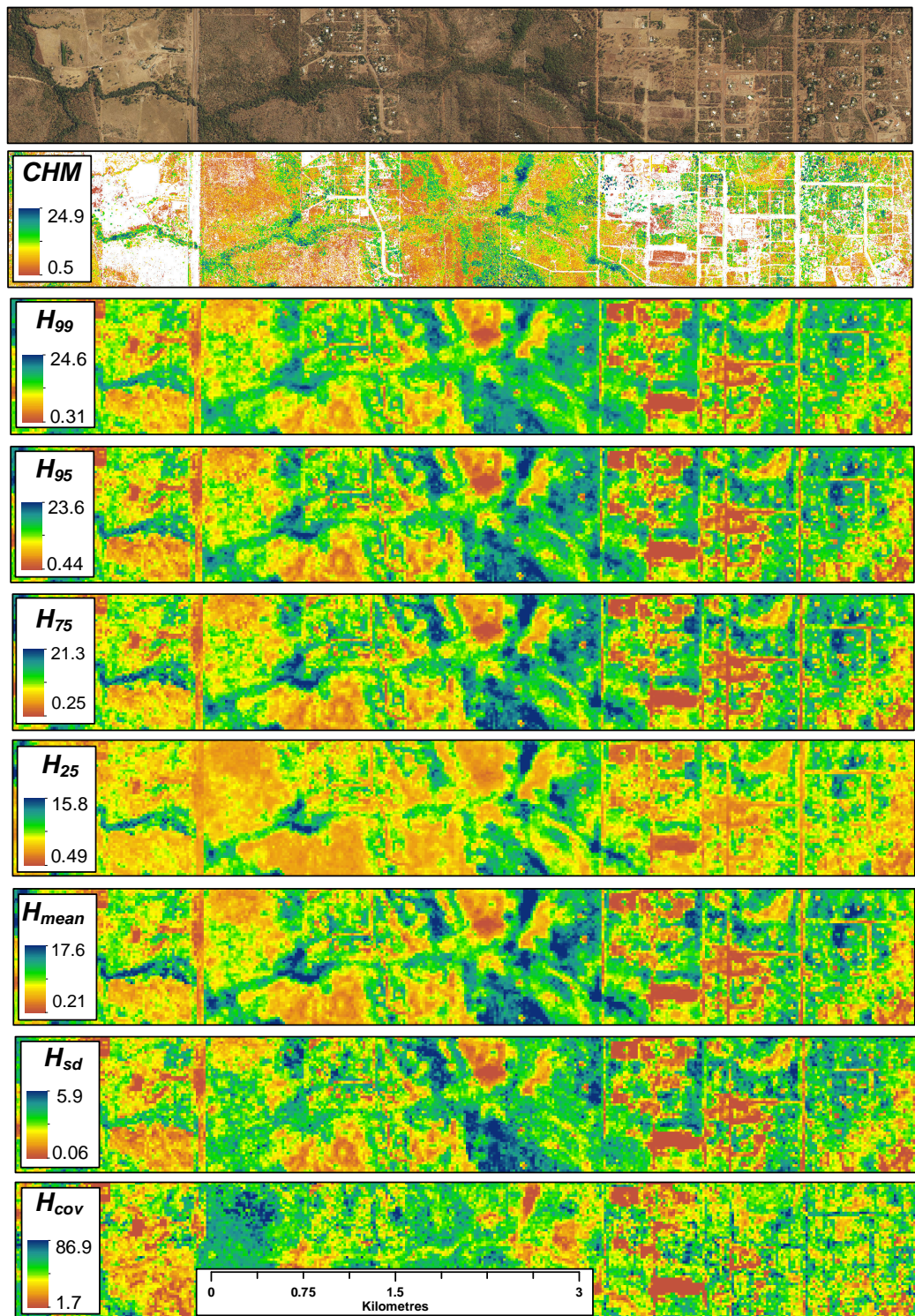


Fig. 4.5 Example of the structural metrics applied to Sentinel-2 at 20 m spatial resolution, along with LiDAR canopy height (1 m) and very high resolution digital aerial photography.

4.3.1.3 Sentinel-2 10 m

The predictor variables used to produce each of the models using Sentinel-2 imagery at 10 m spatial resolution are shown in Figure 4.6. A range of vegetation indices, band ratios and single bands were used in each of the models with the number of variables ranging between 26 and 33. All models were composed of a combination of predictor variables derived from the annual (a) and dry season (d) composites. One predictor variable SWIR2/SWIR1(d) featured in all seven models, while ten variables (SWIR1/RE1(d), SWIR2/Red(d), CVI(a), CVI(d), Green(a), NDRE1(d), RE1/NIR(a), RE1/NIR(d), Red(d) and SWIR1/Green(a)) occurred six times. The accuracy statistics for the seven models derived from the two validation datasets (Val01 and Val02) are detailed in Table 4.6. The distribution of the predicted and observed values for both validation datasets are represented in violin plots Figure 4.7. For the Val01 dataset H_{99} was the highest performing model with an R^2 value of 0.77 and RMSE% of 27.1%, followed by H_{95} which had a similar distribution in height values. Both H_{75} and H_{mean} had similar RMSE% values with 34.5 and 36.8 respectively. Of the two models measuring structural variability H_{sd} had the strongest relationship with RMSE% of 39.0 while H_{cov} recorded 43.3. The lowest accuracy recorded was for H_{25} with R^2 value of 0.49 and RMSE% of 60.7, with predictions of heights generally overestimated, as seen in the distribution of the predicted and observed values (Figure 4.7). The results for the independent validation dataset Val02 were similar to Val01 with a decrease in overall accuracy for each of the seven metrics. Overall the height range and distribution of the independent validation dataset were lower (Figure 4.7). This would have contributed to the difference in values between the two validation datasets, however there is clearly an increase in bias for H_{99} , H_{95} , H_{75} , H_{cov} and H_{25} .

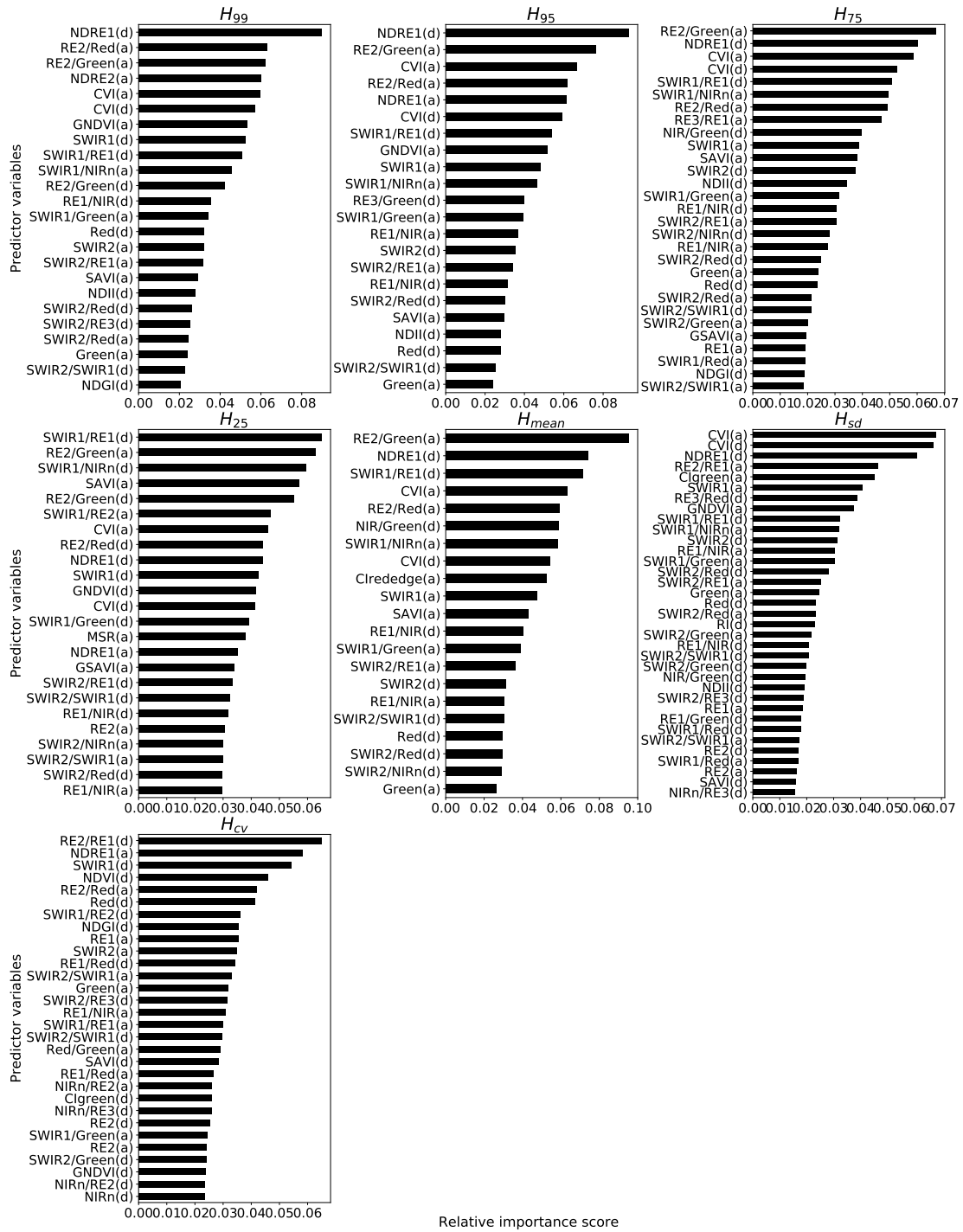


Fig. 4.6 Bar plots showing the predictor variables and relative importance score for each of the models predicting tree structure metrics from Sentinel-2 (10 m) imagery.

Table 4.6 Model accuracy statistics for tree structure metrics derived from Sentinel-2 imagery at 10 m spatial resolution for validation dataset Val01 (n=37,000) and Val02 (n=29,811).

Dataset/Metric	R ²	RMSE	RMSE%	BIAS	BIAS %
Val01					
H ₉₉ (m)	0.77	3.1	27.1	0.002	0.02
H ₉₅ (m)	0.76	3.1	28.5	0.001	0.01
H ₇₅ (m)	0.70	3.1	34.5	0.016	0.18
H ₂₅ (m)	0.49	3.0	60.7	0.076	1.55
H _{mean} (m)	0.68	2.5	36.8	0.033	0.47
H _{sd} (m)	0.66	1.1	39.0	0.016	-0.58
H _{cov} (%)	0.49	17.1	43.3	0.384	-0.97
Val02					
H ₉₉ (m)	0.70	3.0	33.8	-0.137	-1.52
H ₉₅ (m)	0.70	2.9	34.0	-0.152	-1.79
H ₇₅ (m)	0.65	2.8	40.2	-0.100	-1.44
H ₂₅ (m)	0.45	2.5	67.3	0.207	5.65
H _{mean} (m)	0.64	2.2	41.8	-0.001	-0.01
H _{sd} (m)	0.60	1.0	44.5	-0.030	-1.33
H _{cov} (%)	0.40	19.7	48.0	-2.651	-6.45

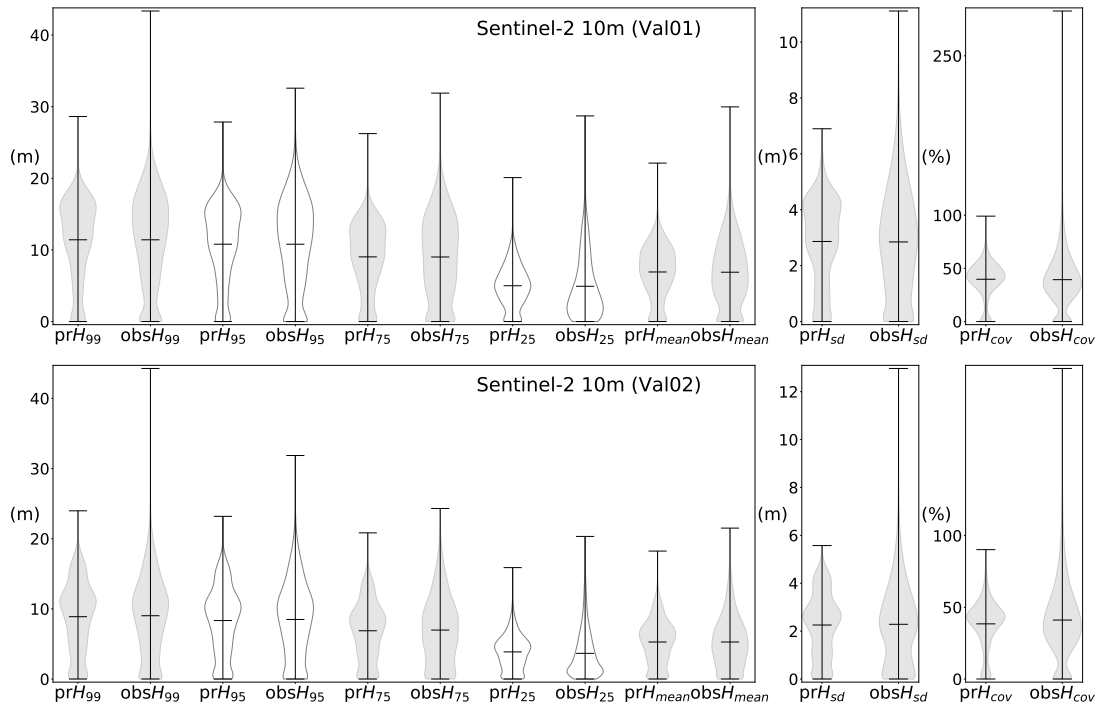


Fig. 4.7 Violin plots showing summary statistics (mean, min, max) and the distribution of the observed (LiDAR derived) and predicted tree structure metrics from Sentinel-2 at spatial resolution 10 m for validation datasets Val01 and Val02.

4.3.1.4 Sentinel-2 20 m

The importance score and each of the predictor variables used to produce the structural models from Sentinel-2 at 20 m spatial resolution are shown in Figure 4.8. The number of variables used in the final candidate models ranged from 26 to 33. Predictor variables consisted of vegetation indices, band ratios and spectral bands from both the annual and dry season composites were used in each of the models, with $\approx 55\%$ derived from the annual composite. Predictor variables that featured in all seven models, included the SWIR2/Green(a), Green(a) and CVI(a), while SWIR1/Red(d), SWIR1/Green(a), RE1/Red(d), SWIR1/Red(a), CVI(d), SWIR2(d), SWIR1(a), and SWIR2/Red(d) occurred six times. Accuracy statistics for both validation datasets are presented in Table 4.7. Violin plots representing the distribution of the predicted and observed values for each model are shown in Figure 4.9. For the Val01 dataset, R^2 values for the seven models ranged from 0.82 to 0.59 with RMSE% values between 25.6 and 51.9. Both H_{99} and H_{95} recorded the highest accuracy, with R^2 of 0.81 and 0.82 with RMSE% values 25.6 and 25.8 respectively. The accuracy statistics for the independent validation (Val02) dataset were very similar to Val01. Structural metrics H_{99} and H_{95} for Val02 were also the best performing models with R^2 values of 0.78 and 0.79 and RMSE% values of 25.9 and 25.8 respectively. In both validation datasets H_{25} was the lowest performing model, with RMSE% above 50%. While RMSE% values for each of the models were similar for both validation datasets, bias values for Val02 with exception for H_{mean} varied when compared with the Val01 results.

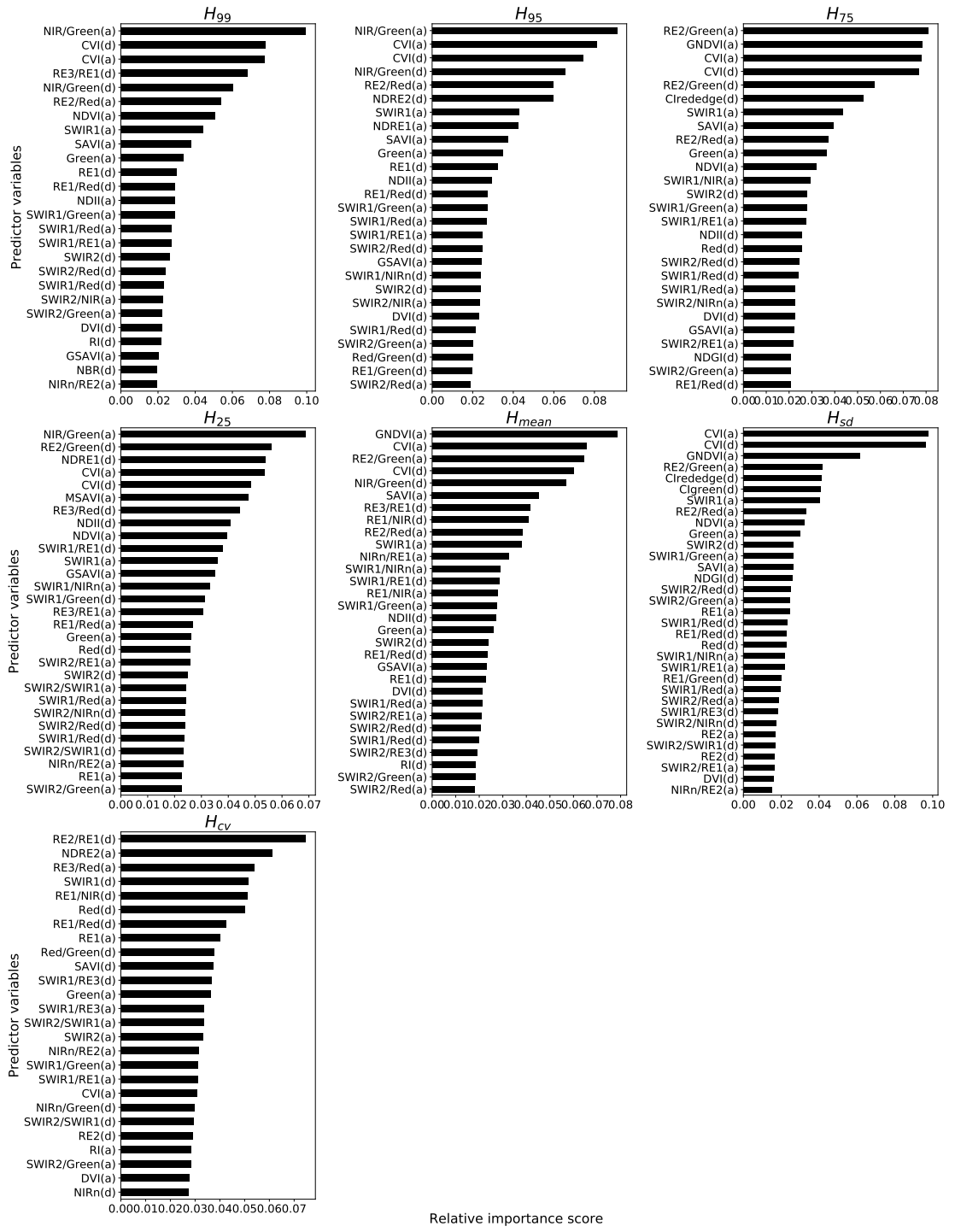


Fig. 4.8 Bar plots showing the predictor variables and relative importance score for each of the models predicting tree structure metrics from Sentinel-2 (20 m) imagery.

Table 4.7 Model accuracy statistics for tree structure metrics derived from Sentinel-2 imagery at 20 m spatial resolution for validation dataset Val01 (n=37,000) and Val02 (n=29,922).

Dataset/Metric	R ²	RMSE	RMSE%	BIAS	BIAS %
Val01					
H_{99} (m)	0.81	2.9	25.6	0.021	0.18
H_{95} (m)	0.82	2.7	25.8	0.016	0.16
H_{75} (m)	0.79	2.5	29.8	0.018	0.22
H_{25} (m)	0.60	2.2	51.9	0.052	1.25
H_{mean} (m)	0.78	1.9	30.7	0.029	0.47
H_{sd} (m)	0.77	0.9	32.8	0.013	0.48
H_{cov} (%)	0.59	14.5	35.2	0.272	0.66
Val02					
H_{99} (m)	0.78	2.7	25.9	-0.123	-1.18
H_{95} (m)	0.79	2.5	25.8	-0.202	-2.10
H_{75} (m)	0.75	2.3	30.3	-0.107	-1.42
H_{25} (m)	0.52	1.9	55.4	0.150	4.31
H_{mean} (m)	0.74	1.7	30.8	-0.006	-0.11
H_{sd} (m)	0.73	0.9	32.4	-0.041	-1.51
H_{cov} (%)	0.53	15.7	34.4	-1.013	-2.23

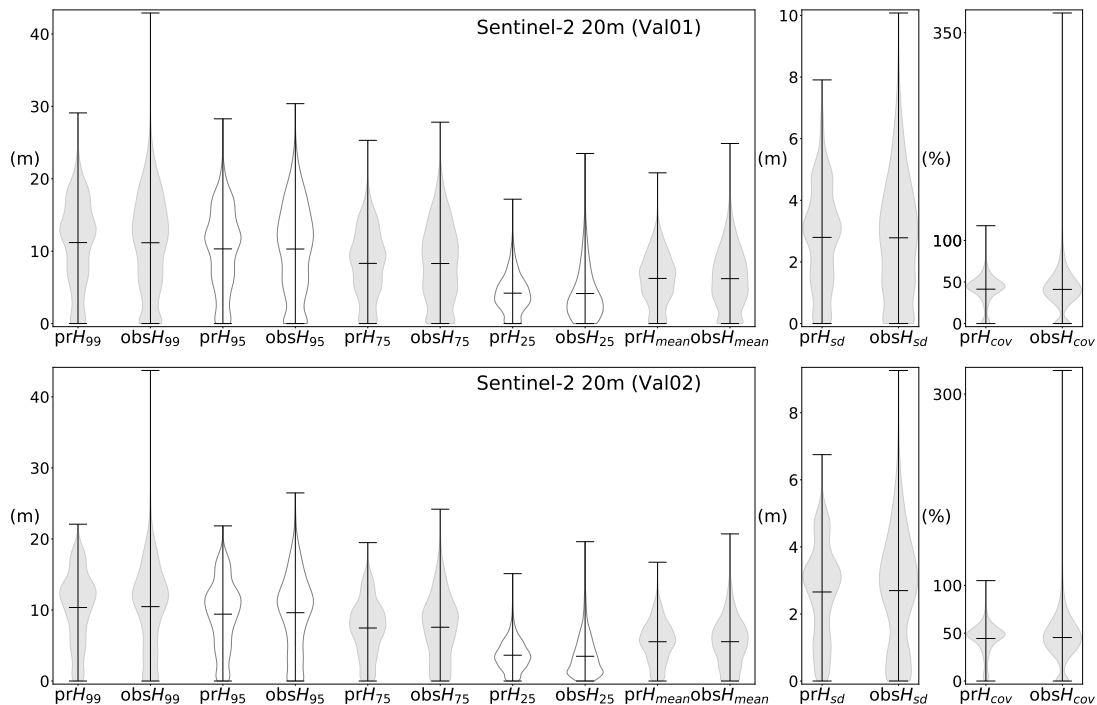


Fig. 4.9 Violin plots showing summary statistics (mean, min, max) and the distribution of the observed (LiDAR derived) and predicted tree structure metrics from Sentinel-2 at spatial resolution 20 m for validation datasets Val01 and Val02.

4.3.1.5 Sentinel-2 30 m

The number of predictor variables and relative importance scores for each structural metrics modelled from Sentinel-2 at 30 m spatial resolution is shown in Figure 4.10. The number of predictor variables used in each of the seven models ranged from 21 to 35. A number of vegetation indices, band ratios and spectral bands were used in each model, derived from both the annual and dry season composites. Three variables CVI(a), SWIR1/Green(a) and SWIR1/RE1(d) were used in all seven models. Eight predictor variables (SWIR2/SWIR1(d), SWIR2/Red(a), CVI(d), RE1(d), RE1/NIR(a), RE1/NIR(d), SWIR2/Green(a) and SWIR1/Green(d)) occurred six time. The vegetation index CVI featured as the most important variable for five of the seven models. Models accuracy statistics for validation datasets Val01 and Val02 are presented in Table 4.8. Summary statistics showing the distribution of the predicted and observed values for each structural metric is shown in Figure 4.11. The overall accuracy for the majority of the models were high for both validation datasets (Val01 and Val02). Five of the structural metrics (H_{99} , H_{95} , H_{75} , H_{mean} and H_{sd}) recorded RMSE% values below 30%. The structural metrics H_{99} and H_{95} for both Val01 and Val02 recorded the highest overall accuracy with R^2 values ranging from 0.80 to 0.76 and RMSE% values between 22.9 and 24.1. The lowest accuracy was recorded for H_{25} with RMSE% values of 47.3 (Val01) and 49.1 (Val02). Bias values for both validation datasets were generally low, with exception for H_{cov} (Val01 and Val02) and H_{25} (Val02).

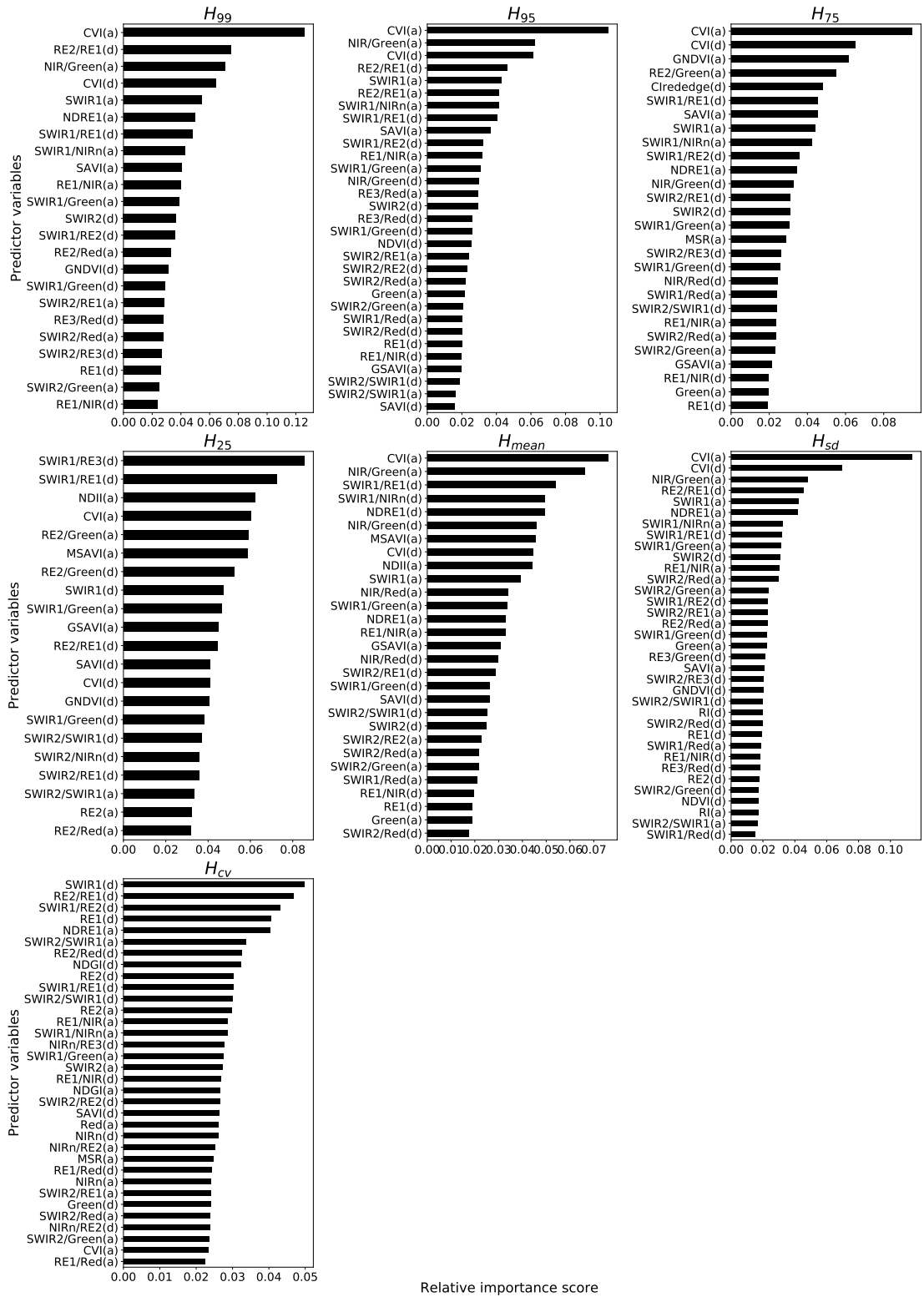


Fig. 4.10 Bar plots showing the predictor variables and relative importance score for each of the models predicting tree structure metrics from Sentinel-2 (30 m) imagery.

Table 4.8 Model accuracy statistics for tree structure metrics derived from Sentinel-2 imagery at 30 m spatial resolution for validation dataset Val01 (n=37,000) and Val02 (n=29,864).

Dataset/Metric	R ²	RMSE	RMSE%	BIAS	BIAS %
Val01					
H_{99} (m)	0.76	3.1	22.9	-0.010	-0.08
H_{95} (m)	0.78	2.8	23.2	-0.010	-0.08
H_{75} (m)	0.76	2.5	26.5	-0.002	-0.02
H_{25} (m)	0.60	2.1	47.3	0.026	0.60
H_{mean} (m)	0.76	1.9	26.9	0.006	0.09
H_{sd} (m)	0.71	1.0	29.4	0.009	0.26
H_{cov} (%)	0.48	15.5	32.4	0.306	0.64
Val02					
H_{99} (m)	0.80	2.6	23.6	0.012	0.11
H_{95} (m)	0.80	2.4	24.1	0.069	0.70
H_{75} (m)	0.78	2.1	27.2	0.067	0.88
H_{25} (m)	0.58	1.7	49.1	0.186	5.46
H_{mean} (m)	0.77	1.5	27.5	0.067	1.21
H_{sd} (m)	0.75	0.8	29.7	0.012	0.43
H_{cov} (%)	0.52	14.3	30.5	-0.194	-0.41

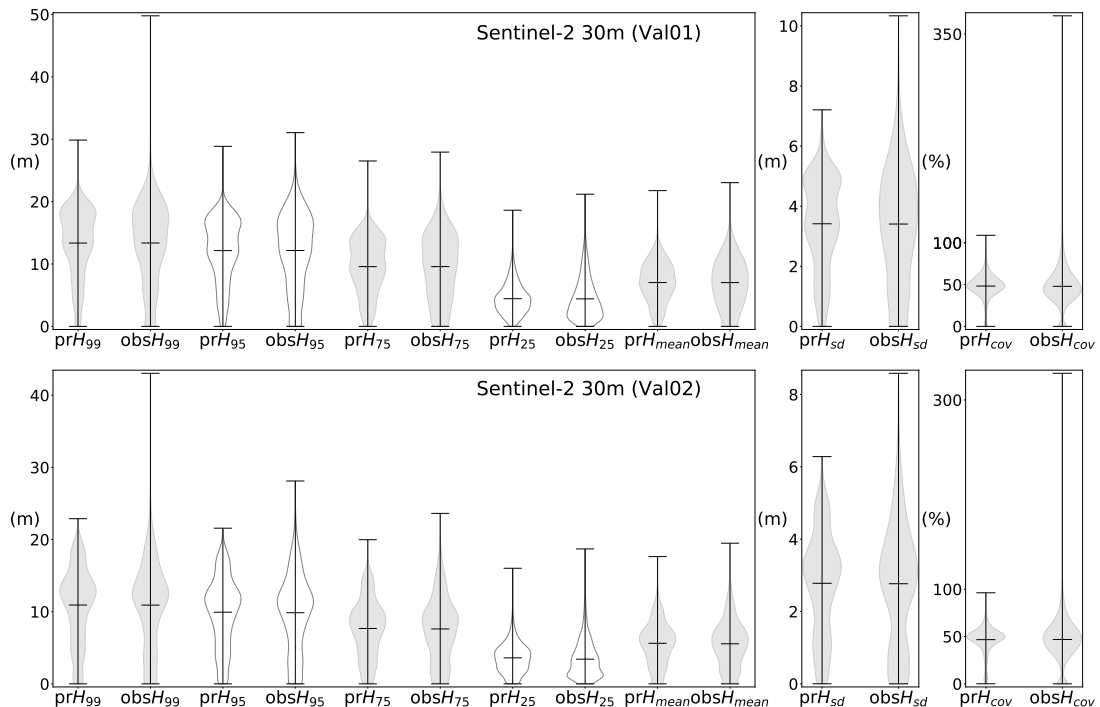


Fig. 4.11 Violin plots showing summary statistics (mean, min, max) and the distribution of the observed (LiDAR derived) and predicted tree structure metrics from Sentinel-2 at spatial resolution 30 m for validation datasets Val01 and Val02.

4.3.1.6 Landsat-8 30 m

The variable importance scores for the seven structural metrics modelled from Landsat-8 imagery are presented in Figure 4.12. The number of predictor variables used in each model ranged from 16 to 25, consisting of a variety of vegetation indices, band ratios and spectral bands derived from the annual and seasonal composite. Six of the predictor variables (CVI(a), SWIR2/Red(d), SWIR2/Red(a), CVI(d), SWIR1/Green(a), SWIR1/Green(d)) occurred in all models. The band ratios SWIR1/Red(a) and SWIR1/Red(d) occurred in six models. For five models (H_{99} , H_{95} , H_{75} and H_{sd}) the vegetation index CVI was the most important predictor variable. Accuracy statistics for the two validation datasets (Val01 and Val02) are presented in Table 4.9. Violin plots showing the distribution and summary statistics for the predicted and observed values are presented in Figure 4.13. RMSE% values for both validation datasets ranged from 24.0 to 49.9, with four metrics (H_{99} , H_{95} , H_{75} and H_{mean}) recording values below 30%. The metrics H_{99} and H_{95} recorded the highest overall accuracy with R^2 values between 0.77 and 0.74 and RMSE% of 24.0 and 25.7, bias results were higher for both H_{99} and H_{95} in the Val02 dataset. Both H_{sd} and H_{cov} recorded RMSE% values between 30.2 and 34.4, while H_{25} was the lowest performing model with RMSE% of 49.7 and 49.9 for Val01 and Val02 respectively. While the bias values were low they did increase for all metrics for Val02.

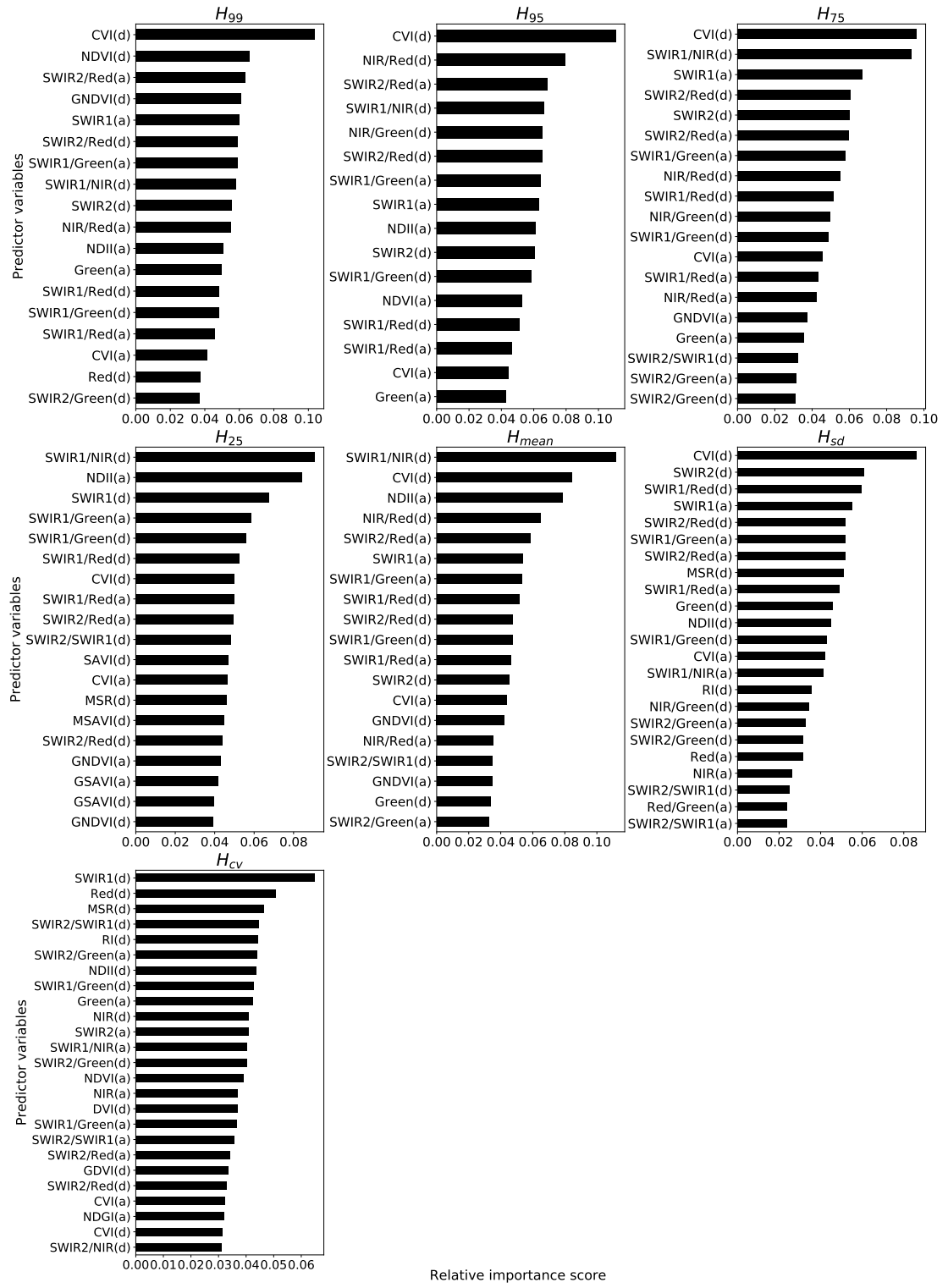


Fig. 4.12 Bar plots showing the predictor variables and relative importance score for each of the models predicting tree structure metrics from Landsat-8 (30 m) imagery.

Table 4.9 Model accuracy statistics for tree structure metrics derived from Landsat-8 imagery at 30 m spatial resolution for validation dataset Val01 (n=37,000) and Val02 (n=29,727).

Dataset/Metric	R ²	RMSE	RMSE%	BIAS	BIAS %
Val01					
H ₉₉ (m)	0.74	3.2	24.0	0.053	0.39
H ₉₅ (m)	0.74	3.0	24.6	0.054	0.44
H ₇₅ (m)	0.73	2.7	27.7	0.044	0.45
H ₂₅ (m)	0.55	2.2	49.7	0.039	0.89
H _{mean} (m)	0.72	2.0	28.4	0.035	0.49
H _{sd} (m)	0.69	1.0	30.2	0.021	0.61
H _{cov} (%)	0.42	16.6	34.4	-0.217	-0.45
Val02					
H ₉₉ (m)	0.77	2.7	25.0	0.277	2.54
H ₉₅ (m)	0.77	2.5	25.7	0.220	2.22
H ₇₅ (m)	0.75	2.2	29.1	0.120	1.58
H ₂₅ (m)	0.56	1.7	49.9	0.144	4.20
H _{mean} (m)	0.75	1.6	29.0	0.113	2.03
H _{sd} (m)	0.72	0.9	31.4	0.054	1.93
H _{cov} (%)	0.52	14.3	30.5	0.817	1.74

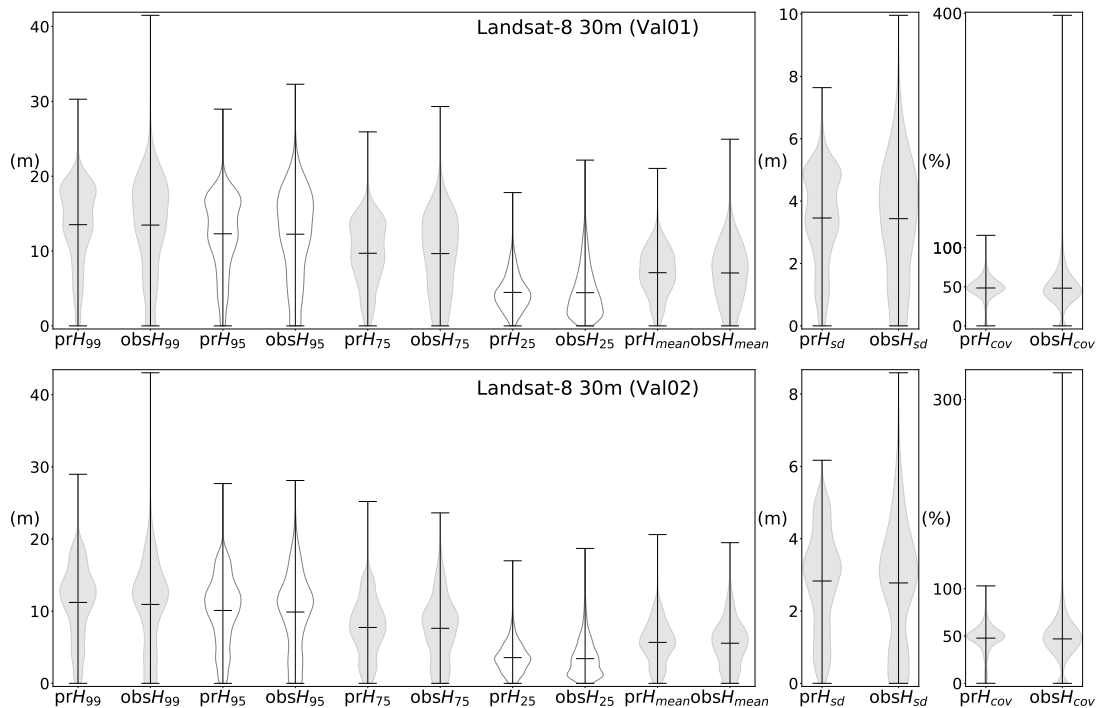


Fig. 4.13 Violin plots showing summary statistics (mean, min, max) and the distribution of the observed (LiDAR derived) and predicted tree structure metrics from Landsat-8 at spatial resolution 30 m for validation datasets Val01 and Val02.

4.4 Discussion

Predictive models for tree canopy structure metrics were developed for Sentinel-2 at spatial scales of 10 m, 20 m and 30 m and for Landsat-8 at 30 m, enabling the production of mapping products detailing a number of tree canopy structure metrics. The first map of forest 99th percentile canopy height (H₉₉) derived from Sentinel-2 imagery at 10 m spatial resolution for our study area is shown in Figure 4.14. These products have the

potential to be used in a variety of applications including vegetation mapping, natural resource management, land use change, and habitat mapping for biodiversity.

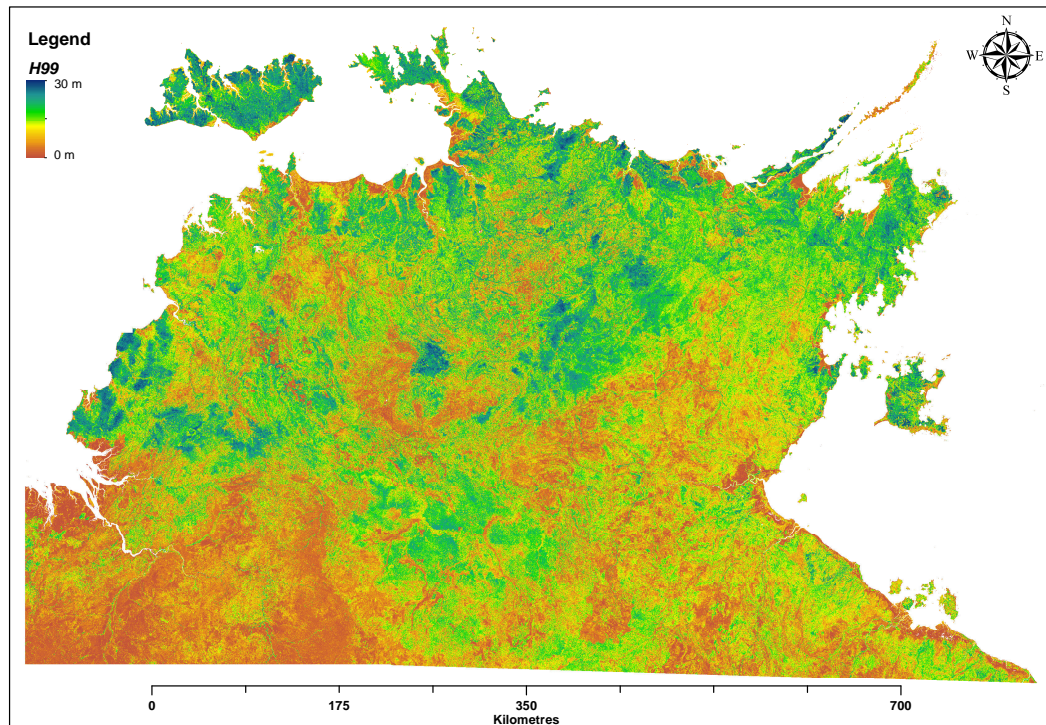


Fig. 4.14 Estimates of forest 99th percentile canopy height (H_{99}) derived from 2018 Sentinel-2 satellite imagery at 10 m spatial resolution for the northern half of the Northern Territory.

4.4.1 Important predictor variables

Predictor variables for both Sentinel-2 and Landsat-8 were produced from two seasonal composites (annual and dry season) for the year of each LiDAR capture. The use of multi-seasonal composites enabled us to exploit the change in spectral response in vegetation communities over the study area (Williams et al. 1997). Estimates of H_{mean} were obtained from a single date Landsat-5 TM image in the Darwin region, with an overall with R^2 and RMSE values of 0.53 and 2.8 m respectively (Staben et al. 2018). In this study H_{mean} predicted from Landsat-8 in the same region improved with RMSE values of 2.0 m for the Val01 and 1.6 m for Val02 dataset. While the improved radiometric properties of the Landsat-8 sensor (Wulder et al. 2019) are likely to be contributing to the higher overall accuracy observed in this study, the additional number of predictor variables contrasting the seasonal responses in vegetation communities is also likely to have had a positive impact. Higginbottom et al. (2018) developed models predicting fractional woody cover in South African semi-arid savanna and found that using multi-seasonal (wet and dry season) composites produced higher levels of accuracy. The results of this study clearly demonstrate that the additional information available in the

seasonal composites were important to the development of the models, with all models comprising of parameters derived from both the annual and dry season composites. In a number of the models, the same parameter (e.g. CVI) derived from both the annual and dry season composites featured in the model (Figures 4.6, 4.8, 4.10 and 4.12).

The additional red-edge bands available with Sentinel-2 sensor were found to be important and featured in all models produced from the three spatial scales. Lang et al. (2019) used convolutional neural networks to produce vegetation height mapping at 10 m spatial resolution from Sentinel-2 across two distinct regions: Switzerland (Europe) and Gabon (tropics) and reported that the higher resolution bands (10 m) contained most of the relevant information. The importance of the 10 m bands in the Lang et al. (2019) study was attributed to the fact that individual trees were represented by single pixels which enhanced the textural features used in the modeling. In this study, texture parameters were not used and both the 10 m and 20 m spectral bands were found to be important and featured in all the Sentinel-2 models.

4.4.2 Scale effects

For all the seven tree canopy metrics, overall performance increased along with a decrease in spatial resolution. Sentinel-2 at 30 m had the strongest relationship across all structural metrics, followed by Landsat-8 and Sentinel-2 at 20 m. There was very little difference between the performance of most models for both Sentinel-2 at 20 m and Landsat-8 with differences in RMSE% scores of $\approx 2\%$. Sentinel-2 at 10 m recorded the lowest accuracy across all models with $\approx 10\%$ difference in RMSE% compared with Sentinel-2 at 30 m. One factor contributing to the reduction in the overall accuracy of the 10 m models is likely due to misregistration errors between the training and validation datasets and the Sentinel-2 10 m spectral bands. In some cases, the 10 m pixels representing the spectral response of tree crowns were offset when compared to the LiDAR canopy height models. In Figure 4.15, the tree canopy represented by the LiDAR canopy height model can be seen to be offset from the Sentinel-2 pixels and shows that a number of the pixels covered by the extent of canopy height model were influenced by shadow. As the spatial resolution increases the effect of the misregistration is minimised, reducing the noise in the training data and overall variance in the validation datasets. The misregistration errors in the 10 m models are likely to have contributed to a reduction in the overall accuracy scores for each of the models.

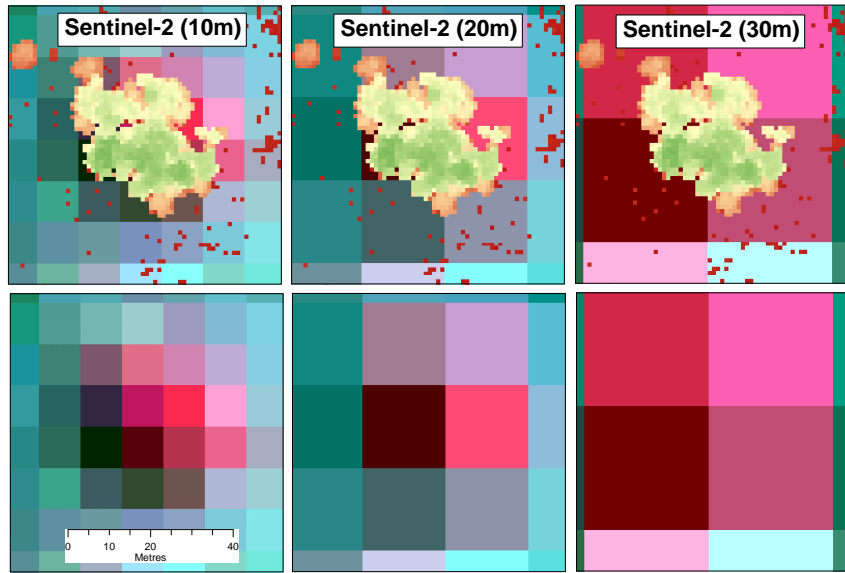


Fig. 4.15 Example of the misregistration errors between the LiDAR canopy height model and the 10 m Sentinel-2 pixels and the influence of different spatial resolutions in absorbing this error. All Sentinel-2 imagery displayed in the NIR, Red and Green spectral bands.

While model performance was lower for models derived from the 10 m Sentinel-2 imagery, the increased spatial resolution does provide increased detail in areas where woody vegetation has been cleared along narrow corridors or sharp changes in ecotone, such as mangrove forests and upland woodland communities (for an example see figure 4.16). The increased detail available at the 10 m spatial scale is significant and would be particularly important for some applications such as detection of land use change and vegetation mapping, however the suite of Landsat sensors at 30 m spatial resolution offers the potential to investigate change in forest structure over a 30 year time period.

4.4.3 Structural metrics performance

Of the seven structural metrics, both H_{99} and H_{95} , representing maximum canopy height recorded the strongest relationship with any of the four test model sets. The differences in the accuracy (based on both validation datasets) for H_{99} models produced from Sentinel-2 at 10 m, 20 m and 30 m and Landsat-8 were small with R^2 values ranging from 0.81 and 0.70 and RMSE% between 33.8 and 22.9. Overall model accuracy declined moving down the height profiles H_{75} , H_{mean} and H_{25} for all model sets. The accuracy of the two metrics characterising structural variability H_{sd} and H_{cov} improved as pixel size increased, with Sentinel-2 at 30 m recording RMSE% values marginal better than Landsat-8. While the additional red-edge bands available with Sentinel-2 featured as important predictor variables, the results of this study show

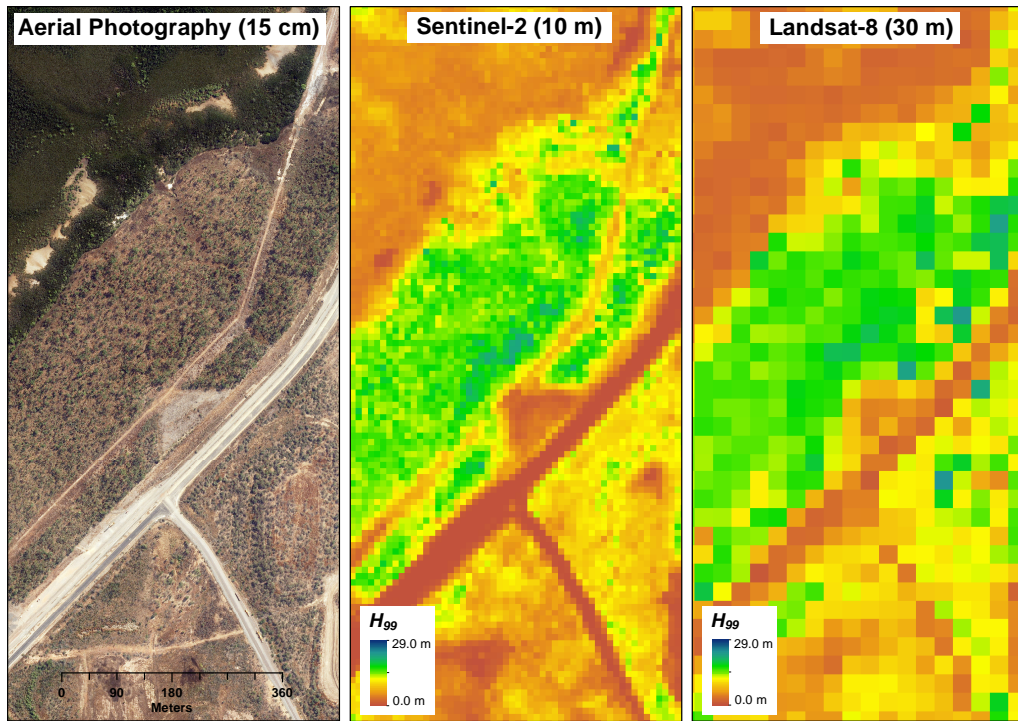


Fig. 4.16 Differences in the level of mapping detail due to scale effects for the H_{99} Sentinel-2 at 10 m and Landsat-8 30 m spatial resolution.

that they did not significantly improve any of the seven models' performance, when compared with Landsat-8. The validation dataset Val02 was used to assess how well the models generalised to unseen data, with the results showing that there was an increase in bias with many of the models. The increase in bias for the Val02 may indicate that the statistics derived from Val01 datasets are an optimistic assessment of the models accuracy due to the fact that the Val01 dataset is likely to be highly autocorrelated with the training dataset. Model development was undertaken on imagery captured in locations across the study area over three different time periods (2016, 2017, 2018), which is likely to have increased the variance in the reflectance values of the predictor variables and is likely to improve the generalisation ability of the models (Jin et al. 2018, Lang et al. 2019).

4.4.4 Characterising tree canopy structural variability

The models developed in this study characterise different aspects of forest structure. The maximum tree height for given pixels were represented by the metrics H_{99} and H_{95} which had a similar height distributions, while the distribution of the remaining metrics were more distinct and highlighted the variability in tree canopy structure. In figure 4.17, the structure metrics H_{99} , H_{mean} and H_{cov} models are displayed as a three band composite. This band combination of structural metrics helps to highlight the

variability in the forest structure across the landscape. For example the combination of these three metrics enable areas dominated by tall canopies such as the monsoon rain forest at Holmes Jungle Nature park to be identified (shown in figure 4.18), as there is little difference in the height values for H_{99} and H_{mean} , while the H_{cov} values are relatively low.

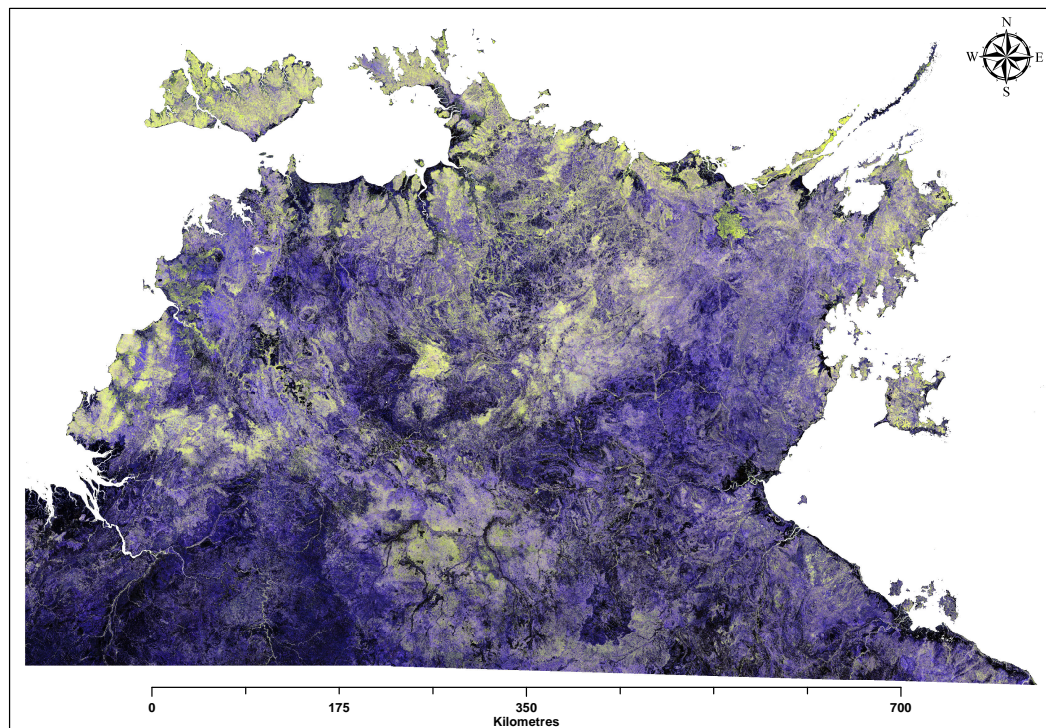


Fig. 4.17 Estimates of tree canopy structure (H_{99} , H_{mean} and H_{cov}) displayed as a three band composite (Red = H_{99} , Blue = H_{mean} and Green = H_{cov}), derived from 2018 Sentinel-2 satellite imagery at 10 m spatial resolution for the northern half of the Northern Territory.

In the open forests and woodlands which often contain a mid stratum of woody vegetation there is a greater difference between maximum (H_{99}) and mean (H_{mean}) canopy heights, with the increase in variability reflected in the values of H_{cov} . In areas with very little or no woody vegetation (dark areas in the imagery), the values for H_{99} , H_{mean} and H_{cov} are all very low. Stands of tall trees which are generally long lived and contain hollows are very important habitat for a number of fauna species in northern Australia (Woolley et al. 2018). The structural metrics developed in this study have the potential to identify the spatial distribution of tall trees and assist in the mapping of important habitats across the landscape. While this study aimed to produce quantitative models, the results for the structural metric H_{25} were low and limit its use, however as a mapping product it does appear to highlight areas of tall trees. Further investigation, including fieldwork is required to understand and validate what is being identified in

the H_{25} product and the different patterns visible in the three band composite imagery.

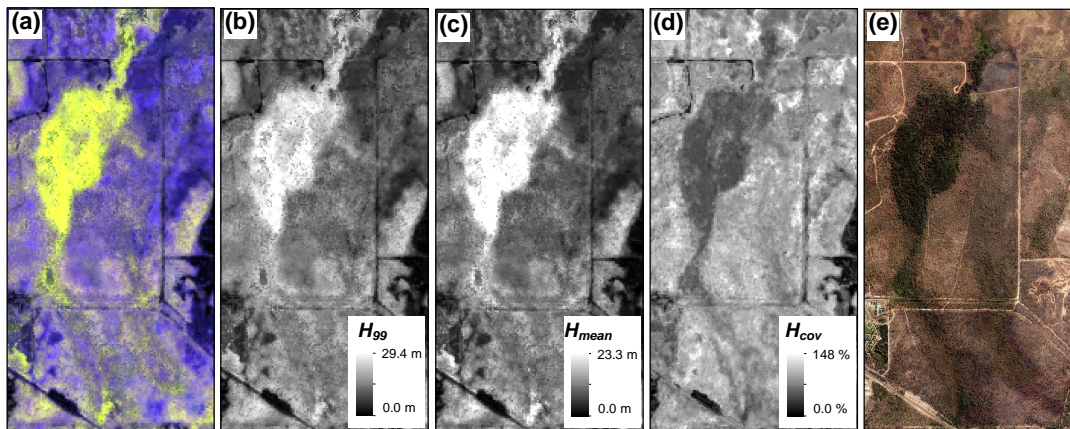


Fig. 4.18 Example of tree canopy structure metrics displayed as a three band composite (a), H_{99} (b), H_{mean} (c) and H_{cov} (d) estimated from Sentinel-2 at 10 m spatial resolution. The 15 cm digital aerial photograph (e) was captured in 2018.

4.5 Conclusion.

This study has demonstrated the utility of optical satellite sensors Sentinel-2 MSI and Landsat-8 OLI for estimating forest structural metrics across the Northern Territory, Australia. Seven structural metrics, characterising tree canopy structure were obtained from LiDAR canopy height models (1 m spatial resolution) to use as training and validation data. The random forest algorithm was used to produce regression models at 10 m, 20 m and 30 m spatial resolution for Sentinel-2 and at 30 m for Landsat-8 imagery. Seasonal composites (annual and dry season) were produced for both Sentinel-2 and Landsat-8 to use as the predictor variables to provide an annual estimate of the tree canopy structural metrics. Seven models were developed estimating a range of canopy structural metrics including, canopy height percentiles ($H_{99}, H_{95}, H_{75}, H_{25}$), mean (H_{mean}), standard deviation (H_{sd}) and coefficient of variation (H_{cov}) for three spatial scales. Overall, model accuracy was found to improve as spatial resolution decreased, with models produced at 30 m recording the highest overall accuracy. For Sentinel-2, the red-edge bands featured as important predictor variables, however they did not significantly improve model performance when compared with the models derived from Landsat-8, at 30 m spatial resolution. Of the seven models, H_{99} (representing maximum canopy height) had the strongest relationship for both Sentinel-2 and Landsat-8 with R^2 values ranging from 0.81 and 0.70 and RMSE% between 33.8 and 22.9. While model accuracy declined with a reduction in spatial scale, models at 10 m spatial resolution provided much higher level of detail across the landscape, making them valuable for certain applications such as land use change and vegetation mapping. While the spatial detail in the 30 m products is reduced, the Landsat archive offers

the potential to assess both spatial and temporal change in forest structure across the Northern Territory, however further work is required to assess how well the Landsat-8 models generalise to Landsat-7 and Landsat-5 sensors. The methods produced in this study show that multiple LiDAR datasets captured across time and space can be used as training data to develop robust models predicting a variety of tree canopy structural metrics from Sentinel-2 and Landsat-8 satellite sensors. While the models were developed over an extensive area across the Northern Territory, it likely that the methodology can be applied more broadly across northern Australia. This study has produced mapping products with the potential to enhance understanding of savanna ecosystems and presents the first mapping product at 10 m spatial resolution, giving greater insight into tree canopy structure across northern Australia.

CHAPTER 5

Remote sensing of structural dynamics of woody vegetation in northern Australia impacted by severe tropical cyclone Monica

Thesis context: The focus of this chapter is on the development of a remote sensing product to enable investigation of the impact of tropical cyclones on the the structural dynamics of woody vegetation. This study is the culmination of the research undertaken in chapters 2, 3 and 4 and demonstrates the utility of remotely sensed products for assessing cyclone impacts on native vegetation at a regional scale.

Abstract

Mapping products were developed to provide insight into the spatial and temporal dynamics of woody vegetation structure in northern Australia's savannas. Annual estimates of canopy cover and height derived from Landsat satellite imagery were combined to produce a structural classification product for a 30 year period (1988-2017). Landsat estimates of woody foliage projective cover (FPC) were validated and corrected for bias using estimates of FPC obtained from aerial photography. The bias corrected Landsat FPC were then converted to canopy cover using a generalised model developed from field data across Australia. The Landsat estimates of CC were then validated using independent field data, while the Landsat canopy height estimates were validated using canopy height models derived from LiDAR. The structural classification scheme developed in this study took into account the Australian national classification scheme, structural attributes of the vegetation in the study area and the error in both the Landsat CC and canopy height estimates. The structural mapping product was then used to investigate the dynamics of woody vegetation in a region ($\approx 11,500 \text{ km}^2$) impacted by severe tropical cyclone Monica in 2006. It was estimated that a total area of $3,551 \text{ km}^2$ was substantially impacted by cyclone Monica. The rate of recovery was assessed and shows that the region is steadily recovering, with 70 km^2 estimated to still be severely impacted in 2017. The proportion of each structural class between the years 2004 and 2017 was used to gain insight into the structural dynamics and recovery of woody vegetation post cyclone Monica. The results show that recovery is occurring across the region, however the dynamics observed between the structural classes suggest that the region is still recovering 11 years after the cyclone.

5.1 Introduction

Tropical cyclones occur on a frequent basis across the northern Australian coastline (Cook and Nicholls 2009). The destructive winds associated with these cyclones can have a major impact on both the man-made and natural environment. The impact of cyclonic winds are greatest on the coastal regions, however they also have the potential to cause significant disturbance further inland (e.g. Cyclone Monica). The impact on native vegetation can be substantial, resulting in major structural changes to vegetation communities. A number of studies have reported on the impact of cyclones on vegetation in Australia's Northern Territory (Stocker 1976, Fox 1980, Cameron et al. 1983, Bowman and Panton 1994b, Cook and Goyens 2008, Staben and Evans 2008, Williamson et al. 2011, Hutley et al. 2013, Russell-Smith et al. 2019). These studies have used a number of different methods ranging from collection of field data, aerial photography and satellite imagery. Although cyclones are frequent and have the potential to be a major disturbance agent in coastal and subcoastal ecosystems across northern Australia (Murphy 1984), there is limited information on the impact and potential role they play in driving the structure of these communities (Cook and Goyens 2008). A number of studies have looked at landscape change (woody cover) in vegetation communities in the Alligator Rivers Region of the Northern Territory (Banfai and Bowman 2006, Bowman and Dingle 2006, Banfai and Bowman 2007, Lehmann et al. 2008, 2009, Bowman et al. 2010). These studies used manual interpretation techniques of aerial photography spanning a 40 year period (1964, 1984, 1991 and 2004) to measure changes in woody cover, and in general reported a trend in woody expansion and densification (Williamson et al. 2011). These studies also looked at a range of possible drivers responsible for the changes observed which included increased rainfall, changes in feral animal populations, increased CO₂ levels and changes in fire regimes. Notably the effects of wind as a disturbance factor were largely not considered as a possible contributor to the changes they observed. While no definitive reason could be given for the changes observed in Bowman and Dingle (2006), Lehmann et al. (2008, 2009), Bowman et al. (2010), it was suggested that research at a regional scale may help to gain a better understanding of the factors (Williamson et al. 2011).

Hutley et al. (2013) quantified the impact of cyclone Monica using the empirical models developed by Cook and Goyens (2008) to estimate the severity of tree damage. They also used satellite imagery (moderate resolution imaging spectroradiometer (MODIS)) to assess gross primary productivity (GPP) and fire frequency post cyclone Monica. They reported that GPP was suppressed for four years after cyclone Monica and that the increased fuel loads from destruction of the tree canopy did not dramatically shift

fire regimes, however there was evidence that fires were more frequent in areas with high levels of damage. It was estimated the on-ground fuel loads as a result of cyclone Monica had the potential to represent $\approx 10\%$ of Australia's accountable green house emissions. Nevertheless, they concluded that the carbon balance is likely to be dominated by fire and termite consumption rather than infrequent extreme disturbance events such as cyclone Monica. They suggested that tracking recovery of highly damaged areas, monitoring fuel consumption and the rate of return of woody vegetation is required to gain a better understanding of cyclone disturbance and the impact it has on savanna structure and function (Hutley et al. 2013). Understanding change in woody vegetation structure is also important for biodiversity conservation management (Levick et al. 2019). Disturbance from cyclone and fire was found to be related to the availability of tree hollows, which are important habitat for many declining fauna species (Woolley et al. 2018). Understanding both the spatial and temporal distribution of the impact of cyclones on the structure of woody vegetation is important as it has the potential to increases the accuracy of carbon stock estimates (Cook et al. 2015, O'Grady et al. 2000, Hutley et al. 2013) and assist in identifying the location of large hollow-bearing trees, which are a keystone habitat in northern Australia for many fauna species (Woolley et al. 2018). It is clear from the level of disturbance a cyclone can have on a savanna ecosystems there is a need to gain a better understanding of their influence at a regional scale. Cook and Goyens (2008) proposed that to understand the role of tropical cyclones in the dynamics of the savanna ecosystems of northern Australia will require the knowledge of “(i) their immediate impacts; (ii) subsequent recovery processes and especially any interaction with fires; (iii) effects on landscape processes; and (iv) the probability of recurrence”.

The aim of this study is to produce information that enables both spatial and temporal analysis of the dynamics of woody vegetation structure, at a regional scale. Remotely sensed data offers a cost-effective way to investigate landscape change across northern Australia (Staben et al. 2016). In particular, the spatial and temporal resolution of the Landsat suite of satellites offers a unique record of northern Australia's landscape. The Landsat open (free) data policy has greatly enhanced its use (Wulder, Masek, Cohen, Loveland and Woodcock 2012). While Landsat data have become freely available, suitable methods need to be developed and applied to ensure accurate information can be derived from them. The objectives of this study are (1) to develop an annual mapping product that details the spatial and temporal distribution of woody vegetation structure between the years 1988 and 2017 using the Landsat sensors; and (2) investigate the impact of severe tropical cyclone Monica (2006) and subsequent recovery of woody vegetation across northern Australia. In this paper, we detail the development of the structural classification mapping product which is based on Landsat estimates of hor-

izontal (Armston et al. 2009) and vertical structure (chapter 4), including validation of the Landsat products using field data, digital aerial photography and LiDAR. We also present new insights in the structural dynamics of woody vegetation for a region impacted by severe tropical cyclone Monica (2006), including estimates of the area severely impacted and the subsequent recovery.

5.2 Data and Methods

The development of the structural classification products involved a number of broadly defined steps which include (1) validation of both the Landsat woody foliage projective cover (FPC) and tree height mapping products using digital aerial photography and LiDAR canopy height models, (2) development of a model to correct the bias in Landsat woody FPC, (3) conversion of the Landsat bias corrected woody FPC product to canopy cover (CC) using models derived from field data, (4) defining the structural classification scheme and, (5) producing the structural classification mapping product from the Landsat CC and canopy height products (Fig 5.1).

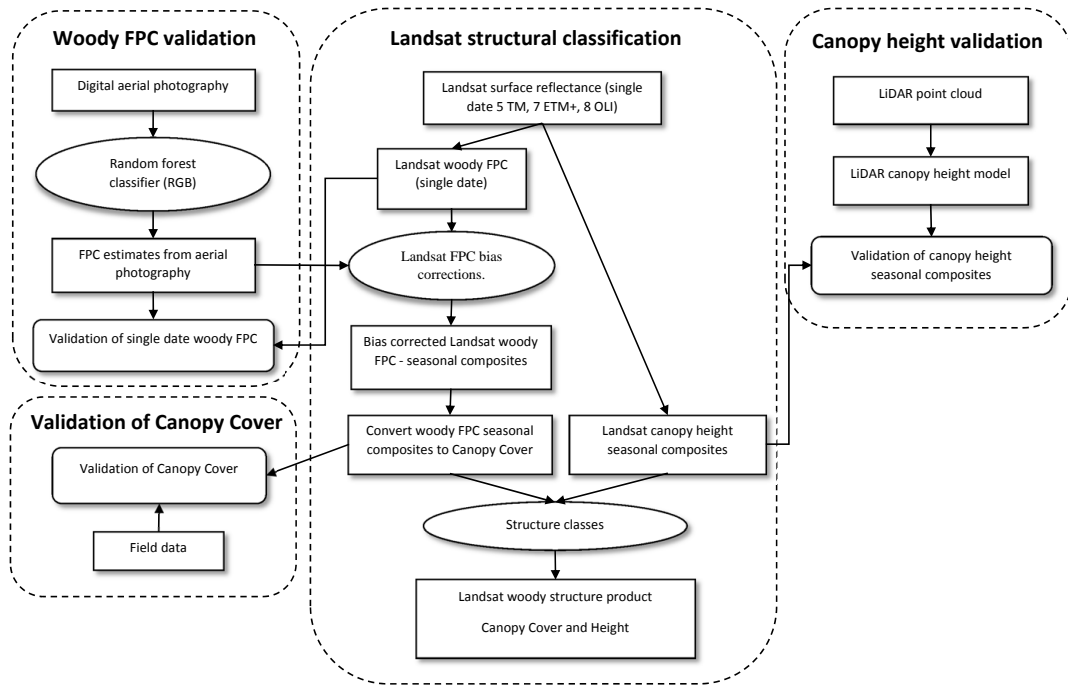


Fig. 5.1 Schematic showing the work flow used to produce the Landsat tree structure mapping product.

The following sections detail the development of the structural classification mapping products and the methodology used to investigate the impact of severe tropical cyclone Monica.

5.2.1 Study area

The study was undertaken in the northern Australian wet-dry tropics covering an area of approximately 355,500 km² in the Northern Territory (NT) (Figure 5.2). Temperatures across the study area are generally high all year with the mean annual maximum temperatures of 32°C on the coast (Darwin) to 34°C for inland regions, such as Katherine. The region is influenced by a monsoonal climate with the majority of the rainfall occurring between the months of October and April (McDonald and McAlpine 1991), with a distinct rainfall gradient moving south (Cook et al. 2015). Mean annual rainfall for Darwin on the north coast is 1725 mm, and 790 mm for Borroloola in the south east of the study area (<http://www.bom.gov.au/>).

The study area consists of a broad variety of vegetation communities dominated by savanna woodlands, open woodlands and open forests. Small areas of wet and dry rainforests are scattered across the region (Bach 2002, Wilson et al. 1990), with extensive areas of Mangroves forests found along the coastal regions (Lymburner et al. 2019, Duke et al. 2017). Large areas of coastal floodplain are dominated by herbaceous species, however woody plants such as *Melaleuca* spp. are found along the margins and can form extensive forests (Cowie et al. 2000). Vegetation on the sandstone plateaus consists of a mix of woodlands and shrublands, with patches of *Allosyncarpia* forest found within the gorges dissecting the plateaus (Wilson et al. 1990, Woinarski et al. 2006). The extensive savanna woodlands and open forests found on the undulating lateritic plains and plateaus are largely dominated by *Eucalyptus* and *Corymbia* species (Wilson et al. 1990). *Eucalyptus* species *E. tetrodonta* and *E. miniata* are the most dominant tree species found in the northern Australian woodlands (Woolley et al. 2018) and often consist of a mid-stratum of mixed semi-deciduous to deciduous trees and shrubs and grasses (Williams et al. 1997).

The case study in this paper focuses on dynamics of vegetation structure in the region impacted by intense tropical cyclone Monica in April 2006. Cyclone Monica developed in the Coral Sea, intensifying into a cyclone on the 17th April before moving in a westerly direction across the Cape York Peninsula into the Gulf of Carpentaria (Durden 2010). Cyclone Monica continued to develop as it moved in a westerly direction, making landfall at Junction Bay on the Northern Territory coastline (35 km west of Maningrida) as an intense category 5 system (Cook and Goyens 2008). The category 5 storm weakened as it moved inland in a south westerly direction, with maximum wind gusts of 118 km h⁻¹ at the town of Jabiru and 12 hours after first making landfall it had weakened to a tropical low over the city of Darwin (BOM 2019 <http://www.bom.gov.au/cyclone/history/monica.shtml> accessed 09/10/2019).

5.2.2 Satellite imagery

This study uses two existing models developed to predict information on horizontal (Armston et al. 2009) and vertical woody structure in chapter 4 from Landsat satellite imagery. Three Landsat sensors are utilised, Landsat-5 Thematic Mapper (TM), Landsat-7 Enhanced Thematic Mapper Plus (ETM+) and Landsat-8 Operational Land Imager (OLI). A number of pre-processing steps were applied to all of the Landsat imagery used in this study including, atmospheric correction using 6S radiative transfer code and application of a bi-directional reflectance distribution function (BRDF) model to take into account topographic illumination effects, producing surface reflectance values at nadir and a solar zenith angle of 45° (Flood 2014). Readers are referred to Flood et al. (2013) for a detailed description of the image pre-processing steps applied in this study. Cloud, shadow and water were also masked from the single date imagery. As large areas of the study area are burnt each year (Edwards et al. 2013), fire scars were masked using burnt area mapping product automatically derived from the single date Landsat imagery (Goodwin and Collett 2014). The Landsat imagery used in this study was captured between the years 1988 and 2018.

5.2.2.1 Landsat horizontal structure (Foliage projective cover)

Foliage projective cover (FPC) is the percentage of the sample site covered by the vertical projection of green foliage for woody vegetation, was used to characterise the horizontal structure. Estimates of woody FPC were obtained from single date Landsat imagery. These single date estimates of woody FPC were produced using a multiple linear regression model developed from field data, collected in the state of Queensland (QLD), Australia (Armston et al. 2009). The Landsat based woody FPC product is used by the Queensland Government for the Statewide Landcover and Trees Study (SLATS), and is routinely produced for all Landsat imagery captured across the Northern Territory under a collaborative agreement between the QLD and NT Governments. To obtain an annual estimate of woody FPC for each year seasonal composites were produced from Landsat imagery captured between the months of May and September. During these months, the grassy understorey is largely senescent and there is a greater spectral separability between woody and non-woody vegetation (Staben et al. 2018). The woody FPC seasonal composites for each year were produced using a multidimensional medoid (median) detailed in Flood (2013). Validation of the woody FPC products was undertaken using digital aerial photography across the study area, which is detailed in section 5.2.4.

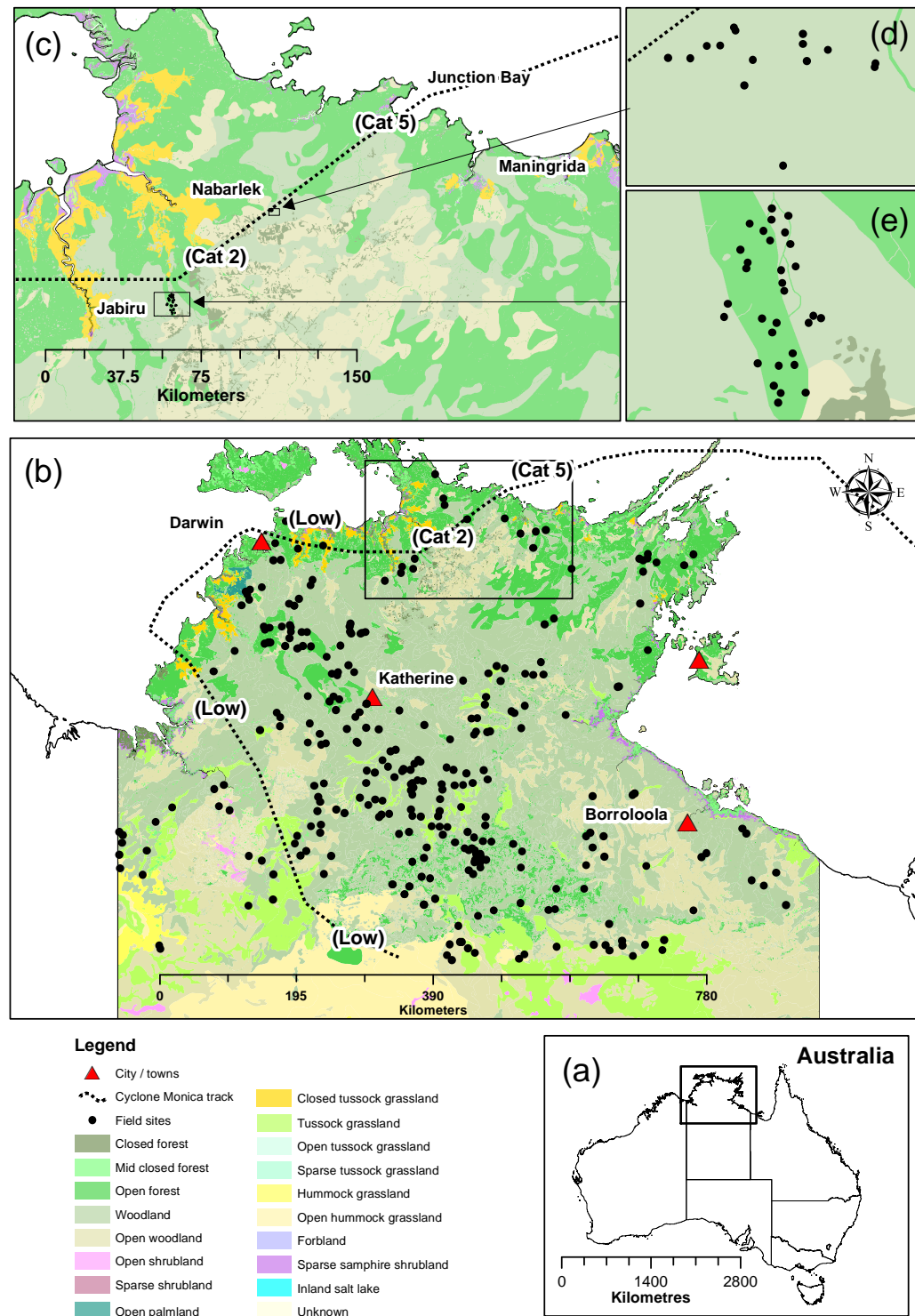


Fig. 5.2 Location of the study area in the Northern Territory, Australia (a) along with the track for cyclone Monica (BOM 2019), locations of the field sites used in this study and broad-scale vegetation structure (NVIS 1M) (b). The region used to assess the impact of cyclone Monica is also shown (c) and field sites at Narbarlek mine lease (d) and Gulungul Creek Catchment adjacent the town of Jabiru (e).

5.2.2.2 Landsat vertical structure (Canopy height)

Annual estimates of vertical tree structure were obtained from Landsat imagery using a random forest model predicting maximum canopy height for each pixel (chapter 4). Training data for the model were derived from 1 m LiDAR canopy height models captured across the NT in 2016, 2017 and 2018. For each 30 m Landsat pixel the 99th percentile height values (representing maximum canopy height) were calculated from the 1 m canopy height models. Predictor variables used in the modelling were derived from two Landsat surface reflectance seasonal composites representing the annual and dry season (May-September) for each year. Validation of the canopy height product using airborne LiDAR captured in 2011 and field sites measured in 2006 was undertaken as detailed in section 5.2.3.

5.2.2.3 Field data

A number of historic field datasets were available to assess the accuracy of the CC and tree canopy height estimates. Canopy Cover (CC) estimates measured using a point intercept method were available from 92 sites captured in 2000 (Meakin et al. 2001) and 212 sites measured as part of the Northern Territory Governments Rangelands monitoring program were available between 2016 and 2018. All CC estimates were from 100 m × 100 m plots using a point-based intercept method, which obtains measurements at 1 m intervals along 100 m tapes using a densiometer sight tube (Stumpf 1993). The tapes were either configured in a star shape (three 100 m tapes) for plots measured in 2016–2018 (Staben et al. 2016) or two 100 m tapes running parallel at a distance of approximately 100 m (Meakin et al. 2001).

In 2006, a total of 46 field plots (30 m × 30 m) were sampled to assess the impact of cyclone Monica on vegetation in the Gulungul Creek Catchment (near the town of Jabiru) and the Nabarlek mine lease (Figure 5.2 (e) (d)). Field sites were selected using a stratified random approach based on a classified 2005 Landsat image for the Gulungul Creek Catchment and for the Nabarlek mine lease land unit mapping (Day and Czachorowski 1982) were used (Saynor et al. 2009). The 31 plots in the Gulungul catchment were located within natural vegetation communities. Three of the plots at Nabarlek were located in rehabilitated areas and the remainder in natural vegetation communities (Staben et al. 2009, Saynor et al. 2009). A number of parameters were measured for trees (≥ 2 m in height) within each plot including; identification to species level (fallen and standing), tree height (standing trees visual estimated and fallen trees measured), diameter at breast height (DBH), tree fall orientation and assessment of the level of damage using one of 11 descriptors detailed in Table 5.1.

Table 5.1 Eleven status codes describing the level of impact of cyclone Monica on each tree ≥ 2 m in height.

Status Code	Description	Status Code	Description
AS	Alive standing undamaged	DU	Dead uprooted
ASS	Alive standing snapped trunk	DL	Dead leaning
ASB	Alive standing broken limbs	DSN	Dead snapped trunk
AU	Alive uprooted	DSC	Main trunk dead standing coppicing at base
AL	Alive leaning	DUC	Main trunk dead uprooted coppicing at base
		DS	Dead standing

The tree damage descriptors were used to produce CC and tree height statistics pre (2005) and post (2006) Cyclone Monica. All tree measurements were used to produce statistics representing 2005, while for 2006 four status codes (AS, ASS, ASB, AL) were used to produce the tree height statistics and five (AS, ASS, ASB, AL, AU) were used to produce the CC estimates. As CC was not directly measured in the field sites, estimates were derived from the basal area measurements for each plot by first predicting FPC from total plot basal area (Armston et al. 2009) and then CC from FPC (Fisher et al. 2018). The individual tree heights were used to calculate the 99th percentile tree height for each 30x30 m plot. The Landsat estimates of tree canopy height (H_{99}) and CC from for 2005 and 2006 were then compared with field estimates for each of the 46 field sites, accuracy was assessed using the statistics coefficient of determination (Zar 1984), RMSE and BIAS. The RMSE and BIAS are defined as;

$$RMSE = \sqrt{\frac{\sum (x_i - y_i)^2}{n}} \quad (5.1)$$

$$BIAS = \frac{1}{n} \sum_{i=1}^n x_i - \bar{y} \quad (5.2)$$

where n is the number of observations, y_i are the observed and x_i the predicted structural metrics and \bar{y} is the mean of y_i .

5.2.3 Validation of Landsat canopy height product

Airborne LiDAR captured over the Kakadu region in 2011 were used to validate the Landsat canopy height product. This LiDAR dataset was captured over a extensive area covering a broad range of vegetation communities with a focus on the Kakadu flood-plains. To reduce the computational time required to produce the LiDAR canopy height models, a subset of the LiDAR dataset representing a broad range of vegetation communities was selected covering an area approximately 3,780 ha (Fig 5.3). The LiDAR used in this study were captured using a Leica ALS60 sensor between 22nd October and 16th November 2011 at a flying height of 1409 m (AGL). The laser foot print was

0.32 m with an average point spacing of 2 points per m² and horizontal and vertical spatial accuracy of 0.8 m and 0.3 m respectively. We produced canopy height models from the LiDAR point clouds following the same methodology in chapter 4 which used the open source software Fusion http://forsys.cfr.washington.edu/fusion/fusion_overview.html. This involved producing surface models to enable the canopy heights to be normalised to the ground surface. To account for the senescent native grasses about 0.5 m tall when the LiDAR data were captured (Setterfield et al. 2010) pixels in the canopy height models between 0 and 0.51 m were removed from further analysis as they may represent the highest z value for a given pixel in the canopy height model.

Polygon grids based on the 30 m Landsat pixels were produced over the extent of the LiDAR canopy height models. The 99th percentile canopy height values were calculated from the LiDAR derived canopy height model for each of the 30 m polygon grids and compared with the Landsat derived estimates resulting in a validation dataset of 42,000 points. The accuracy of the 99th percentile canopy height values were assessed using the coefficient of determination (Zar 1984), root mean squared error (RMSE) and BIAS.

5.2.4 Validation of the Landsat Woody FPC product

Previous studies have successfully demonstrated that very high resolution imagery can be used to obtain cover estimates of woody vegetation (Sharp and Bowman 2004, Fenham and Fairfax 2007, Coggins et al. 2008, Staben et al. 2016, Higginbottom et al. 2018, Whiteside and Bartolo 2018, Melville et al. 2019, Barnetson et al. 2019). Staben et al. (2016) have shown that estimates of woody FPC can be reliably estimated from digital aerial photography when compared with field plots across our study area. To assess the Landsat woody FPC product we obtain estimates of woody FPC from subsets of digital aerial photograph mosaics captured between the years 2008-2018 across the study area. The digital aerial photography used in this study were captured using either a Vexcel Ultracam D or Ultracam X large-format digital camera on a fixed wing aircraft. The aerial photography was processed by commercial contractors producing a true colour (red, green, blue) orthorectified mosaic with a dynamic range of 8 bit, with a reported spatial accuracy of 1 m (Staben et al. 2016).

To obtain the woody FPC estimates from the aerial photography we used a supervised classification technique based on the machine-learning algorithm random forest. Random forest produces an ensemble of decision trees built from a bootstrap sample of the training data. The combined ensemble of decision trees reduces the risk of overfitting

and produces more accurate results (Breiman 2001). The random forest classifier is relatively easy to parameterise and requires a minimum of two parameters to be set. These parameters include the number of trees and the number of predictor variable used to grow the trees (Pedregosa et al. 2011). In this study, the number of trees and the number of predictor variables were set to 200 and ‘auto’ respectively. The ‘auto’ parameter in the random forest classifier is calculated as the square root of all features. The random forest algorithm implemented in this study is based on the open source python programming language and the scikit-learn machine-learning library (Pedregosa et al. 2011). Training and validation data were selected from a number of aerial photograph mosaics located across the NT. Five classes were defined representing either woody green, non-woody green, bare, shadow and branch/trunk (Table 5.2. A total of 17,012 pixels (vector point file) were visually assessed and assigned to one of the five classes. To assess the accuracy of the classification, 80% of the 17,012 points were randomly selected to train the classifier, while 3,403 data points were used to produce an error matrix. All 17,012 data points were then used to train the final classifier which was applied to plots across the aerial photography to estimate woody FPC.

Table 5.2 Description of the classes used in the development of the digital aerial photography random forest classifier

Class	Description
Woody green	Green leaf for all woody vegetation
Non-woody green	Green leaf from all non-woody vegetation
Bare	Bare ground and senescent vegetation (woody and non-woody)
Shadow	Shadow
Branch/trunk	Branches and trunks of woody vegetation

Field data collected over 1 ha plots covering at least 3x3 Landsat pixels were used to develop the Landsat woody FPC product used in this study (Armston et al. 2009). To replicate the size of the field plots used to develop the woody FPC model we obtained woody FPC estimates from the aerial photography over an area covering 3×3 Landsat pixels (0.81 ha). A total of 6,305 plots were selected representing a broad range of vegetation communities from across the study area. A grid of 90×90 m (representing 3×3 Landsat pixels) were generated over each of the aerial photography mosaics. For the majority of aerial mosaics, the plots were randomly selected from the grid, however for rainforest communities plots were manually selected to obtain a larger sample size and for the smaller subsets of the aerial mosaics the entire area was used to assess the Landsat woody FPC product. For each of the 90×90 m plots the woody FPC estimate was calculated from the aerial photography by summing the total number of pixels classified as green woody vegetation and dividing it by the total number of pixels per plot. Estimates of Landsat woody FPC were then obtained for each of the 6,305 plots using cloud free Landsat images captured closest to the date of the aerial photography.

The accuracy of the woody FPC product was assessed using the statistics coefficient of determination (R^2), RMSE and BIAS.

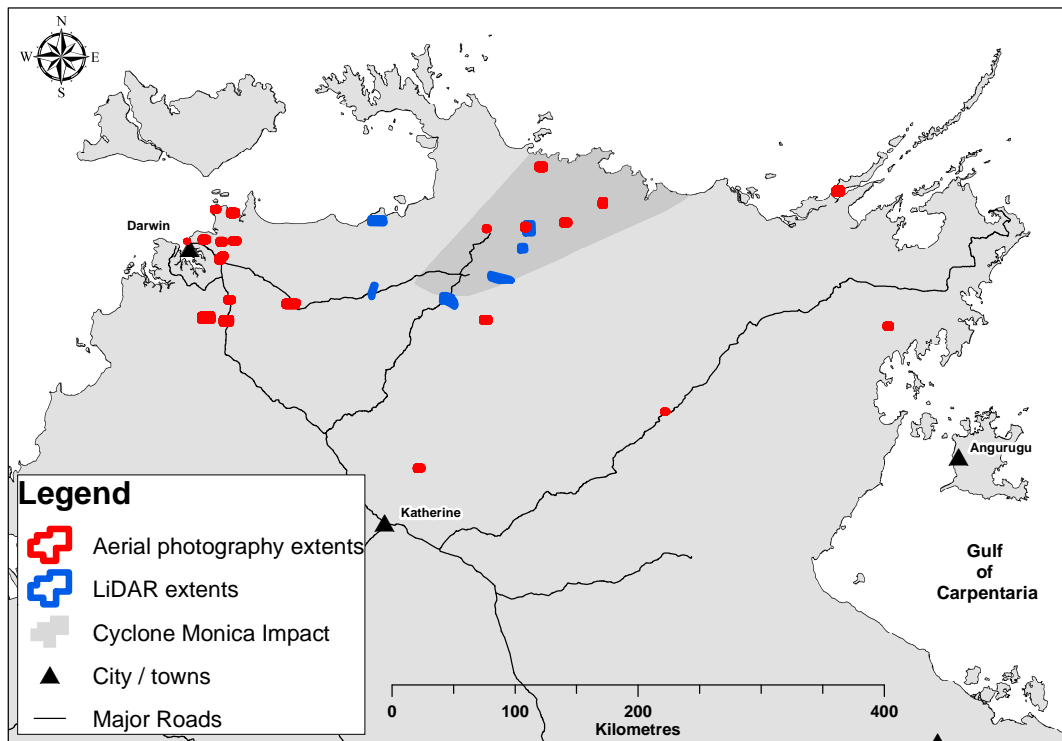


Fig. 5.3 Location of the digital aerial photographs and LiDAR used to validate the woody FPC and canopy height estimates from Landsat imagery.

5.2.5 Correcting the bias in Landsat satellite estimates of foliage projective cover.

A number of studies have shown that the relationship between canopy cover and Landsat derived indices or products in our study area is non-linear and follows a sigmoid curve (Staben and Evans 2008, Lymburner et al. 2019). To correct the systematic bias observed during the validation of the Landsat woody FPC product used in this study we developed a model using the aerial photography woody FPC estimates as the dependent variable and Landsat FPC product as the independent variable based on a sigmoidal equation;

$$LsatC_{FPC} = 100 * (1 - \exp(-k * FPC^b)) \quad (5.3)$$

where FPC is the estimate obtained from the single date Landsat imagery, k and b represent the fitting constants. Seventy percent of the 6,305 aerial photograph plots were randomly selected to train the sigmoid function and remaining 30 % were used to independently validate the accuracy of the model. The accuracy of the model was assessed using the statistics coefficient of determination (R^2), RMSE and BIAS.

5.2.6 Converting foliage projective cover to canopy cover

Canopy cover is commonly used to describe the structure in Australian vegetation communities (Lewis et al. 2008). Fisher et al. (2018) developed a generalised equation to enable prediction of CC from FPC using the following form;

$$CC = 1 - (1 - FPC)^{1.86} \quad (5.4)$$

This function has been fit using a wide range of field data across the Australian continent, including field data collected in the NT between the years 2009 and 2015 (Fisher et al. 2018). It should be noted that none of the field sites used in this study were used by Fisher et al. (2018) to develop equation 5.4.

5.2.7 Structural classification

The structural classification used in this study has been defined by CC and height which is commonly used to describe structural formations for woody vegetation in Australia (Sun et al. 1997, Lewis et al. 2008, Thackway et al. 2007, Scarth et al. 2019). A number of classification schemes have been used to define vegetation structure in Australia. The National Vegetation Inventory System (NVIS) classification scheme has been developed by Commonwealth, State and Territory governments and has been adopted by the NT Governments vegetation mapping program (Brocklehurst et al. 2007, Lewis et al. 2008). The NVIS classification scheme utilises floristic, cover and height information to define 23 major vegetation groups across Australia (Scarth et al. 2019). In this study, the structural classes were adapted from NVIS and (Walker and Hopkins 1990) classification schemes with CC represented by six categories, while height were grouped into four (Table 5.3). The definition of the CC classes in this study took into account both the NVIS classification scheme and the measurement error in the Landsat derived CC estimates. The CC values used to define the closed forest, open forests and woodlands followed the NVIS classification scheme while the lower value used to define the open woodland class (<5 %) took into account the measurement error in the Landsat CC estimates and followed Walker and Hopkins (1990) scheme. The woodland class was split into two CC ranges ($lc = 20\text{-}35\%$) and ($hc = 35\text{-}50\%$) to assist in the detection of change between these classes and take into account measurement error in the mapping product. The structural formations defined in this study represented woody vegetation (e.g. Trees, palms and shrubs) with CC values between 5 and 100 %. Due to the measurement error in the Landsat CC estimates the "isolated trees" class was not used in this study, with any pixels <5 % CC classified as grassland. The height classes were represented by four classes and followed the NVIS nomenclature (Tall, Mid, Low

and Very Low), however the height ranges were modified to represent vegetation communities across the study area. Estimates of height >20 m were considered tall, while heights between 10–20 m were considered Mid. The height values for the Low class ranged between 6–10 m, while the very low class was represented by height values <6 m. As with the Landsat CC products any height estimates for pixels with CC values between 0–5 % were not used due to the uncertainty in the height estimates.

Table 5.3 Description of the structural formation classes used in this study, canopy cover classes are based on the NVIS/Walker and Hopkins scheme and the height classes have been adapted from Walker and Hopkins/NVIS scheme taking into account the measurement error in the Landsat derived CC and canopy height products and structural characteristic of woody vegetation in the study area.

Canopy Cover	Height Range			
	>20 m	10-20 m	6-10 m	<6 m
>80 %	Closed forest-Tall	Closed forest-Mid	Closed forest-Low	Closed forest-Very low
50-80 %	Open forest-Tall	Open forest- Mid	Open forest-Low	Open forest-Very low
35-50 %	Woodland(hc)-Tall	Woodland(hc)-Mid	Woodland(hc)-Low	Woodland(hc)-Very low
20-35 %	Woodland(lc)-Tall	Woodland(lc)-Mid	Woodland(lc)-Low	Woodland(lc)-Very low
5-20 %	Open woodland-Tall	Open woodland-Mid	Open woodland-Low	Open woodland-Very low
0-5 %	Grassland	Grassland	Grassland	Grassland

5.2.8 Time series Analysis.

Analysis of the structural classification product was undertaken to assess the impact of Cyclone Monica on woody vegetation. This analysis included identifying annual disturbance and rates of recovery post Cyclone Monica. The area of each structural class was calculated for each year between 2004 and 2017 to investigate the dynamics of woody vegetation over the region ($\approx 11,500 \text{ km}^2$) impacted by the cyclone.

5.2.8.1 Change detection.

Possible change in structural classes were identified for each year between 1988 and 2017 for the region shown in Fig 5.2 (c). A methodology was developed to identify any change (substantial loss) between the 21 structural classes. This methodology took into account (1) limitations (error) of the structural classification product to accurately discriminate adjoining classes, (2) natural variation in CC as a result of seasonal variation and (3) limitations of the models to accurately predict CC or canopy height in areas of low tree density. A matrix was used to identify when substantial change was considered to have occurred for a particular class (the decision matrix is provided in the supplementary material Fig B.1). To also assist in removing the seasonal variation between years the majority class for each pixel was calculated from all available years prior to the year being assessed. For example, if the year 2006 was being assessed the mode was calculated for each pixel in a layer stack produced from the structural classified products between 1988 and 2005. This gave an estimate of the long-term structural

class for each pixel in 2005. Each pixel in the 2006 structural classification was then evaluated against the long-term class in 2005 and assessed as changed based on the range of classes defined in the decision matrix. A graphical examples of the change detection analysis described above is shown for two sites in Fig 5.4.

5.2.8.2 Recovery estimates.

The rate of recovery for areas impacted by Cyclone Monica were estimated using the change detection analysis for the years 2006 and 2017. As there is sufficient data (18 years) prior to Cyclone Monica, the change detection is based on the long term class value (mode) the subsequent recovery from the disturbance event can be assessed, as individual pixels will be identified as change until they return to the original class or within the class ranges defined as not substantially different to the original class in Fig B.1. To identify the rate of recovery the change detection layers, between 2006 and 2017 were totaled, resulting in values ranging from 0 to 12. Pixels with the value of 0 were not identified in the initial change detection in 2006 and are not assessed further while pixel values of 1 to 11 indicate the time taken to recover and pixel values of 12 have been estimated to have not yet recovered and still substantially different. Missing data in 2006 structural classification were not included in any analysis post cyclone Monica. This analysis does not take into account additional disturbance after the impact of cyclone Monica however, areas that were disturbed post cyclone Monica (2007 to 2017) but were not assessed as disturbed in 2006 are not identified in the change/recovery analysis.

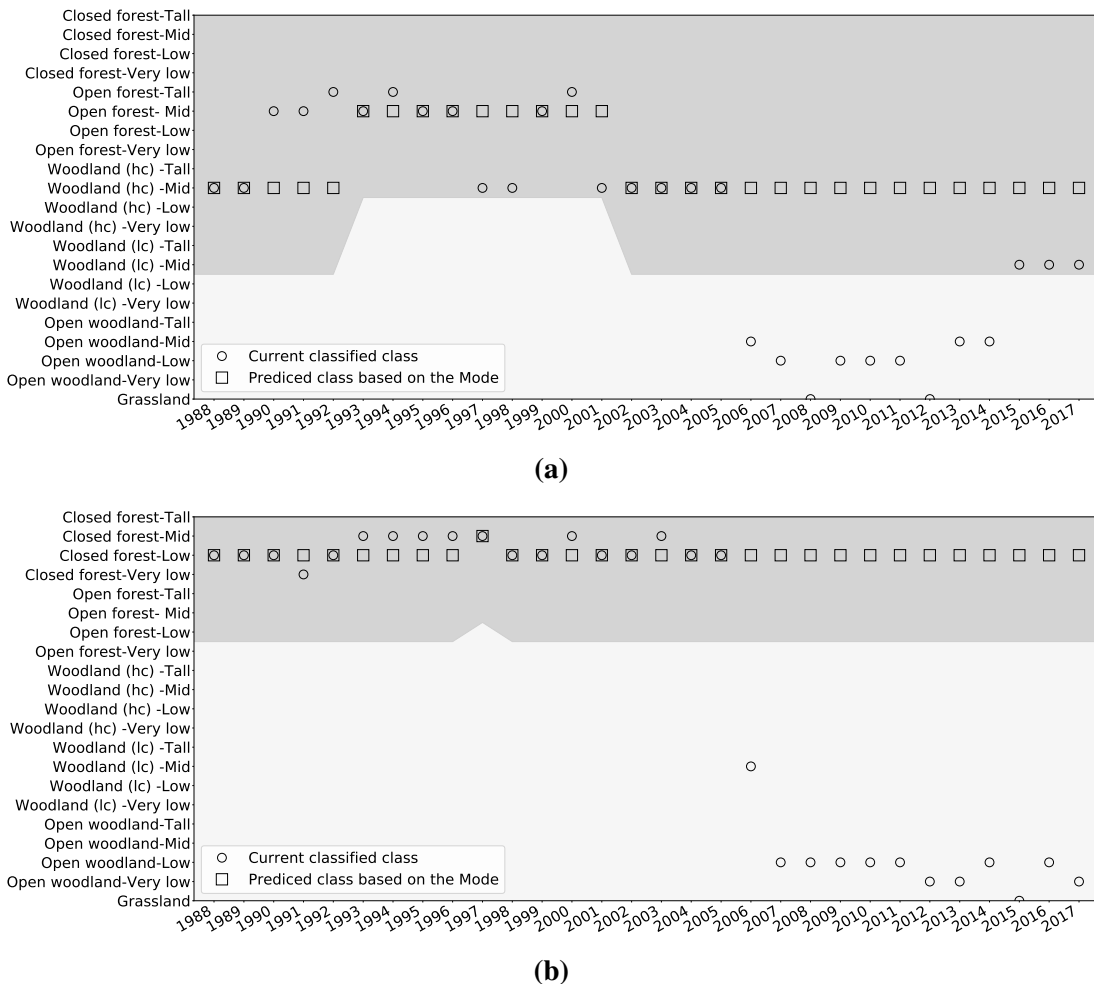


Fig. 5.4 Graphical representations of the change detection analysis undertaken for each pixel over a 30 year period for (a) Eucalyptus Open forest and (b) Mangrove forest. Each of the 21 structural classes are shown on the y axis and year on the x axis. The circles represents the classification assigned to the pixel for each year and the squares represent the long term classification based on the mode. The light grey area represents the range of classes considered to be substantially different from the long term class which is identified as change, whereas the dark grey regions represent no change.

5.2.8.3 Time series analysis of structural class spatial coverage.

Estimates of the spatial coverage for each of the structural formation classes was calculated for each year from 2004 to 2017 over an area $\approx 11,500 \text{ km}^2$. The boundary for the area of interest (AOI) was defined based on the area identified as significant change in 2006, the AOI boundary is shown in Fig 5.16. Areas of coastal floodplains dominated with grasslands within the AOI were also removed due to error in the structural formation classes in these regions (discussed further in section 5.4). For each year, the percentage area covered by each structural class over the $11,500 \text{ km}^2$ area were calculated to produce time series plots detailing change in spatial coverage between the years 2004 and 2017.

5.3 Results

5.3.1 Woody FPC validation and bias corrections

The aerial photograph plots were randomly split into a training ($n=4,413$) and validation ($n=1,892$) dataset with mean woody FPC of 29.7 % and 30.3 % respectively. An example of the classified aerial photography used to produce estimates of woody FPC is shown in Fig 5.5.

5.3.1.1 Accuracy of aerial photograph classifier

The overall accuracy of the random forest classifier using 3,403 independent validation point was 94 %, with the producer and user accuracy for the five classes being high and ranging from 76.6 % to 99.5 % (Table 5.4). The woody green class recorded high user and producer accuracy, with 96.5 and 92.1 % respectively. Commission and omission error was low for most classes, however commission error was higher for the woody green class with the highest misclassification occurring with the non-woody green class. While the aerial photography used in this study were captured during the dry season when most of the grassy understory is senescent, in some situations photosynthetic grass was present in low lying areas and drainage depressions. The confusion between the woody green and non-woody green classes may have resulted in overestimation of the woody FPC in some plots.

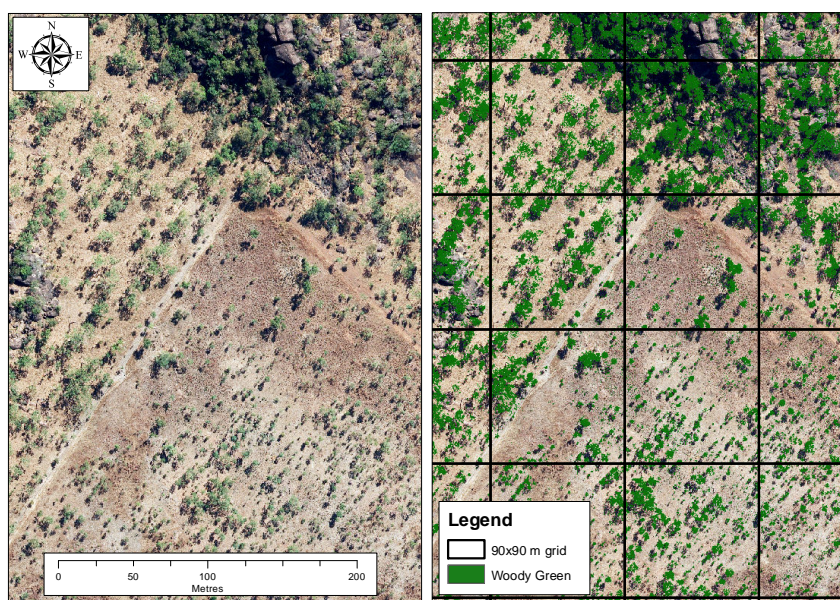


Fig. 5.5 Example of the digital aerial photograph (2013) and the woody green class, with the 90x90 m grid overlay.

Table 5.4 Error matrix for the aerial photo classification

Classified data	Reference data						Users accuracy
	Woody green	Non-woody green	Bare	Shadow	Branch Trunk	Total	
Woody green	1089	15	19	1	5	1129	96.5 %
Non-woody green	66	329	7			402	81.8 %
Bare	14		875	3	24	916	95.5 %
Shadow	4		6	818		828	98.8 %
Branch / Trunk	10		20		98	128	76.6 %
Total	1183	344	927	822	127	3403	
Producers accuracy	92.1 %	95.6	94.4	99.5	77.2		
Overall accuracy 94.3 %							

5.3.1.2 Validation and bias correction

The training dataset was used to assess the relationship between woody FPC estimates derived from the aerial photography and the single date Landsat imagery (Fig 5.6). The relationship between the digital aerial photography and single date Landsat derived woody FPC estimates recorded a R^2 of 0.56, RMSE of 11.5 % and bias of 2.9. While the overall bias is relatively low, there is clearly an overestimation of Landsat woody FPC below ≈ 20 % and an underestimation above ≈ 50 %. The increase in Landsat FPC values below 38 % is evident with a majority of the data points below the 1:1 line (Fig 5.6a). To correct for the systematic bias observed in the relationship between aerial photograph and Landsat derived woody FPC we fit a sigmoidal function to the training dataset Fig 5.6b. The fitting constants for the non-linear model (eq. 5.3) were $k = 0.000435$ and $b = 1.909$ which applied to the single date Landsat woody FPC and the accuracy of the bias correction was assessed using the aerial photograph validation dataset.

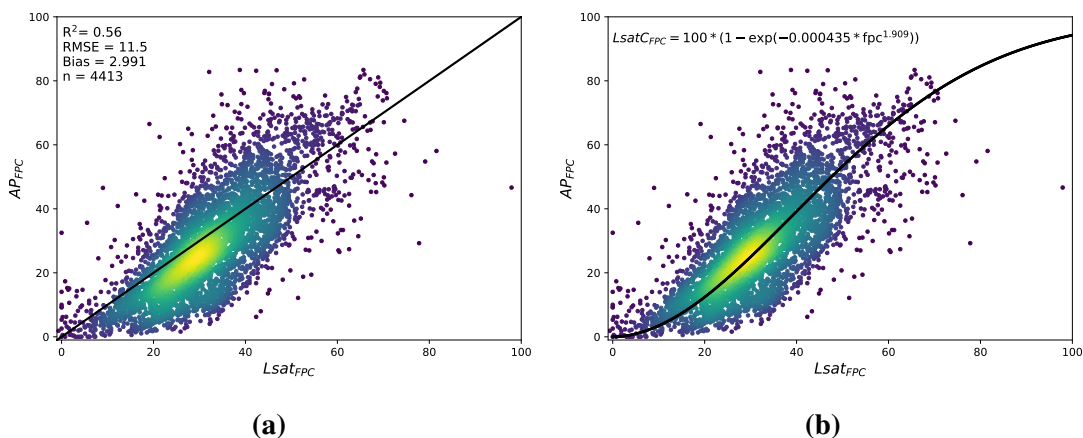


Fig. 5.6 (a) Scatter plots showing the predicted (woody FPC from single date Landsat TM, ETM+ and OLI) and observed (aerial photo derived FPC) for sites located across the Northern Territory between the years 2008 and 2018 and (b) the non-linear fitted line used to correct the bias in Landsat woody FPC estimates.

Scatter plots showing woody FPC estimates derived from both Landsat with and without bias correction and digital aerial photograph are shown in Figure 5.7. Comparisons

between the uncorrected and corrected Landsat woody FPC estimates show that there was only a slight improvement in the R^2 and RMSE error, however overall bias for the corrected data was reduced. The improvement in the relationship between the corrected Landsat and aerial photograph estimates of woody FPC is clear, with the distribution of the data points spread around the 1:1 line. Predictions of Landsat corrected woody FPC below 30 % were improved while data were more dispersed around the 1:1 line above 50 % FPC.

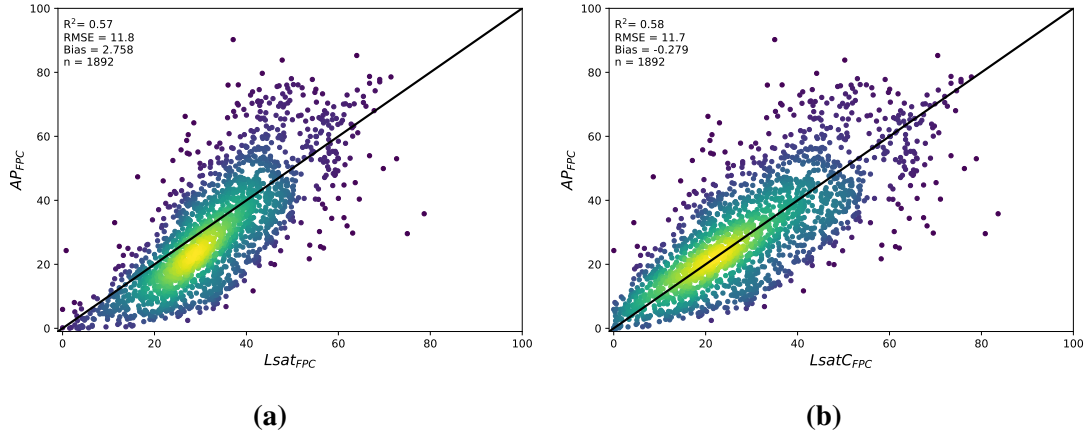


Fig. 5.7 Scatter plots showing the relationship between woody FPC estimates obtained from digital aerial photography and single date Landsat satellite imagery for (a) uncorrected and (b) bias corrected data. The black line represents the 1:1 line.

5.3.2 Conversion of FPC to CC

The Landsat seasonal woody FPC composites were first corrected for bias (eq. 5.3) before converting them to CC using eq. 5.4 (Fisher et al. 2018). The Landsat seasonal CC estimates were then compared with field measured CC for 304 sites measured in the years 2000, 2016, 2017 and 2018 across the study area (locations shown in Fig 5.2). The predicted and observed data were scattered around the 1:1 line, with a R^2 of 0.51 and RMSE of 13 % Fig 5.8. The Landsat CC estimates were slightly underestimated compared to the field measured CC with a bias of -3.55.

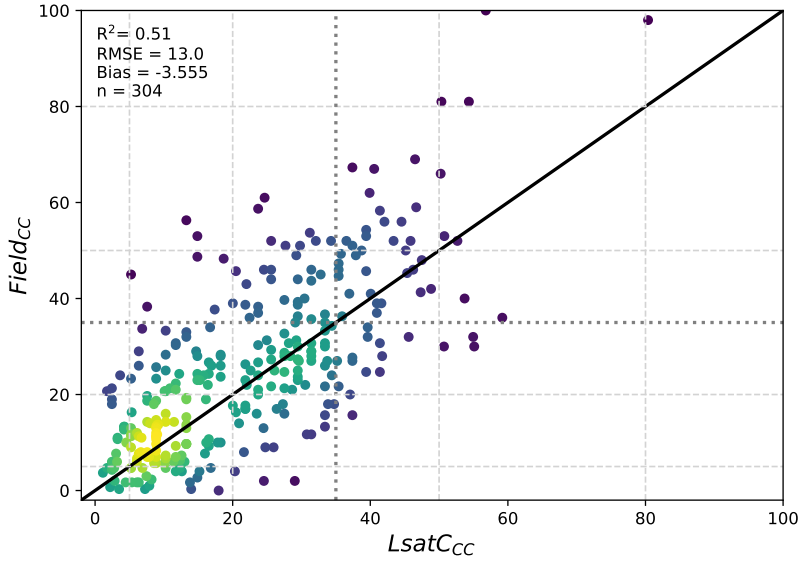


Fig. 5.8 Scatter plots showing the predicted and observed CC estimates obtained from Landsat seasonal composites and field sites across the study area for the years 2000, 2016, 2017 and 2018. The black line represents the 1:1 line and the grey dashed lines represent the CC cover class ranges used in this study.

Estimates of CC obtained from field total basal area measurements and Landsat pre (2005) and post (2006) cyclone Monica are shown in Figure 5.9. Canopy Cover was overestimated from Landsat in 2005 with a R^2 of 0.58 and RMSE of 13 % which is similar to the results of the CC derived from point intercept data (Figure 5.8). The results for 2006 show that there was a general reduction in CC post cyclone (2006) with a R^2 of 0.39 and RMSE of 15.2 %.

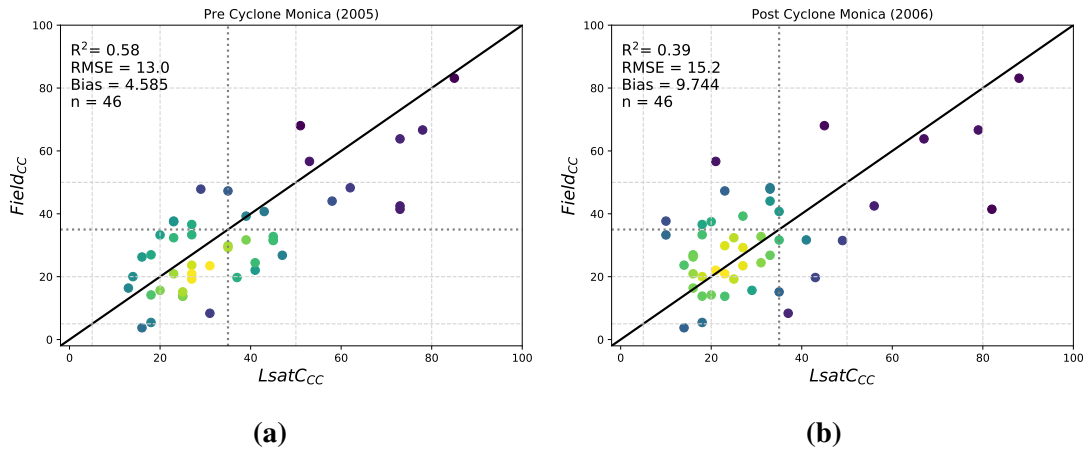


Fig. 5.9 Scatter plots showing the predicted and observed CC estimates obtained from Landsat seasonal composites and field sites ($30\text{ m} \times 30\text{ m}$) impacted by cyclone Monica (a) 2005 and (b) 2006. The black line represents the 1:1 line. The location of the field sites is shown in Figure 5.2

5.3.3 Validation of tree height

Tree canopy height parameter (H_{99}) representing the maximum canopy height for a 30×30 m Landsat pixel were obtained from a subset of the LiDAR dataset (captured in 2011) were compared to the estimates predicted from 2011 Landsat seasonal composites (Landsat path/row: 105/068, 105/069, 104/068 and 104/069). A scatter plot showing the predicted and observed data for the 42,000 pixels assessed is shown in Fig 5.10. The results show the data scattered around the 1:1 line with a low bias of -0.667, R^2 of 0.48 and a RMSE of 4.3 m. While the majority of the data points are scattered around the 1:1 line there are significant number of data points under predicting heights above 20 m. The Landsat model is also underestimating heights in the 12–15 m height range, which will result in an overestimation in the 6–10 m height class. The results also show that the model is predicting non-zero canopy heights for pixels with no observed canopy.

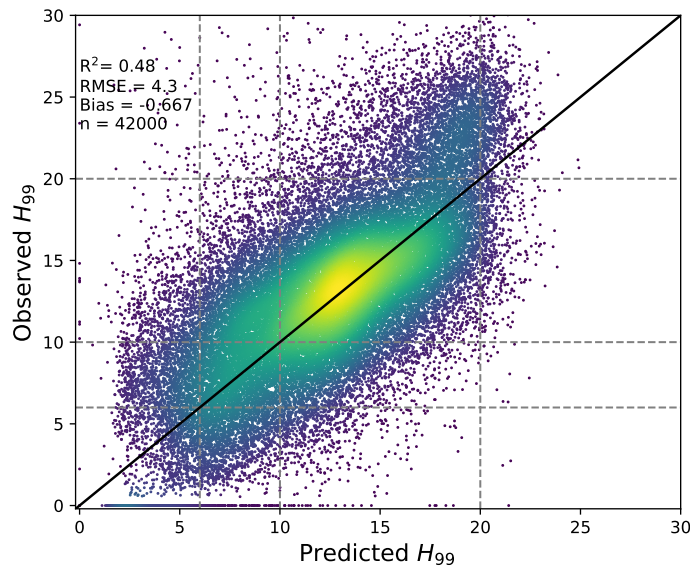


Fig. 5.10 Scatter plot showing the predicted (Landsat satellite seasonal composite) and observed (LiDAR) results for the validation of the canopy height metric H_{99} . The black line represents the 1:1 line and the grey dashed lines represent the height class ranges used in this study.

Comparison between field measured tree height (H_{99}) for the 46 plots and estimates derived from Landsat seasonal composites for 2005 and 2006 are shown in Figure 5.11. The validation statistics were similar for both years, with R^2 of 0.35 and RMSE of 3.6 for 2005. The results for 2006 reflect a loss of taller trees in the plots with R^2 of 0.39 and RMSE of 3.1.

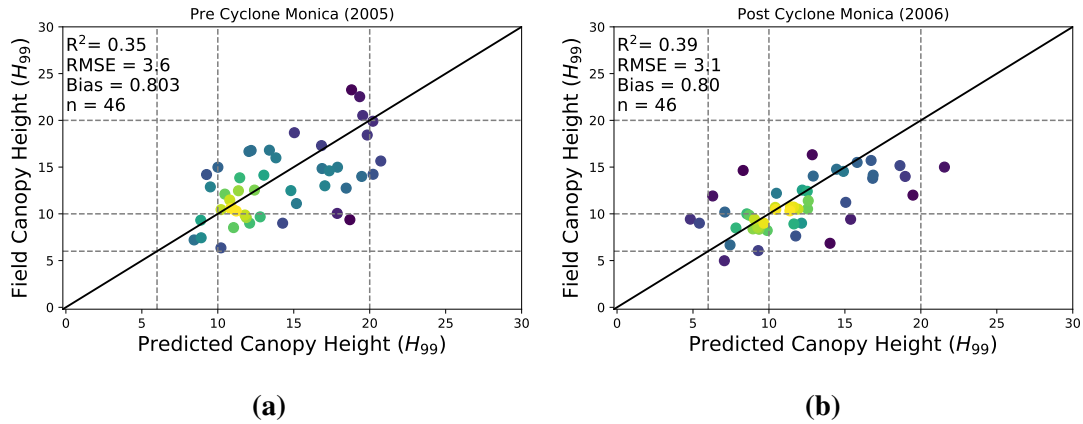


Fig. 5.11 Scatter plots showing the predicted and observed tree canopy height (H_{99}) estimates obtained from Landsat seasonal composites and field sites ($30\text{ m} \times 30\text{ m}$) impacted by cyclone Monica (a) 2005 and (b) 2006. The black line represents the 1:1 line. The location of the field sites is shown in Figure 5.2

5.3.4 Structural formation classes

Structural formation classes were produced from annual Landsat seasonal composites of canopy height and CC estimates. The structural formation classification for 2017 over the northern half of the NT is shown in Fig 5.12. The percentage area covered by each of the 21 classes was calculated from the mapping product shown in Fig 5.12. Woodlands were the dominant class covering approximately 55 % of the area with the majority from the two mid height range (10–20 m) classes (Fig 5.13). Approximately 28 % of the study area consisted of open woodland with the highest proportions (15.5 %) recorded in the low height range. Open forest covered approximately 8 % of the region with the majority also found in the mid height range. Closed forest covered the smallest area, representing 0.8 % of the region with height ranges predominately in the low and mid classes while grasslands were estimated to cover 6.6 % of the region.

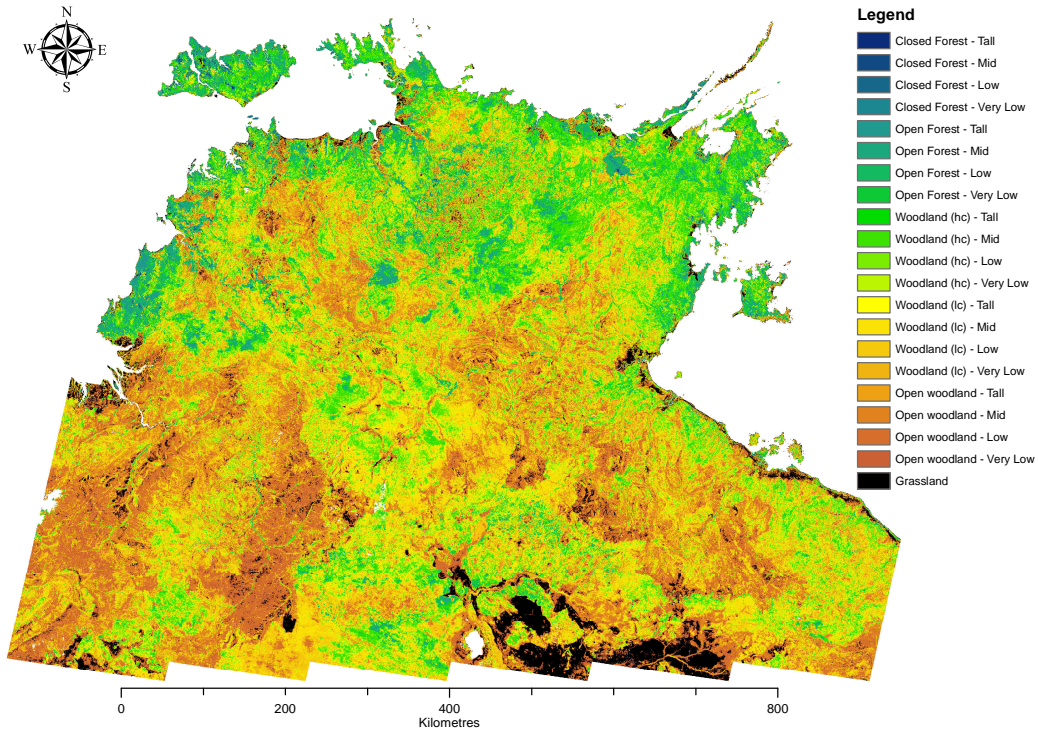


Fig. 5.12 Structural formation classification for the year 2017 across the study area (Landsat path/rows: 106/68-72, 105/68-72, 104/68-72, 103/68-72, 102/68-72, 101/71-72).

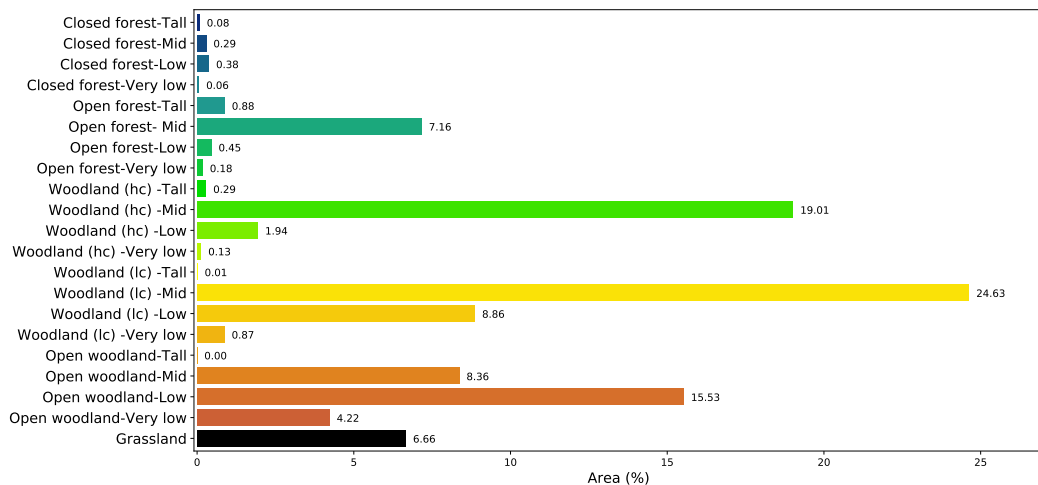


Fig. 5.13 The percentage area covered for each of the structural formation classes for the 2017 mapping shown in Fig 5.12.

5.3.5 Time series analysis - Cyclone Monica

Landsat derived CC and tree canopy height for both 2005 and 2006 were used to investigate impact of cyclone Monica. The 2005 image was subtracted from the 2006 imagery to identify areas of change in both the CC and tree height products Figure 5.14. The

area impacted by cyclone Monica is very evident with significant areas of change in both the CC and tree canopy height products along the track of cyclone Monica. The initial impact of cyclone Monica on the Wessel Islands is evident along with the impact at Junction Bay and inland to the town of Jabiru.

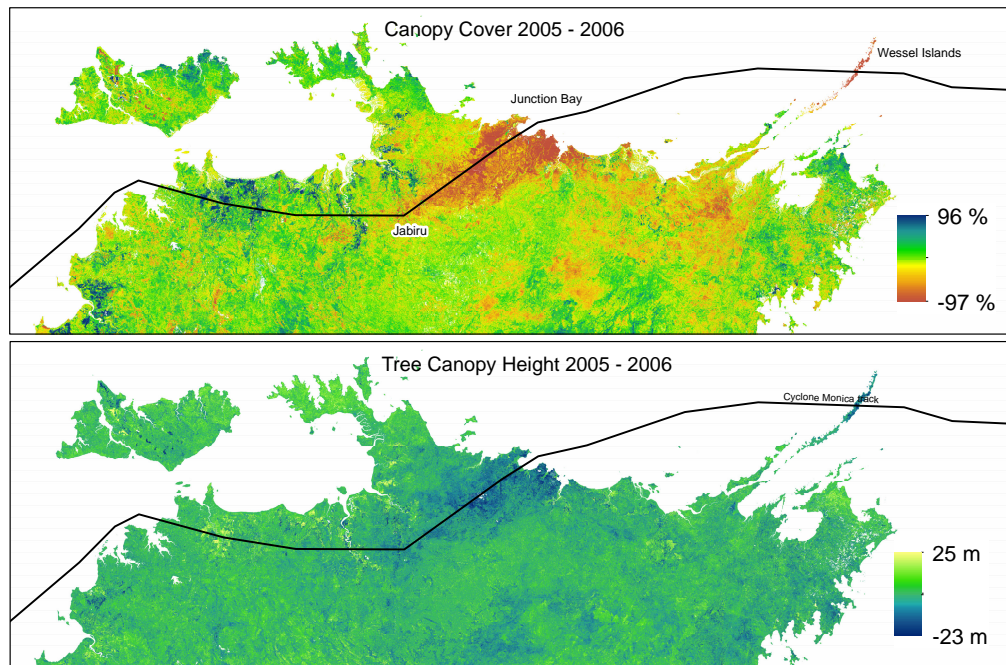


Fig. 5.14 Maps showing the extent of change in canopy cover and tree canopy height between 2005 and 2006 for the top-end of the Northern Territory.

The structural classification were produced for the region impacted by severe tropical Cyclone Monica for the years 1988 to 2017. An example of the structural formation mapping for the years 2005, 2006 and 2017 are shown in Fig 5.15. The impact of Cyclone Monica is clearly visible in 2006 with large areas of change visible along the cyclone track. A larger area was impacted east of the cyclone track due to the influence of the forward motion on the cyclonic winds which are increased on the east and reduced in the west (Hutley et al. 2013). The recovery 11 years after cyclone Monica is evident in the 2017 mapping. Analysis of the time series was undertaken to quantify the change visible in 2006 and subsequent recovery using the methodology described in section 5.2.8. A summary of the results for the change detection analysis from 2006 to 2017 for the area impacted by Cyclone Monica is shown in Fig 5.16. The change detection map shows that damage occurred along a 75 km extent on the coast with extensive area impacted ≈ 90 km inland, damage then starts to tapering off towards the town of Jabiru. Using the area identified as severely impacted by cyclone Monica, we defined an area of interest (AOI) covering $\approx 11,500 \text{ km}^2$, the extent is shown in Fig 5.16. Based on the change detection analysis the area identified as severely impacted

in 2006 is estimated to cover an area of 3,551 km². The rate of recovery post Cyclone Monica for the preceding 11 years was estimated using the annual change detection layer and shows that one year after Cyclone Monica (2007) a total of 714 km² were estimated to have recovered Fig 5.17. The total area estimated to still be severely impacted steadily declined over the 11 years, with an area of ≈ 70 km² estimated to be still severely impacted in 2017.

The area covered by each structural formation class for each year between 2004 and 2017 was obtained from the 11,500 km² AOI impacted by Cyclone Monica. The results for five of the major classes representing the percentage of area covered by each structural classes over the period two years prior and 11 years post cyclone Monica are presented in Figure 5.18 and in the supplementary material B.2. The impact of cyclone Monica in 2006 is evident, with reductions in the Open forest-Mid, Woodland(hc)-Mid and to a lesser degree the Closed forest-Mid classes. The loss of taller trees and reduction in CC is evident, with a sharp increase in the area mapped as Open woodland-Low in 2006. Areas mapped as Open woodland-Mid and Open Woodland-Very Low increased and there was a slight increase in the area classified as grasslands. The results show that recovery post cyclone Monica is occurring, with increases in area for the Woodland(hc)-Mid and Open Forest-Mid classes and a decrease in the Open woodland-Low class. The results show that the recovery of the Open forest-Mid class is still below the level pre-cyclone Monica, while the Woodland(hc)-Mid class recovered to similar levels in 2014. The results suggest that the Closed forest-Mid class was declining prior to 2006 and it is currently still below the 2005 levels. Both the Closed forest-Tall and Low class decline in 2006, with no real recovery evident for the Closed forest-Tall class while the the results indicate the area of Closed forest-Low class is similar to the 2006 levels.

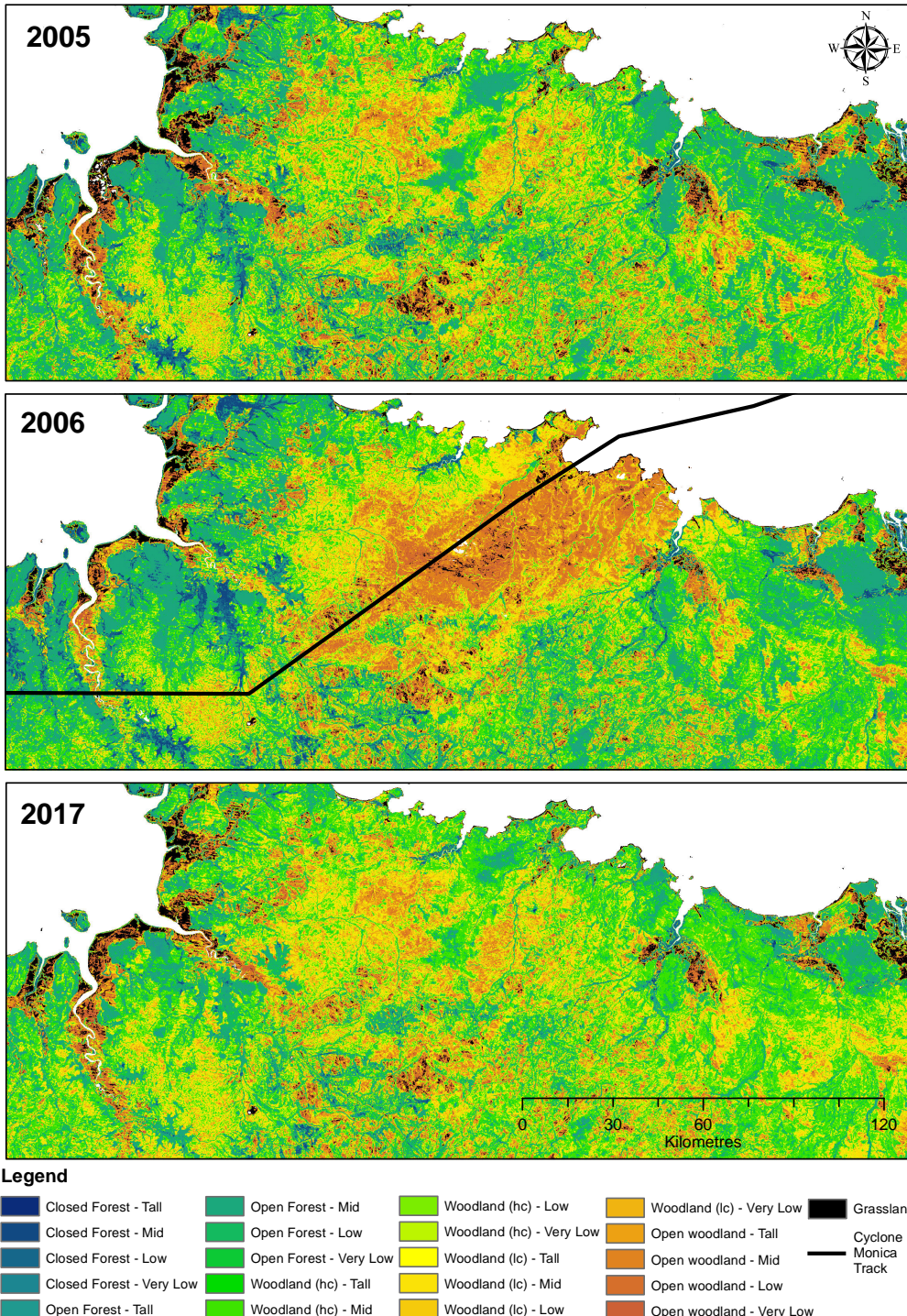


Fig. 5.15 Structural formation maps for the years 2005, 2006 and 2017 over the region impacted by severe tropical cyclone Monica.

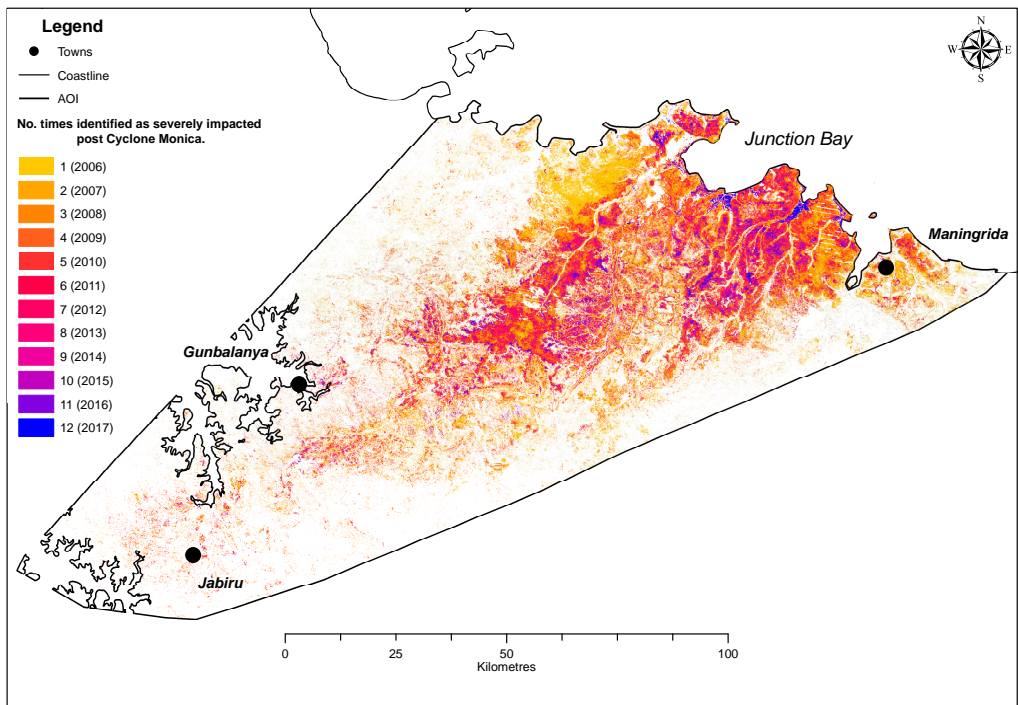


Fig. 5.16 Summary of the change detection analysis undertaken post severe tropical Cyclone Monica. The initial pixels ($30 \times 30 m$ area) identified as significant change are shown for 2006 along with the total number of times these pixels have been classified as a structure class below the long term structural class recorded in 2005 (pre Cyclone Monica).

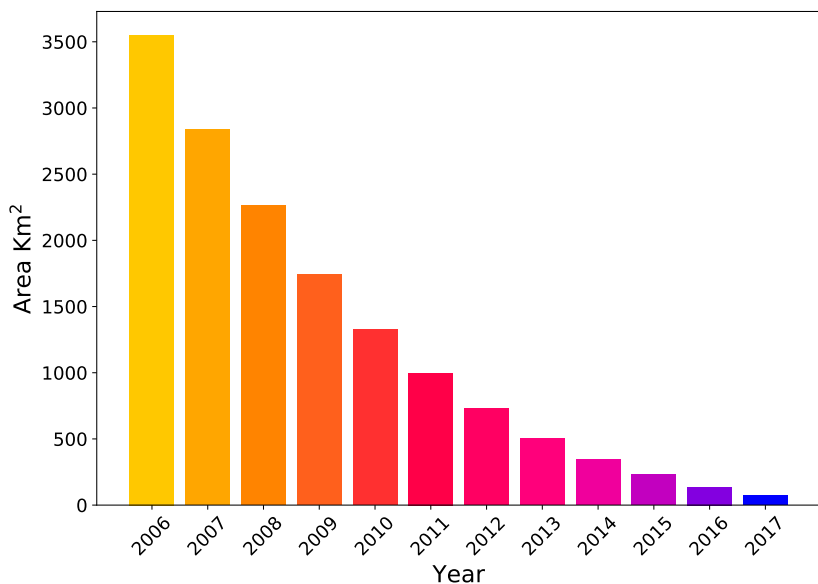


Fig. 5.17 Annual estimates of total area identified as severely impacted by Cyclone Monica in 2006 and the subsequent years until 2017 for the regions shown in Fig 5.16.

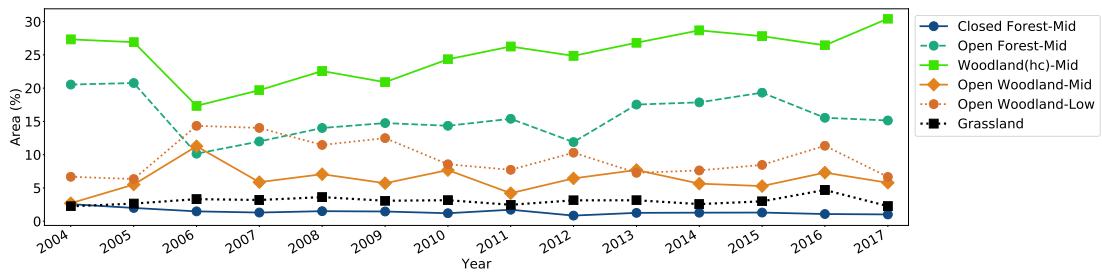


Fig. 5.18 Time series plot showing the percentage area covered by six major structural formation classes for the years 2004 to 2017 over the region impacted by cyclone Monica (Extent shown in Fig 5.16).

5.4 Discussion

5.4.1 Development of the structural formation mapping product.

5.4.1.1 Landsat CC.

The estimates of CC were derived from Landsat model predicting woody FPC developed by Armston et al. (2009). The accuracy assessment showed that the single date Landsat woody FPC product was overestimating FPC in areas with lower tree density and cover, and underestimating in high cover (Fig 5.11a). The bias observed in this study are similar to Armston et al. (2009), who assessed the accuracy of their model using LiDAR derived woody FPC estimates (Fig 8 page 20 Armston et al. (2009)). The overestimation of woody FPC in lower cover ranges has been observed in other products derived from Landsat in Australia (including our study area) and has been attributed to the presence of a green understory visible thought the sparse canopy (Gill et al. 2017). The single date woody FPC products used to produce the seasonal composites were captured during the dry season (May and September) when the majority of the understory grasses are senescent (Staben et al. 2018). While the seasonal composites were produced from imagery captured in the dry season, areas such as drainage lines and lower lying area may still have photosynthetic non-woody vegetation, which would increase the estimated FPC values for these areas. Another area with overestimation of woody FPC is the extensive fresh water wetlands across the study area. These wetland often contain flood waters early in the dry season that progressively dry and contain large areas of photosynthetic non woody vegetation later into the dry season (Cowie et al. 2000). In an attempt to reduce the observed bias in the Landsat FPC, a sigmoid function was fitted using the aerial photograph estimates of FPC as the dependent variable. Assessment of the bias correction (using an independent validation dataset) clearly showed a reduction in the bias, however there was only a very slight improvement in the overall RMSE.

In Australia, CC is a common metric used to characterise horizontal woody vegetation structure (Lewis et al. 2008, Fisher et al. 2018). The bias corrected Landsat woody FPC seasonal composites were used to estimate CC for each year between 1988 and 2017. The generalised equation developed by Fisher et al. (2018) to predict CC from FPC was developed from a range of field site across the Australian continent, including a significant number located across our study area. A total of 350 field sites located across our study area were used to assess the accuracy of the CC derived from the Landsat seasonal composites. None of the field sites used in this study were used in the development of the generalised equation Fisher et al. (2018). The results show that there was reasonable agreement between the annual Landsat CC and field based estimates obtained from the 1 ha sites (using point intercept measurements) with a RMSE of 13 %. The results obtained from the 30 m × 30 m sites pre (2005) cyclone Monica were similar to the 1 ha field sites and for 2006 there was an increase in the RMSE (15.2 %) and an overall reduction in CC, post cyclone Monica. The majority of the data points below 20 % CC showed good agreement with the field data however data points are dispersed around the 1:1 line and the number of field sites available to assess CC above 60 % were minimal. The CC class ranges are show as the dashed grey lines in Fig 5.8 and show that a a number of the sites in the Woodland(lc) class 20-35 % were underestimated by Landsat CC. A number of the data field sites in the 5-20 % class range were also overestimated by Landsat CC. To enable assessment of CC values above 60 % the single date bias corrected Landsat and aerial photograph FPC validation dataset were converted to CC and show that similar error was occurring across all the CC class ranges (Fig 5.19). Woodlands are the dominant structural class in our study area so to reduce chance of detecting false change between both the Woodland class and either the Open woodland or Open forest class we produced sub classes identifying low (20-35 %) and high (35-50 %) cover values. This was undertaken to take into account the error in the CC data and increased the flexibility in defining the rules in the change matrix (Fig B.1).

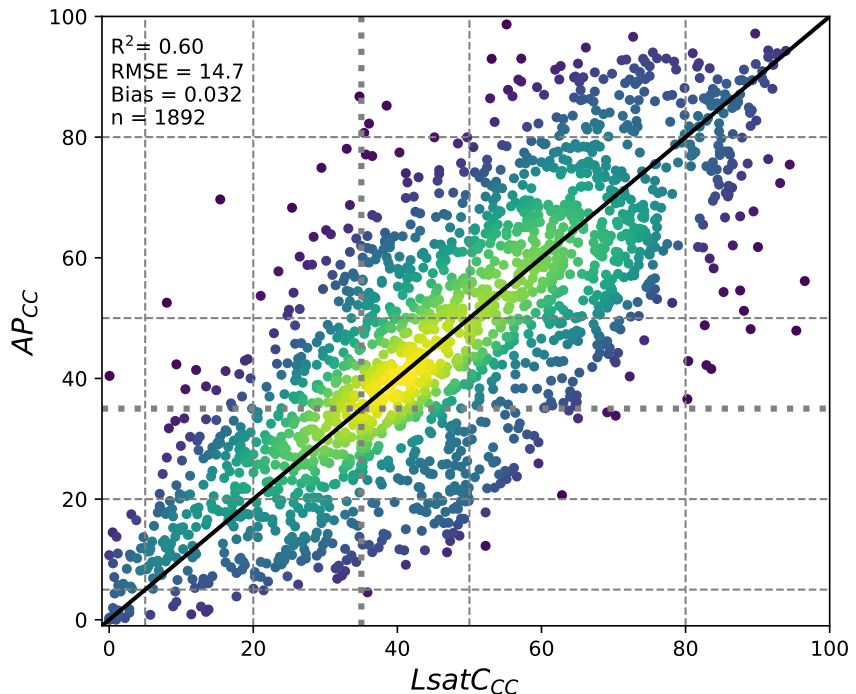


Fig. 5.19 Scatter plots showing the predicted and observed CC estimates obtained from Landsat single dates imagery and digital aerial photography across the study area for the years 2008-2018. The black line represents the 1:1 line and the grey dashed lines represent the CC cover class ranges used in this study.

5.4.1.2 Landsat Canopy Height

The vertical structural information used in this study was obtained from Landsat annual and seasonal composites which estimated the maximum canopy height of the trees (H_{99}) for each pixel (Chapter 4). The Landsat canopy height model used in this study was developed for Landsat-8 OLI sensor which were trained on canopy height metrics data obtained from a number of canopy height models (1 m) derived from LiDAR captured across our study area. While the model was developed using Landsat-8 annual and seasonal composites, the surface reflectance values were converted to predict Landsat-7 reflectance values using coefficients published in Flood (2014), enabling the model to be directly applied to both Landsat-7 and Landsat-5 sensors. The accuracy of the H_{99} canopy height model produced from Landsat-8 (detailed in chapter 4) using two validation datasets, reported overall R^2 values of 0.74 and 0.77 and RMSE of 3.2 and 2.7. The seasonal composites used to assess the accuracy of the canopy height model were a combination of Landsat-5 TM and Landsat-7 ETM+ sensors captured in 2011. The overall accuracy of the canopy height model was lower than the results in chapter 4 with R^2 values of 0.48 and RMSE of 4.3. The validation results obtained from the 30 m × 30 m field sites pre and post cyclone Monica were lower than the 2011 results, with RMSE of 3.6 and 3.1 for 2005 and 2006 respectively. The overall reduction in

tree canopy height is also apparent post cyclone Monica and the results show that for a number of sites the Landsat predicted height was overestimated. There are a number of factors that could explain the difference between the results in this study and chapter 4. While the LiDAR used to train the Landsat-8 OLI model were captured across a variety of landscapes across the Northern Territory, the increased error observed in this study may reflect differences in vegetation communities not represented in the training dataset used to develop the canopy height model. Direct comparisons between the accuracy of mean canopy height predicted from models using single date Landsat-5 image ($R^2 = 0.53$ and RMSE = 2.8) (Staben et al. 2018) and Landsat-8 seasonal composites in chapter 4 ($R^2 = 0.72$, RMSE = 2.0) show that there was an improvement in the results for Landsat-8. The use of seasonal composites may explain the improved accuracy of the Landsat-8 sensors or it could reflect differences in the overall radiometric quality between the three Landsat sensors (5,7 and 8). The results of the accuracy assessment in this study and in chapter 4 indicate that there could be more error in the height estimates derived from Landsat-5 and Landsat-7 between 1988 and 2012, with an improvement from 2013 with the introduction of Landsat-8.

5.4.1.3 Structural Classification

Landsat derived estimates of CC and canopy height were used to produce a structural formation classification mapping product, covering three decades between 1988 to 2017. The structural classification used in this study were guided by the nationally adopted NVIS classification scheme developed by Commonwealth, State and Territory governments (Brocklehurst et al. 2007, Lewis et al. 2008). Where possible the NVIS classification scheme was adopted, however we also took into account the error in the Landsat derived CC and canopy height products and the structural characteristics of the vegetation communities in our study area. The NVIS classification scheme was developed to characterise a diverse range of vegetation communities across the continent of Australia (Scarth et al. 2019). To account for measurement error in the Landsat CC and canopy height products, a number of the NVIS classes were altered. As discussed in section 5.4.1.1, the Woodland class was split into two sub classes to enable more flexibility in defining the rules in the change detection analysis. The lower and upper bounds of the NVIS CC range (20-50 %) for the Woodland class were retained enabling users to combine the two Woodland sub classes if required. The Open woodland class in this study used the CC range of 5-20 % (Walker and Hopkins 1990) which differed from the NVIS classification which uses 0.25-20 % (Brocklehurst et al. 2007). The lower bound of 5 % was chosen as 0.25 % used in the NVIS class was not reliably predicted by the Landsat model. Both the NVIS and Walker and Hopkins (1990) classification schemes have an ‘isolated trees’ class which was not used in this study. All values below 5 %

were classified as grassland as the accuracy of both the CC and canopy height products were low in areas with very few trees and low cover.

The ranges used to define the vertical structure differed from the NVIS classification and took into account the height of vegetation communities across the study area. The height range of 10–20 m was selected as this represents the dominant vegetation communities across the study area. While the accuracy assessment shows that areas >20 m are underestimated, this class was retained as it still highlighted important areas such as rainforest patches (Closed forest-Tall) in the mapping product. Below 10 m the 6 m height was used to separate classes into low and very low classes. The height ranges are important as communities such as Mangrove forests are generally classified in the Closed forest low and very low classes. While this study does not attempt to distinguish between woody shrubs or trees. The <6 m height range was used as it is associated with shrubs in the Open woodland class which are predominately located in the more southern regions of our study area.

There are a number of limitations which need to be taken into account when using the structural formation mapping products. While seasonal composites were used to reduce the influence of non-woody vegetation, there is error over the floodplains and in areas of agriculture. Non-woody agriculture is often misclassified as woody vegetation due to the photosynthetically active crops as a result of irrigation during the dry season. The extensive floodplains will often be flooded and covered with photosynthetically active aquatic grasses and sedges that become senescent later into the dry season (Ward et al. 2014), which resulted in misclassification of the grasslands in these areas. While there are areas of extensive forest across the floodplains it is difficult to reliably separate the woody and non-woody pixels at the Landsat scale. Further work is required to produce grassland masks to enable analysis of the extensive forest on the floodplains such as the Arufura swamp. Due to the failure of scan line corrector (SLC) of the Landast-7 sensor, there is striping visible in some areas of the annual mapping product as a result of distinct changes in classification. In some instances, the change in class in these areas is due to error in the height class (e.g. change from Mid to Low ranges) or associated with a change in the CC classes. The striping in the annual structural formation classification mapping is likely to be reflecting the seasonal changes over the year in woody vegetation across the study area (Williams et al. 1997, Myers et al. 1997). Ma et al. (2013) have also observed the inter-annual seasonal variability in the vegetation across the study area. The inter-annual and annual variability in the single date imagery combined with the total number of cloud free images available for a given year, all contributed to the variability in the CC and canopy height values, which results in class variation between years. The variability between years could also be due to the

occurrence of natural and prescribed fires, which occur across large areas in the study area (Edwards et al. 2013). The burnt areas masked from the Landsat imagery used in this study are mapped automatically (Goodwin and Collett 2014) and it is likely that the influence of burnt areas were not entirely removed from the production of the Landsat CC and canopy height product, resulting in reduction in values for both CC and canopy height. Producing structural formation mapping products over multiple years reduces the variability seen in the annual mapping products. An example showing the reduction of the striping error clearly visible in the 2017 structural formation mapping and a tri-annual structural formation mapping product calculated from 2015, 2016, 2017 using the mode class value is shown in Fig 5.20.

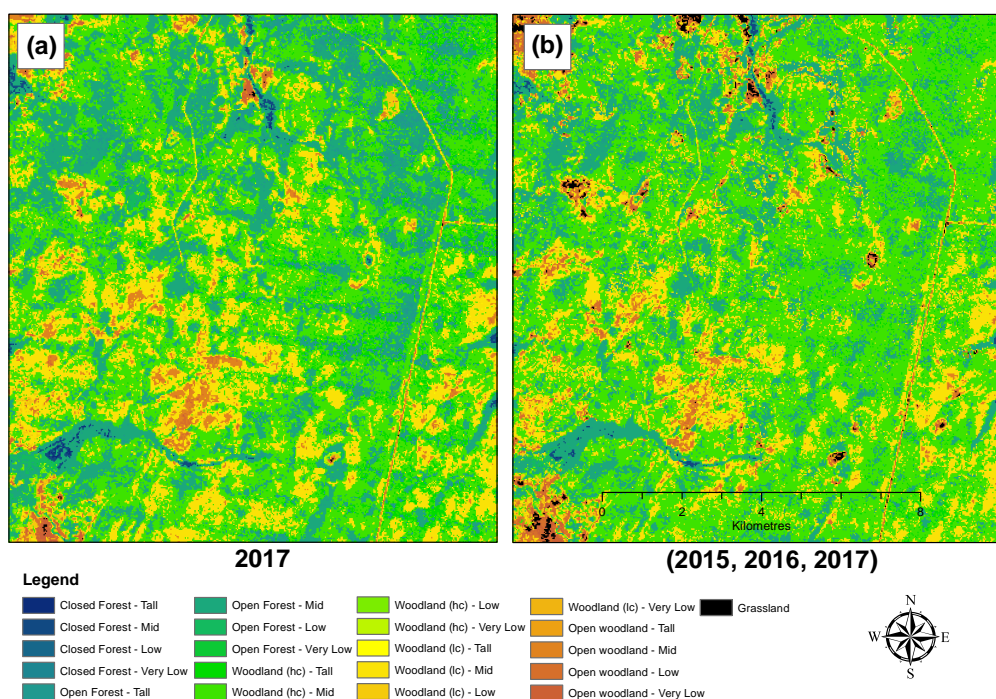


Fig. 5.20 Example of the (a) Structural formation classification for 2017 and (b) the structural formation classification produced from three years of data 2015, 2016 and 2017.

5.4.2 Assessment of Cyclone Monica

The immediate impact of cyclone Monica on the Northern Territory is clearly visible in (Fig 5.14), with a reduction in both CC and tree canopy height between 2005 and 2006. While the focus of this study is on the mainland of the Northern Territory, the impact of cyclone Monica on the Wessel Islands is evident in reductions of CC and tree canopy height. The difference analysis between 2005 and 2006 shown in Fig 5.14 enables the magnitude of change in CC and tree canopy height to be quantified. The impact of severe tropical Cyclone Monica on the woody vegetation is clearly visible

when compared with the 2005 and 2006 structural formation mapping (Fig 5.15). The spatial distribution of the area impacted by Cyclone Monica mapped in this study is similar to a tree isodamage map produced by Hutley et al. (2013) which used estimates of tree damage derived from aerial and field surveys and wind speed estimates along the track of Cyclone Monica (Cook and Goyens 2008). The results of this study indicate that recovery of the woody vegetation is occurring, with the area considered severely impacted steadily declining over the 11 years assessed. Russell-Smith et al. (2019) undertook a tree recruitment study in two locations in the NT, including field sites located in the coastal and sub-coastal regions impacted by cyclone Monica, which were measured in 2006 (3 months after cyclone Monica), 2007, 2011 and 2016. They reported that mean stem basal area for all plots was estimated to be $9.8 \text{ m}^2/\text{ha}$ at the time of cyclone Monica and that extensive structural devastation was evident, by 2016 stem basal area had recovered to $\approx 6.5 \text{ m}^2/\text{ha}$. Between 2011 and 2016 at one of their sub-coastal plots, stem basal area increased from 5.3 to $11.8 \text{ m}^2/\text{ha}$, attributed to significant eucalyptus stem recruitment (Russell-Smith et al. 2019). Estimates from the change/recovery analysis in this study indicate that between 2006 and 2011 $\approx 62\%$ of the area initially assessed as severely impacted (based on the decision matrix Fig. B.1) had recovered. In 2017, it was estimated that an area of 70 km^2 was still significantly impacted. The spatial distribution of these areas is shown in Fig 5.2.8 and shows that a large number of these areas are located on or within $\approx 30 \text{ km}$ of the coast. The greatest concentration of these areas is in the Mangrove forests where there has been no regrowth since 2006 and the remnants of dead Mangroves are still evident in high resolution satellite imagery captured in 2015 (source: ESRI World imagery). While some areas of Mangroves forest impacted by cyclone Monica are recovering, it may take several decades for some areas to recover. Mangroves forest located in Darwin Harbour ($\approx 350 \text{ km}$ east of Junction Bay) were moderately and severely impacted as a result of cyclone Tracy in 1974 (Stocker 1976). In some of the severely impacted areas, there was still evidence of dead trees 26 years after cyclone Tracy (Ferwerda et al. 2007) with recovery only starting to appear two decades after the cyclone (Staben et al. 2018). A large number of the areas assessed as still significantly impacted appear to be located on areas of bright soil. Inspection of high resolution imagery in a number of these areas show that there was significant wind-throw, with large numbers of tree trunks still visible. An example of the tree damage visible in aerial photography captured in 2013 in a area with bright soil is shown in Fig 5.21, In 2015 the tree damage is similar (see Google Earth Lat: -12.226310, Long: 133.287477). It should be noted that not all areas identified as severely impacted for a given year have not started to recover. The change detection analysis used in this study was based on the conditions detailed in Fig. B.1, which takes into account the long term structural formation classification of each pixel, which in turn determines when a pixel is considered to have

reached the minimum structural formation class identifying it as recovered. The condition matrix took into account the measurement error in the CC and canopy height models and also the natural seasonal fluctuations in woody vegetation (section 5.2.8), which was not considered a significant change. While the change analysis highlights areas significantly altered the magnitude of the change needs to be taken into account. A number of other potential factors such as; land use change, fire or tropical storms need to be taken into account as they have the potential to contribute to change observed in the structure of woody vegetation, post cyclone Monica. Change in land use can result in the loss of native vegetation however, it is not likely to have changed significantly in the study area as this region is sparsely populated with very limited development (Staben and Edmeades 2017). Localised tropical storms have the potential to cause minor to severe damage to woody vegetation (Franklin et al. 2010) and other cyclone's such as cyclone Nathan which impact the study area in 2015. Cyclone Nathan initially made landfall on the east coast of the Northern Territory as a category 2 storm (C.1) and continued to move westward over Elcho Island before moving over the Arafura Sea. Cyclone Nathan continued to track in a westerly direction over the Arafura Sea before making landfall as a category 1 storm over Junction Bay, it then moved in a south westerly direction overland before weakening to below tropical cyclone intensity near the towns of Gunbalanya and Jabiru (<http://www.bom.gov.au/cyclone/history/Nathan-2015.shtml>). While cyclone Nathan impacted the study area as low intensity storm (in comparison to cyclone Monica) it is likely to have caused damage to areas recovering from Monica in 2006.

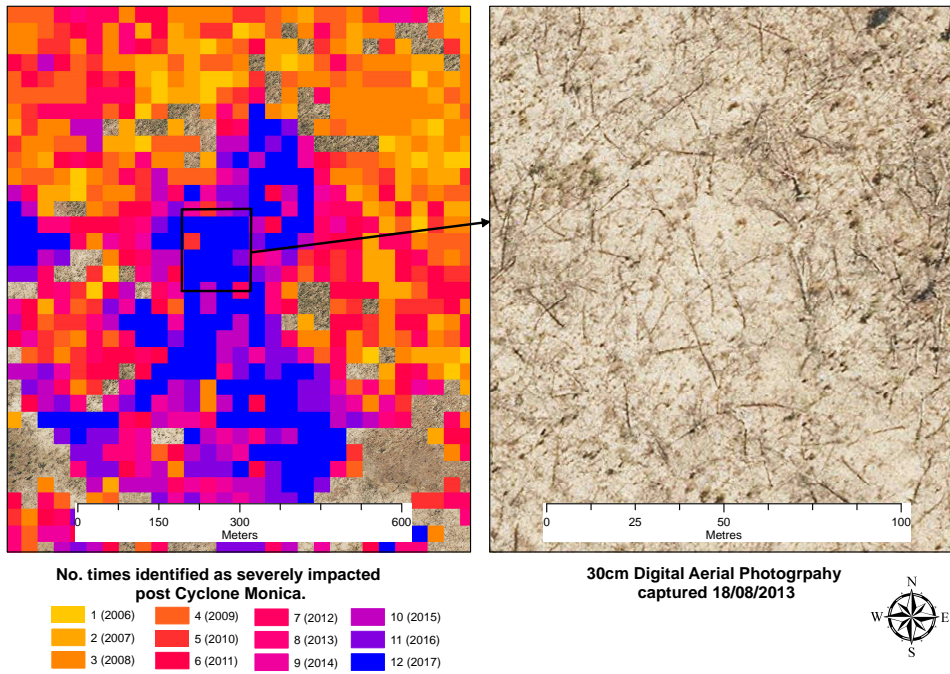


Fig. 5.21 Example the disturbance/recovery mapping product and an area estimated as not recovered, in 2017. The digital aerial photography was captured in August 2013 and the damage is still evident. This site is located at Lat -12.226310 Long 133.287477 and in 2015 the damage is still evident in high resolution satellite imagery in Google Earth.

To gain further insight into the the structural dynamics of woody vegetation impacted by cyclone Monica in the region, the proportion of each class was calculated. The initial impact of cyclone Monica is clear in the time series analysis with an increase in the number of pixels classified as Open Woodland-Low and decreases in areas of higher woody cover and taller trees. There are a number of trends evident which indicate that woody vegetation is recovering, with increases in the Woodland(hc)-Mid and to a lesser extent in the Open forest-Mid class. In contrast, the area classified as Closed forest-Mid appears to be in decline prior to cyclone Monica with no real increase in area over the next 11 years. The area mapped as Open Woodland-Mid class increased significantly in 2006 and is shown to reduce to a similar level pre cyclone Monica in 2007. This rapid reduction in the area of the Open Woodland-Mid class in 2007 is likely to reflect the recovery of trees with less damage. The loss of branches and defoliation in the canopy in areas not significantly impacted are likely to recover rapidly (Stocker 1976, Cook and Goyens 2008). The area mapped as Open Woodland-Low increased after the cyclone and then gradually declines which is likely to reflect the slower recovery of trees, particularly in areas significantly damaged. In 2015 there is a slight decrease in the area mapped as Woodland(hc)-mid and an increase in Open woodland-Mid and Open Woodland-Low classes which may reflect the impact of cyclone Nathan, which followed a similar track to cyclone Monica. In 2016 the area

mapped as Woodland(hc)-mid and Open Forest-Mid declined further while the Open Woodland-Mid, Open Woodland-Low and grassland classes increased. In 2017 there was an increase in the area mapped as Woodland(hc)-Mid and decreases to close to the 2014 levels for the Open woodland-Mid, Open Woodland-Low and grassland classes. Cyclone Nathan impacted the region as a low intensity category 1 storm which is more likely to result in canopy defoliation and damage to branches which has potential to recover more rapidly however, other factors such as fire may be also influencing the results observed. Fire occurs frequently across the top-end of the Northern Territory (Edwards et al. 2013) and has been shown to impact woody vegetation structure (Williams et al. 1999). Further work is required to identify the interactions between other disturbance factors such as fire on the recovery process of woody vegetation in the savanna's of northern Australia. The dynamics observed between the structural formation classes and the change/recovery analysis indicate that while there has been recovery over the 11 years post cyclone Monica the regions is still in a state of recovery with some areas still significantly impacted.

5.5 Conclusion

Landsat derived estimates of Canopy Cover (CC) and canopy height were combined to produce a woody vegetation structural classification mapping product. The CC estimates were derived from the Landsat woody FPC product (Armston et al. 2009) which were validated using estimates of woody FPC derived from digital aerial photography captured across the study area. Based on the aerial photography validation assessment, bias corrections were applied to the Landsat woody FPC prior to converting them to CC using a generalised model developed from field data collected across Australia (Fisher et al. 2018). The accuracy of the annual Landsat CC estimates (RMSE of 13 %) were then assessed using field data from 304 sites collected across the study area in the years 2000, 2016, and 2017. Canopy height estimates were derived from Landsat seasonal composites (Chapter 4), which were validated (RMSE = 4.3 m) using canopy height models derived from LiDAR acquired in 2011. The structural classification scheme used in this study was based on the Australian national (NVIS) classification scheme and took into account the error in both the Landsat CC and canopy height estimates and consideration of the structural attributes of the vegetation in the region. It should be noted, that as the structural mapping product is developed from continuous data any classification scheme can be applied to the Landsat CC and canopy height products to produce the required class ranges. Annual and inter-annual seasonal changes are likely to account for some of the error in the Landsat woody FPC and canopy height products used to produce the annual structural mapping product. It is recommended that further work is undertaken to investigate using multiple years (e.g. 3–5) to reduce the

error in the structural mapping product. The Landsat CC and canopy height estimates were used to produce annual structural classification mapping products over a 30 year period, impacted by severe tropical cyclone Monica. A change detection method was developed to identify the areas impacted by cyclone Monica and it was estimated that an area of 3,551 km² was severely impacted in 2006. Over the next decade, the areas assessed as severely impacted gradually decreased, however in 2017 it was estimated that a total of 70 km² was still severely impacted. The impact of cyclone Monica in many of the areas identified as severely impacted were still visible in both high resolution aerial photography captured in 2013 and satellite imagery in 2015. The area covered by each structural class was used to gain insight into the dynamics of woody vegetation in the 11,500 km² between the years 2004 and 2017. The proportion of each structural class shows the initial impact of cyclone Monica in 2006 and subsequent recovery of woody vegetation. The results clearly show the impact of cyclone Monica in 2006 and indicate that substantial recovery has occurred, but some areas still have not completely recovered from the effects of Tropical Cyclone Monica.

CHAPTER 6

Conclusion

The aim of this thesis was the development of remote sensing products and techniques enabling the assessment of the impact of tropical cyclones on natural vegetation communities in the wet-dry tropics of northern Australia. Remote sensing methods were developed that enabled analysis of vegetation structure dynamics at a regional scale over a 30 year period across the top-end of the Northern Territory. The first three research chapters (2,3 and 4) focused on the development of these remote sensing products. Chapter 2 focused on the use of digital aerial photography as a surrogate for the collection of field data to validate and calibrate satellite derived woody FPC. Chapter 3 and 4 focused on development of techniques to quantify and map vertical structure attributes of woody vegetation. Chapter 5 utilised the research in chapters 2, 3 and 4 to combined both horizontal (woody FPC) and vertical (tree height) derived from Landsat sensors to develop annual mapping products identifying 21 vegetation structural classes for the period 1988 to 2017. A change detection method was developed to investigate the impact of severe tropical cyclone Monica on native vegetation communities using the annual structural classification product. The research in the thesis provides new information on tree structure attributes for vegetation communities across the Northern Territory at a scale (spatial and temporal) not previously available. The analysis of the region (Australian mainland) impacted by severe tropical cyclone Monica, demonstrated the utility of the new techniques developed in this thesis to identify areas of damage and any subsequent recovery. The methodology and results presented in this thesis have improved insight into the role tropical cyclones play as a natural disturbance agent on savanna ecosystems at a regional scale. In doing so, this work contributes more broadly to the global understanding of the ecological impacts of cyclones, for a biome that is poorly understood. The outcomes of this thesis are a resource contributing to the protection of important ecosystems and supporting long-term ecologically sustainable development across the Northern Territory. The following sections briefly summarise the major findings, details the limitations and the contribution of each research chapter to the overall aim of the thesis, followed by a section summarising the key contribution to new knowledge and recommendations for future work.

6.0.1 Chapter 2 - Obtaining biophysical measurements of woody vegetation from high resolution digital aerial photography in tropical and arid environments: Northern Territory, Australia

The objective of chapter 2 was to “***investigate the utility of very high resolution digital aerial photography to be used as a surrogate for the collection of field data***”.

The findings of this study identified that there is a strong relationship between field-measured woody UMG_{FPC} and AP_{GWC} derived from aerial photography captured across a broad range of vegetation communities in the Northern Territory. Evidence of the relationship was further highlighted by the close agreement of live SBA predicted from both UMG_{FPC} and AP_{GWC} using allometric relationship developed from field measured data. The use of aerial photography to obtain woody FPC estimates has advantages for sites with low tree density, as it samples the entire image ensuring all trees are detected. A number of limitations were identified that need to be taken into account when using the methodology developed in this study. The results showed that in areas of very high cover it is possible that woody FPC is underestimated due to shadow masking the green foliage. The supervised classification method used in this study, relies on an operator selecting the training samples for each image being classified. If the operator is not familiar with the objects visible in the imagery, the results are likely to be erroneous. The major contribution of this chapter to the overall aim of the thesis is that it shows that accurate estimates of woody FPC can be obtained from digital aerial photography. This is particularly relevant when the satellite imagery used such as Landsat-5 TM (used in chapter 5) is no longer operational and historical field estimates are required coincident with the image overpass.

6.0.2 Chapter 3 - Modelling LiDAR derived tree canopy height from Landsat TM, ETM+ and OLI satellite imagery:a machine learning approach.

The objective of chapter 3 was to “***Investigate the utility of Landsat-5 TM satellite sensors to predict woody vegetation canopy height across a range of vegetation communities in the wet-dry tropics of northern Australia***”.

A random forest regression algorithm was developed to predict canopy height from a single date Landsat-5 TM scene. Training data for the model were derived from a 1 m canopy height model produced from LiDAR captured in 2009. A three-stage approach was used to tune the random forest regression model. Independent data ($n = 30,500$) was used to validate the accuracy of the model resulting in an overall $R^2 = 0.53$, RMSE of 2.8 m. For two of the dominant vegetation communities in the study area, Mangrove

forests and Eucalyptus communities, RMSE values of 2.9 m and 2.5 m were achieved respectively. The model was also applied to Landsat-7 Enhanced Thematic Mapper Plus (ETM+) resulting in an R^2 of 0.49 and RMSE of 2.8 m. A number of limitations were identified with the model developed in this study. When the model was applied to Landsat imagery captured between 1987 and 2016, the results showed that there was variability between canopy height estimates likely caused by seasonal variations in the image capture dates and difference in sensors characteristics. Also one limitation of the random forest regression model is that it will not extrapolate beyond the range of values in the training dataset. While the minimum and maximum heights in the validation dataset did not exceed the values in the training dataset, further work was required to assess how well the random forest model transfers beyond the current study area. The major contribution of the research undertaken in chapter 3 to the thesis was the demonstration that canopy height can be predicted from Landsat imagery at moderate to high levels of accuracy. The robustness of the model across a range of vegetation communities and three different Landsat sensors also illustrated that the approach could be successfully used to explore changes in woody vegetation canopy height through time.

6.0.3 Chapter 4 - Broad-scale mapping of tree canopy structure using optical satellite sensors, Sentinel-2 MSI and Landsat-8 OLI

The objective of chapter 4 was to *“Investigate the utility of optical satellite imagery, Sentinel-2 MSI and Landsat-8 OLI in predicting seven forest structural parameters to produce annual forest structure maps across northern Australia.”*

This study developed and evaluated seven random forest regression models predicting a range of structural metrics characterising tree canopy structure from Sentinel-2 MSI and Landsat-8 OLI satellite sensors. To assess different spatial resolutions and enable comparisons with Landsat-8 imagery, models were developed at 10 m, 20 m and 30 m spatial resolution for Sentinel-2. To address limitations identified in chapter 3, the models developed in this study used seasonal composites (annual and dry season) produced for both Sentinel-2 and Landsat-8 as the predictor variables. In addition, training datasets were generated from three LiDAR datasets captured across a much larger area of the NT. Model accuracy was found to improve as spatial resolution decreased, with models produced at 30 m recording the highest overall accuracy (Tables 4.8 and 4.9). The additional red-edge bands available for Sentinel-2 imagery featured as important predictor variables, however they did not significantly improve model performance when compared with the Landsat-8 models. Of the seven models H_{99} (representing maximum canopy height) had the strongest relationship for both Sentinel-2 and Landsat-8 with R^2 values ranging from 0.81 and 0.70 and RMSE% be-

tween 33.8 and 22.9. Model accuracy declined with a reduction in spatial resolution however, models at 10 m spatial resolution provide much higher level of detail across the landscape, making them relevant for certain applications such as land use change and vegetation mapping. While the validation of the models developed in this study was rigorous, one limitation of this study (particularly in the context of this thesis) was the need to assess how well the Landsat-8 models generalise when applied to seasonal composites produced from all three Landsat sensors. The major contribution of this chapter to the aim of the thesis are (1) the overall improvement of the accuracy of the tree structure models, (2) identification of the optimal tree structure metric (H_{99}), and (3) development of a regional scale mapping product that provides insight into the vertical tree canopy structural metrics, which has been validated across a broad range of vegetation communities in the NT.

6.0.4 Chapter 5 - Investigating structural dynamics of woody vegetation in northern Australia impacted by severe tropical cyclone Monica, using remote sensing

The final research chapter (5) in this thesis consisted of two core objectives: “**(1) development of an annual mapping product, detailing the spatial and temporal distribution of woody vegetation structure between 1988 and 2017 using the Landsat suite of sensors, and (2) investigate the impact of severe tropical cyclone Monica (2006) and assess the subsequent recovery of woody vegetation (2017).**”.

Research from chapters 2, 3 and 4 were used to achieve the first objective in chapter 5, which produced a woody structural classification mapping product based on estimates of canopy cover and canopy height derived from Landsat sensors. The CC estimates were derived from Landsat woody FPC product (Armston et al. 2009), which were validated using estimates of woody FPC derived from digital aerial photography captured across the study area. To address the limitations identified in chapter 2, an automated classifier was developed to obtain estimates of woody FPC from digital aerial photography ($n = 6,305$). The woody FPC estimates obtained from the aerial photography were then used to correct the bias observed in the Landsat based woody FPC estimates prior to converting them to CC using a generalised model developed from field data collected across Australia (Fisher et al. 2018). Accuracy of the annual Landsat CC estimates (RMSE of 13 %) were assessed using field data from 304 sites collected across the study area in the years 2000, 2016, and 2017. Validation of the H_{99} tree height was also undertaken to assess how well the Landsat-8 model (chapter 4) transferred to Landsat seasonal composites produced from 2011 Landsat-5 and Landsat-7 imagery (RMSE = 4.3 m). The Landsat CC and canopy height estimates were used to produce annual structural classification mapping product over a 30 year period. The 21 structural

classes were defined taking to account a number of factors which included: the Australian national (NVIS) classification scheme, error in both the Landsat CC and height estimates, and consideration of the structural attributes of the vegetation in the region.

The annual structural mapping product was then used to investigate the dynamics of woody vegetation in a region ($\approx 11,500 \text{ km}^2$) impacted by severe tropical cyclone Monica in 2006. The accuracy assessment of the Landsat derived canopy cover and tree height products enabled limitations of these data to be identified, which was taken into account when developing the change detection methodology. It was estimated that an area of $3,551 \text{ km}^2$ was substantially impacted by cyclone Monica and that the region impacted is steadily recovering, with an area of 70 km^2 estimated to still be severely impacted in 2017. The proportion of each structural class was used to gain insight into the structural dynamics and recovery of woody vegetation post cyclone Monica, the results suggesting that the region is still in a state of recovery. A number of limitations were identified in the structural classification mapping product. This included the mapping of woody classes in areas dominated by non-woody vegetation that is photosynthetically active during the dry season (e.g. floodplains and areas of agriculture). Variability between structural classes was also evident between years, which in some situations is likely to represent true change, however, a number of factors are likely to have also influenced the variability observed. For instance, striping effects were visible in the structural classification product due to the failure of the scan line corrector error in the Landsat-7 imagery, and regions which were burnt were not successfully removed from the single date imagery prior to production of the seasonal composites. These factors need to be taken into account when using the structural mapping product. The major contributions of this chapter to the overall aim of the thesis are (1) the development of a structural classification mapping product that enables analysis of vegetation structural dynamics over three decades across the northern half of the Northern Territory, (2) development of a change detection methodology that enables areas substantially impacted by tropical cyclones to be quantified and assessed at a regional scale, demonstrated by the cyclone Monica case study.

6.0.5 Contributions to knowledge

This thesis focused on the development of remote sensing methods and creation of mapping products that enable greater insight into the dynamics of vegetation structure in the wet-dry tropics of northern Australia. A number of different remote sensing platforms were used in this thesis, including digital aerial photography, LiDAR and multispectral satellite sensors (Landsat and Sentinel-2). The major contributions to knowledge in this thesis is the development of techniques and remote sensing products (digital aerial ph-

tography and multispectral satellite data) which provide new insight and ways to assess tree structural dynamics in the savanna ecosystems of northern Australia.

In chapters 2 and 5, techniques were developed to quantify woody vegetation cover from digital aerial photography. The results in chapter 2 show that there is a strong relationship between foliage projective cover obtained from both aerial photography and field measurements across a broad range of vegetation communities across the Northern Territory. To our knowledge this is the first study that looks at the relationship between field measured woody FPC (measured using the Australian national standard methodology), based on an extensive field dataset covering a diverse range of vegetation communities, and biophysical parameters from digital aerial photography in the NT. In chapter 5, methodology and code were developed using machine learning techniques to automatically extract large quantities of information from digital aerial photography, at a scale suitable for use validation and calibration of satellite sensors, as demonstrated in chapter 5 (section 5.3.1.2).

In chapter 3 and 4 research was undertaken to develop methodology and techniques to quantify vertical woody vegetation structural metrics from Landsat satellite sensors, enabling annual analysis over satellite imagery acquired between 1988 to the present day. Models were also developed to quantifying vertical tree canopy structural metrics from Sentinel-2 satellite sensors for three spatial resolutions (10 m, 20 m, 30 m), enabling annual analysis from 2016 to present. The tree canopy models developed in this thesis provide the opportunity to assess the dynamics of tree canopy height at a spatial and temporal scale, previously unavailable across the northern half of the Northern Territory. Furthermore, the tree canopy height model developed for the Sentinel-2 sensor at 10 m spatial resolution is the first mapping product at this scale, providing information on the tree canopy height at a broad-scale.

The remote sensing methods developed in chapter 5 enabled annual analysis of horizontal and vertical structural dynamics at a broad-scale. These new methods enable analysis of the structural mapping products, providing greater insight into the spatial and temporal dynamics of vegetation structure in the savanna ecosystems of northern Australia. Despite the significant impact tropical cyclones can have on the dynamics of vegetation structure, there has been very little focus on the long term impacts these natural disturbance events have on savanna ecosystems. Understanding of the ecological role tropical cyclones play in savanna ecosystems is limited in both northern Australia Cook and Goyens (2008), Hutley et al. (2013) and at a global scale (Lin et al. 2020). Furthermore the global understanding of tropical cyclones on ecosystem structure and function, over the last three decades is likely to be biased towards the northern hemi-

sphere (Lin et al. 2020). This thesis has made a major methodological contribution enabling quantitative mapping of the impacts of tropical cyclones as a natural disturbance agent on savanna ecosystems across northern Australia. This thesis provides new ways to assess the immediate impact and the longer-term influence of tropical cyclones on ecosystem structure and function. One of the unique aspects of this work is that the methodology has been applied to long timeseries of satellite data advancing knowledge and insight into the influence of tropical cyclones on savanna ecosystems, over three decades across northern Australia.

The research undertaken in chapters 2, 3, 4 and 5 of this thesis has been extended to other applications in the Northern Territory for the development of vegetation mapping products. The algorithms developed in this thesis are now used operationally in remote sensing monitoring programs contributing to a greater understanding of vegetation structure in northern Australia. In doing so, this work contributes to identify and protect significant ecosystems assisting long-term ecologically sustainable development in northern Australia.

6.0.6 Current operational use of the products developed in this thesis

The remote sensing methods and products developed in this thesis have been applied and used operationally for a number of projects by the Northern Territory Government and Department of Environment and Natural Resources. The relevant chapters of this thesis and a brief summary of the projects using the output from this thesis are:

- Chapter 2 and 5 - concepts and the methodology used to extract biophysical parameters from digital aerial photography has been applied in a project (<https://denr.nt.gov.au/water/water-management/darwin-harbour>) developing a long-term mangrove monitoring program for Darwin Harbour (Staben et al. 2019).
- Chapter 2 - The methodology developed in chapter 2 to extract biophysical parameters from digital aerial photography was used to assess the accuracy of a number of Landsat satellite derived woody FPC products (Aubault H. (in prep) Comparison of woody cover based on aerial photography and remote imagery. Technical Report, Department of Environment and Natural Resources.)
- Chapter 3 and 4 - the height structural metrics predicted from both Landsat and Sentinel-2 were used as input parameters in the development of a mapping product identifying mangrove extent and land use. This is also associated with the development of a long-term mangrove monitoring program for Darwin Harbour (Sun and Staben 2019).

- Chapter 3 and 4 - Both Landsat and Sentinel-2 tree structure products are being used in the assessment of land clearing applications.
- Chapter 4 - Landsat and Sentinel-2 tree structure products have been used as inputs into species distribution models, which are used for biodiversity conservation.
- Chapter 4 and 5 - Both Landsat and Sentinel-2 mapping products (Sentinel-2 tree canopy metrics, and Landsat structural classification) are being used as inputs for the production of a vegetation map covering an area of 80,000 km² across the Beetaloo Basin in the Northern Territory.

6.0.7 Recommendations for future work

While the focus of this thesis was on the development of remote sensing products to enable the investigation of the impact of tropical cyclones on native vegetation, the methodology and products have the potential to be used for a range of applications (as demonstrated above). It is recommended that future work focuses on addressing a number of the limitations identified in the Landsat structural classification mapping products, including;

- investigating the suitability of producing mapping products from data captured over multiple years in attempt to reduce the variability seen in the annual mapping products and,
- development of masks (similar to the concept of cloud masking) which enables grasslands and agricultural areas to be efficiently removed from further analysis.

It is recommended that additional LiDAR datasets covering a range of ecosystems across the study area are used to validate existing tree canopy models and develop new models. The existing Sentinel-2 tree canopy metric (H_{99}) was used to characterise tree canopy height across the 80,000 km² area of the Beetaloo Basin. While no LiDAR datasets were available across the Beetaloo Basin to train the Sentinel-2 model (chapter 4), it was successfully used to characterise tree canopy height across this broad region and it is recommended that future work is undertaken to develop tree canopy models for the entire Northern Territory. In addition to using airborne LiDAR data, it is recommended that future work investigates the use of spaceborne LiDAR captured by the Global Ecosystem Dynamics Investigation (GEDI) project (Dubayah et al. 2020), to validate and calibrate tree structure models.

The canopy height models developed in chapter 4 were based on predictor variables derived from individual spectral bands, band ratios and indices from seasonal com-

posites. If sufficient LiDAR training datasets are available, it is also recommended that additional predictor variables such as texture metrics and ancillary datasets such as topographic metrics and climatic variables are investigated in any new model development. The use of a range of texture metrics have been found to be useful as predictor variables in models predicting biomass and classification products however, there may be difficulties using texture due to the way texture metrics are calculated (using global min and max values for each spectral band). The variability in values representing the same feature between the annual seasonal composites may make it difficult to use for time series analysis. It is recommended that future work investigates the potential use of texture metrics in the model development based on seasonal composites, derived from multiple years, as the reduced variability between years may be sufficient to enable them to be used. It is also recommended that the use of ancillary datasets such as topographic metrics and climatic variables are investigated as predictor variables in any development of the tree canopy models across the entire Northern Territory.

In chapter 4, several tree canopy metrics were modeled from both Landsat and Sentinel-2. It is recommended that further work is undertaken to explore the relationship between the seven structural models and the patterns observed when these models are combined to produce a three band composite image. While the results for the structural metric H_{25} were low and limit its use, as a mapping product it does appear to highlight areas of tall trees in the imagery. It is recommended that further work (including field work) is undertaken to gain a better understanding of the patterns and validate these mapping products, as they have the potential to identify regions dominated by tall trees, which are important habitat for a number of fauna species (Woolley et al. 2018).

This thesis demonstrated that remote sensing can be used to quantify and assess the impact of tropical cyclones on native vegetation. Estimates of vegetation structure at 30 m spatial resolution are now currently available between 1988 and 2019. Numerous cyclones have impacted the Northern Territory coastline over this time period (e.g. C.1) and it is recommended that further work is undertaken to map and quantify the impact of cyclones on native vegetation structure over this period. To assist in identifying the magnitude of damage, it is also recommended that work is undertaken to define damage severity classes, based on changes in tree canopy height and canopy cover layers pre and post any cyclone event. Quantifying and mapping the impact of cyclones on the structural dynamics of native vegetation in the savannas of northern Australia is important, as it has the potential to improve the estimates of carbon stocks and provide important information for biodiversity conservation management. This thesis has made a substantial contribution to achieving this aim.

REFERENCES

- Ahmed, O. S., Franklin, S. E., Wulder, M. A. and White, J. C. (2015), ‘Characterizing stand-level forest canopy cover and height using Landsat time series, samples of airborne LiDAR, and the Random Forest algorithm’, *ISPRS Journal of Photogrammetry and Remote Sensing* **101**, 89–101.
- URL:** <http://www.sciencedirect.com/science/article/pii/S0924271614002755>
- Alleaume, S., Dusseux, P., Thierion, V., Commagnac, L., Laventure, S., Lang, M., Féret, J. B., Hubert-Moy, L. and Luque, S. (2018), ‘A generic remote sensing approach to derive operational essential biodiversity variables (EBVs) for conservation planning’, *Methods in Ecology and Evolution* **9**(8), 1822–1836.
- Allen, K. J., Brookhouse, M., French, B. J., Nichols, S. C., Dahl, B., Norrie, D., Prior, L. D., Palmer, J. G. and Bowman, D. J. (2019), ‘Two climate-sensitive tree-ring chronologies from Arnhem Land, monsoonal Australia’, *Austral Ecology* **44**(4), 581–596.
- Anderson, A. N., Braithwaite, R. W., Cook, G. D., Corbett, L. K., Williams, R. J., Douglas, M. M., Gill, M. A., Setterfield, S. A. and Muller, W. J. (1998), ‘Review article Fire research for conservation management in tropical savannas : Introducing the Kapalga fire experiment’, *Australia Journal of Ecology* **23**(May 1997), 95–110.
- Armston, J. D., Denham, R. J., Danaher, T. J., Scarth, P. F. and Moffiet, T. N. (2009), ‘Prediction and validation of foliage projective cover from Landsat-5 TM and Landsat-7 ETM + imagery’, *Journal of Applied Remote Sensing* **3**(August), 1–28.
- Armston, J., Disney, M., Lewis, P., Scarth, P., Phinn, S., Lucas, R., Bunting, P. and Goodwin, N. (2013), ‘Direct retrieval of canopy gap probability using airborne waveform lidar’, *Remote Sensing of Environment* **134**, 24–38.
- URL:** <http://linkinghub.elsevier.com/retrieve/pii/S003442571300062X>
- Asbridge, E., Lucas, R., Rogers, K. and Accad, A. (2018), ‘The extent of mangrove change and potential for recovery following severe Tropical Cyclone Yasi, Hinchinbrook Island, Queensland, Australia’, *Ecology and Evolution* **8**(21), 10416–10434.
- Avitabile, V., Baccini, A., Friedl, M. a. and Schmullius, C. (2012), ‘Capabilities and limitations of Landsat and land cover data for aboveground woody biomass estimation of Uganda’, *Remote Sensing of Environment* **117**, 366–380.
- URL:** <http://linkinghub.elsevier.com/retrieve/pii/S0034425711003609>
- Bach, C. S. (2002), ‘Phenological patterns in monsoon rainforests in the Northern Ter-

- ritory, Australia', *Austral Ecology* **27**(5), 477–489.
- URL:** <http://doi.wiley.com/10.1046/j.1442-9993.2002.01209.x>
- Baldi, P., Brunak, S., Chauvin, Y., Andersen, C. A. F. and Nielsen, H. (2000), 'Assessing the accuracy of prediction algorithms for classification: an overview', *BIOINFORMATICS REVIEW* **16**(5), 412–424.
- Banfai, D. S. and Bowman, D. M. (2006), 'Forty years of lowland monsoon rainforest expansion in Kakadu National Park, Northern Australia', *Biological Conservation* **131**(4), 553–565.
- URL:** <http://linkinghub.elsevier.com/retrieve/pii/S0006320706000954>
- Banfai, D. S. and Bowman, D. M. (2007), 'Drivers of rain-forest boundary dynamics in Kakadu National Park, northern Australia: A field assessment', *Journal of Tropical Ecology* **23**(1), 73–86.
- Bannari, A., Morin, D., Bonn, F. and Huete, A. R. (1995), 'A review of vegetation indices', *Remote Sensing Reviews* **13**(1), 95–120.
- URL:** <http://dx.doi.org/10.1080/02757259509532298>
- Barlow, J., Martin, Y. and Franklin, S. E. (2003), 'Detecting translational landslide scars using segmentation of Landsat ETM+ and DEM data in the northern Cascade Mountains, British Columbia', *Canadian Journal of Remote Sensing* **29**(4), 510–517.
- URL:** <http://www.tandfonline.com/doi/abs/10.5589/m03-018>
- Barnes, E., Clarke, T., Richards, S., Colaizzi, P., Haberland, J., Kostrzewski, M., Waller, P., Choi, C., Riley, E., Thompson, T., Lascano, R., Li, H. and Moran, M. (2000), Coincident detection of crop water stress, nitrogen status and canopy density using ground based multispectral data, in P. C. Robert, R. H. Rust and W. E. Larson, eds, 'Proceedings of the 5th International Conference on Precision Agriculture, Bloomington, Minnesota, USA, 16–19 July, 2000.', American Society of Agronomy, Bloomington.
- Barnetson, J., Phinn, S. and Scarth, P. (2019), 'Mapping woody vegetation cover across Australia's arid rangelands: Utilising a machine-learning classification and low-cost Remotely Piloted Aircraft System', *International Journal of Applied Earth Observation and Geoinformation* **83**, 101909.
- Belgiu, M. and Drăgu, L. (2016), 'Random forest in remote sensing: A review of applications and future directions', *ISPRS Journal of Photogrammetry and Remote Sensing* **114**.
- Benz, U. C., Hofmann, P., Willhauck, G., Lingenfelder, I. and Heynen, M. (2004), 'Multi-resolution, object-oriented fuzzy analysis of remote sensing data for GIS-ready information', *ISPRS Journal of Photogrammetry and Remote Sensing* **58**(3–4), 239–258.
- Blaschke, T. (2010), 'Object based image analysis for remote sensing', *ISPRS Journal of Photogrammetry and Remote Sensing* **65**(1), 2–16.

- URL:** <http://linkinghub.elsevier.com/retrieve/pii/S0924271609000884>
- Blaschke, T., Hay, G. J., Kelly, M., Lang, S., Hofmann, P., Addink, E., Queiroz Feitosa, R., van der Meer, F., van der Werff, H., van Coillie, F. and Tiede, D. (2014), 'Geographic Object-Based Image Analysis - Towards a new paradigm', *ISPRS Journal of Photogrammetry and Remote Sensing* **87**, 180–191.
- Bowman, D., Boggs, G. S., Prior, L. D. and Krull, E. S. (2007), 'Dynamics of Acacia aneura-Triodia boundaries using carbon (14C and 13C) and nitrogen (15N) signatures in soil organic matter in central Australia', *The Holocene* **17**(3), 311–318.
- URL:** <http://hol.sagepub.com/cgi/doi/10.1177/0959683607076442>
- Bowman, D. M. J. S. and Dingle, J. K. (2006), 'Late 20th century landscape-wide expansion of Allosyncarpia ternata (Myrtaceae) forests in Kakadu National Park, northern Australia', *Australian Journal of Botany* **54**(8), 707.
- URL:** <http://www.publish.csiro.au/?paper=BT05202>
- Bowman, D. M. J. S., Latz, P. K. and Panton, W. J. (1994), 'Pattern and Change in an Acacia aneura Shrubland and Triodia Hummock Grassland Mosaic on Rolling Hills in Central Australia', pp. 25–37.
- Bowman, D. M. J. S., Murphy, B. P. and Banfai, D. S. (2010), 'Has global environmental change caused monsoon rainforests to expand in the Australian monsoon tropics?', *Landscape Ecology* **25**(8), 1247–1260.
- URL:** <http://link.springer.com/10.1007/s10980-010-9496-8>
- Bowman, D. and Panton, W. (1994a), 'Fire and cyclone damage to woody vegetation on the north coast of the Northern Territory, Australia', *Australian Geographer* **25**(1), 32–25.
- Bowman, D. and Panton, W. (1994b), 'Fire and cyclone damage to woody vegetation on the north coast of the Northern Territory, Australia', *Australian Geographer* **25**(1), 32–35.
- URL:** <http://www.tandfonline.com/doi/abs/10.1080/00049189408703096>
- Breiman, L. (2001), 'Random Forests', *Machine Learning* **45**(1), 5–32.
- Brock, J. (1995), Remnant Vegetation Survey Darwin To Palmerston Region, Technical report, Greening Australia N.T., Darwin.
- URL:** <http://hdl.handle.net/10070/239792>
- Brocklehurst, P. and Edmeades, B. (1996), Mangrove survey of Darwin Harbour Northern Territory (N.T.), Technical report, Dept. of Lands, Planning and Environment, Darwin.
- URL:** <http://www.territorystories.nt.gov.au/handle/10070/213495>
- Brocklehurst, P., Lewis, D., Napier, D. and Lynch, D. (2007), Northern Territory Guidelines and Field Methodology for Vegetation Survey and Mapping, Technical report, Department of Natural Resources, Environment and the Arts. Northern Territory Government, Palmerston.

- Brown, L., Chen, J. M., Leblanc, S. G. and Cihlar, J. (2000), 'A Shortwave Infrared Modification to the Simple Ratio for LAI Retrieval in Boreal Forests An Image and Model Analysis', *Remote Sensing of Environment* **71**(1), 16–25.
- URL:** <http://www.sciencedirect.com/science/article/pii/S0034425799000358>
- Browning, D. M., Archer, S. R. and Byrne, A. T. (2009), 'Field validation of 1930s aerial photography : What are we missing ?', *Journal of Arid Environments* **73**(9), 844–853.
- URL:** <http://dx.doi.org/10.1016/j.jaridenv.2009.04.003>
- Buckley, R. (1981), 'Soils and vegetation of central Australian sandridges II. Sandridge vegetation in the Uluru National Park Area, Northern Territory, Australia', *Australian Journal of Ecology* **6**(4), 345–351.
- URL:** <https://doi.org/10.1111/j.1442-9993.1981.tb01494.x>
- Buschmann, C. and Nagel, E. (1993), 'In Vivo Spectroscopy and Internal Optics of Leaves as Basis for Remote Sensing of Vegetation.', *International Journal of Remote Sensing* **14**, 711–722.
- Cameron, D., Rance, S. and Lukitsch, P. (1983), 'Tree damage in Darwin parks and gardens during cyclones Tracy and Max', *Landscape Planning* **10**(2), 89–108.
- URL:** <http://linkinghub.elsevier.com/retrieve/pii/0304392483900540>
- Campbell, J. (1996), *Introduction to Remote Sensing*, 2nd edn, The Guilford Press, New York and London.
- Carrasco, L., Giam, X., Paps, M. and Sheldon, K. S. (2019), 'Metrics of lidar-derived 3D vegetation structure reveal contrasting effects of horizontal and vertical forest heterogeneity on bird species richness', *Remote Sensing* **11**(7).
- Carreiras, J. M., Pereira, J. M. and Pereira, J. S. (2006), 'Estimation of tree canopy cover in evergreen oak woodlands using remote sensing', *Forest Ecology and Management* **223**(1-3), 45–53.
- URL:** <http://linkinghub.elsevier.com/retrieve/pii/S0378112705006808>
- Chambers, J. Q., Fisher, J. I., Zeng, H., Chapman, E. L., Baker, D. B. and Hurtt, G. C. (2007), 'Hurricane Katrina's carbon footprint on U.S. Gulf Coast forests', *Science* **318**(5853), 1107.
- Chen, J. M. (1996), 'Optically-based methods for measuring seasonal variation of leaf area index in boreal conifer stands', *Agricultural and Forest Meteorology* **80**(2-4), 135–163.
- URL:** <http://linkinghub.elsevier.com/retrieve/pii/0168192395022910>
- Chi, C. H., McEwan, R. W., Chang, C. T., Zheng, C., Yang, Z., Chiang, J. M. and Lin, T. C. (2015), 'Typhoon Disturbance Mediates Elevational Patterns of Forest Structure, but not Species Diversity, in Humid Monsoon Asia', *Ecosystems* **18**(8), 1410–1423.
- Clewley, D., Lucas, R., Accad, A., Armston, J., Bowen, M., Dwyer, J., Pollock, S.,

- Bunting, P., McAlpine, C., Eyre, T., Kelly, A., Carreiras, J. and Moghaddam, M. (2012), ‘An Approach to Mapping Forest Growth Stages in Queensland, Australia through Integration of ALOS PALSAR and Landsat Sensor Data’, *Remote Sensing* **4**(12), 2236–2255.
- URL:** <http://www.mdpi.com/2072-4292/4/8/2236/>
- Coggins, S., Coops, N. C. and Wulder, M. A. (2008), ‘Initialization of an insect infestation spread model using tree structure and spatial characteristics derived from high spatial resolution digital aerial imagery’, *Canadian Journal of Remote Sensing* **34**(6), 485–502.
- Cohen, W. B. and Goward, S. N. (2004), ‘Landsat’s Role in Ecological Applications of Remote Sensing’, *BioScience* **54**(6), 535–545.
- Cohen, W. B., Maiersperger, T. K., Gower, S. T. and Turner, D. P. (2003), ‘An improved strategy for regression of biophysical variables and Landsat ETM+ data’, *Remote Sensing of Environment* **84**(4), 561–571.
- Congalton, R. G. and Green, K. (2009), *Assessing the accuracy of remotely sensed data: principles and practices, Second edition.*, CRC Press, Talyor and Francis Group.
- Cook, G. D. and Goyens, C. M. a. C. (2008), ‘The impact of wind on trees in Australian tropical savannas: lessons from Cyclone Monica’, *Austral Ecology* **33**(4), 462–470.
- URL:** <http://doi.wiley.com/10.1111/j.1442-9993.2008.01901.x>
- Cook, G. D. and Heerdegen, R. G. (2001), ‘Spatial variation in the duration of the rainy season in monsoonal Australia’, *International Journal of Climatology* **21**(14), 1723–1732.
- URL:** <http://doi.wiley.com/10.1002/joc.704>
- Cook, G. D., Liedloff, A. C., Cuff, N. J., Brocklehurst, P. S. and Williams, R. J. (2015), ‘Stocks and dynamics of carbon in trees across a rainfall gradient in a tropical savanna’, *Austral Ecology* **40**(7), 845–856.
- URL:** <http://doi.wiley.com/10.1111/aec.12262>
- Cook, G. D., Liedloff, a. C., Eager, R. W., Chen, X., Williams, R. J., O’Grady, a. P. and Hutley, L. B. (2005), ‘The estimation of carbon budgets of frequently burnt tree stands in savannas of northern Australia, using allometric analysis and isotopic discrimination’, *Australian Journal of Botany* **53**(7), 621.
- URL:** <http://www.publish.csiro.au/?paper=BT04150>
- Cook, G. D. and Nicholls, M. J. (2009), ‘Estimation of tropical cyclone wind hazard for Darwin: Comparison with two other locations and the Australian wind-loading code’, *Journal of Applied Meteorology and Climatology* **48**(11), 2331–2340.
- Coops, N., Delahaye, A. and Pook, E. (1997), ‘Estimation of Eucalypt Forest Leaf Area Index on the South Coast of New South Wales using Landsat MSS Data’, *Australian Journal of Botany* **45**(5), 757.
- URL:** <http://www.publish.csiro.au/?paper=BT96021>

- Cowie, I., Short, P. and Osterkamp Madsen, M. (2000), *Floodplain Flora. A Flora of the Coastal Floodplains of the Northern Territory, Australia*, Australian Biological Resources Study, Canberra.
- Cuff, N. and Brocklehurst, P. (2015), *Leaf and coarse fuel accumulation and relationships with the vegetation attributes in 'evergreen'tropical eucalypt savannas*. In: *Carbon Accounting and Savanna Fire Management.*, CSIRO Publishing.
- Cutler, D. R., Edwards, T. C., Beard, K. H., Cutler, A., Hess, K. T., Gibson, J. and Lawler, J. J. (2007), 'Random forests for classification in ecology.', *Ecology* **88**(11), 2783–92.
- URL:** <http://www.ncbi.nlm.nih.gov/pubmed/18051647>
- Danaher, T., Armston, J. and Collett, L. (2004), A Regression Model Approach for Mapping Woody Foliage Projective Cover Using Landsat Imagery in, in 'International Geoscience and Remote Sensing Symposium (IGARSS)', number C, Anchorage, pp. 523–527.
- Davies, H. F., McCarthy, M. A., Firth, R. S., Woinarski, J. C., Gillespie, G. R., Andersen, A. N., Rioli, W., Puruntatameri, J., Roberts, W., Kerinaua, C., Kerinaua, V., Womatakimi, K. B. and Murphy, B. P. (2018), 'Declining populations in one of the last refuges for threatened mammal species in northern Australia', *Austral Ecology* **43**(5), 602–612.
- Day, K. and Czachorowski, A. (1982), Land Units of the Nabarlek Mine Area, Northern Territory. , Technical report, Land Conservation Unit, Conservation Commission of the NT, Darwin.
- de Gouvenain, R. C. and Silander, J. A. (2003), 'Do Tropical Storm Regimes Influence the Structure of Tropical Lowland Rain Forests?', *BIOLOGICA* **35**(2), 166–180.
- Dorigo, W., Lucieer, A., Podobnikar, T. and Carni, A. (2012), 'Mapping invasive Fallopia japonica by combined spectral, spatial, and temporal analysis of digital orthophotos', *International Journal of Applied Earth Observation and Geoinformation* **19**(1), 185–195.
- Dowdy, A. J. (2014), 'Long-term changes in Australian tropical cyclone numbers', *Atmospheric Science Letters* **15**(4), 292–298.
- Dubayah, R., Blair, J. B., Goetz, S., Fatoyinbo, L., Hansen, M., Healey, S., Hofton, M., Hurt, G., Kellner, J., Luthcke, S., Armstrong, J., Tang, H., Duncanson, L., Hancock, S., Jantz, P., Marselis, S., Patterson, P. L., Qi, W. and Silva, C. (2020), 'The Global Ecosystem Dynamics Investigation: High-resolution laser ranging of the Earth's forests and topography', *Science of Remote Sensing* **1**, 100002.
- Duke, N. C., Kovacs, J. M., Griffiths, A. D., Preece, L., Hill, D. J., Van Oosterzee, P., Mackenzie, J., Morning, H. S. and Burrows, D. (2017), 'Large-scale dieback of mangroves in Australia's Gulf of Carpentaria: A severe ecosystem response, coincidental with an unusually extreme weather event', *Marine and Freshwater Research*

- 68**(10), 1816–1829.
- Durden, S. L. (2010), ‘Remote Sensing and Modeling of Cyclone Monica near Peak Intensity’, *Atmosphere* **1**(1), 15–33.
- URL:** [http://www.mdpi.com/2073-4433/1/1/15/](http://www.mdpi.com/2073-4433/1/1/15)
- Edwards, A. C., Maier, S. W., Hutley, L. B., Williams, R. J. and Russell-smith, J. (2013), ‘Remote Sensing of Environment Spectral analysis of fire severity in north Australian tropical savannas’, *Remote Sensing of Environment* **136**, 56–65.
- URL:** <http://dx.doi.org/10.1016/j.rse.2013.04.013>
- Edwards, A. C. and Russell-Smith, J. (2009), ‘Ecological thresholds and the status of fire-sensitive vegetation in western Arnhem Land, northern Australia: implications for management’, *International Journal of Wildland Fire* **18**(2), 127.
- URL:** <http://www.publish.csiro.au/?paper=WF08008>
- Ekstrand, S. (1996), ‘Landsat TM-Based Forest Damage Assessment : Correction for Topographic Effects’, *Photogrammetric Engineering and Remote Sensing* **62**(2), 151–161.
- Eriksson, H. M., Eklundh, L., Kuusk, A. and Nilson, T. (2006), ‘Impact of understory vegetation on forest canopy reflectance and remotely sensed LAI estimates’, *Remote Sensing of Environment* **103**(4), 408–418.
- URL:** <http://linkinghub.elsevier.com/retrieve/pii/S0034425706001556>
- Escadafal, R. and Huete, A. (1991), ‘Improvement in remote sensing of low vegetation cover in arid regions by correcting vegetation indices for soil ”noise”’, *Comptes Rendus de l'Academie des Sciences. Serie 2* **312**(11), 1385–1391.
- URL:** https://inis.iaea.org/search/search.aspx?orig_q=RN:46046803
- Fensham, R. J., Bray, S. G. and Fairfax, R. J. (2007), ‘Evaluation of aerial photography for predicting trends in structural attributes of Australian woodland including comparison with ground-based monitoring data.’, *Journal of environmental management* **83**(4), 392–401.
- URL:** <http://www.ncbi.nlm.nih.gov/pubmed/16828220>
- Fensham, R. J. and Fairfax, R. J. (2007), ‘Effect of photoscale , interpreter bias and land type on woody crown-cover estimates from aerial photography’, *Australian Journal of Botany* **55**, 457–463.
- Fensham, R. J., Fairfax, R. J., Holman, J. E. and Whitehead, P. J. (2002), ‘Quantitative assessment of vegetation structural attributes from aerial photography’, *International Journal of Remote Sensing* **23**(11), 2293–2317.
- URL:** <http://www.tandfonline.com/doi/abs/10.1080/01431160110106050>
- Ferwerda, J. G., Ketner, P. and McGuinness, K. A. (2007), ‘Differences in regeneration between hurricane damaged and clear-cut mangrove stands 25 years after clearing’, *Hydrobiologia* .
- Fisher, A., Scarth, P., Armston, J. and Danaher, T. (2018), ‘Relating foliage and crown

- projective cover in Australian tree stands', *Agricultural and Forest Meteorology* **259**, 39–47.
- Flood, N. (2013), 'Seasonal composite landsat TM/ETM+ Images using the medoid (a multi-dimensional median)', *Remote Sensing* **5**(12), 6481–6500.
- Flood, N. (2014), 'Continuity of reflectance data between landsat-7 ETM+ and landsat-8 OLI, for both top-of-atmosphere and surface reflectance: A study in the australian landscape', *Remote Sensing* **6**(9), 7952–7970.
- Flood, N. (2017), 'Comparing Sentinel-2A and Landsat 7 and 8 using surface reflectance over Australia', *Remote Sensing* **9**(7).
- Flood, N., Danaher, T., Gill, T. and Gillingham, S. (2013), 'An Operational Scheme for Deriving Standardised Surface Reflectance from Landsat TM/ETM+ and SPOT HRG Imagery for Eastern Australia', *Remote Sensing* **5**(1), 83–109.
- URL:** <http://www.mdpi.com/2072-4292/5/1/83>
- Foody, G. M., Boyd, D. S. and Cutler, M. E. (2003), 'Predictive relations of tropical forest biomass from Landsat TM data and their transferability between regions', *Remote Sensing of Environment* **85**(4), 463–474.
- URL:** <http://linkinghub.elsevier.com/retrieve/pii/S0034425703000397>
- Foran, B. D. and Cellier, K. M. (1980), 'An evaluation of large scale aerial photography for assessing range condition in central Australia.', *Australian Rangeland Journal* **2**(3), 189–200.
- Fox, R. E. (1980), Deciduous vine thickets of the Darwin area and effects of cyclone 'Tracy' 25 December 1974, Technical report, Parks and Wildlife, Technical Bulletin Number Two, Conservation Commission of the Northern Territory,, Darwin, NT.
- Franklin, D. C., Brocklehurst, P. S., Lynch, D. and Bowman, D. M. J. S. (2007), 'Niche differentiation and regeneration in the seasonally flooded Melaleuca forests of northern Australia', *Journal of Tropical Ecology* **23**(04), 457.
- URL:** http://www.journals.cambridge.org/abstract_S0266467407004130
- Franklin, D. C., Gunton, R. M., Schatz, J. and Lawes, M. J. (2010), 'Resprouting responses of trees in a fire-prone tropical savanna following severe tornado damage', *Austral Ecology* **35**(6), 685–694.
- URL:** <http://doi.wiley.com/10.1111/j.1442-9993.2009.02075.x>
- Gao, T., Zhu, J., Zheng, X., Shang, G., Huang, L. and Wu, S. (2015), 'Mapping spatial distribution of larch plantations from multi-seasonal landsat-8 OLI imagery and multi-scale textures using random forests', *Remote Sensing* **7**(2), 1702–1720.
- García, M., Saatchi, S., Casas, A., Koltunov, A., Ustin, S. L., Ramirez, C. and Balzter, H. (2017), 'Extrapolating forest canopy fuel properties in the California Rim fire by combining airborne LiDAR and landsat OLI data', *Remote Sensing* **9**(4).
- Gill, A. M., Ryan, P. G., Moore, P. H. R. and Gibson, M. (2000), 'Fire regimes of World Heritage Kakadu National Park., Australia', *Austral Ecology* **25**(6), 616–625.

- URL:** <http://doi.wiley.com/10.1111/j.1442-9993.2000.tb00067.x>
- Gill, T., Johansen, K., Phinn, S., Trevithick, R., Scarth, P. and Armston, J. (2017), ‘A method for mapping Australian woody vegetation cover by linking continental-scale field data and long-term Landsat time series’, *International Journal of Remote Sensing* **38**(3), 679–705.
- URL:** <https://www.tandfonline.com/doi/full/10.1080/01431161.2016.1266112>
- Gitelson, A. A., Viña, A., Arkebauer, T. J., Rundquist, D. C., Keydan, G. and Leavitt, B. (2003), ‘Remote estimation of leaf area index and green leaf biomass in maize canopies’, *Geophysical Research Letters* **30**(5).
- Goldbergs, G., Levick, S. R., Lawes, M. and Edwards, A. (2018), ‘Hierarchical integration of individual tree and area-based approaches for savanna biomass uncertainty estimation from airborne LiDAR’, *Remote Sensing of Environment* **205**, 141–150.
- Goodwin, N. R. and Collett, L. J. (2014), ‘Development of an automated method for mapping fire history captured in Landsat TM and ETM+ time series across Queensland, Australia’, *Remote Sensing of Environment* **148**, 206–221.
- Grömping, U. (2009), ‘Variable Importance Assessment in Regression: Linear Regression versus Random Forest’, *The American Statistician* **63**(4), 308–319.
- Grove, S. J., Turton, S. M. and Siegenthaler, D. T. (2000), ‘Mosaics of canopy openness induced by tropical cyclones in lowland rain forests with contrasting management histories in northeastern Australia’, *Journal of Tropical Ecology* **16**, 883–894.
- Gruber, M. and Reitinger, B. (2008), ‘UltraCamX, the largeformat digital aerial camera system by Vexcel Imaging/Microsoft.’, *International archives of photogrammetry and remote sensing Spatial Information Science*. **XXXVII**(B1), 665–670.
- Hansen, M. C., Potapov, P. V., Goetz, S. J., Turubanova, S., Tyukavina, A., Krylov, A., Kommareddy, A. and Egorov, A. (2016), ‘Mapping tree height distributions in Sub-Saharan Africa using Landsat 7 and 8 data’, *Remote Sensing of Environment* **185**, 221–232.
- URL:** <http://www.sciencedirect.com/science/article/pii/S0034425716300530>
- Harvey, K. and Hill, G. (2001), ‘Vegetation mapping of a tropical freshwater swamp in the Northern Territory, Australia: a compariosn of aerial photography, Landsat TM and SPOT satellite imagery’, *International Journal of Remote Sensing* **22**(15), 2911–2925.
- Heartsill Scalley, T., Scatena, F. N., Lugo, A. E., Moya, S. and Estrada Ruiz, C. R. (2010), ‘Changes in structure, composition, and nutrients during 15 yr of hurricane-induced succession in a subtropical wet forest in Puerto Rico’, *Biotropica* **42**(4), 455–463.
- Higginbottom, T. P., Symeonakis, E., Meyer, H. and van der Linden, S. (2018), ‘Mapping fractional woody cover in semi-arid savannahs using multi-seasonal composites from Landsat data’, *ISPRS Journal of Photogrammetry and Remote Sensing* **139**, 88–

102.

URL: <https://doi.org/10.1016/j.isprsjprs.2018.02.010>

Hill, G. J. E. and Carter, J. L. (1999), ‘The role of remote sensing and GIS technologies for indigenous resource management in northern Australia.’, *Australian Biologist* **12**, 6–12.

Hill, R., Boyd, D. S. and Hopkinson, C. (2011), ‘Relationship between canopy height and Landsat ETM+ response in lowland Amazonian rainforest.’, *Remote Sensing Letters* **2**(3), 203–212.

URL: <http://eprints.bournemouth.ac.uk/17133/1/licence.txt>

Hudak, A. T., Lefsky, M. A., Cohen, W. B. and Berterretche, M. (2002), ‘Integration of lidar and Landsat ETM+ data for estimating and mapping forest canopy height’, *Remote Sensing of Environment* **82**(2-3), 397–416.

URL: <http://linkinghub.elsevier.com/retrieve/pii/S0034425702000561>

Huete, A. R. (1988), ‘A Soil-Adjusted Vegetation Index (SAVI).’, *Remote Sensing of Environment* **25**, 295–309.

Hunt, E. R. and Rock, B. N. (1989), ‘Detection of Changes in Leaf Water Content Using Near- and Middle-Infrared Reflectances’, **54**, 43–54.

Hutley, L. B., Evans, B. J., Beringer, J., Cook, G. D., Maier, S. W. and Razon, E. (2013), ‘Impacts of an extreme cyclone event on landscape-scale savanna fire, productivity and greenhouse gas emissions’, *Environmental Research Letters* **8**(4), 045023.

Ji, L., Zhang, L., Wylie, B. K. and Rover, J. (2011), ‘On the terminology of the spectral vegetation index (NIR - SWIR)/(NIR + SWIR)’, *International Journal of Remote Sensing* **32**(21), 6901–6909.

Jiang, Z., Huete, A. R., Chen, J., Chen, Y., Li, J., Yan, G. and Zhang, X. (2006), ‘Analysis of NDVI and scaled difference vegetation index retrievals of vegetation fraction’, *Remote Sensing of Environment* **101**(3), 366–378.

Jin, S., Su, Y., Gao, S., Hu, T., Liu, J. and Guo, Q. (2018), ‘The Transferability of Random Forest in Canopy Height Estimation from Multi-Source Remote Sensing Data’, *Remote Sensing* **10**(8), 1183.

Joyce, K. E., Belliss, S. E., Samsonov, S. V., McNeill, S. J. and Glassey, P. J. (2009), ‘A review of the status of satellite remote sensing and image processing techniques for mapping natural hazards and disasters’, *Progress in Physical Geography* **33**(2), 183–207.

URL: <http://ppg.sagepub.com/cgi/doi/10.1177/0309133309339563>

Joyce, K. E., Phinn, S. R., Roelfsema, C. M., Neil, D. T. and Dennison, W. C. (2004), ‘Combining Landsat ETM+ and Reef Check classifications for mapping coral reefs: a critical assessment from the southern Great Barrier Reef, Australia’, *Coral Reefs* **23**(1), 21–25.

URL: <http://link.springer.com/10.1007/s00338-003-0357-7>

- Karfs, R. A., Abbott, B. N., Scarth, P. F. and Wallace, J. F. (2009), ‘Land condition monitoring information for reef catchments : a new era’, *Rangeland Journal* **31**(1), 69–86.
- Karlson, M., Ostwald, M., Reese, H., Sanou, J., Tankoano, B. and Mattsson, E. (2015), ‘Mapping Tree Canopy Cover and Aboveground Biomass in Sudano-Sahelian Woodlands Using Landsat 8 and Random Forest’, *Remote Sensing* **7**(8), 10017–10041.
- URL:** <http://www.mdpi.com/2072-4292/7/8/10017/htm>
- Khosravipour, A., Skidmore, A. K., Isenburg, M., Wang, T. and Hussin, Y. A. (2014), ‘Generating Pit-free Canopy Height Models from Airborne Lidar’, *Photogrammetric Engineering and Remote Sensing* **80**(9), 863–872.
- Labrecque, S., Fournier, R. A., Luther, J. E. and Piercey, D. (2006), ‘A comparison of four methods to map biomass from Landsat-TM and inventory data in western Newfoundland’, *Forest Ecology and Management* **226**, 129–144.
- Laliberte, A. S., Browning, D. M., Herrick, J. E. and Gronemeyer, P. (2010), ‘Hierarchical object-based classification of ultra-high-resolution digital mapping camera (DMC) imagery for rangeland mapping and assessment’, *Journal of Spatial Science* **55**(1), 101–115.
- URL:** <http://www.tandfonline.com/doi/abs/10.1080/14498596.2010.487853>
- Laliberte, A. S., Fredrickson, E. L. and Rango, A. (2007), ‘Combining Decision Trees with Hierarchical Object-oriented Image Analysis for Mapping Arid Rangelands’, *Photogrammetric Engineering and Remote Sensing* **73**(2), 197–207.
- Lang, N., Schindler, K. and Wegner, J. D. (2019), ‘Country-wide high-resolution vegetation height mapping with Sentinel-2’, *Remote Sensing of Environment* **233**, 111347.
- URL:** <https://linkinghub.elsevier.com/retrieve/pii/S0034425719303669>
- LAStools (2017), ‘LAStools, Efficient LiDAR Processing Software (version 170822, academic), obtained from <http://rapidlasso.com/LAStools>’.
- Leberl, F. and Gruber, M. (2005), Ultracam-D : Understanding some Noteworthy Capabilities, in F. D, ed., ‘Photogrammetric Week.’, Wichmann-Verlag, Stuttgart,Germany, pp. 57–68.
- Leberl, F., Gruber, M., Ponticelli, M. and Wiechert, A. (2012), ‘The ultracam story’, *International Archives of the Photogrammetry, Remote Sensing and Spatial Information Sciences* **XXXIX**(B1), 39–44.
- Lehmann, C. E. R., Prior, L. D. and Bowman, D. M. J. S. (2009), ‘Decadal dynamics of tree cover in an Australian tropical savanna’, *Austral Ecology* **34**(6), 601–612.
- URL:** <http://doi.wiley.com/10.1111/j.1442-9993.2009.01964.x>
- Lehmann, C. E. R., Prior, L. D., Williams, R. J. and Bowman, D. M. J. S. (2008), ‘Spatio-temporal trends in tree cover of a tropical mesic savanna are driven by landscape disturbance’, *Journal of Applied Ecology* **45**(4), 1304–1311.
- URL:** <http://doi.wiley.com/10.1111/j.1365-2664.2008.01496.x>
- Levick, S. R., Richards, A. E., Cook, G. D., Schatz, J., Guderle, M., Williams, R. J.,

- Subedi, P., Trumbore, S. E. and Andersen, A. N. (2019), ‘Rapid response of habitat structure and above-ground carbon storage to altered fire regimes in tropical savanna’, *Biogeosciences* **16**(7), 1493–1503.
- Lewis, D. L., Brockelhurst, P. B., Thackway, R. and Hill, J. V. (2008), ‘Adopting national vegetation guidelines and the National Vegetation Information System (NVIS) framework in the Northern Territory.’, *Cunninghamia* **10**(4), 557–567.
- URL:** www.rbgsyd.nsw.gov.au/science/Scientific_publications/cunninghamia
- Lewis, D., Phinn, S. and Arroyo, L. (2013), ‘Cost-Effectiveness of Seven Approaches to Map Vegetation Communities — A Case Study from Northern Australia’s Tropical Savannas’, *Remote Sensing* **5**(1), 377–414.
- URL:** <http://www.mdpi.com/2072-4292/5/1/377/>
- Lewis, R. J. and Bannar-Martin, K. H. (2012), ‘The Impact of Cyclone Fanele on a Tropical Dry Forest in Madagascar’, *Biotropica* **44**(2), 135–140.
- Li, H., Mausel, P., Brondizio, E. and Deardorff, D. (2010), ‘A framework for creating and validating a non-linear spectrum-biomass model to estimate the secondary succession biomass in moist tropical forests’, *ISPRS Journal of Photogrammetry and Remote Sensing* **65**(2), 241–254.
- URL:** <http://linkinghub.elsevier.com/retrieve/pii/S0924271610000031>
- Lim, K., Treitz, P., Wulder, M. A., St-Onge, B. and Flood, M. (2003), ‘LiDAR remote sensing of forest structure’, *Progress in Physical Geography* **27**(1), 88–106.
- Lin, T. C., Hogan, J. A. and Chang, C. T. (2020), ‘Tropical Cyclone Ecology: A Scale-Link Perspective’, *Trends in Ecology and Evolution* **35**(7), 594–604.
- Lindenmayer, D. B., Burns, E. L., Tennant, P., Dickman, C. R., Green, P. T., Keith, D. A., Metcalfe, D. J., Russell-Smith, J., Wardle, G. M., Williams, D., Bossard, K., deLacey, C., Hanigan, I., Bull, C. M., Gillespie, G., Hobbs, R. J., Krebs, C. J., Likens, G. E., Porter, J. and Vardon, M. (2015), ‘Contemplating the future: Acting now on long-term monitoring to answer 2050’s questions’, *Austral Ecology* **40**(3), 213–224.
- Lindenmayer, D. B., Likens, G. E., Andersen, A., Bowman, D., Bull, C. M., Burns, E., Dickman, C. R., Hoffmann, A. a., Keith, D. a., Liddell, M. J., Lowe, A. J., Metcalfe, D. J., Phinn, S. R., Russell-Smith, J., Thurgate, N. and Wardle, G. M. (2012), ‘Value of long-term ecological studies’, *Austral Ecology* **37**(7), 745–757.
- URL:** <http://doi.wiley.com/10.1111/j.1442-9993.2011.02351.x>
- Lucas, R. M., Ellison, J. C., Mitchell, A., Donnelly, B., Finlayson, M. and Milne, A. K. (2002), ‘Use of stereo aerial photography for quantifying changes in the extent and height of mangroves in tropical Australia’, *Wetlands Ecology and Management* **10**, 161–175.
- Ludwig, J. A., Hindley, N. and Barnett, G. (2003), ‘Indicators for monitoring minesite rehabilitation: trends on waste-rock dumps, northern Australia’, *Ecological Indicators* **3**(3), 143–153.

URL: <http://linkinghub.elsevier.com/retrieve/pii/S1470160X03000384>

- Luque, S., Pettorelli, N., Vihervaara, P. and Wegmann, M. (2018), 'Improving biodiversity monitoring using satellite remote sensing to provide solutions towards the 2020 conservation targets', *Methods in Ecology and Evolution* **9**(8), 1784–1786.
- Lymburner, L., Bunting, P., Lucas, R., Scarth, P., Alam, I., Phillips, C., Ticehurst, C. and Held, A. (2019), 'Mapping the multi-decadal mangrove dynamics of the Australian coastline', *Remote Sensing of Environment* **111**:185.
- Ma, X., Huete, A., Yu, Q., Coupe, N. R., Davies, K., Broich, M., Ratana, P., Beringer, J., Hutley, L. B., Cleverly, J., Boulain, N. and Eamus, D. (2013), 'Spatial patterns and temporal dynamics in savanna vegetation phenology across the north australian tropical transect', *Remote Sensing of Environment* **139**, 97–115.
- Mannel, S., Price, M. and Hua, D. (2006), 'A method to obtain large quantities of reference data', *International Journal of Remote Sensing* **27**(3), 623–627.
- Marques, A., Martins, I. S., Kastner, T., Plutzar, C., Theurl, M. C., Eisenmenger, N., Huijbregts, M. A., Wood, R., Stadler, K., Bruckner, M., Canelas, J., Hilbers, J. P., Tukker, A., Erb, K. and Pereira, H. M. (2019), 'Increasing impacts of land use on biodiversity and carbon sequestration driven by population and economic growth', *Nature Ecology and Evolution* **3**(4), 628–637.
- Mascaro, J., Asner, G. P., Knapp, D. E., Kennedy-Bowdoin, T., Martin, R. E., Anderson, C., Higgins, M. and Chadwick, K. D. (2014), 'A tale of two "Forests": Random Forest machine learning aids tropical Forest carbon mapping', *PLoS ONE* **9**(1), 12–16.
- Matasci, G., Hermosilla, T., Wulder, M. A., White, J. C., Coops, N. C., Hobart, G. W. and Zald, H. S. (2018), 'Large-area mapping of Canadian boreal forest cover, height, biomass and other structural attributes using Landsat composites and lidar plots', *Remote Sensing of Environment* **209**, 90–106.
- McDonald, N. and McAlpine, J. (1991), Floods and droughts: the northern climate., in C. Haynes, M. Ridpath and M. Willimans, eds, 'Monsoonal Australia. Landscape Ecology and Man in The Northern Lowlands.', A. A. Balkema, Rotterdam, pp. 19–29.
- McGeoch, M. A., Butchart, S. H. M., Spear, D., Marais, E., Kleynhans, E. J., Symes, A., Chanson, J. and Hoffmann, M. (2010), 'Global indicators of biological invasion: Species numbers, biodiversity impact and policy responses', *Diversity and Distributions* **16**(1), 95–108.
- Meakin, C., Owen, G., Brocklehurst, P. and Lewis, D. (2001), NORFOR Mapping the forest cover of the NT: Document 1 Field methodology and FPC indexing., Technical report, Northern Territory. Department of Lands, Planning and the Environment, Darwin.

URL: <https://www.territorystories.nt.gov.au/jspui/handle/10070/299146>

- Mellor, A., Boukir, S., Haywood, A. and Jones, S. (2015), ‘Exploring issues of training data imbalance and mislabelling on random forest performance for large area land cover classification using the ensemble margin’, *ISPRS Journal of Photogrammetry and Remote Sensing* **105**.
- Mellor, A., Haywood, A., Stone, C. and Jones, S. (2013), ‘The Performance of Random Forests in an Operational Setting for Large Area Sclerophyll Forest Classification’, *Remote Sensing* **5**(6), 2838–2856.
- URL:** <http://www.mdpi.com/2072-4292/5/6/2838/>
- Melville, B., Fisher, A. and Lucieer, A. (2019), ‘Ultra-high spatial resolution fractional vegetation cover from unmanned aerial multispectral imagery’, *International Journal of Applied Earth Observation and Geoinformation* **78**, 14–24.
- Morgan, J. L., Gergel, S. E. and Coops, N. C. (2010), ‘Aerial Photography: A Rapidly Evolving Tool for Ecological Management’, *BioScience* **60**(1), 47–59.
- Moulin, S., Bondeau, A. and Delecolle, R. (1998), ‘Combining agricultural crop models and satellite observations: From field to regional scales’, *International Journal of Remote Sensing* **19**(6), 1021–1036.
- URL:** <http://www.tandfonline.com/doi/abs/10.1080/014311698215586>
- Muir, J., Schmidt, M., Tindall, D., Trevithick, R., Scarth, P. and Stewart, J. (2011), Field measurement of fractional ground cover : a technical handbook supporting ground cover monitoring for Australia, Technical report.
- Müller, A. C. and Guido, S. (2016), *Introduction to Machine Learning with Python; A Guide for Data Scientists*, 1 edn, O’Reilly Media, Inc., 1005 Gravenstein Highway North, Sebastopol, CA 95472, United States of America.
- Murphy, B. P., Lehmann, C. E. R., Russell-smith, J. and Lawes, M. J. (2014), ‘Fire regimes and woody biomass dynamics in Australian savannas’, *Journal of Biogeography* **41**, 133–144.
- Murphy, B. P., Russell-Smith, J. and Prior, L. D. (2010), ‘Frequent fires reduce tree growth in northern Australian savannas: Implications for tree demography and carbon sequestration’, *Global Change Biology* **16**(1), 331–343.
- Murphy, K. (1984), *Big Blow up North: A History of Tropical Cyclones in Australia’s Northern Territory*, University Planning Authority, Darwin.
- Myers, B. A., Duff, G. A., Eamus, D., Fordyce, I. R., O’Grady, A. and Williams, R. J. (1997), ‘Seasonal Variation in Water Relations of Trees of Differing Leaf Phenology in a Wet–Dry Tropical Savanna near Darwin, Northern Australia’, *Australian Journal of Botany* **45**(2), 225.
- URL:** <http://www.publish.csiro.au/?paper=BT96015>
- Nicholas, A. M., Franklin, D. C. and Bowman, D. M. (2009), ‘Coexistence of shrubs and grass in a semi-arid landscape: A case study of mulga (*Acacia aneura*, Mimosaceae) shrublands embedded in fire-prone spinifex (*Triodia pungens*, Poaceae)

- hummock grasslands', *Australian Journal of Botany* **57**(5), 396–405.
- Nott, J. (2006), 'Tropical Cyclones and the Evolution of the Sedimentary Coast of Northern Australia', *Journal of Coastal Research* **22**1, 49–62.
- URL:** <http://www.bioone.org/doi/abs/10.2112/05A-0005.1>
- Noy, I. (2016), 'Tropical storms: The socio-economics of cyclones', *Nature Climate Change* **6**(4), 343–345.
- O'Grady, A. P., Eamus, D. and Hutley, L. B. (1999), 'Transpiration increases during the dry season: patterns of tree water use in eucalypt open-forests of northern Australia.', *Tree physiology* **19**(9), 591–597.
- URL:** <http://www.ncbi.nlm.nih.gov/pubmed/12651533>
- Oshiro, T. M., Perez, P. S. and Baranauskas, J. A. (2012), 'How Many Trees in a Random Forest?', *Lecture Notes in Computer Science* **7376**(July), 154–168.
- Ota, T., Ahmed, O., Franklin, S., Wulder, M., Kajisa, T., Mizoue, N., Yoshida, S., Takao, G., Hirata, Y., Furuya, N., Sano, T., Heng, S. and Vuthy, M. (2014), 'Estimation of Airborne Lidar-Derived Tropical Forest Canopy Height Using Landsat Time Series in Cambodia', *Remote Sensing* **6**(11), 10750–10772.
- URL:** <http://www.mdpi.com/2072-4292/6/11/10750/>
- O'Grady, A. P., Chen, X., Eamus, D. and Hutley, L. B. (2000), 'Composition, leaf area index and standing biomass of eucalypt open forests near darwin in the northern territory, australia', *Australian Journal of Botany* **48**(5), 629–638.
- Pal, M. (2005), 'Random forest classifier for remote sensing classification', *International Journal of Remote Sensing* **26**(1), 217–222.
- URL:** <http://www.tandfonline.com/doi/abs/10.1080/01431160412331269698>
- Paling, E., Kobryn, H. and Humphreys, G. (2008), 'Assessing the extent of mangrove change caused by Cyclone Vance in the eastern Exmouth Gulf, northwestern Australia', *Estuarine, Coastal and Shelf Science* **77**(4), 603–613.
- URL:** <http://linkinghub.elsevier.com/retrieve/pii/S0272771407004866>
- Pascual, C., García-Abril, A., Cohen, W. B. and Martín-Fernández, S. (2010), 'Relationship between LiDAR-derived forest canopy height and Landsat images', *International Journal of Remote Sensing* **31**(5), 1261–1280.
- URL:** <http://www.tandfonline.com/doi/abs/10.1080/01431160903380656>
- Pedregosa, F., Grisel, O., Weiss, R., Passos, A. and Brucher, M. (2011), 'Scikit-learn : Machine Learning in Python', *Journal of Machine Learning Research* **12**, 2825–2830.
- Pereira, H. M., Ferrier, S., Walters, M., Geller, G. N., Jongman, R. H., Scholes, R. J., Bruford, M. W., Brummitt, N., Butchart, S. H., Cardoso, A. C., Coops, N. C., Dulloo, E., Faith, D. P., Freyhof, J., Gregory, R. D., Heip, C., Höft, R., Hurt, G., Jetz, W., Karp, D. S., McGeoch, M. A., Obura, D., Onoda, Y., Pettorelli, N., Reyers, B., Sayre, R., Scharlemann, J. P., Stuart, S. N., Turak, E., Walpole, M. and Wegmann,

- M. (2013), ‘Essential biodiversity variables’, *Science* **339**(6117), 277–278.
- Pettorelli, N., Laurance, W. F., O’Brien, T. G., Wegmann, M., Nagendra, H. and Turner, W. (2014), ‘Satellite remote sensing for applied ecologists: opportunities and challenges’, *Journal of Applied Ecology* **51**(4), 839–848.
- URL:** <http://doi.wiley.com/10.1111/1365-2664.12261>
- Pettorelli, N., Wegmann, M., Skidmore, A., Mücher, S., Dawson, T. P., Fernandez, M., Lucas, R., Schaepman, M. E., Wang, T., O’Connor, B., Jongman, R. H., Kempeneers, P., Sonnenschein, R., Leidner, A. K., Böhm, M., He, K. S., Nagendra, H., Dubois, G., Fatoyinbo, T., Hansen, M. C., Paganini, M., de Klerk, H. M., Asner, G. P., Kerr, J. T., Estes, A. B., Schmeller, D. S., Heiden, U., Rocchini, D., Pereira, H. M., Turak, E., Fernandez, N., Lausch, A., Cho, M. A., Alcaraz-Segura, D., McGeoch, M. A., Turner, W., Mueller, A., St-Louis, V., Penner, J., Vihervaara, P., Belward, A., Reyers, B. and Geller, G. N. (2016), ‘Framing the concept of satellite remote sensing essential biodiversity variables: challenges and future directions’, *Remote Sensing in Ecology and Conservation* **2**(3), 122–131.
- Powell, S. L., Cohen, W. B., Healey, S. P., Kennedy, R. E., Moisen, G. G., Pierce, K. B. and Ohmann, J. L. (2010), ‘Quantification of live aboveground forest biomass dynamics with Landsat time-series and field inventory data: A comparison of empirical modeling approaches’, *Remote Sensing of Environment* **114**(5), 1053–1068.
- URL:** <http://linkinghub.elsevier.com/retrieve/pii/S0034425709003745>
- Preston, R. A. (1987), Use of Landsat 5 MSS imagery to map cyclone damage to rainforest in North Queensland, in ‘4th Australasian Remote Sensing Conference’, Adelaide.
- Pruitt, J. N., Little, A. G., Majumdar, S. J., Schoener, T. W. and Fisher, D. N. (2019), ‘Call-to-Action: A Global Consortium for Tropical Cyclone Ecology’, *Trends in Ecology and Evolution* **34**(7), 588–590.
- Pu, R., Xu, B. and Gong, P. (2003), ‘Oakwood crown closure estimation by unmixing Landsat TM data’, *International Journal of Remote Sensing* **24**(22), 4422–4445.
- URL:** <http://www.tandfonline.com/doi/abs/10.1080/0143116031000095989>
- Qi, J., Chehbouni, A., Huete, A., Kerr, Y. and Sorooshian, S. (1994), ‘A modified soil adjusted vegetation index’, *Remote Sensing of Environment* **48**(2), 119–126.
- URL:** <https://www.sciencedirect.com/science/article/pii/0034425794901341>
- Renó, V. F., Novo, E. M., Suemitsu, C., Rennó, C. D. and Silva, T. S. (2011), ‘Assessment of deforestation in the Lower Amazon floodplain using historical Landsat MSS/TM imagery’, *Remote Sensing of Environment* **115**(12), 3446–3456.
- URL:** <http://linkinghub.elsevier.com/retrieve/pii/S0034425711002902>
- Ringrose, S., Matheson, W., Matlala, C. J. S. S., Neill, T. O., Patricia, A. and Werner, P. A. (1994), ‘Vegetation spectral reflectance along a north-south vegetation gradient in northern Australia’, *Journal of Biogeography* **21**(1), 33–47.

- URL:** <https://www.jstor.org/stable/2845602?origin=JSTOR-pdf>
- Robinson, T., van Klinken, R. and Metternicht, G. (2008), ‘Spatial and temporal rates and patterns of mesquite (*Prosopis* species) invasion in Western Australia’, *Journal of Arid Environments* **72**(3), 175–188.
- URL:** <http://linkinghub.elsevier.com/retrieve/pii/S0140196307001620>
- Rodriguez-Galiano, V. F., Ghimire, B., Rogan, J., Chica-olmo, M. and Rigol-sanchez, J. P. (2012), ‘ISPRS Journal of Photogrammetry and Remote Sensing An assessment of the effectiveness of a random forest classifier for land-cover classification’, *ISPRS Journal of Photogrammetry and Remote Sensing* **67**, 93–104.
- URL:** <http://dx.doi.org/10.1016/j.isprsjprs.2011.11.002>
- Rogers, K., Lymburner, L., Salum, R., Brooke, B. P. and Woodroffe, C. D. (2017), ‘Mapping of mangrove extent and zonation using high and low tide composites of Landsat data’, *Hydrobiologia* pp. 1–20.
- URL:** <http://link.springer.com/10.1007/s10750-017-3257-5>
- Rosso, P. H., Klonus, S., Ehlers, M. and Tschach, E. (2008), ‘Comparative properties of fourairborne sensors and their applicability to land surface interpretation.’, *The International Archives of the Photogrammetry, Remote Sensing and Spatial Information Sciences*. **XXXVII**(B1).
- Roughgarden, J., Running, S. W. and Matson, P. A. (1991), ‘What Does Remote Sensing Do For Ecology?’, *Ecology* **72**(6), 1918–1922.
- URL:** <http://doi.wiley.com/10.2307/1941546>
- Roy, D. P., Ju, J., Mbow, C., Frost, P. and Loveland, T. (2010), ‘Accessing free Landsat data via the Internet: Africa’s challenge’, *Remote Sensing Letters* **1**(2), 111–117.
- URL:** <http://www.tandfonline.com/doi/abs/10.1080/01431160903486693>
- Roy, D., Zhang, H., Ju, J., Gomez-Dans, J., Lewis, P., Schaaf, C., Sun, Q., Li, J., Huang, H. and Kovalskyy, V. (2016), ‘A general method to normalize Landsat reflectance data to nadir BRDF adjusted reflectance’, *Remote Sensing of Environment* **176**, 255–271.
- Russell-Smith, J., Evans, J., Macdermott, H., Brocklehurst, P., Schatz, J., Lynch, D., Yates, C. and Edwards, A. (2019), ‘Tree recruitment dynamics in fire-prone eucalypt savanna’, *Ecosphere* **10**(3), e02649.
- URL:** <https://onlinelibrary.wiley.com/doi/abs/10.1002/ecs2.2649>
- Samani Majd, A. M., Bleiweiss, M. P., DuBois, D. and Shukla, M. K. (2013), ‘Estimation of the fractional canopy cover of pecan orchards using Landsat 5 satellite data , aerial imagery , and orchard floor photographs’, *International Journal of Remote Sensing* **34**(16), 37–41.
- URL:** <https://doi.org/10.1080/01431161.2013.800951>
- Saynor, M., Staben, G., Hancock, G., Fox, G., Calvert, G., Smith, B., Moliere, D. and Evans, K. (2009), Impact of Cyclone Monica on catchments within the Alligator

- Rivers Region – Data. Internal Report 557, Technical report, Supervising Scientist, Darwin.
- Scarth, P., Armston, J. and Danaher, T. (2008), On the relationship between crown cover, foliage cover and leaf area index., in ‘Proceedings of the 14th Australasian RemoteSensing and Photogrammetry Conference’, Darwin, Australia.
- Scarth, P., Armston, J., Lucas, R. and Bunting, P. (2019), ‘A Structural Classification of Australian Vegetation Using ICESat/GLAS, ALOS PALSAR, and Landsat Sensor Data’, *Remote Sensing* **11**(2), 147.
- Scarth, P., Roder, A. and Schmidt, M. (2010), Tracking grazing pressure and climate interaction?the role of Landsat fractional cover in time series analysis., in ‘15th Australasian Remote Sensing and Photogrammetry Conference’, 13th–17th September 2010.
- Setterfield, S. A., Rossiter-Rachor, N. A., Hutley, L. B., Douglas, M. M. and Williams, R. J. (2010), ‘Turning up the heat: The impacts of Andropogon gayanus (gamba grass) invasion on fire behaviour in northern Australian savannas’, *Diversity and Distributions* **6**, 854–861.
- Sharp, B. R. and Bowman, D. M. J. S. (2004), ‘Net woody vegetation increase confined to seasonally inundated lowlands in an Australian tropical savanna, Victoria River District, Northern Territory’, *Austral Ecology* **29**(6), 667–683.
- URL:** <http://doi.wiley.com/10.1111/j.1442-9993.2004.01407.x>
- Skidmore, A. K., Pettorelli, N., Coops, N. C., Geller, G. N., Hansen, M., Lucas, R., Mücher, C. A., O’Connor, B., Paganini, M., Pereira, H. M., Schaepman, M. E., Turner, W., Wang, T. and Wegmann, M. (2015), ‘Environmental science: Agree on biodiversity metrics to track from space’, *Nature* **523**(7561), 403–405.
- URL:** <http://www.nature.com/doifinder/10.1038/523403a>
- Smale, D. A., Wernberg, T., Oliver, E. C., Thomsen, M., Harvey, B. P., Straub, S. C., Burrows, M. T., Alexander, L. V., Benthuysen, J. A., Donat, M. G., Feng, M., Hobday, A. J., Holbrook, N. J., Perkins-Kirkpatrick, S. E., Scannell, H. A., Sen Gupta, A., Payne, B. L. and Moore, P. J. (2019), ‘Marine heatwaves threaten global biodiversity and the provision of ecosystem services’, *Nature Climate Change* **9**(4), 306–312.
- Sohn, Y. and Mccoy, R. M. (1997), ‘Mapping Desert Shrub Rangeland Using Spectral Unmixing and Modeling Spectral Mixtures with TM Data’, *Photogrammetric Engineering and Remote Sensing* **63**(6), 707–716.
- Sripada, R. P., Heiniger, R. W., White, J. G. and Meijer, A. D. (2006), ‘Aerial color infrared photography for determining early in-season nitrogen requirements in corn’, *Agronomy Journal*.
- Staben, G. and Edmeades, B. (2017), Northern Territory Land Use Mapping for Biosecurity 2016. Technical Report 18/2017D,, Technical report, Department of Environment and Natural Resources, Northern Territory Government, Darwin.

- Staben, G., Lucieer, A., Evans, K., Scarth, P. and Cook, G. (2016), ‘Obtaining biophysical measurements of woody vegetation from high resolution digital aerial photography in tropical and arid environments: Northern Territory, Australia’, *International Journal of Applied Earth Observation and Geoinformation* **52**, 204–220.
- URL:** <http://linkinghub.elsevier.com/retrieve/pii/S0303243416300939>
- Staben, G., Lucieer, A. and Scarth, P. (2018), ‘Modelling LiDAR derived tree canopy height from Landsat TM, ETM+ and OLI satellite imagery—A machine learning approach’, *International Journal of Applied Earth Observation and Geoinformation* **73**, 666–681.
- Staben, G., McGregor, R., Brocklehurst, P., Cuff, N. and Benham, K. (2019), Exploring the utility of Unmanned Aerial Systems (UAS) to quantify mangrove biophysical parameters in Darwin Harbour, Technical report, Department of Environment and Natural Resources, Northern Territory Government, Darwin, NT.
- Staben, G., Saynor, M., Moliere, D., Hancock, G. and Evans, K. (2009), Assessment of the significance of extreme events in the Alligator Rivers Region – impact of Cyclone Monica on Gulungul Creek catchment, Ranger minesite and Nabarlek area. In eriss research summary 2007–2008. eds Jones DR and Webb A, Supervising Scientist Report 200, Technical report, Supervising Scientist, Darwin.
- Staben, G. W. and Evans, K. G. (2008), ‘Estimates of tree canopy loss as a result of Cyclone Monica , in the Magela Creek catchment northern Australia’, *Austral Ecology* **33**(4), 562–569.
- Staben, G. W., Pfitzner, K., Bartolo, R. and Lucieer, A. (2012), ‘Empirical line calibration of WorldView-2 satellite imagery to reflectance data : using quadratic prediction equations’, *Remote Sensing Letters* **3**(6), 521–530.
- URL:** <https://www.tandfonline.com/doi/abs/10.1080/01431161.2011.609187>
- Stocker, G. C. (1976), Report on cyclone damage to natural vegetation in the Darwin area after cyclone Tracey 25 December 1974, Technical report, Forestry and Timber Bureau, Leaflet No. 127, Canberra.
- Stojanova, D., Panov, P., Gjorgjioski, V., Kobler, A. and Džeroski, S. (2010), ‘Estimating vegetation height and canopy cover from remotely sensed data with machine learning’, *Ecological Informatics* **5**(4), 256–266.
- Strobl, C., Boulesteix, A.-L., Kneib, T., Augustin, T. and Zeileis, A. (2008), ‘Conditional variable importance for random forests’, *BMC Bioinformatics* **9**(1), 307.
- URL:** <http://dx.doi.org/10.1186/1471-2105-9-307>
- Stumpf, K. (1993), The estimation of forest vegetation cover descriptions using a vertical densitometer.
- URL:** <https://www.researchgate.net/publication/237510073>
- Suganuma, H., Abe, Y., Taniguchi, M., Tanouchi, H., Utsugi, H., Kojima, T. and Yamada, K. (2006), ‘Stand biomass estimation method by canopy coverage for appli-

- cation to remote sensing in an arid area of Western Australia', *Forest Ecology and Management* **222**(1-3), 75–87.
- Sun, D., Hnatiuk, R. J. and Neldner, V. J. (1997), 'Review of vegetation classification and mapping systems undertaken by major forested land management agencies in Australia', *Australian Journal of Botany* **45**(6), 929–948.
- Sun, J. and Staben, G. (2019), Development of an integrated long-term mangrove monitoring program for Darwin Harbour Sub-project B: Development of methodology to map mangrove forest extent using satellite sensors, Technical Report No. 41/2019, Technical report, Darwin, NT.
- Thackway, R., Lee, A., Donohue, R., Keenan, R. J. and Wood, M. (2007), 'Vegetation information for improved natural resource management in Australia', *Landscape and Urban Planning* **79**(2), 127–136.
- Trimble (2013), Trimble eCognition Developer 8.9 User Guide, Technical report, München: Germany Trimble Documentation.
- Tucker, C. J. (1979), 'Red and photographic infrared linear combinations for monitoring vegetati', *Remote sensing of Environment* **8**, 127–150.
- Turton, S. (2008), 'Editorial Cyclones Larry and Monica : ecological effects of two major disturbance events', *Austral Ecology* **33**, 365–367.
- Turton, S. M. (2012), 'Securing Landscape Resilience to Tropical Cyclones in Australia's Wet Tropics under a Changing Climate: Lessons from Cyclones Larry (and Yasi)', *Geographical Research* **50**(1), 15–30.
- URL:** <http://doi.wiley.com/10.1111/j.1745-5871.2011.00724.x>
- Vicente-Serrano, S. M., Pérez-Cabello, F. and Lasanta, T. (2008), 'Assessment of radiometric correction techniques in analyzing vegetation variability and change using time series of Landsat images', *Remote Sensing of Environment* **112**(10), 3916–3934.
- Vincini, M., Frazzi, E. and D'Alessio, P. (2008), 'A broad-band leaf chlorophyll vegetation index at the canopy scale', *Precision Agriculture* **9**(5), 303–319.
- Walker, J. and Hopkins, M. S. (1990), Vegetation., in R. C. McDonald, R. F. Isbell, J. G. Speight, J. Walker and M. S. Hopkins, eds, 'Australian Soil and Land Survey Field Handbook. Second Edition (Yellow Book).', 2 edn, Inkata Press, Melbourne, pp. 58–56.
- Wallace, B. J., Behn, G. and Furby, S. (2006), 'Vegetation condition assessment and monitoring from sequences of satellite imagery', *Ecological Management and Restoration* **7**(June), 31–36.
- Wallace, J. F., Caccetta, P. a. and Kiiveri, H. T. (2004), 'Recent developments in analysis of spatial and temporal data for landscape qualities and monitoring', *Austral Ecology* **29**(1), 100–107.
- URL:** <http://doi.wiley.com/10.1111/j.1442-9993.2004.01356.x>
- Wang, K., Franklin, S. E., Guo, X. and Cattet, M. (2010), 'Remote Sensing of Ecology,

- Biodiversity and Conservation: A Review from the Perspective of Remote Sensing Specialists', *Sensors* **10**(11), 9647–9667.
- URL:** <http://www.mdpi.com/1424-8220/10/11/9647/>
- Wang, W., Qu, J. J., Hao, X., Liu, Y. and Stanturf, J. A. (2010), 'Post-hurricane forest damage assessment using satellite remote sensing', *Agricultural and Forest Meteorology* **150**(1), 122–132.
- Ward, D., Petty, A., Setterfield, S., Douglas, M., Ferdinands, K., Hamilton, S. and Phinn, S. (2014), 'Floodplain inundation and vegetation dynamics in the Alligator Rivers region (Kakadu) of northern Australia assessed using optical and radar remote sensing', *Remote Sensing of Environment* **147**, 43–55.
- Webb, L. (1958), 'Cyclones as an ecological factor in tropical lowland rain-forest, North Queensland.', *Australian Journal of Botany* **6**(3), 220–228.
- URL:** <https://doi.org/10.1071/BT9580220>
- Whiteside, T. G. and Bartolo, R. E. (2018), 'A robust object-based woody cover extraction technique for monitoring mine site revegetation at scale in the monsoonal tropics using multispectral RPAS imagery from different sensors', *International Journal of Applied Earth Observations and Geoinformation* **73**, 300–312.
- Whiteside, T. G., Boggs, G. S. and Maier, S. W. (2011), 'International Journal of Applied Earth Observation and Geoinformation Comparing object-based and pixel-based classifications for mapping savannas', *International Journal of Applied Earth Observations and Geoinformation* **13**(6), 884–893.
- URL:** <http://dx.doi.org/10.1016/j.jag.2011.06.008>
- Wilkes, P., Jones, S. D., Suarez, L., Mellor, A., Woodgate, W., Soto-Berelov, M., Haywood, A. and Skidmore, A. K. (2015), 'Mapping forest canopy height across large areas by upscaling ALS estimates with freely available satellite data', *Remote Sensing* **7**(9), 12563–12587.
- Williams, R. J., Cook, G. D., Gill, a. M. and Moore, P. H. R. (1999), 'Fire regime, fire intensity and tree survival in a tropical savanna in northern Australia', *Austral Ecology* **24**(1), 50–59.
- URL:** <http://doi.wiley.com/10.1046/j.1442-9993.1999.00946.x>
- Williams, R. J. and Douglas, M. (1995), 'Windthrow in a tropical savanna in kakadu national park, northern australia', *Journal of Tropical Ecology* **11**(4), 547–558.
- Williams, R. J., Myers, B. A., Muller, W. J., Duff, G. A. and Eamus, D. (1997), 'Leaf phenology ofwoody species in a northern Australian tropical savanna.', *Ecology* **78**(8), 2542–2558.
- Williams, R. J., Zerihun, A., Montagu, K. D., Hoffman, M., Hutley, L. B. and Chen, X. (2005), 'Allometry for estimating aboveground tree biomass in tropical and subtropical eucalypt woodlands: towards general predictive equations', *Australian Journal of Botany* **53**(7), 607.

URL: <http://www.publish.csiro.au/?paper=BT04149>

Williamson, G. J., Boggs, G. S. and Bowman, D. M. J. S. (2011), ‘Late 20th century mangrove encroachment in the coastal Australian monsoon tropics parallels the regional increase in woody biomass’, *Regional Environmental Change* **11**(1), 19–27.

URL: <http://link.springer.com/10.1007/s10113-010-0109-5>

Wilson, B. A. and Bowman, D. M. J. S. (1987), ‘Fire , storm , flood and drought : The vegetation ecology of Howards Peninsula , Northern Territory , Australia’ , *Australian Journal of Ecology* **12**, 165–174.

Wilson, B. A., Brocklehurst, P., Clark, M. and Dickinson, K. (1990), Vegetation survey of the Northern Territory, Technical Report No. 49., Technical report, Conservation Commission of the Northern Territory, Darwin.

URL: <http://www.territorystories.nt.gov.au/bitstream/10070/228438/1/LRD90049.pdf>

Woinarski, J. C., Hempel, C., Cowie, I., Brennan, K., Kerrigan, R., Leach, G. and Russell-Smith, J. (2006), ‘Distributional pattern of plant species endemic to the Northern Territory, Australia’ , *Australian Journal of Botany* **54**(7), 627–640.

Woodcock, C. E., Macomber, S. A., Pax-lenney, M. and Cohen, W. B. (2001), ‘Monitoring large areas for forest change using Landsat : Generalization across space , time and Landsat sensors’ , **78**, 194–203.

Woolley, L. A., Murphy, B. P., Radford, I. J., Westaway, J. and Woinarski, J. C. (2018), ‘Cyclones, fire, and termites: The drivers of tree hollow abundance in northern Australia’s mesic tropical savanna’ , *Forest Ecology and Management* **419-420**, 146–159.

Wulder, M. A., Loveland, T. R., Roy, D. P., Crawford, C. J., Masek, J. G., Woodcock, C. E., Allen, R. G., Anderson, M. C., Belward, A. S., Cohen, W. B., Dwyer, J., Erb, A., Gao, F., Griffiths, P., Helder, D., Hermosilla, T., Hipple, J. D., Hostert, P., Hughes, M. J., Huntington, J., Johnson, D. M., Kennedy, R., Kilic, A., Li, Z., Lymburner, L., McCorkel, J., Pahlevan, N., Scambos, T. A., Schaaf, C., Schott, J. R., Sheng, Y., Storey, J., Vermote, E., Vogelmann, J., White, J. C., Wynne, R. H. and Zhu, Z. (2019), ‘Current status of Landsat program, science, and applications’ , *Remote Sensing of Environment* **225**, 127–147.

URL: <https://linkinghub.elsevier.com/retrieve/pii/S0034425719300707>

Wulder, M. a., Masek, J. G., Cohen, W. B., Loveland, T. R. and Woodcock, C. E. (2012), ‘Opening the archive: How free data has enabled the science and monitoring promise of Landsat’ , *Remote Sensing of Environment* **122**, 2–10.

URL: <http://dx.doi.org/10.1016/j.rse.2012.01.010>

Wulder, M. A., White, J. C., Coggins, S., Ortlepp, S. M., Coops, N. C., Heath, J. and Mora, B. (2012), ‘Digital high spatial resolution aerial imagery to support forest health monitoring: the mountain pine beetle context’ , *Journal of Applied Remote Sensing* **6**(1), 062527–1.

Wulder, M. A., White, J. C., Fournier, R. A., Luther, J. E. and Magnussen, S. (2008),

- ‘Spatially Explicit Large Area Biomass Estimation: Three Approaches Using Forest Inventory and Remotely Sensed Imagery in a GIS’, pp. 529–560.
- Wulder, M. A., White, J. C., Nelson, R. F., Næsset, E., Ørka, H. O., Coops, N. C., Hilker, T., Bater, C. W. and Gobakken, T. (2012), ‘Lidar sampling for large-area forest characterization: A review’, *Remote Sensing of Environment* **121**, 196–209.
URL: <http://dx.doi.org/10.1016/j.rse.2012.02.001>
- Xu, B., Gong, P. and Pu, R. (2003), ‘Crown closure estimation of oak savannah in a dry season with Landsat TM imagery: Comparison of various indices through correlation analysis’, *International Journal of Remote Sensing* **24**(9), 1811–1822.
URL: <http://www.tandfonline.com/doi/abs/10.1080/01431160210144598>
- Zar, J. H. (1984), *Biostatistical Analysis*, second edn, Prentice-Hall, Inc, Englewood Cliffs, New Jersey (07632).

Appendices

Appendix A

Supplementary material - Chapter 3

Table A.1 Details of the Landsat imagery used in the production of the time series plots.

Sensor	WRS-2 path/row	Capture date
Landsat 5TM	106/69	30/05/1987
Landsat 5TM	106/69	01/04/1989
Landsat 5TM	106/69	04/04/1990
Landsat 5TM	106/69	07/06/1990
Landsat 5TM	106/69	07/04/1991
Landsat 5TM	106/69	09/05/1991
Landsat 5TM	106/69	12/04/1993
Landsat 5TM	106/69	28/04/1993
Landsat 5TM	106/69	30/05/1993
Landsat 5TM	106/69	15/04/1994
Landsat 5TM	106/69	01/05/1994
Landsat 5TM	106/69	17/05/1994
Landsat 5TM	106/69	20/05/1995
Landsat 5TM	106/69	20/04/1996
Landsat 5TM	106/69	23/04/1997
Landsat 5TM	106/69	10/04/1998
Landsat 5TM	106/69	26/04/1998
Landsat 5TM	106/69	28/05/1998
Landsat 5TM	106/69	29/04/1999
Landsat 7ETM+	106/69	25/05/2000
Landsat 7ETM+	106/69	10/04/2001
Landsat 7ETM+	106/69	26/04/2001
Landsat 7ETM+	106/69	28/05/2001
Landsat 7ETM+	106/69	13/04/2002
Landsat 7ETM+	106/69	29/04/2002
Landsat 7ETM+	106/69	31/05/2002
Landsat 7ETM+	106/69	16/04/2003
Landsat 7ETM+	106/69	02/05/2003
Landsat 5TM	106/69	10/04/2004
Landsat 7ETM+	106/69	18/04/2004
Landsat 5TM	106/69	26/04/2004
Landsat 7ETM+	106/69	04/05/2004
Landsat 5TM	106/69	13/04/2005
Landsat 7ETM+	106/69	21/04/2005
Landsat 5TM	106/69	29/04/2005

Continued on next page

Table A.1 –continued from previous page

Sensor	WRS-2 path/row	Capture date
Landsat 5TM	106/69	15/05/2005
Landsat 5TM	106/69	31/05/2005
Landsat 5TM	106/69	02/05/2006
Landsat 7ETM+	106/69	10/05/2006
Landsat 5TM	106/69	18/05/2006
Landsat 7ETM+	106/69	26/05/2006
Landsat 5TM	106/69	03/06/2006
Landsat 5TM	106/69	05/05/2007
Landsat 5TM	106/69	05/04/2008
Landsat 7ETM+	106/69	13/04/2008
Landsat 7ETM+	106/69	29/04/2008
Landsat 5TM	106/69	07/05/2008
Landsat 7ETM+	106/69	31/05/2008
Landsat 5TM	106/69	08/06/2008
Landsat 5TM	106/69	26/05/2009
Landsat 7ETM+	106/69	05/05/2010
Landsat 7ETM+	106/69	06/06/2010
Landsat 7ETM+	106/69	24/05/2011
Landsat 7ETM+	106/69	11/04/2013
Landsat 8OLI	106/69	19/04/2013
Landsat 7ETM+	106/69	27/04/2013
Landsat 8OLI	106/69	08/05/2014
Landsat 8OLI	106/69	24/05/2014
Landsat 8OLI	106/69	09/04/2015
Landsat 8OLI	106/69	11/05/2015
Landsat 8OLI	106/69	27/05/2015
Landsat 8OLI	106/69	13/05/2016
Landsat 7ETM+	106/69	21/05/2016

Appendix B

Supplementary material - Chapter 5

Decision matrix used to define when substantial change (loss) had occurred between each structural formation class in the change detection methodology developed in this study. The grey cells represent classes where significant change is considered to have occurred for the class representing the year being assessed.

		Year Assessed																	
		Previous Year																	
		Gl	Owv	Owi	Own	Owt	Wt (lc)	Wt (tc)	Wt (hc)	Wm (lc)	Wm (tc)	Wm (hc)	Orv	Orf	Ofm	Cfv	Cfi	Cfm	Cft
Gl																			
Owv																			
Owi																			
Own																			
Owt																			
Wt (lc)																			
Wt (tc)																			
Wm (lc)																			
Wt (hc)																			
Wm (hc)																			
Orv																			
Ofm																			
Ofr																			
Cfv																			
Cfi																			
Cfm																			
Cft																			

Year Assessed
 Previous Year

No Change

 Change

 Gl = Grassland
 Owv = Open woodland very low
 Owi = Open woodland low
 Own = Open woodland mid
 Owt = Open woodland tall
 Wt (lc) = Woodland (lc) very low
 Wt (tc) = Woodland (tc) low
 Wt (hc) = Woodland (hc) mid
 Wt (hc) = Woodland (hc) tall
 Wm (lc) = Woodland (lc) very low
 Wm (tc) = Woodland (tc) low
 Wm (hc) = Woodland (hc) mid
 Wm (hc) = Woodland (hc) tall
 Orv = Open forest very low
 Orf = Open forest low
 Ofm = Open forest mid
 Ofm = Open forest tall
 Cfv = Closed forest very low
 Cfi = Closed forest low
 Cfm = Closed forest mid
 Cft = Closed forest tall

Fig. B.1 Decision matrix showing the conditions used to identify change (loss) between structural formation classes.

Bar chart showing the coverage of each structural formation class for the region impacted by Cyclone Monica between the years 2004 and 2017.

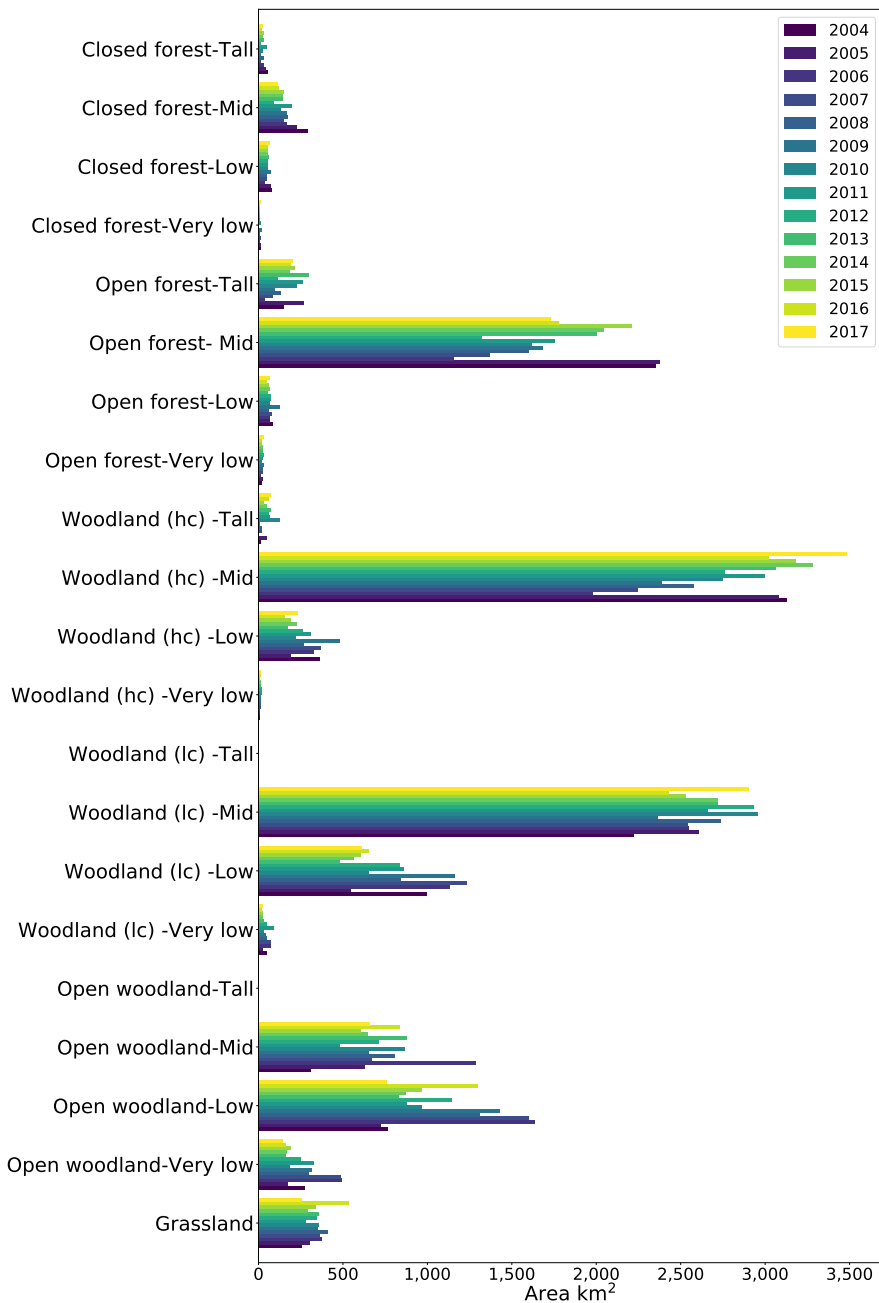


Fig. B.2 Bar graph detailing the coverage (km²) of each structural formation class for the years 2004 to 2017 over the region impacted by Cyclone Monica (Extent shown in Fig 5.16).

Appendix C

Supplementary material - Chapter 6

Example of the structural classification mapping product showing the impact of two cyclone's, Lam and Nathan which impacted the Arnhem Land region in 2015. Cyclone Lam is the strongest cyclone to impact the Northern Territory since cyclone Monica in 2006.

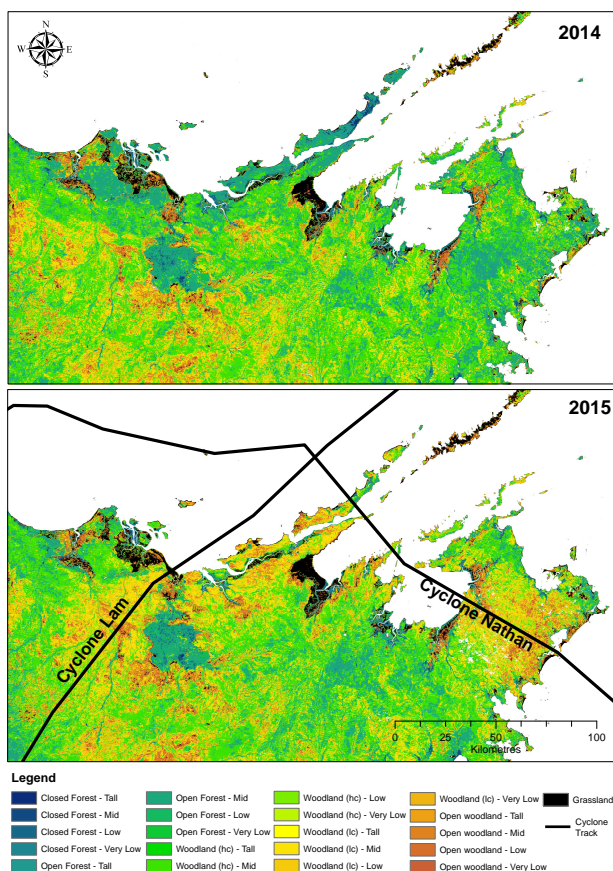


Fig. C.1 Example of the structural classification mapping product showing the impact of two cyclone's, Lam and Nathan which impacted the Arnhem Land region in 2015.